# TRANSIENT ANALYSIS OF AGED CONCRETE DAM-FOUNDATION COUPLED SYSTEM

Thesis Submitted in Partial Fulfillment of the Requirements

for the Degree of

***DOCTOR OF PHILOSOPHY***

*by*

AVIJIT BURMAN

ROLL No. 04610401


**DEPARTMENT OF CIVIL ENGINEERING**

**INDIAN INSTITUTE OF TECHNOLOGY GUWAHATI**

**GUWAHATI-781039**

# CERTIFICATE

This is to certify that the thesis entitled **"Transient Analysis of Aged Concrete Gravity Dam-Foundation Coupled System"** submitted by **Avijit Burman** Roll No. 04610401 to the Indian Institute of Technology Guwahati, for the award of the degree of Doctor of Philosophy in Civil Engineering is a record of bonafide research work carried out by him under my supervision and guidance. The thesis work, in my opinion, has reached the requisite standard fulfilling the requirement for the degree of Doctor of Philosophy.

The results contained in this thesis have not been submitted in part or full to any other University or Institute for award of any degree or diploma.

(Dr. S. Sreedeep)
Associate Professor
Department of Civil Engineering
Indian Institute of Technology Guwahati
Guwahati-781039, INDIA.

Guwahati

Date:

# STATEMENT

I do hereby declare that the matter embodied in this thesis is the result of investigations carried out by me in the Department of Civil Engineering, Indian Institute of Technology Guwahati, Guwahati, Assam, India.

In keeping with the general practice of reporting scientific observations, due acknowledgements have been made wherever the work described is based on the findings of other investigators.

Guwahati 781039

Date: (AVIJIT BURMAN)

# ACKNOWLEDGEMENT

First and foremost, I would like to extend my heartfelt thanks to my supervisor, Dr. S. Sreedeep. Frequent discussions with him have cleared many critical questions regarding this thesis. His energetic and friendly ways have always remained a constant source of inspiration for me. Without his constant guidance and perseverance, this work could have never been completed.

For the first three years of my stay in IIT Guwahati as a full time PhD student, I was fortunate to have Dr. Damodar Maity as my supervisor. Even after he left IITG, he continued to extend his helping hand towards me. I offer my sincerest gratitude to Dr. Damodar Maity who supported me throughout this thesis work with his knowledge and extreme patience. His in-depth knowledge has always been a beacon of light whenever I felt lost inside a dark tunnel. Not only on the academic front, on the personal front too, I found his advises absolutely invaluable.

I am extremely indebted to Dr. Anjan Dutta, Dr. Sujit Dash and Dr. S. K. Kakoty for their critical suggestions on my work and their constant support.

I would also like to thank all the staffs of Department of Civil Engineering, IIT Guwahati for their cooperation. In my daily work I was blessed with a friendly and cheerful group of fellow students. I would like to thank Bibhash, Bidyut, Kaushik, Rajendra, Tarapada, Debashis, Subham, Bedabrata, Pallav, Avishek and all my friends back home in my place.

Finally I would like to thank my mother and my wife whose constant support during days of uncertainties and anxieties helped me to overcome those difficult phases of my life. I am also very much grateful to my colleagues in BIT Mesra for their cooperation in seeing this work through.

AVIJIT BURMAN
Research Scholar
Dept. of Civil Engineering, IIT Guwahati

# ABSTRACT

The seismic behavior of concrete dams has been the subject of extensive research during the past decades because of concern for dam safety during earthquakes. Concrete dams are distinguished from other structures because of their huge size and their interactions with the adjacent reservoir and underlying foundation. The safety evaluation of the concrete gravity dams subjected to severe seismic excitations is really very complex as they create coupling effect with the underlying foundation. The interaction among dam, reservoir and its foundation may alter the actual behavior of the dam considerably than what is obtained from the consideration of the dam alone. Therefore, it is necessary to take into account the coupled dam-foundation-reservoir interaction effects for the sound design of the concrete dam. While the structural models are relatively simpler, foundation models are often complicated due to their unbounded nature and nonlinear stress-strain characteristics. Because of nonlinear stress-strain behavior of soil/rock material, it is important to consider its effect while carrying out soil-structure interaction analysis. An attempt is made here to develop a method to assess the effect of soil-structure interaction on the seismic response of dam to make its design more realistic.

Due to ageing, the dams are subjected to severe environmental effects, which may lead to loss of stiffness as well as strength due to material degradation. Since the dam face is in constant contact with water, concrete degradation due to hygro-mechanical loading is inevitable and should be considered in the analysis procedure. This ageing process of concrete leads to loss of stiffness and strength of the material. Therefore, to assess the behavior of the dam at a later stage of its life, it is important to determine the proper strength of the concrete at a certain age. An approach to include the time dependent degradation of concrete owing to various environmental factors is presented. Both the aged dam and foundation domains are analyzed separately with the interaction effects at the dam-foundation interface enforced by a developed iterative scheme. In the present work, an appropriate method is presented to truncate infinite foundation domain with absorbing dampers. The finite element method is used to model both dam and foundation. The results obtained from present dam-foundation interaction analyses presents the trends to be expected for a concrete gravity dam at a later stage after construction which may help a designer in the decision making process.

# List of Figures

# List of Tables

# List of Symbols

| | |
|---|---|
| $[M]$ | The mass matrix of the structure |
| $[C]$ | The damping matrix of the structure = $\alpha'[M]+\beta'[K]$ |
| $[K]$ | The structural stiffness matrix |
| $\{u\}$ | The vector of nodal point displacements relative to ground |
| $[L]$ | The matrix which determines the hydrodynamic forces from pressures. |
| $\{p\}$ | Pressure at dam-reservoir interface |
| $a_g$ | Ground acceleration |
| $\alpha'$ | Mass proportional damping constant |
| $\beta'$ | Stiffness proportional damping constant |
| $\zeta_r$ | Fraction of critical damping |
| $\omega_r$ | Natural frequency of vibration in the $r^{th}$ mode of vibration |
| $C_s$ | A coefficient |
| $\alpha_h$ | Seismic coefficient |
| $\rho_f$ | Density of water |
| $H_f$ | Depth of water in the reservoir |
| $p$ | Hydrodynamic pressure at any point $(x,y)$ in the reservoir |
| $c$ | Acoustic velocity in water |
| $g$ | Gravitational acceleration |
| $n$ | Wave number ($n = 2\pi/\lambda$) |
| $\lambda$ | Wavelength of the pressure oscillations |
| $k$ | Bulk modulus of water ($k = c^2/\rho_f$) |
| $T$ | Period of horizontal ground vibrations |
| $\sigma_{ij}, s_{ij}$ | Stress tensor, deviatoric stress tensor |
| C | Cohesion of the soil particles |
| $\phi$ | Angle of internal friction |
| $\sigma_1, \sigma_2, \sigma_3$ | Principal stresses |
| $I_1, I_2, I_3$ | Stress invariants |
| $J_1, J_2, J_3$ | Deviatoric stress invariants |
| $W_d$ | The distortional energy per unit volume of the material |
| $\mu$ | Poisson's ratio |
| $E_d$ | Modulus of elasticity or Young's modulus |

| | |
|---|---|
| $u, v$ | Displacement, velocity functions |
| $x, y$ | Cartesian coordinates |
| $N_{di}, [N]$ | Shape functions for eight node quadrilateral element. |
| $[J]$ | Jacobian matrix |
| $\{u\}, \{\dot{u}\}, \{\ddot{u}\}$ | Displacement, velocity and accelerations at any point in a continuum |
| $\gamma, \beta$ | Parameters in average acceleration integration method |
| $i$ | Iteration count |
| $\varepsilon$ | Tolerance |
| $\Delta t, \Delta t_{cr}$ | Time step, Critical time step |
| $F, f$ | External force vector |
| $T$ | Time period |
| $\omega, \omega_n$ | Frequency, natural frequency |
| $\xi$ | Damping ratio |
| $\theta$ | Parameter in Wilson-$\theta$ method, Lode angle |
| $\{\sigma\}$ | Stresses in a continuum |
| $\{\varepsilon\}$ | Strains in a continuum |
| $d$ | Damage variable |
| $W(\varepsilon, d)$ | Strain energy |
| $Y$ | Thermodynamic force associated with damage |
| $d_{gi}$ | Orthotropic degradation index |
| $d_g$ | Isotropic degradation index |
| $[D]$ | Constitutive matrix of any material |
| $[D_d]$ | Degraded constitutive matrix of any material |
| $\phi$ | Total porosity of concrete |
| $\phi_0, \phi_c, \phi_m$ | Initial porosity, chemical porosity and mechanical porosity of concrete |
| $d_m$ | Scalar degradation index |
| $\kappa^0$ | A variable representing the initial degradation status |
| $\kappa$ | A variable representing the current degradation status |
| $a_s, \alpha_c, \beta_c$ | Material parameters |
| $f_t$ | Static tensile strength |
| $E_0$ | Elastic modulus of the non-degraded material |
| $E_m$ | Degraded elastic modulus due to porosity of concrete |
| $\varsigma$ | A parameter representing effect of ageing process as a function of time |
| $\tau_a$ | Characteristic time of the ageing process |
| $f(t)$ | Compressive strength of concrete as a function of time |
| $\delta u_i$ | A virtual displacement field |
| $\{q\}$ | Nodal values of displacement for an eight nodded quadrilateral element |

| | |
|---|---|
| $[B]$ | Strain displacement matrix |
| $\{\sigma_e\}$ | Elemental stress vector |
| $\{q_e\}$ | Elemental displacement vector |
| $p$ | Hydrodynamic pressure at the upstream face of the dam |
| $a_n$ | The magnitude of acceleration normal to the upstream face of the dam |
| $\rho$ | The mass density of water |
| $H$ | The height of water at the upstream side of the dam |
| $y$ | The variation of distance in the vertical direction |
| $\sigma_1, \sigma_3$ | Major and minor principal stresses |
| $E_i$ | Initial slope of the stress-strain curve |
| $K$ ,$n$ | Modulus number, modulus exponent |
| $Pa$ | Atmospheric pressure |
| $R_f$ | Failure ratio |
| $c$ | Cohesion of soil/rock material. |
| $\phi$ | Angle of internal friction of soil/rock material |
| $E_T$ | Tangent Young's modulus for a Duncan-Chang material |
| $E_{ur}$ | Young's modulus for unloading and reloading |
| $K_{ur}$ | Unloading-reloading modulus number |
| $B$ | Bulk modulus |
| $K_b$ , $m$ | Bulk modulus number, bulk modulus exponent |
| $\sigma(s), \tau(s)$ | Normal and shear stresses on the boundary |
| $u(s), v(s)$ | Normal and shear displacements on the boundary |
| $C_x$ | Damping coefficient of a dashpot |
| $C_n, C_t$ | Damper coefficient in normal and tangential directions |
| $c_s, c_p$ | Shear and compressional wave velocities |
| $G$ | Shear modulus |
| $A_1, A_2$ | Effective factors along normal and tangential |
| $G$ | Shear modulus |
| $x, \dot{x}, \ddot{x}$ | Displacement, velocity and acceleration respectively for any domain. |
| $M, C, K$ | Mass, damping and stiffness matrix for any domain |
| $f$ | External force vector |
| $f_{if}$ | Vector composed of interaction forces |
| $i$ | Iteration count |
| $\varepsilon$ | Tolerance |
| $\Delta t$ | Time step |

## Units Used

In the present work, SI units have been used all throughout. They are listed as below:

| | |
|---|---|
| Force: | N, kN |
| Density: | $kg/m^3$ |
| Length/Distance: | m |
| Temperature: | Degree (Celsius) |

# CONTENTS

# CHAPTER 1

# INTRODUCTION

## 1.1 GENERAL

A concrete gravity dam is a huge structure made up of plain cement concrete. It is generally built in a river terrain to block the flow of water and release it according to our convenience to generate hydro electrical energy. Apart from the generation of electricity, it also helps in irrigation and countless other activities by channeling the water of the reservoir in proper way. One of its main activities is to support the water in the reservoir which lies adjacent to it. In order to support the huge mass of reservoir water, the dam has to withstand the overturning and the sliding forces caused by the reservoir water. The stability of the dam against the overturning and the sliding forces caused by the reservoir water is derived mainly from its gravitational weight (Leger and Katsouli, 1989). The cost associated with the building of a dam project is generally in the order of billions of rupees. Also, habitation, cultivation and numerous other industries grow on the downstream side of the dam. Therefore, it is of utmost importance to ensure the safety of the dam because a massive failure will certainly lead to huge loss of properties and the lives of people (Gogoi, 2007).

During any earthquake, the dam body is subjected to hydrodynamic forces which is a time dependent phenomenon and changes its direction depending upon direction of the ground acceleration. The issues of seismic safety of dams have attracted increased attention from the researchers and analysts all over the world because a large number of dams have been commissioned recently in many earthquake prone areas or in places where some active seismic faults exist (Chopra, 1968, 1975). A very important structure like a concrete gravity dam is often designed and constructed for a lifetime of more than 100 years. The dam face remains in contact with the adjacent reservoir water throughout its lifetime and as a result, the concrete gets seriously degraded by the effects of various hygro-chemo-mechanical actions. Over a longer period of time, such close proximity with water leads to the change of the strength of concrete. Therefore, any analysis of the dam at a later stage of its life considering its initial undamaged concrete strength is bound to be grossly inadequate. In order to truly asses the behavior of the dam under any type of loading, whether static or dynamic, the proper strength of the material at any stage of its lifetime should be considered (Gogoi and Maity, 2007).

It is a well known fact that the concrete gains strength after being laid. It is customary to assume the 28 days strength as the full strength of concrete, but experimental evidences (Washa et. al., 1989) show that concrete develops strength beyond 28 days. This gain of strength continues for a certain time. After that, the strength of the concrete assumes a constant value. For proper estimation of the behavior of concrete gravity dam, this phenomenon also entails to be evaluated. During the lifetime of a dam, the factors and the parameters which are responsible for the deterioration of the strength of the concrete due to various hydro-chemo-mechanical actions should be identified. Besides that, it is also very much important to develop proper mathematical models to facilitate determination of the response of a concrete gravity dam which have suffered degradation under the action of various environmental processes over time.

The response of a structure during an earthquake depends on the characteristics of the ground motion, the surrounding soil, and the structure itself. In general the seismic analysis of buildings and other engineering structures is often based on the assumption that the foundation corresponds to a rigid block, which is subjected to a horizontal, unidirectional acceleration. For the structure on the rigid foundation, the horizontal motion can be applied directly on the base of the structure. The input acceleration resulting in the applied horizontal inertial loads will be constant over the height of the structure. During the earthquake, an overturning moment and transverse shear acting at the base will develop. As the rock is very stiff, these two stress resultants will not lead to any (additional) deformation at the base (Leger and katsouli, 1989). The resulting horizontal displacement of the base is thus equal to the control motion; no rocking motion arises at the base. For a given control motion, the seismic response of the structure depends on the properties of the structure alone. For the structure founded on flexible soil, the motion of the base of the structure will be different from the free-field motion because of the coupling of the structure-soil system. This is due to the following reasons: First, the inability of the foundation to conform to the deformations of the free-field motion would cause the motion of the base of the structure to deviate from the free-field motion. Second, the dynamic response of the supporting structure itself would induce deformation of the supporting soil. This process, in which the response of the soil influences the motion of the structure and response of the structure influences the motion of the soil, is referred to as ***soil-structure interaction (SSI)***. The nature and the amount of interaction depend on the respective properties of soil and foundation domains (Zhang, Wegner and Haddow, 1999).

If the foundation is rigid, the energy received by the structure from the base during an earthquake, can be dissipated only through material damping mechanisms, such as viscous damping, plastic deformations *etc*. Material damping is due to the inelastic behavior of the soil supporting the foundation. Radiation damping is a purely geometric effect that exists at low as well as high strain amplitudes. For typical foundations, radiation damping is much higher than the material damping (Wolf, 1988). Therefore, it is indispensable to consider radiation damping during vibration analysis of the structure. Several kinds of modeling techniques had been developed for this purpose including viscous boundary, transmitting boundary, boundary elements and infinite elements.

The effect of soil-structure interaction is recognized to be important and cannot, in general be neglected. For the design of the critical facilities, especially nuclear power-plants and concrete gravity dams, very complex analyses are required which are based on recent research results, some of which have not been fully evaluated. This has led to a situation where soil-structure interaction has become a highly challenging research area.

## 1.2 IMPORTANCE OF SOIL-STRUCTURE INTERACTION EFFECT

The effect of soil-structure interaction may be very significant on the dynamic response of many structures and foundation systems. Sometimes, avoidance of the effect of the soil-structure interaction may be advantageous from point of view of computational cost, as the consideration of it would increase accuracy of the computed results very marginally. Sometimes, disregarding its effect may lead to grossly inaccurate analysis as in the case of structure lying on a relatively less stiff foundation. Whether the neglect of its effects is conservative or unconservative depends on the details of the problem at hand and must be evaluated on a case-by-case basis. If a lightweight flexible structure is built on a very stiff rock foundation, a valid assumption is that the input motion at the base of the structure is same as the free-field earthquake motion. This assumption is valid for a large number of building systems since most of the building type structures are approximately 90 percent voids, and it is not unusual that the weight of the structure is excavated before the structure is built (Wolf, 1985). However, if the structure is very massive and stiff, such as a concrete gravity dam and nuclear power plants and with that if the foundation is relatively flexible, the motion at the base of the structure may be significantly different than the free-field surface motion. As the earthquake response of a

structure is dependent on the time period and the period of vibration of a given structure increases with decreasing soil stiffness it is now realized that for calculating the response of a structure considering a fixed base and ignoring the effect of soil can lead to serious errors. Because the maximum stresses and deflections in the system are modified significantly from the values that would have developed if it were on a rigid foundation, it is intuitively recognized that the effect of soil-structure interaction increases with the increase of foundation flexibility and vice versa (Wolf, 1985, 1988). So, while analyzing massive structures resting on flexible foundation we must take soil-structure interaction into consideration.

## 1.3 COMPONENTS OF SOIL-STRUCTURE INTERACTION

### 1.3.1 Modeling of Structure

The dimensions of the structure are finite. Structure models are characterized by *stick models, lumped mass and finite elementt models.* Proper constitutive modeling has to be used in order to represent the behavior of the structure accurately under dynamic loading condition. Generally, linear elastic material properties are considered to be satisfactory under ordinary conditions. But, in extraordinary cases i.e., if the loading is very high or under some other specific circumstances, consideration of a nonlinear elasto-plastic model may become necessary.

### 1.3.2 Modeling of Soil

Soil behaves strongly nonlinearly when excited by the high magnitude of earthquakes. A material model is a mathematical relationship describing the stress-strain behavior of a material, and is called a *"constitutive model"*. The constitutive models that are used to characterize the bahaviour of geologic materials include primarily the following 4 types of models: a) Linear elastic models, b) Nonlinear elastic models, c) Elasto-plastic models and d) Elastovisco-plastic models. Soil being heterogeneous, anisotropic and nonlinear in force-displacement characteristics, consideration of linear behavior may not always suffice. Therefore we have to use either elasto-plastic model or a nonlinear elastic model to represent true stress-strain behavior of soil. In the present work, a nonlinear, elastic model known as Duncan-Chang model (1970) is adopted for the purpose of modeling the foundation domain.

### 1.3.3 Modeling of Radiation Boundary Condition

In a finite element model, the foundation domain has to be truncated somewhere which is inaccurate from the point of view of physical representation of the domain. Applying the roller or fixed boundary conditions at the truncated boundary implies that certain amount of fixity is introduced which will lead to the reflection of on-going seismic waves. Therefore, certain boundary condition should be adopted so that the traveling waves are allowed to pass unhindered. These boundary conditions are known as radiation or transmitting boundary conditions or non-reflecting boundary conditions. In a FEM model, non-reflecting boundary conditions as suggested by Lysmer and Kuhlemeyer (1969) may be adopted to satisfy the radiation condition. The infinite element (Bettess, 1970) also satisfies the radiation boundary conditions which may be used to model the semi-infinite foundation domain. The analytical solution required for the boundary element method satisfies the requirement of radiation condition properly which makes it an attractive method for representing semi-infinite domains. However, amongst all these methods, the first boundary condition suggested by Lysmer and Kuhlemeyer (1969) are still used because of their attractive physical implications and computational simplicity. In the present work, the viscous boundaries suggested by Lysmer and Kuhlemeyer (1969) have been adopted which use dashpots to absorb the energy of the on-going waves and thus, minimize their reflection from the truncated boundary into the computational domain.

### 1.3.4 Modeling of Coupled Dam-Foundation System

Having modeled the structure, foundation and the radiation boundary condition, it is important to model the interaction effect that arises between soil and structure. In direct method of soil-structure interaction the soil and structure domain is modeled as a whole and the interaction effect is incorporated in the generated matrices. This method gives rise to large sizes of matrices which may require considerable time to solve and computer memory for storage (Gogoi, 2007). On the other hand, the indirect method breaks the whole system into two sub-systems and the interaction effect is generated by means of iterative processes (Von Estorff and Hagen, 2005). This method helps us to work with smaller matrices which may lead to saving of time and storage memory. However, the choice of a particular method depends entirely on the analyst's preference.

## 1.4 OBJECTIVE OF THE STUDY

The objective of the present investigation is to develop (i) a suitable boundary condition for the finite element analysis of unbounded soil domain considering its material nonlinearity, (ii) an iterative technique for the dam-foundation coupled system and (iii) an effective algorithm to predict the seismic response of new and aged dams with and without the presence of reservoir water.

## 1.5 ORGANIZATION OF THE REPORT

The outline of the thesis report is as follows.

*Chapter 1 - Introduction*: An illustration of several key concepts, importance of SSI and Objective of the present work are presented.

*Chapter 2 - Literature Review*: In this chapter an overview of the relevant literature review and basic methodologies in SSI analysis are given chronologically. Finally, the summary of the literature review and detailed scope of the present work is outlined.

*Chapter 3 - Theory and Formulations*: *S*election of numerical technique and theoretical formulations are outlined in this chapter. There are three distinct parts in this chapter. Part A of this chapter describes the methodologies adopted for simulation of ageing of concrete material, which plays a significant role in the final assessment of its behavior at a later stage of its construction. Part B describes the nonlinear material adopted for the description of the nonlinear stress-strain behavior of the foundation material. Part C describes the iterative procedure adopted for the simulation of the interaction between dam and the underlying foundation.

*Chapter 4 - Results and Discussions*: Results of the response analyses for various problems and discussions on the results are presented in three parts in this chapter. Part A shows the results of the degradation model used to represent the deterioration of concrete over a longer period of time due to various hydro-chemo-mechanical analyses. The nonlinear behavior of the foundation is presented in part B and the results related to dam-foundation interaction analyses are presented in part C of this chapter.

*Chapter 5 - Conclusions:* This chapter comprises of conclusions on the present work and reviews the scope for further work.

# CHAPTER 2

# REVIEW OF LITERATURE

## 2.1 INTRODUCTION

This chapter deals with a comprehensive review of literature on some of the important soil-structure interaction problems. During the last few decades a significant amount of research activity had been devoted towards the area of soil-structure interaction. The problem becomes still more complex when the effect of dynamic load such as earthquake is taken into account. For sound design against dynamic loading, the interactive behavior of soil foundation and structure domain has led to increased interests in the area of soil structure interaction analysis. A concrete gravity dam consists of the structure itself, the reservoir beside it and the foundation below it (Fig. 2.1). Some of these relevant literatures are reviewed chronologically in order to bring out the gradual development in the study of dynamic soil-structure interaction problems. Further, the contributions of different researchers on modeling material nonlinearity of the soil/rock material and processes of ageing of the concrete are discussed. A brief description of some of the existing nonlinear models has been presented. Efforts have been made to highlight the works of various investigators in the development of different local and non-local boundary conditions which are applicable for semi-infinite or infinite domains. A critical appraisal of the reviewed literature is presented at the end of this chapter, before highlighting the scope of the present study.

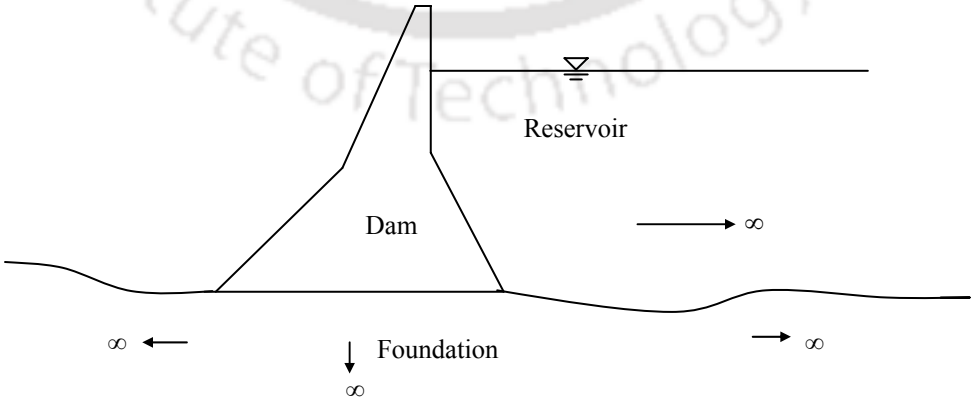


Fig. 2.1 A general dam-reservoir-foundation system

## 2.2 TRADINATIONAL ANALYSIS OF DAM

### 2.2.1 Traditional Static Analysis and Design

The standard static design procedure does not account for the random earthquake motions. The inertia forces induced by the earthquake are statically applied at the centre of gravity of the dam. The limitations of this method are that it disregards the elasticity of the dam, the time varying excitation force and the damping capacity of the dam. Despite these disadvantages, the method is still employed owing to its simplicity. It was shown that if the dynamic character of earthquake forces is ignored, the dynamic analysis does not indicate the actual principal tensile stresses, the region of stress concentration and areas where cracks are likely to occur (Chopra, 1975). A large discrepancy exists between the stress distribution obtained by use of the equivalent static method and that resulting by use of proper dynamic methods (US Army Corps of Engineers, 1977). Another drawback is the assumption of a height-wise uniform seismic coefficient which shows stresses to be greatest at the base of the dam. This has led to the concept of decreasing the concrete strength with increase in elevation. Fenves and Chopra (1987) proposed a simplified response spectrum analysis to determine the structural response, in the fundamental mode of vibration due to the horizontal component of ground motion. This procedure was developed as a hand calculated alternative to the more general analytical procedures that can be used to evaluate the compressive and tensile stresses at locations above the base of the dam. But dynamic analysis results show that the largest stresses actually occur at the upstream and downstream faces in the upper part of gravity dams (Chandrashaker & Humar 1993) in the case of Koyna dam. However, the largest stresses may also occur at the base of the dam depending on dynamic characteristics and geometry.

### 2.2.2 Linear Dynamic Analysis of Dam

Since, a concrete gravity dam is a fairly long structure in the longitudinal direction, the strain in z direction can be assumed to be zero. Therefore, a long structure like a concrete gravity dam is often modeled under plain strain idealization. Earlier, while analyzing a dam against earthquake excitation, people used to consider it as a rigid system situated on

a rigid foundation. While this assumption makes the problem simpler, but it effectively ignores the flexibility effect of the dam and foundation interface i.e. the flexibility of the foundation domain. Ideally, while analyzing, the interaction effect between structure and foundation should be considered in order to take care of the flexibility of the foundation domain. Most of the recent work has incorporated the elastic properties of the dam materials into the mathematical model, which influences the vibration properties of the dam and influences the earthquake response behavior. When flexibility of dam is considered, the hydrodynamic responses show high peaks at the natural frequencies of the system (Saini et al. 1978). Considering the dam as rigid and water to be incompressible, the authors showed that the hydrodynamic forces and dynamic amplification factor remained independent of excitation frequency in a frequency domain analysis. However, when flexibility of dam was considered, the responses were dependent on the excitation frequency. They used the discretized equation of motion in finite element form for the dam subjected to ground motion which is expressed as:

$$[M]\{\ddot{u}\}+[C]\{\dot{u}\}+[K]\{u\}=-[M]a_g(t)+[L]\{p\} \qquad (2.1)$$

Where,

$[M]$ = The mass matrix of the structure

$[C]$ = The damping matrix of the structure = $\alpha'[M]+\beta'[K]$

$[K]$ = The structural stiffness matrix

$\{u\}$ = The vector of nodal point displacements relative to ground

$[L]$ = The matrix which determines the hydrodynamic forces from pressures.

$\{p\}$ = Pressure at dam-reservoir interface

$a_g$ = Ground acceleration

$\alpha'$ = Mass proportional damping constant

$\beta'$ = Stiffness proportional damping constant

In the above expression, dots define differentiation with respect to time, $t$. Damping is expressed as linear combination of the mass and stiffness of the system, where $\alpha'$ and $\beta'$ can suitably be chosen to obtain the desired damping in the system. This type of damping is normally referred to as Rayleigh damping. The Rayleigh damping matrix is

equivalent to using a modal analysis in which damping is expressed as a fraction of critical damping given by

$$\zeta_r = \frac{1}{2}\left[\left(\alpha' / \omega_r\right) + \beta' \omega_r\right] \tag{2.2}$$

where, $\zeta_r$ is the fraction of critical damping and $\omega_r$ is the natural frequency of vibration in the $r^{th}$ mode of vibration. Rayleigh damping does not occur naturally, but is used only for numerical convenience.

#### *2.2.2.1 Three Dimensional Modelling of Dam*

Fok et al. (1986) developed the EACD-3D computer program implementing an analytical procedure for the three-dimensional analysis of earthquake response of concrete dams including the effects of dam-water interaction, water compressibility, and reservoir boundary absorption due to alluvium and sediments at the bottom.

A numerical correlation study was carried out along with an extensive dynamic testing on Outardes 3 gravity dam in northeastern Quebec, Canada (Proulx and Paultre 1997) to evaluate the performance of 2D and 3D models. It was concluded that for earthquake analysis of gravity dams with un-keyed construction joints, a 2D model is reasonable if sliding of vertical blocks is expected. However, for important projects and critical safety evaluation, a 3D analysis was recommended.

Fahjan et al. (2003) proposed a 3D model which accounted for canyon profile and gives accurate response of the structure. However, consideration of a 3D model increases the required computational effort drastically. Unless the dam is located in narrow canyon, for which the 3D analysis gives higher peak acceleration values than the 2D analysis, the extra computational effort required outweighs the extra accuracy of computed result from 3D analysis.

A three-dimensional model can thus be used when the dam geometry or loading is such that plane strain conditions may not be assumed, when the geometry is such that the stability of the dam depends upon stress distribution parallel to its axis, as is the case of a gravity-arch dam which is curved in plan, or when a dam is in a narrow valley. Three-dimensional analysis allows the rigorous determination of what forces will be applied to

the foundation, and where. If 3D behavior is to be considered, features that enable horizontal force transfer such as shear keys or curvature in plane must be present.

### 2.2.3 Nonlinear Dynamic Analysis of Dam

Linear dynamic analysis of a concrete gravity dam would be sufficient if the induced stresses and strains are below the yield point of the material. But, in case of severe earthquake loading, these may exceed the elastic limit. Then, proper nonlinear analysis which takes into account of the changed material stiffness during the loading period would become unavoidable. Though nonlinear analysis is much more complex as well as demanding from the point of view of computational cost, many researchers across the globe have taken this subject very seriously. It was observed that a gravity dam might fail due to the crushing of the toe material, cracking of the upstream material with an increase in uplift pressure and reduction in shear resistance that may result in sliding failure (Copen et al. 1977), even before the failure due to overturning takes place.

The crack band theory (Vargas-Loli & Fenves 1989) has also been used to model tensile cracking to evaluate the nonlinear seismic response of a dam-reservoir system. The use of this theory allows use of large size finite elements. The continuum model proposed by Lemaître and Chaboche (1989) and Krajcinovic (1989) was found to be advantageous over the discrete approach, as it does not require re-meshing. A boundary element (BE) technique was formulated by Pekau et al. (1991) and Batta and Pekau (1996), which was found to be efficient for the analysis of seismic crack propagation due to simplification of the non-linear dynamic problem as it is based on linear elastic fracture mechanics.

Procedures to verify the seismic stability of concrete dams due to overturning and sliding were proposed by Léger and Katsouli (1989) and Chavez and Fenves (1995). Léger and Katsouli (1989) used gap-friction elements having nonlinear constitutive relation to model possible vertical separation and sliding of dam interface. They introduced a parameter called PNBC (Percentage of base not in contact) as an very important factor required to determine the sliding characteristics of the dam on the foundation. The seismic fragility assessment using a probabilistic model (Tekie & Ellingwood 2003) indicated that sliding along the dam-foundation interface is likely if the

dam is subjected to an earthquake with a magnitude of the maximum credible earthquake (MCE) as specified by the U.S. Army Corps of Engineers.

A dynamic nonlinear analysis may be adopted if cracks are present in the dam body, if the soil at the site where the dam is constructed is soft, heterogeneous having cracks, faults and fissures; and if possibilities of strong earthquakes occurring at the site are high. The choice of nonlinear analysis procedure to adopt will mainly depend on the geometry, material and dynamic characteristics of the dam-reservoir-foundation system.

## 2.3 HYDRODYNAMIC PRESSURE ON DAMS

In the design methods, as specified by U.S. Bureau of Reclamation in Design Standards No.2 (1965, 66) and Design manual (1976), the dynamic interaction behavior of the elastic dam, reservoir water and foundation rock system was not considered. Instead, the effect of hydrodynamic pressure on the dam is considered according to the "added mass approach" as suggested by Westargaard (1933). The Indian Standards Code (IS: 1893-1984) adopted the following expression originally proposed by Zangar (1952):

$$p = C_s \alpha_h \rho_f H_f \tag{2.3}$$

where,

$C_s$ = A coefficient to be determined experimentally (varies with shape and depth)

$\alpha_h$ = Seismic coefficient

$\rho_f$ = Density of water

$H_f$ = Depth of water in the reservoir

The above expression could be used for determination of pressure against the inclined upstream face of rigid dams due to horizontal earthquakes. The forces associated with the inertia of dam were expressed as the product of seismic coefficient taken to be constant over the surface of the dam, with values ranging between 0.05 and 0.1; the weight of the dam per unit surface area expressed as a function of location. This analytical expression has been found to be useful for minor works or for preliminary design of major works, giving the hydrodynamic pressure distribution in the upstream face of the dam to calculate total horizontal force and the overturning moment above any elevation of the dam.

The vibrating movements of an earthquake induce a concrete gravity dam to be in a state of forced vibration, where the acceleration of the dam-reservoir interface subsequently induces pressure waves in the reservoir. This undulatory system, which develops temporarily in the reservoir, entails pressure wave propagation that can be expressed mathematically by the wave equation as

$$\frac{\partial^2 p}{\partial x^2}+\frac{\partial^2 p}{\partial y^2}=\frac{1}{c^2}\frac{\partial^2 p}{\partial t^2} \tag{2.4}$$

where $p$ is the hydrodynamic pressure at any point $(x,y)$ in the reservoir and $c$ is the acoustic velocity in water. Different methods of solution of eq. (2.4) allow an estimation of hydrodynamic pressure considering the dam to be a rigid structure. In a simplified seismic analysis of dams, the effect of the reservoir systems is incorporated by imposing the hydrodynamic force at the dam-reservoir interface.

Westergaard (1933) determined the hydrodynamic pressure in the reservoir considering that the dam and the foundation are rigid, the dam is rectilinear and of infinite length, the upstream face of the dam is vertical, the excitation force is harmonic and develop horizontally in a direction normal to the crest length, the reservoir is of infinite length and the water in the reservoir is compressible. The analytical expression prescribed to determine hydrodynamic pressure at a depth $y$ from the bottom of the reservoir can be given as:

$$p=\frac{8\alpha_h \rho_f H_f}{\pi^2}\sum_{n=1,3,5..}^{\infty}\frac{1}{n^2 c_n}\sin\left(\frac{n\pi y}{2H_f}\right) \tag{2.5}$$

Where,

$$c_n=\sqrt{1-\frac{16\rho_f H_f^2}{n^2 gkT^2}} \tag{2.6}$$

In the above expressions, $\alpha_h$ is the ratio measuring the intensity of earthquake *i.e.*, the maximum horizontal component of acceleration of the dam-reservoir interface in the normal direction divided by gravitational acceleration $g$, $n$ is the wave number ($n = 2\pi/\lambda$) where $\lambda$ denotes the wavelength of the pressure oscillations, $k$ is the bulk modulus of water ($k = c^2/\rho_f$) and $T$ is the period of horizontal ground vibrations. The author proposed the added mass approach to determine the hydrodynamic pressure exerted on the vertical

upstream face of the rigid dam during earthquake. The dynamic action of the reservoir on the dam was visualized as an added mass, as if a certain body of water moved with the dam while the remainder of the reservoir remained inactive. The added mass effect was found to be neither too large nor negligible. The author suggested a series solution of the wave equation. Simple expressions were also suggested with relevant approximations for satisfactory performance of some practical problems. The distribution of hydrodynamic pressure along the reservoir depth may be either parabolic (Westergaard 1933) or elliptic (von Kármán, 1933 and Werner and Sundquist, 1949).

The modeling of interaction effects in the field of earthquake analysis of dams has a long tradition. The first to study these types of problem was Westergaard (1933). He considered the problem of fluid-structure interaction of a two-dimensional dam-reservoir system subjected to horizontal earthquake ground motion. The dam was assumed to be rigid and the reservoir was supposed to be semi-infinite and of constant depth. With analytical methods he derived the pressure distribution in the fluid at the dam-reservoir interface. His finding was that the interaction forces are proportional to the acceleration of the earthquake ground motion such that they may be approximated by a mass density distributed in a parabolic manner over the height of the dam. This technique is called added mass approach. A key argument used to motivate this solution was that the dominant energy content of the earthquake ground motion is related to the spectral components being significantly smaller than the first eigen frequency of the reservoir. Clearly, this argument can not be seriously advocated today: The spectra of registered earthquake ground motions records show significant amplitudes over a wide range of frequencies. But at that time very little was known about earthquake ground motion.

The added mass approach of Westergaard allows us to model an important effect of fluid-structure interaction which is in close agreement with more elaborated models. Because of the additional mass, the eigen frequencies of the coupled dam-reservoir system relevant for the earthquake response of the dam are significantly lower than those of the dam alone. However, the added mass approach doesn't consider any radiation damping so that energy dissipation is only due to the structural damping of the dam. Nevertheless, because of its simplicity, it has been one of the most frequently used models for the numerical analysis of dams in engineering practice.

In his first of a long series of publications devoted to interaction effects on dams, Chopra (1967) studied the effects of compressibility on the fluid-structure interaction forces. He found that significant errors may occur if the compressibility of the fluid is neglected. The assumed incompressibility of water was the subject of many studies because it greatly simplifies the modeling of fluid-structure interaction. In incompressible water, waves propagate with infinite speed such that the interaction forces are proportional to the accelerations imposed to the fluid. Therefore, no convolution integrals must be evaluated.

Bustamante and Flores (1966) proposed a simple computational method for estimating the transient hydrodynamic pressure to overcome the difficulties faced in computing using 1966 generation of computers. The validity of modal analysis to determine the hydrodynamic pressures caused by earthquakes was established.

In the references discussed so far the interaction forces during earthquake ground motion were applied as external forces to the dam. The response of the dam didn't contribute to the interaction forces because it was assumed to be rigid. Chopra (1968) studied the effects of a flexible dam on the interaction forces by modeling the dam as a mass-dashpot-spring system. The parameters of this system were defined by considering the first eigen mode of a triangular shaped dam. He showed that the natural frequencies of the coupled dam-reservoir system are different from those of the two uncoupled subsystems. He found that the compressibility of water can be neglected if the ratio of the first eigen frequency of the dam to the first eigen frequency of the reservoir is larger than two. In this dam-reservoir model was used to compute the response of the dam subjected to horizontal earthquake ground acceleration (Chopra, 1970). He found that the response of the dam significantly increases if the fluid-structure interaction is considered.

Since the classical work by Westergaard (1933), Bounaani et al. (2003) felt the need of a simplified expression for hydrodynamic pressure (much in the essence of the expression derived by Westergaard). However, these simplified formulas are generally based on many restricting assumptions, such as neglecting water compressibility and reservoir bottom absorption. Numerical studies carried out with models that account for these energy dissipating mechanisms in the reservoir, have shown that the changes to the hydrodynamic pressure can be considerably important, and moreover not always on the

conservative side (Chopra and Fenves, 1984). The authors derived an easy to use technique to get a reliable estimate of the earthquake-induced hydrodynamic pressures on gravity dams, by proposing closed-form formulas for the eigenvalues involved when solving the fluid–dam interaction problem.

## 2.4 CONCRETE DEGRADATION

Usually, concrete dams always remain in contact with water since they are built to retain the reservoir water. Concrete is a porous material and has a very large internal surface that strongly interacts with water (Gogoi, 2007; Steffens et al., 2003). Capillary surface tension, capillary forces develop in the concrete pores leading to interaction at the solid-fluid interfaces. These water induced stresses are related to the degree of saturation. As the saturation level of concrete pores increases, the material strength gradually reduces. At the macro-level, this effect is manifested in the form of decrease of the elastic stiffness. Also, structural deformations may occur due to inhomogeinities of the material and the non-uniform moisture. Deformations on the micro-level may lead to large stresses that induce micro-cracks. A state of damage may be induced already in the unloaded structure, which affects not only the apparent macroscopic material strength but also the permeability of the material. Hence, it is important to estimate material degradation with ageing. Moreover, during the entire lifetime, the dams may be subjected to harsh environmental conditions and various types of loading induced by earthquakes, impacts due to blasts, freezing and thawing that may affect material degradation. Since the scope of the present work is to predict the dynamic behavior of an ageing dam, a number of relevant literatures are reviewed and presented in brief.

The fifty years investigations on long-term properties of concrete have been initiated as far back as 1910 by Withey (1961) and successfully continued and expanded by Washa et al. (1989), they were not followed by more recent research. Generally, the old concrete is very rarely an object of contemporary direct investigations. It remains largely unstudied neither experimentally nor analytically. Recently, Levtchitch et al. (2004) carried out some studies on the static compressive and tensile strength, elastic modulus and deformation characteristics for concrete cubes taken from buildings which were about 25 years old. However, authentic description of the behavior of aged concrete

of different characteristic strength is not readily available. Such a study may be carried out which will provide more meaningful insight into the behavior of old concrete.

Hydration of cement is a highly exothermic chemical reaction. After pouring of the concrete during the construction of massive structures like concrete gravity dams the temperature may rise up to 50°-60°C. As the rate of hydration slows down, the temperature decreases resulting in thermal shrinkage that leads to thermal stresses. All the Portland cement concrete undergoes hydration and proper hydration is necessary for strength development. Byforse (1980) observed that the improper hydration of concrete may affect the long-term mechanical properties of concrete while investigating the properties of early age concrete.

Experimental evidence (Tu and Niu 1988) shows that during construction autogeneous strain stabilizes after 70 days (Fig. 2.2). If in a system, no moisture movement is allowed to or from the concrete mix with temperature remaining constant, the autogenous shrinkage is observed to take place. Shetty (1988) found that such deformations are important for mass concrete in the interior of a concrete dam.

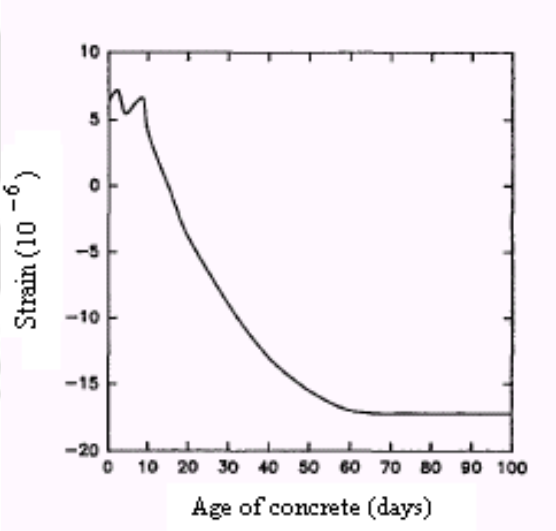


Fig. 2.2 Experimental data of autogenous deformation (Tu & Niu 1988)

Some non-ageing constituents like hardened cement gel constituting of tri and dicalcium silicate hydrates are primarily responsible for the hydration of concrete at the micro-level (Bazant, 1994). Ulm and Coussy (1995) explored the theory of reactive porous media for modelling of concrete at early ages. The thermodynamic imbalance

between the chemical constituents is referred to as the prime factor responsible for hydration of cement in their theory. The intrinsic relationship between heat generation, ageing and autogeneous shrinkage is also derived by the authors.

A new physical theory and constitutive model considering effects of long term ageing and drying on concrete creep which was an improvement over the solidification theory of ageing based on volume growth approach is proposed by Bazant et al. (1997). Bazant and Xiang (1997) proposed a solution procedure to predict the design lifetime of concrete considering crack growth and long time loading. The results obtained by measuring the time rate of crack mouth opening in notched concrete specimens subjected to constant load of almost one month are described by a previously proposed time-dependent generalization of the R-curve model. In the R-curve model the rate of crack growth is a function of the ratio of the stress intensity factor to the R-curve. The time curves of crack opening terminate with an infinite slope, indicating the lifetime.

Cervera et al. (1999, 2000a, b) proposed a thermo-chemical model to simulate the hydration and ageing process of concrete considering creep and damage in a roller compacted concrete dam. The evolution of temperature, elastic moduli, compressive and tensile stress distribution inside the dam can be predicted in terms of ageing degree at any time during the construction process and also during the first few years following the completion of the dam. This procedure can be applied to understand the effect of some major variables such as the placing temperature, the starting date and the placing speed on the construction process. In the long term, ageing of concrete is affected by the concentration of various constituents in the concrete mix, chemical reactions such as calcium leaching or alkali-silica reaction, moisture transport and loading due to submergence in water. According to Cervera et al. (2000b), the consideration of creep is significant if the stress analysis includes simulation of construction process. This is because rheological effects are most evident for early age concrete.

Lindvall (2001) determined the mathematical co-relationship of the service life of concrete structures which are dependent on material properties, construction process and the environmental effects. The deterioration of concrete strength is further accounted to the transport in porous materials. Various empirical relationships exist based on the performance of the concrete structures to account for the service life of the structure. The

performance based design methodologies and probabilistic methods have also been used to predict the service life of the concrete structures. Probabilistic methods require extensive statistical quantifications of the parameters in the mathematical models. Concrete compositions, environmental actions on the surface of the structure are some of the very important factors which govern the characteristics of these statistical parameters. Bangert et al. (2003) evaluated the long-term material degradation in concrete structures due to a chemically induced degradation processes and calcium leaching.

Alkali-Silica Reaction (ASR) approach to determine the degradation of the concrete structures was proposed by Steffens et al. (2003). A comprehensive mechanical model was proposed for the material swelling with a hydro-chemo-mechanical approach, to study structural effects of ASR. A two-stage mechanism to account for the swelling characteristics was introduced in the model namely i) the formation of an amorphous gel for with a characteristic time of reaction and (ii) the quantity of water interacting with the gel. The ageing effect on the material degradation and structural response is validated with experimental results.

Sain and Kishen (2003) proposed a fatigue crack propagation law for concrete based on the effect of overloads and loading frequencies. The crack propagation nature in a concrete member under constant load was characterized by employing static fracture theory. The effect of creep is to decrease the elastic modulus of the structure. The authors concluded that creep is pre-dominant in the initial stage of the structure but the actual failure occurs due the growth of the cracks which are time dependent.

Peyer, Royet and Boissier (2006) proposed three fold methods on concrete dam to support expert diagnosis and risk analysis namely (*i*) an ageing functional model based on the failure mode and effect analysis (FMEA) method using a causal graph representation of ageing scenarios leading to loss of functions; (*ii*) a qualitative method of describing dam ageing historical data and representing trends in performance loss; and (*iii*) qualitative methods to assess the risk of performance loss of dams and their components. The research produced a knowledge database on dam mechanisms. Also, an ageing historical database was compiled from dams that have experienced deterioration. Finally, computer aided methods to assist engineers in diagnosis and risk analysis tasks were also proposed.

The existing literatures confirm that the thermal stresses are very important to determine the behavior at an early stage of a massive concrete structure. In the long term, ageing of concrete is mainly affected by environmental conditions. Creep in concrete affects only initial stage of structural performance. In order to take into account of the various detrimental effects of concrete degradation due to hygro-chemo-mechanical causes in the long run, a proper methodology should be devised to suitably predict the dam-foundation interaction behaviors under strong earthquake loadings.

## 2.5 MODELING OF FOUNDATION

Any soil-structure interaction problem has to deal with the underneath foundation which is in all probability, made up of soil/rock. Modeling soil/rock behavior by finite element method is again a very challenging work. A lot of literatures could be found where the soil foundation has been treated as a linear, elastic material whose stress-strain properties strictly follow Hook's law. But, the stress-strain behavior is essentially nonlinear in nature. Therefore, it is of utmost importance that the nonlinear behavior of soil/rock foundation should be properly modeled by the use of a proper constitutive model in order to truly asses the behavior of structure during SSI analysis. In the present work, a nonlinear elastic-plastic model namely Hoek-Brown (1988) model has been found to be useful to simulate the nonlinear stress-strain characteristics of soil/rock. In the next section, a brief description of different nonlinear constitutive models generally used for the purpose of modeling soil/rock material has been presented. A detailed and chronological description of various plasticity models used for the purpose of simulating geomaterials have been eloquently discussed by Scott (1985) in his 49$^{th}$ Terzaghi lecture.

### 2.5.1 Material Nonlinearity

Because the present work consists of modeling the nonlinearity of soil and then coupling the nonlinear soil with the structural response, the following literature review is focused on both the nonlinear soil modeling considering proper constitutive matrix (mainly elastic-plastic modeling) and the soil-structure interaction itself. A brief review of the relevant literatures has been presented in a chronological order.

For numerical simulation of soil by finite element method it is necessary to consider a proper constitutive model. Because the behaviour of soil is nonlinear, a nonlinear isotropic constitutive model is no more applicable for use in finite element program. A lot of methods have already been adopted for modeling the behaviour of soil. The different models which have been used in modeling of geomaterials can be categorized into elastic, plastic, elastic-plastic, visco-elastic, visco-plastic and elastic-viscoplastic models etc.

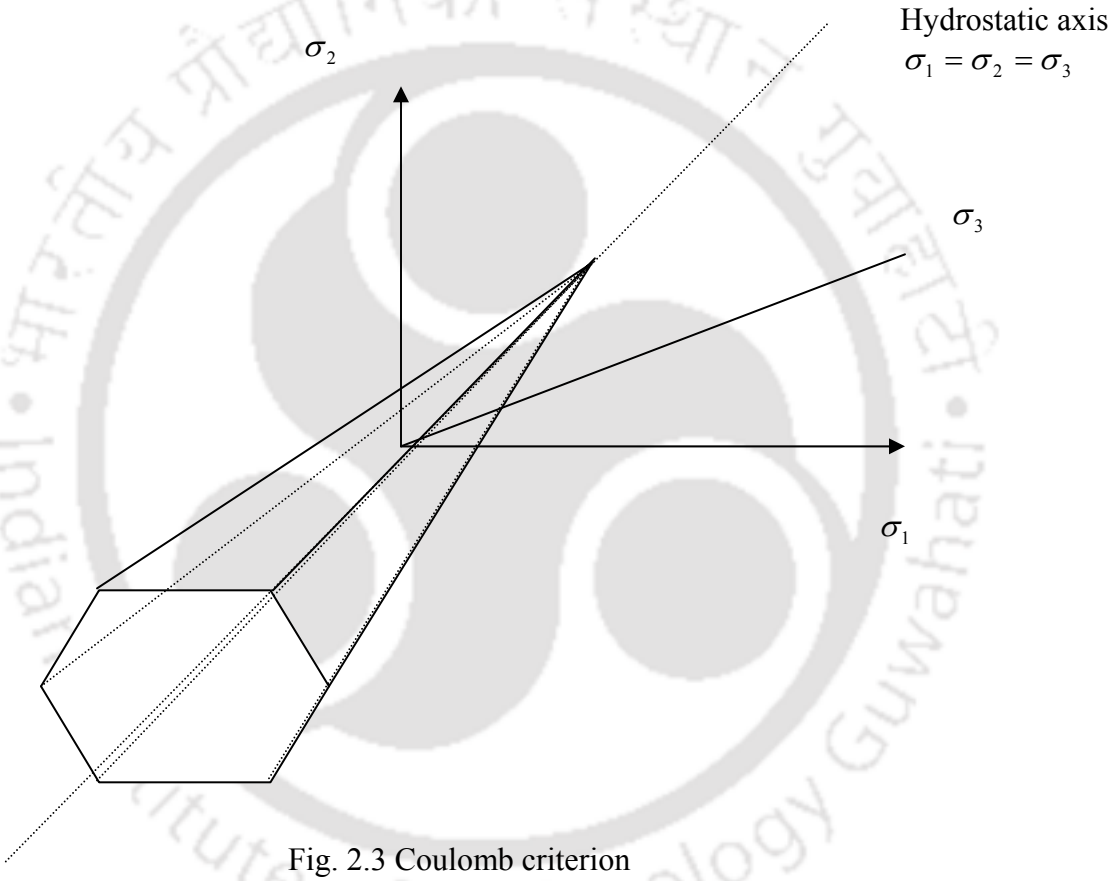


Fig. 2.3 Coulomb criterion

Amongst the elastic models, hyperelastic and hypoelastic models were the first developments in simulating the behaviour of the soil numerically. These nonlinear models were used to model the soil staying within the framework of elasticity. After that the plastic, elastic-plastic, viscoelastic, viscoplastic models came into the picture of numerical modeling of soil behaviors. A detailed description of all the different types of models which have been used in the numerical simulation of the behavior of soil is

beyond the scope of this text. Some very popular models which have been used extensively in the history of soil mechanics (such as Coulomb model, Fig. 2.3) and other elastic-plastic models have been briefly described here. However, some relevant historical developments in modeling of geomaterials have been presented below.

The most widely used yield criterion in soil mechanics for geomaterials dates back to1773 and is credited to Coulomb. This criterion is known as Coulomb's yield criterion (1773) which depends on various parameters such as stresses, strains and history of loading. The general form of yield surface ***f*** for isotropic materials can be expressed as

$$\textbf{\textit{f(invariants of }}\sigma_{ij}\textbf{\textit{)}} = f_c \tag{2.5}$$

The Coulomb criterion states that the failure occurs when the shear stress $\tau$ and the normal stress $\sigma$ acting on any element in the material satisfy the linear equation:

$$|\tau| + \sigma \tan\phi - c = 0 \tag{2.6}$$

where,

c = Cohesion of the soil particles

$\phi$ = Angle of internal friction

The origin of metal plasticity dates back to a series pf papers by Tresca beginning in 1864. The first proposed yield surface (or the maximum shear stress criterion) is now known as the Tresca criterion. Tresca (1864) proposed a yield criterion of the form

$$f \text{ (invariants of } s_{ij}) = f_c \tag{2.7}$$

where,

$s_{ij}$ = Deviatoric stress tensor

For the special case of $\sigma_1 \geq \sigma_2 \geq \sigma_3$, the Tresca yield criterion can be written as:

$$\frac{1}{2}(\sigma_1 - \sigma_3) = k \tag{2.8}$$

where $\sigma_1$ and $\sigma_3$ are the maximum and minimum principal stresses.

k = Yield stress of the material determined from pure shear test.

More generally equation (2.8) can be written in the form:

$$\left[(\sigma_1 - \sigma_2)^2 - 4k^2\right]\left[(\sigma_2 - \sigma_3)^2 - 4k^2\right]\left[(\sigma_3 - \sigma_1)^2 - 4k^2\right] = 0 \tag{2.9}$$

Saint Venant (1870) used the Tresca criterion to determine the state of stress in a physically deforming cylinder subjected to two dimensional states of stress. In this process, he developed a constitutive relation for a rigid, perfectly plastic material. Later, Levy extended Saint Venant's equation to the 3-dimensional case. Prandtl (1924) considered elastic components of strain-rates when formulating the constitutive equation.

Von Mises (1913) introduced a new yield criterion for metals which proved to be more convenient for numerical solutions than the Tresca criterion. This yield condition is known as Von Mises criterion (or the octahedral shear or distortion energy criterion). Von Mises yield criterion (or the maximum shear energy criterion) implies that the plastic behaviour begins when the distortional energy reaches a critical value. The distortional energy per unit volume of the material, $W_d$, due to elastic shear deformation prior to yielding can be represented by,

$$W_d = \frac{1+\mu}{E} J_2 \tag{2.10}$$

Where,

$\mu$ = Poisson's ratio

E = Modulus of elasticity

Since $W_d$ is a function of second stress invariant of the deviatoric stress tensor, $J_2$, the Von Mises criterion is also called the $J_2$ theory or the octahedral shear stress criterion. It has the simple form:

$$J_2 - k^2 = 0 \tag{2.11}$$

Von Mises (1928) used this criterion and developed a constitutive relation based on the normality concept that relates the plastic strain rates to the yield surface.

The first major advance in the extension of metal plasticity to soil plasticity was made in a paper "Soil Mechanics and Plastic Analysis or Limit Design" by Drucker and Prager (1952). In this paper, the authors extended the Coulomb criterion to 3-dimensional problem. Drucker and Prager (1952) proposed a perfectly plastic model (shown in Fig. 2.4) which neglects the influence of $J_3$ on the cross sectional shape of the failure surface, can be considered as the first attempt to approximate the well known Coulomb criterion by a simple smooth function. This criterion is expressed as the function of the first

invariant of the stress tensor $I_1$ , and the second invariant of deviatoric stress tensor, $J_2$, together with two material constants $\alpha$ and $k$. It has the simple form:

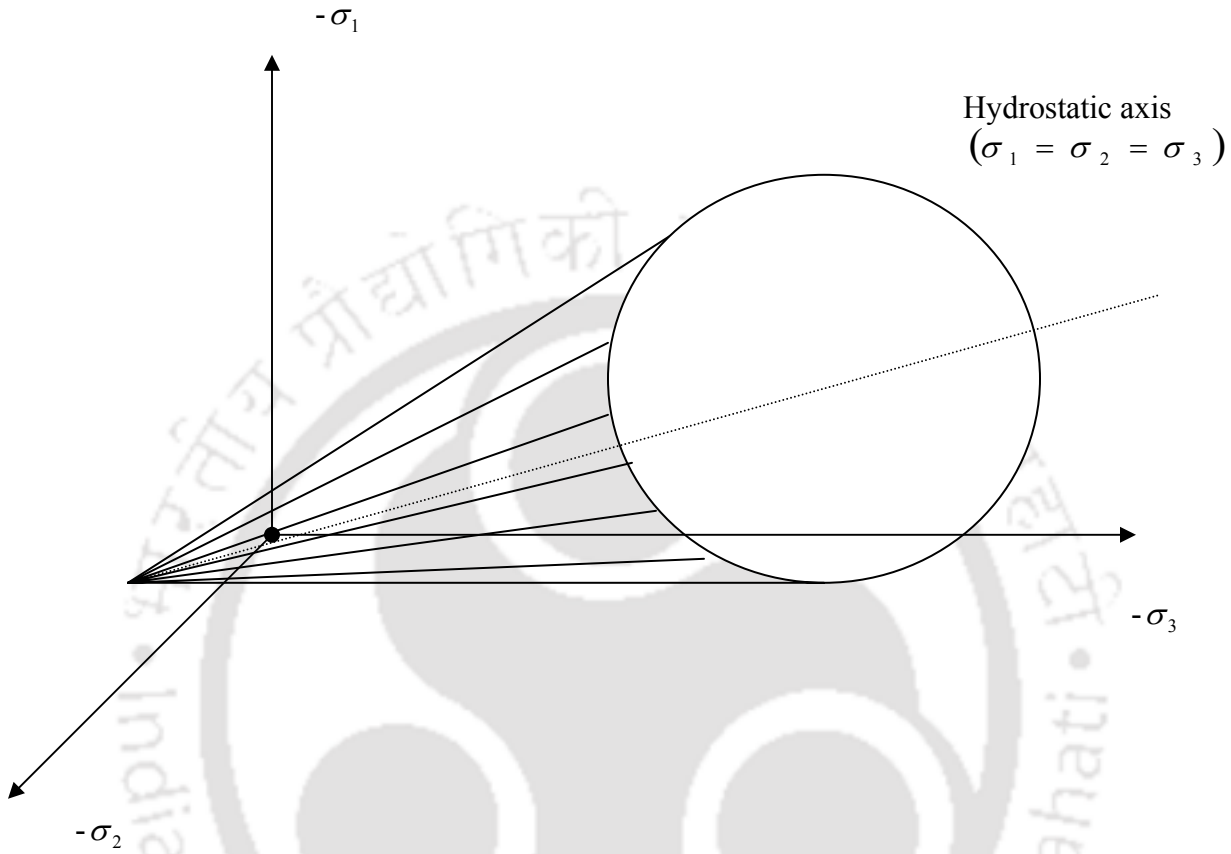


Fig. 2.4 Drucker-Prager criterion

$$f = \alpha I_1 + \sqrt{J_2} - k = 0 \tag{2.12}$$

Where $\alpha$ and $k$ can be related to the Coulomb material constants $c$ and $\phi$ in the following way:

$$\alpha = \frac{2Sin\phi}{\sqrt{3}(3 - Sin\phi)} \tag{2.13}$$

$$k = \frac{6cCos\phi}{\sqrt{3}(3 - Sin\phi)} \tag{2.14}$$

Drucker et al. (1957) proposed an extended Von Mises model with a convex end cap because Drucker-Prager model cannot predict plastic volumetric strain or compaction of soil materials during hydrostatic loading.

Duncan and Chang (1970) proposed the hyperbolic model for describing the nonlinear stress-strain behavior of soils. This model is still very much popular because of its computational simplicity. However, this model suffers from the fact that it overestimates the dilatancy property of soil. DiMaggio and Sandler (1971) proposed a modified failure surface, which is asymptotically parallel to the $I_1$ axis for higher values of $I_1$. This failure surface was proposed to improve the difficulty arising from much higher prediction of dilatancy than that observed in experiments by the extended Von Mises model.

Frantziskonis et al. (1986) provided a simplified approach for the non-associative behavior of granular (geologic) materials. The basic concept is that the plastic potential can be obtained by controlling or correcting the yield function used for associative plasticity. This is achieved by correcting the hardening, evolution or growth function, which involves only one additional parameter above those for the associative model. Determination of constants and verification with respect to two granular soils tested under a variety of multiaxial stress paths are presented. It is shown that incorporation of the non-associative behavior through the correction of the growth function yields remarkably satisfactory predictions for volumetric and stress-strain responses of the material.

Desai and Galagoda (1989) developed a plasticity based constitutive model for anisotropic behavior of soils and implemented in a finite element program. The model was based on the generalized Biot's theory and used for dynamic non-linear response analysis of porous materials. The model allows for an inelastic response during loading, unloading and reloading. The procedure was verified with respect to closed form solutions for wave propagation in porous media. The model was used to predict the behavior of a realistic structure-saturated porous soil system subjected earthquake loading and performed both linear and non-linear analyses. They found that, in comparison with linear analysis the non-linear response showed increased magnitudes and zones of

concentration of pore water pressures, horizontal displacements and shear stresses and decreased magnitude of vertical displacements.

Torkamani and Alsanusi (1989) discussed the mathematical formulations in the incremental theory of plasticity, which is based on the mixed hardening rule and linear yield surface. A three parameter, uniaxial symmetric, linear yield surface suitable for tension and compression yield stress material is presented. This yield condition, along with the mixed hardening and the associated flow rules is used to formulate the constitutive laws for sides and corners of the yield surface. The formulation is based on incremental plasticity with the assumption of small displacements and is suitable for plane stress problems under monotonic cyclic loading. The mixed hardening rule, which is mathematically modeled, could be changed to either kinematic or isotropic hardening by a simple change in the model. This hardening rule could handle different degrees of Bauschinger effect, as opposed to kinematic hardening, which assumes only an ideal Bauschinger effect, or isotropic hardening, which does not account for the effect at all. The theory is applied to a ductile material using the finite element method and cyclic loading.

Griffiths (1990) claimed that the use of numerical methods such as finite elements to make accurate predictions of failure or collapse of geomaterials must utilize a suitable failure criterion that is able to represent the shear strength for all stress paths likely to be encountered. The best-known failure criterion is that of Mohr-Coulomb, but several others have been proposed. Using a dimensionless form of principal stress space, the author reviewed some of these other criteria in a unified way by presenting them in terms of equivalent Mohr-coulomb friction angle implied at various locations on their periphery.

The Hoek-Brown criterion was first introduced in early eighties. Hoek-Brown (1980) found that the peak triaxial compressive strength of isotropic rock is related to confining stress based on various rock types. The strengths and limitations of this criterion were again proposed in an update in 1988 (Hoek-Brown, 1988). It was then proposed that the correct use of this criterion should be decided on the nature of rock mass, which does not contain any discontinuities, and the volume of rock under consideration might contain four or more closely spaced and almost uniform

discontinuity sets. In 1997, a generalized Hoek-Brown failure criterion was published for accommodating hard and soft rock masses (Hoek and Brown, 1997). Since then this criterion has been widely used in geotechnical and rock engineering problems.

Barros, Marques and Martins (1991) presented an elastoplastic model with a non-associated law to be used in structural problems. In non-associated plasticity the system of equations of the tangential stiffness method is non-symmetric. This inconvenience can be overcome by defining a new material, with associated law, equivalent to the initial one. In this case the system of equations becomes symmetric. In the method presented by the author, this symmetric system is modified, with nonlinear part of the stiffness matrix being transferred to the load vector, and the resulting system being solved by an iterative process.

Sitharam, Majhi and Verma (2005) showed the usefulness and efficiency of the Practical Equivalent Continuum model proposed by Sitharam et al. (2001) and Sitharam and Madhavi Latha (2002), in simulating jointed rock mass. This model estimates the properties of jointed rock mass from the properties of intact rock and a joint factor ($J_f$), which is the integration of the properties of joints to take care of the effects of frequency, orientation and strength of joint. The authors built a FLAC-3D program called FISH for modeling jointed rocks using Duncan and Chang hyperbolic model (1970). The model has been validated first with simple elemental tests for different rocks with different joint configurations at different confining pressures. Further, this has been applied for a case study of a large underground power house cavern in Himalayas. The analysis has been done under various stages of excavation, assigning null model available in FLAC-3D for simulating the excavation. The settlement observations reported from the field studies carried out in the Nathpa Jhakri power house cavern in India were compared with the predicted observations from the 3-D numerical analysis using this model.

### 2.5.2 Integration of Nonlinear Constitutive Equations

Apart from the development of the constitutive models for describing the nonlinear stress-strain behavior under various types of loading conditions, researchers have also devoted a lot of effort on finding out the ways to incorporate these nonlinear constitutive models in the integration procedure. Depending upon the types of loading (i.e. static or

dynamic), various algorithms were developed which could be used in a general purpose finite element program. Unlike the implementation of linear, elastic material properties which obeys Hook's law, the nonlinear algorithms work in a more complicated way. Most of the nonlinear algorithms are of incremental, iterative types where loads are applied in increments and iterations are carried out within each load increment to achieve the equilibrium between the applied forces and the resistive forces. This process is known as Newton-Raphson method. The get the displacements, strains and stresses at a particular load step; the quantities are added to those values of the previous load step. This way, the nonlinear behavior of the material is simulated through a piecewise linear process. For dynamic problems, several numerical techniques were developed to integrate the dynamic equilibrium equation of the structural systems in time domain. Besides the very popular implicit Newmark (1959) algorithm there exists another class of method called implicit-explicit methods. Implicit-explicit schemes were first introduced by Belytschko and Mullen (1977) and were given an alternative form by Hughes and Liu (1978) and Park et al (1977).

Bathe et al. (1980) formulated some finite element procedures for the analysis of elastic-plastic response. A consistent large displacement and large strain formulation is summarized, a versatile elastic-plastic model applicable to the analysis of metals and geologic materials are presented, the choice of an appropriate finite element discretization is discussed, and some effective methods for the solution of the nonlinear finite element equations are briefly summarized. Finally, to illustrate the strength and shortcomings of the procedure used the result of some sample analyses are presented and evaluated.

Clarke and Hancock (1990) described the incremental-iterative solution techniques for geometrically non-linear analyses. The solution method described are based on a modified Newton-Raphson approach, meaning that the tangent stiffness matrix is computed at the commencement of each load step but is then held constant throughout the equilibrium iterations. A consistent mathematical notation is employed in the description of the iterative and load increment strategies, enabling the simple inclusion of several solution options in a computer program. The iterative strategies investigated are iteration at constant load, iteration at constant displacement, iteration at constant 'arc-length', iteration at constant external work, iteration at minimum

unbalanced displacement norm and iteration at constant 'weighted response'. The load increment schemes include strategies based on number of iterations required to achieve convergence in the previous load step, strategies based on the current "stiffness parameters" and a strategy based on a parabolic approximation to the load-deflection response. Criteria for detecting when the applied external load increment should reverse are also described. A challenging example of a circular arch exhibiting snap-through (load-limit point) behavior and snap back (displacement limit point) is solved using several different iterative and load increment strategies. The performance of the solution schemes is evaluated and conclusions are drawn.

Sloan and Booker (1992) discussed the problems associated with the integration of constitutive relationships for Tresca and Mohr-Coulomb materials under conditions of plane strain. Wei, Peric and Owen (1996) presented a consisted algorithm, which combines the advantages of the exact time integration of the Prandtl-Reuss elastoplastic models and the quadratic asymptotic convergence of Newton-Raphson iteration strategies. The consistent modulus is evaluated by a full linearization of the exact stress update procedure. Numerical tests for a thin wall tube subjected to combined loads of tension and torsion are performed. For comparison purpose, the results of radial return methods are also given.

Apart from these, a huge amount of literatures exist on the different methods developed till date for nonlinear integration of the static and dynamic equilibrium equation. A comprehensive review on this subject can be found in the paper authored by Clarke and Hancock (1990).

## 2.6 INTERACTION AND RADIATION CONDITION

Most civil engineering structures are elements of much larger systems, called here the overall system, containing several other system components. When subjected to transient loads, these structures interact with the other components of the overall system such that a continuous transfer of energy is established between them. The effects of interaction on the dynamic behavior of these structures are determined by the mechanical properties of all the components of the overall system, the interaction mechanism and the type of dynamic loading. Dams belong exactly to this category of structures, they interact with

the foundation rock and with the reservoir. The kind and intensity of the interaction depends on the physical processes that occur at the interfaces of the dam with the foundation rock and the reservoir. As an example, the effects of the interaction on the dam will be different if a dam is allowed to slip on the foundation or not.

A class of interaction problems requiring special methods for its analysis is that involving overall systems which are much larger in size than the structure itself. Typical examples are foundations resting on rock or soil or dams interacting with the reservoir and the foundation rock. The size of the overall system is so large that its direct modeling, e.g. with finite elements, is virtually impossible because of the tremendous effort needed to compute a solution. In addition, usually engineers are mainly interested on the response of the structure and its close neighborhood so that an accurate modeling is only needed for a small subdomain of the overall system. Therefore, the overall system is subdivided by a suitable imposed boundary, the so-called artificial boundary $\Gamma_B$, in two sub-systems (Figure 2.5). One subsystem, the inner domain or near field $\Omega_N$, contains the structure and its close neighborhood. This near field may behave nonlinearly. It is usually modeled in detail by finite elements or similar numerical methods.

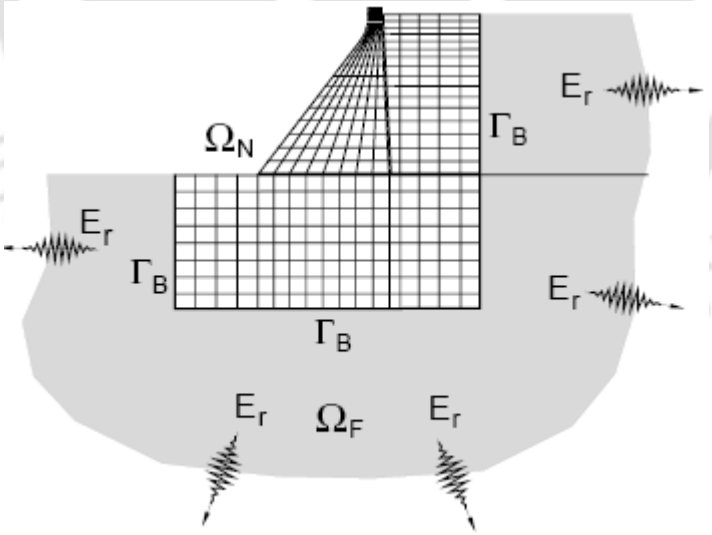


Fig. 2.5 Near field $\Omega_N$, far field $\Omega_F$, artificial boundary $\Gamma_B$ and energy $E_\Gamma$ radiated to infinity because of radiation damping

The second sub-system, the outer domain or far field $\Omega_F$, is modeled by methods that are usually quite different from the finite element method. Usually, the far field is simplified in the sense that it is assumed to be infinite in at least one of its dimensions. This model assumption is certainly justified if the distant parts of the physical boundaries have little or no appreciable effect on the response of the structure and its close neighborhood. Moreover, it is usually assumed that the far field has regular properties (e.g. isotropy, homogeneity etc.) and that it behaves linearly. These premises are introduced to provide a reasonably simple solution of the far field. However, they are even reasonable from a physical point of view. In fact, we may expect that isolated confined inhomogeneities situated far away from the structure have small effects on its response.

The unboundedness of the far field has an important consequence in wave dynamics: waves travelling in the unbounded direction are not reflected back to the near field. Because waves transport energy, we obtain a mechanism which irreversibly transfers energy from the near field to the far field. This mechanism is called radiation damping and extracts energy from the near field. Its effect on the response of structures is similar to that of viscous damping where a part of the mechanical energy of a structure is irreversibly transformed into heat. In both cases, the response of the structure is appreciably reduced. For this kind of problem, the accurate modeling of radiation damping becomes a central issue. This is exactly the case for dams interacting with the adjacent reservoir and foundation rock.

There exist a number of numerical methods to deal with modeling of unbounded domain. One of them is to specify a particular boundary condition, other than the normally used fixed or roller type of boundary condition, which will allow the impinged waves to pass without being reflected back into the computational domain. These boundary conditions are known as radiating or transmitting or non-reflecting boundary conditions (NRBC's). These NRBC's are nonlocal in nature. Another type of boundary condition uses some absorbing devices (such as viscous dashpots) placed at the sides of the boundaries which absorb the energy of the traveling waves so that they are not reflected back into the computational domain. They are called viscous or absorbing boundaries and they local in space. The use of such boundaries enables the analyst to use

only finite element method in which these boundary conditions are implemented. Other than such local or nonlocal boundaries, one may use coupled finite element and infinite element to model the infinite foundation domain. The infinite elements are very popular for solving problems associated with infinite or semi-infinite domains. Another method which uses coupled finite element and boundary element is also very popular for solving interaction problem related to unbounded domains. The structure is modeled by the FEM and BEM is used to model the unbounded foundation domain. The fundamental solution used in BEM satisfies the radiation condition exactly. Scaled boundary element method or consistent infinite finite element cell technique is another method developed by Wolf (1986) for tackling the radiation condition associated with unbounded domains. A brief review of the various methods used in solving problems related to unbounded domains has been presented in the next section.

## 2.6.1 Numerical Methods to Tackle Radiation Condition

### *2.6.1.1 Finite Element Method*

Finite Element Method is a numerical analysis theory that is widely used for various situations in engineering say, non-homogeneous material conditions, complex geometry and nonlinear stress-strain behavior. Analyses on dynamic soil-structure interaction (SSI) problem with the FEM can be dated from 1960s. Most of the cases, such a problems were performed by 2-dimentional models with plain strain elements. One of the major issues for such analyses is how to treat the infinity of ground stiffness by the finite model. The boundary should be set sufficiently far from the site in general, so as to attenuate the energy of outwardly propagating wave; it will be quite wasteful of time. In the appropriate size of model, reflections of propagating waves on artificial boundary must be avoided, consequently. For this purpose Lysmer and Kuhlemyer (1969) had proposed the transmitting boundary with frequency independent viscous dashpot. The FEM technique was employed by Edwards (1969) in the anchored soil-liquid-tank interaction analysis. Wolf (1985) and Luco and Mita (1987) presented their direct method of soil-structure interaction analysis where the idealized soil-structure system was analyzed in single step. Werkle (1986) studied the dynamic finite analysis of three-dimensional models with a transmitting element.

Modeling the semi-infinite foundation domain by exclusively finite element method necessitates the application of proper boundary conditions so that the traveling waves are not reflected back to the domain of computation leading to the generation of spurious reflections. In the frequency domain, it is well known that an exact NRBC applied to a separable truncation boundary is available through the Dirichlet-to-Neumann (DtN) map (Keller and Givoli, 1989). The DtN map is a nonlocal (integral) operator composed of a series of wave harmonics relating DtN data on the truncation boundary. The DtN map is easily implemented in the finite element method as a 'natural' boundary condition using standard C0 continuous interpolation functions in the frequency domain. There are two main types of NRBCs: *approximate local* NRBCs and *exact nonlocal* NRBCs. Most of the NRBCs belong to the former category. The first local boundary-indeed the first transmitting boundary was proposed by Lysmer and Kuhlemeyer (1969). It is also known as viscous or absorbing boundary since it places viscous dashpots at the boundary to absorb the energy of the traveling waves.

The boundary of Ang and Newmark (1972) evolved based on the idea of "transfer of D' Alembert force", which essentially entails replacing the inertia forces in the wave equation by certain rates of change of stresses. Closely related to Lindman's boundary (1973, 1975) is the family of boundary conditions proposed a few years later by Engquist and Majda (1977) for the scalar wave equation and by Clayton and Engquist (1977) for the elastic wave equation. The boundary conditions proposed by Engquist and Majda (1977) were complicated as they were derived for acoustic and elastic waves described with respect to rectangular as well as cylindrical coordinates. Although, this technique was based on the rational approximation of pseudo-differential operators and was considerably different from Lysmer and Kuhlemeyer (1969) boundary condition, the simplest boundary condition for acoustic waves is equivalent to the viscous boundary condition of Lysmer & Kuhlemeyer. The general form of (Engquist & Majda 1977) $N^{th}$ order boundary condition can be expressed as:

$$\left(\frac{\partial}{\partial x}+\frac{1}{c}\frac{\partial}{\partial t}\right)^{N} u = 0 \qquad (2.11)$$

where the terms within the bracket is the differential operator that is multiplied $N$ times. These local, non-consistent boundaries though accurate are not suitable for dam-reservoir problem as a large near field is required that will result in large computational effort.

Saini et al. (1978) applied the finite element method for simulating the hydrodynamic effects in a dam-reservoir system. Two different approaches were considered to account for the large extent of the reservoir. In the first approach, a non-reflective radiation boundary condition was applied at the far-field boundary of the reservoir. The non-reflective radiation boundary condition was derived from the wave equation (Zienkiewicz and Newton, 1969)

$$p = F_1(n - ct) + F_2(n + ct) \tag{2.12}$$

which represents the wave propagation in a direction $n$ perpendicular to the boundary. In the above equation $F_1$ stands for a wave advancing with a velocity $c$ towards the boundary and $F_2$ for returning wave.

All these local absorbing boundary conditions have found much interest in the context of finite difference methods. Many papers deal with their implementation, accuracy and stability. A detailed overview with supplementary references may be found in the works of Givoli (1992). But these absorbing boundary conditions had much less impact in the context of the finite element method. The first of the few finite element implementations was attempted by Cohen and Jennings (1983) for elastic wave dynamics problems. Using an asymptotic approximation technique they derived boundary conditions which they called paraxial boundary conditions. In the two-dimensional case, the paraxial boundary conditions are equivalent to those of Engquist and Majda (1977). The finite element implementation was very involved because they employed special upwind elements to avoid spurious oscillations originated by non-symmetric terms. The numerical tests showed that the paraxial boundary conditions were not significantly better than the much simpler viscous boundary conditions of Lysmer and Kuhlemeyer (1969).

Liao and Wong (1984) suggested a transmitting boundary which is based on determining the motion at the boundary by extrapolating the motion at the points in the vicinity of the boundary at the earlier times. This concept was very much similar to that of Lindman-Engquist-Majda family of boundary conditions. Also, local NRBCs proposed by Bayliss and Turkel (1980), and Feng (1983) are of worth mentioning. These and other

approximate local NRBCs differ in the way they have been designed and consequently in their performance in various configurations. Refer to the works by Givoli (1991) for an excellent review on the subject. A smaller number of exact nonlocal NRBCs have been devised for various problems in infinite domains (Givoli and Cohen, 1995; Grote and Keller, 1996).

Kausel (1988) examined the most common and well known transmitting boundaries such as Lysmer-Kuhlemeyer, Engquist-Majda, Ang-Newmark, Smith-Kundall and Liao-Wong etc. The author showed that these boundaries are mathematically equivalent and therefore, they should have comparable wave absorbing properties. The author showed that Smith-Kundall boundaries had limited absorbing capacities. Hence, these various transmitting boundaries were essentially alternative realizations of one and the same boundary conditions.

The boundary condition to be applied on the truncated boundary is referred to as the artificial boundary condition or the artificial boundary for short. These boundaries are nonlocal in nature. The boundary conditions proposed by Grote and Keller (1996) were further modified by Thompson and Huan (2000) to improve the scaling of the related first order equations. Using the hierarchy of the local boundary operators proposed by Bayliss and Turkel (1980), Huan and Thompson (2000) as well as Thopmson et al. (2001) re-derived the same form of exact non-reflecting artificial boundary conditions for the two-dimensional and three-dimensional wave equations on the surfaces of a circle and a sphere respectively.

Kellezi (2000) developed alternative FEM based local absorbing boundaries which rendered the computational domain finite. These boundaries were local in both time and space and were completely defined by a pair of symmetric stiffness and damping matrices. As the effort for implementing them was the same as for the impedance boundary condition (BC) considering the angle of incidence, standard assembly procedure could be used. Due to the local nature they also preserved the overall structure of the global equations of motion. Even though the focus was in the time domain the same equations of motions could be used to determine the solution under time-harmonic excitation directly in the frequency domain. Explicit formulae for the element matrices were included in the paper and numerical examples for transient

radiation model problems to illustrate the validity and accuracy of the new procedures were presented. Zhao and Liu (2003) used operator splitting method to derive an exact non reflecting boundary condition on the truncated boundary of the computational domain in time domain. Compared with the derivation of the non- reflecting artificial boundary condition using the previous methods, the present derivation of the non-reflecting artificial boundary condition in this study is simple and straightforward. A very good comparison between local and non local boundaries has been provided by Givoli and Patlashenko (1998) in a tabular form.

#### *2.6.1.2 Coupled Infinite Element and Finite Element Approach*

Ever since Bettes (1977) introduced infinite elements, which may be considered to be a natural extension of finite elements to treat infinite domains, have gained popularity among the researchers throughout the world. Since then, many researchers including Medina and Penzien (1982), Valiappan and Zhao (1992), Khalili et al. (1997) have successfully used infinite elements to model wave propagation problems in infinite domains. This approach requires modeling the near field by FEM and the far field by infinite elements. The shape functions for the infinite elements are obtained from the special form of fundamental solution. But, this form of fundamental solutions might be difficult to be obtained for all kind of problems. The uses of infinite elements have mostly been limited in the frequency domain in spite of their increasing popularity for problems involving infinite domains.

Bettess (1980) reviewed briefly the method of infinite elements. Some new logical and general formulations for infinite elements are presented. The programming techniques to be adopted are also discussed with results for elasticity and potential problems. Beer and Meek (1981) carried out a parametric study which enables the economic modeling of 'infinite domain' type problems. A typical problem is an opening in a stress field in an infinite medium, either two or three dimensions. The strategy is to model around the opening with two or three layers of conventional isoparametric finite elements and surround these with a single layer of 'infinite domain' elements. Several sample problems have been analyzed for circular, square and spherical openings in infinite media, and the results compared with either theoretical or boundary solutions

which include the 'infinite' boundary in their solution technique. Olson and Bathe (1985) also apply an infinite element to transient fluid-structure interaction problems. However, they do not claim that the element will deal with any transient exterior wave problem. They adopt the *Doubly Asymptotic Approximation*, which is widely adopted in coupled exterior fluid-structure analyses. The infinite element methodology supplies the "added mass", low frequency effects, and the high frequency effects are dealt with using a plane damper. The approach is exact in the low frequency and high frequency limits. Good results were obtained by Olson and Bathe for a number of problems. Haggblad and Nordgren (1987) applied infinite elements to transient problems of non-linear soil interaction. Their infinite element was modelled on the mapped infinite elements and also included a damping component, based on the Lysmer and Kuhlemeyer absorbing boundary (1969). They carried out a number of tests of the element and reported that "the implemented infinite elements capture both the transient and static responses reasonably well". They tested the infinite elements both with and without a stiffness component.

Also Von Estorff and Antes (1991) presented a coupling procedure for fluid-structure interaction analysis. While applying these methods to dam related interaction problems, the formulations were carried out in frequency domain in almost all the cases. Viladkar, Godbole and Noorzaei (1990) developed some new mapped three dimensional infinite elements with $1/r$ and $1/\sqrt{r}$ decay type. Detailed mathematical formulation and computer implementation of these elements were presented and numerical results were investigated in conjunction with few soil-structure interaction problems. Viladkar et al. (1991, 1994a) used coupled finite and infinite elements to solve problems related to plane-combined footing soil systems. Again, Viladkar, Godbole and Noorzaei (1994b) studied the behavior of infinite elements in elasto-plastic domain in conjunction with soil-structure interaction analyses.

Yun et al. (2000) developed analytical frequency dependent dynamic infinite elements to model the far field of a two-dimensional layered half-space soil medium for soil-structure interaction analysis. Using the proposed infinite elements, the element mass and stiffness matrices could be obtained in analytical forms of frequency and constant matrices representing the wave propagation characteristics in the far field soil medium. The compliances of rigid strip foundations on a homogenous half-space, on a layered

half-space, and on a layered strip with rigid bed rock were calculated using the proposed formulation, and the results were compared with those by other approaches. The comparison indicated that the proposed infinite elements gave good accurate solutions. The equation of motion including the present frequency-dependent dynamic stiffness matrix for the far field region could be transformed into a time domain equation, and the soil-structure interaction analysis may be carried out in time domain.

#### *2.6.1.3 Coupled Boundary Element and Finite Element Approach*

This numerical technique had been applied to the field of soil-structure interaction by many authors, both in the frequency domain and in the time domain (Antes and Von Estorff (1989). Boundary Integral Equation Method (BIEM) or Boundary Element Method (BEM) had been used by Touhei and Ohmachi (1993) for isotropic and homogeneous materials for both bounded and unbounded domains. No domain discretization was required which was an advantage for practical applications. This approach allows a reduction in spatial dimensionality, and satisfies the Sommerfield radiation conditions at infinity. Hence, the far field of infinite domain need not be modelled. The first limitation of this technique is that the system matrix is non-symmetric, non-positive definite. Secondly, this method is not suitable for anisotropic domains, material and geometrical non-linearities and complex geometry. Cruse (1968) and Cruse and Rizzo (1968) used a direct formulation of the boundary integral method for elastodynamics problems. Manolis and Beskos (1981) applied the Laplace transform to the governing equations of motion. Cole et al. (1978), Antes (1985) and Israil and Banerjee (1990) used BEM in time domain transient analysis. BEM is in general less costly form a computational point of view, compared to the other numerical techniques, since discretization of only the surface of the domain is required.

Boundary element method has also been widely used to tackle soil-structure interaction problems. It is a powerful method for modeling the semi-infinite soil medium since only the boundaries of the unbounded medium are discretized so that the spatial dimension is reduced by one and the radiation condition is satisfied automatically as a part of the fundamental solution. Based on the substructure method, Zienkiewicz et al. (1977) suggested many hybrid methods (coupling methods) where the structure and the

adjacent finite region of soil are discretized by the standard finite element method while the unbounded soil is modeled by the boundary element method. The coupled boundary and finite element methods (BEM-FEM) in time domain have been employed for modeling infinite foundation domain by Spyrakos and Beskos (1986) and Karabalis and Beskos (1984) to investigate two and three dimensional flexible foundations. Touhei and Ohmachi (1993) developed a numerical method by coupling FEM & BEM for dynamic response analyses of dam-foundation-reservoir systems in time domain. During formulation, the weighted residual procedure was applied to the coupling of several equations of motion for solid and fluid in the FE-BE region, and an algorithm similar to the Newmark beta procedure was finally obtained. The algorithm was advantageous in the sense that it took into account all the effects of dam-foundation and reservoir-foundation interactions, as well as of the absorption of both elastodynamic and hydrodynamic waves at the boundaries of the foundation and the reservoir.

Estorff and Kausel (1989) presented results obtained from a finite element-boundary element coupling procedure and discussed their applicability to some representative soil-structure interaction problems. The structures considered were elastic systems, such as foundations, tunnels and filled trenches (modeled by finite element method), which were coupled with homogenous elastic half spaces (modeled by boundary elements). The coupling procedure was formulated entirely in the time domain. Coupled time domain techniques had been used by Karabalis and Beskos (1985), Spyrakos and Beskos (1986), von Estorff and Prabucki (1990) and von Estorff and Antes (1991). Chuhan et al. (1999) accounted for the radiation effects of the infinite layered soil by FE-IE coupling. An equivalent linear approach was employed for approximation of non-linearity of the near-field soil. Effect of relative modulus ratio $E_r/E_s$ of rock and soil on the response of the structure and soil were examined.

Wolf and Song (1996) developed the scaled boundary element method (also known as consistent infinitesimal finite element cell method) by combining the advantages of the boundary element method and the finite element method. This method is exact in radial direction and converges to the exact solution in the finite element sense in the circumferential direction, and is rigorous in space and time. Also boundary integral equation methods (BIEMS) have recently emerged to be very effective for studying wave

propagation problems in unbounded domains in the field of geotechnical engineering. These methods (Dravinski, 1982; Reinoso et al, 1996; Wong, 1982) require only discretization of the boundary and are able to model the radiation conditions at the infinity in exact way. But these methods suffer from the disadvantage of the evaluation of Green's functions which are very demanding from computational point of view. Also the methods are limited to problems involving linear materials only (Kobayashi, 1983). The finite element methods and finite difference methods are useful for problems with complex geometries, but they require the discretization of the entire domain of solution which renders such procedures inefficient for geotechnical problems.

Yazdchi et al. (1999) investigated the effect of different stiffness ratio of structure and foundation material on the overall response of the structure using coupled FE-BE methods. The effect of impedance ratio *($E_f$/Ed i.e,* the ratio of foundation Young's modulus and Young's modulus of the structure*)* on the response of the structure was examined in the context of seismic excitation applied to a dam-foundation prototype. In the analysis, the structure was modeled by FEM and the half space was represented by the BEM. Effects of non-zero initial conditions due to the pre-dynamic loads and/or self-weight of the structure were included in the transient BE formulation. It was shown that for practical cases (such as dam-foundation systems) where initial conditions due to the pre-seismic loads (water pressure) and self-weight of the dam should be considered in the calculation. Zhang, Wegner and Haddow (1999) proposed a new procedure for the analysis of three-dimensional dynamic soil-structure interaction in the time domain. In this study, the soil is modeled as linear elastic solid; however, the methods developed can be adapted to include the effects of soil nonlinearities and hysteretic damping in the soil. A substructure method, in which the unbounded soil is modeled by the scaled boundary finite-element method, is used and the structure is modeled by 8-21 noded 3D isoparametric or subparametric hexahedral elements. Approximations in both time and space were made to calculate acceleration unit-impulse response matrix. The approximations resulted in significant reduction in computational effort with little loss of accuracy and in a very efficient scheme for evaluation of convolution integrals in the calculation of soil-structure interaction forces. The approximations proposed in this paper are also applicable to the boundary element method. A 3D Dynamic Soil-Structure

Interaction Analysis program (DSSIA-3D) is developed considering different types of seismic excitations (S-waves, P-waves, and surface waves). The computer program developed can be used in the analysis of three-dimensional dynamic soil-structure interaction as well as in the analysis of wave scattering and diffraction by three-dimensional surface irregularities. Rizos and Wang (2002) developed a coupled BEM–FEM methodology for 3D wave propagation and soil–structure interaction analysis in the direct time domain. A standard finite element methodology for dynamic analysis along with direct integration in time is coupled to the BEM through a staggered solution approach. Each method provides initial conditions to the other at the beginning of each time step. Elleithy and Tanaka (2003) presented several interface relaxation algorithms for boundary element–boundary element coupling (BEM–BEM) and for finite element–boundary element coupling (FEM–BEM) using sub structuring concept. Separate computations for the BEM and FEM sub-domains and successive update of the boundary conditions at the interfaces are performed until convergence is achieved. The interface relaxation coupling algorithms preserve the nature of the FEM and BEM.

Another class of method called dual reciprocity boundary element method (DRBEM) was introduced by Nardini and Brebbia (1982) for elastodynamic problems and extended to scalar wave propagation problems by Dai (1992). By considering the advantages and disadvantages of the finite element and the boundary element methods for dam-resevoir-foundation interaction problems, the dual reciprocity boundary element method coupled with finite element method was found to be convenient to use in such interaction problems. Kucukarslan (2003) formulated a time domain dynamic analysis of the dam-reservoir-foundation interaction problem by coupling the dual reciprocity boundary element method (DRBEM) for the infinite reservoir and foundation domain and the finite element method for the finite dam domain. An efficient coupling procedure was formulated by using the substructure method. Sharan's boundary (1987) condition at the far end of the infinite fluid domain was implemented. To verify the proposed scheme, numerical examples were solved and compared with available exact solutions and finite-finite element coupling results for the problem of dam-reservoir interaction. Finally, a complete dam-reservoir-foundation interaction problem was solved and the solution was compared with the previously published results.

## 2.7 SOIL STRUCTURE INTERACTION ANALYSIS

The foundation of every structure is situated on soil/rock medium. If the foundation material is very stiff/rigid, then assumption of a rigid base will yield results with sufficient accuracy. In case of a foundation with relatively softer material, the assumption of a rigid base may lead to unsafe analysis. In such cases, it is very important to consider the effect of soil-structure interaction. More often than not, the effect of soil-structure interaction leads to higher displacements and stresses. If the foundation is considered to be rigid, then the behavior of structure under any kind of loading doesn't affect the foundation or vice versa. When the response of the structure under any kind of loading is influenced by the underneath foundation and behavior of the foundation is also altered by the presence of structure, the problem may be categorized as a soil-structure interaction problem. Based upon the types of loading, the soil-structure interaction problem may be further classified as static and dynamic soil-structure interaction problems. If the imposed load on the soil-structure coupled system is static in nature, it can be termed as a static interaction problem. In case of dynamic loading on the coupled system of soil and structure, the problem is termed as dynamic SSI (soil-structure interaction) problem. In next section, some important contributions from some of the leading researchers working in the area of both static and dynamic soil-structure interaction problems have been highlighted.

### 2.7.1 Static Soil-Structure Interaction Problems

SSI analyses for static problems have also attracted a considerable amount of attention among the researchers. Though simple compared to the dynamic soil-structure interaction, many developments have come around in the field of developments of new elements, new boundary conditions and new algorithms to tackle soil-structure interaction problems in general. The techniques developed are generally applicable to both static and dynamic problems as well. However, based on the types of problems investigated, a brief description of the interaction analyses of the static problems is addressed next.

Stefanou (1983) discussed the application of numerical methods, the finite element, the finite difference and dynamic relaxation, for the solution of problems in soil-structure interaction. Hird and Russel (1990) presented an analytical solution for the compression of a long elastic block, bonded along one side to a rigid material. This provided a benchmark for testing the performance of interface elements employed in finite element modeling of soil-structure interaction. Pandey et al. (1994) developed an iterative approach for the soil-structure interaction of tall buildings having closely spaced independent footings. A software package was developed and several plane frame problems were analyzed. Results were compared with those obtained with fixed base analysis. In order to verify the proposed approach, a finite element analysis of a 12storey plane frame (footing modeled as plate and soil as brick element) has also been carried out. Results of the finite element analysis agree closely with the proposed approach. Viladkar et al. (1994) carried out a study of FEM modeling of plane frame-combined footing system subjected to bi-directional loading. The formulation of an interface joint element used to model the interface characteristics has also been presented. Some useful suggestions were given regarding the choice of tangential and normal stiffness of the interface elements. Ng, Pyrah and Anderson (1997) examined CRISP90 interface element, the DRCRISP interface element and a conventional 8-noded quadrilateral element subjected to various loading conditions. Studies revealed that all these interface elements only suitable for monotonic loading which are not tensile along the interface. The CRISP90 interface element was modified by introducing a limiting adhesive strength in the normal direction. The results of single element and other benchmark tests showed that the modified element could satisfactorily model different modes of deformations relevant to SSI problems.

Bose and Das (1997) carried out nonlinear finite element analysis to investigate the stress distribution and load-settlement behaviour of uniformly loaded circular footings of absolute rigidity and absolute flexibility. The nonlinearity of the stress-strain curve of soil was taken into account by adopting a “piecewise” linear model. A hyperbolic stress-strain relationship of the soil was assumed. An analysis was carried out under conditions simulating the experimental setup of the model footing tests, performed on two different types of soil media. Theoretical observations were compared with experimental ones and

good agreement between the above two was found. Kocak and Mengi (2000) developed a 3D SSI model in which, the layered soil medium is divided into thin layers and each thin layer is represented by a parametric model. The parameters of this model are determined, in terms of the thickness and elastic properties of the sub layer. Then, by adding the structure to soil model a three-dimensional finite element model is established for the soil-structure system. For the floors and footings of the structure, rigid diaphragm model is employed. Based on the proposed model, a general computer software is developed. Though the model accommodates both the static and dynamic interaction effects, the program is applied to four examples, which are chosen to be static so that they can be analyzed by the developed program. Based on the results, it is found that the proposed model can be used reliably in SSI analysis. Reports of use of techniques involving BEM-FEM or BEM-BEM coupling for the solution of static problems, are available in the works of El-Gebeily et al (2002), Elleithy and Tanaka (2003). Jahromi et al. (2007) investigated the coupled SSI problems by domain decomposition techniques. Coupling of the separately modeled partitioned subdomains is undertaken with various algorithms based on the sequential iterative Dirichlet-Neumann sub-structuring method, which ensures compatibility and equilibrium at the interface boundaries of the subdomains. The developed tool is used in a case study involving nonlinear soil-structure interaction analysis between a plane frame and soil subjected to ground excavation. This study highlights the relative performance of the various considered coupling algorithms in modeling real soil-structure interaction problems, in which nonlinearity arises in both the structure and the soil, and leads to important conclusions regarding their adequacy for such problems and their future developments as well.

## 2.7.2 Dynamic Soil-Structure Interaction Problems

### *2.7.2.1 Linear Analysis*

Wolf (1985) presented the direct method of soil-structure interaction analysis. Using this method the soil region near the structure and the structure was modeled directly. The idealized soil-structure system was analyzed in single step. A consistent free-field ground motion was applied to the boundaries of the discrete model and the response of the combined soil-structure system was computed. The response of the soil and the structure

obtained was used as input in a second stage analysis to obtain the detailed structural response. This technique limits the extent of soil domain to be considered, and used if the soil deposit rests on rock foundation hence can be used in determining the responses of a concrete gravity dam.

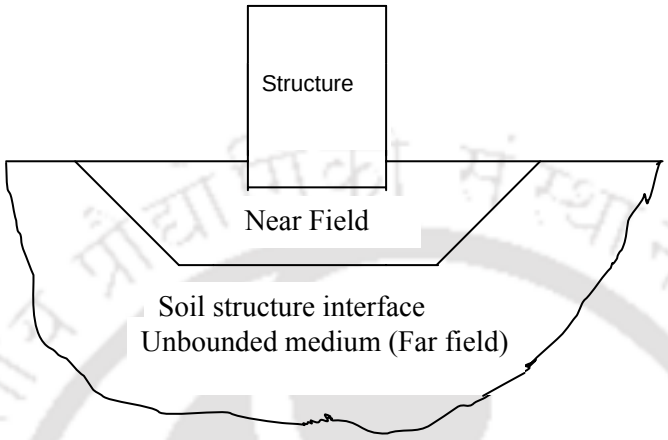


Fig. 2.6 General Soil structure system

Wolf (1985, 1988) also introduced substructure method in which, the soil-structure system may be divided into two substructures: a structure, which may include a portion of non-linear soil or soil with an irregular boundary, and the unbounded soil i.e., the SSI problem was divided into a series of simpler problems, which were solved independently, and the results were then superposed to obtain the response of the structure. Though simple, this method was restricted to simple geometry and linear soil. This approach is often implemented in the frequency domain to account for the frequency dependence of the foundation impedance functions. These substructures are connected by the general soil-structure interface (See Figure 2.6). The unbounded soil is assumed to be linear but the structure could be non-linear. Generally the non-linear soil adjacent to the structure can be treated as a part of the structure, so non-linearity of the soil adjacent to the structure could also be included if necessary. Usually a dynamic soil-structure interaction analysis by the substructure method can be performed in three steps as follows:

I. Determination of seismic free-field input motion along the general soil-structure interface. The seismic free-field input motion can be determined by free field site analysis (Chen, 1980; Wolf, 1988).

II. Determination of the reaction of the unbounded soil on the general soil-structure interface in the form of a displacement-force relationship.

III. Analysis of the bounded soil-structure system under the action of the externally applied transient loading and the ground interaction force determined by steps I and II.

The reaction of the unbounded soil on the general soil-structure interface is represented by a boundary condition in the form of a force-displacement relationship, which is global in both space and time. The boundary-element method is a powerful procedure for modeling the unbounded medium since only the boundaries of the unbounded medium are discretized so that the spatial dimension is reduced by one, and the radiation condition is satisfied automatically as a part of the fundamental solution. Based on the substructure method, many hybrid methods (Zienkiewicz, Kelly and Bettess, 1977; Touhei and Ohmachi, 1993) have been developed where the structure and an adjacent finite region of the soil are discretized by the standard finite-element method while the unbounded soil is modeled by the boundary-element method. However, it is very difficult to derive the fundamental solutions for many cases. The scaled boundary finite-element method which is the alias of the consistent infinitesimal finite-element cell method, (Song and Wolf, 1997, 1998) combines the advantages of the boundary element method and the finite-element method, and no fundamental solution is required. It is exact in the radial direction, converges to the exact solution in the finite-element sense in the circumferential direction, and is rigorous in both space and time. Moser, Antes and Beer (2005) developed a new methodology for analyzing wave propagation problems of plane strain elastodynamics. It is based on a Laplace domain boundary element formulation and Duhamel integrals in combination with the convolution quadrature method (CQM). The CQM is a technique which approximates convolution integrals, in this case the Duhamel integrals, by a quadrature rule whose weights are determined by Laplace transformed fundamental solutions and a multistep method. In order to investigate the accuracy and the stability of the proposed algorithm, some plane wave propagation and interaction problems are solved and the results are compared to analytical solutions and results from finite element calculations. Very good agreement is obtained. The results are very stable with respect to time step size.

Ibhrahimbegovic and Wilson (1990) presented an efficient computational technique for the dynamic analysis of large linear structural systems with local nonlinearities. Various possibilities for base isolation systems were naturally fitted within the proposed framework. In particular, the uplifting of the structure as a natural base isolation concept was addressed. The authors used dynamic substructuring technique and an efficient numerical algorithm using fast nonlinear analysis which accommodated non-proportional damping as a consistent way to reduce significantly the computational effort. Tan and Chopra (1995) extended the available substructure method and available computer program for the earthquake analysis of arch dams, including the effects of dam-reservoir interaction, reservoir absorption, and foundation rock flexibility, was extended to include the effects of dam-foundation rock interaction with inertia and damping effects. Tan and Chopra (1996) further calculated the dynamic response of Morrow Point Dam to ground motion for a wide range of properties of dam, foundation rock, impounded water, and reservoir boundary materials. Based on these response results, the effects of dam-foundation rock interaction (considering damping, inertia, and flexibility of the foundation rock) with empty reservoir were investigated. Finally, the combined effects of dam-foundation rock interaction, dam-water interaction, and reservoir boundary absorption were studied.

Felippa and Park (1980) discussed, in detail, staggered solution procedure for solution of for a variety of coupled field dynamic problems. In a staggered solution procedure the solution state of the coupled system is approached sequentially. Direct solution methods of coupled field problems i.e. soil-structure interaction or fluid-structure interaction problems suffer from the need of excessive storage requirements and computation time. The staggered solution schemes allow us to use reduced matrices for the particular subsystem and also reduce the computational time required to solve the system matrices. Paul et al. (1981) have successfully used staggered solution approach to solve reservoir-dam interaction problems. An example application of the staggered approach in the context of soil-structure interaction analysis is that of Rizos and Wang (2002). The authors developed a partitioned method for soil-structure interaction analysis in the time domain through a staggered solution, where a standard Finite Element Method (FEM) model, representing the structure domain, was coupled to a Boundary Element

Method (BEM) model, representing the soil domain as an elastic half-space. Maity and Bhattachaya (2003) suggested an iterative scheme in conjunction with the staggered solution procedure for the dam-reservoir interaction problems. Since the two systems are dealt with separately, the resulting matrices are always symmetric. However, the staggered approach should be used with great care, since its stability is conditional on the size of time step. Stability and accuracy issues related to the staggered approach typically demand excessively small time steps, rendering this scheme computationally prohibitive for many coupled problems. If a corrective iteration at each time step is employed, where the interface boundary conditions are iteratively updated until convergence is achieved, one obtains an iterative coupling method. Within the iteration procedure at every time step, a relaxation operator may be applied to the interface boundary conditions in order to enable or speed up convergence. In this case, the method can also be called an interface relaxation method. Reports of use of such techniques, involving BEM-FEM or BEM-BEM coupling for the solution of static problems, were made by El-Gebeily et al (2002), Elleithy and Tanaka (2003). Estorff and Hagen (2005) used this coupled FEM-BEM technique for the solution of elastodynamic problems which showed that convergence is influenced by the sub domain mesh density, the material properties and the adopted relaxation scheme. They also discussed the need for a proper relaxation criterion to be used in staggered solution to speed up the convergence. Jahromi et al. (2007) used partitioned analysis technique involving iterative coupling procedure for solving different soil-structure interaction problems.

#### *2.7.2.2 Nonlinear Analysis*

The majority of the work carried out throughout the world in the area of soil structure analysis is restricted to linear analysis. The primary reason for this limitation is mainly the fact that most of analyses have been carried out in frequency domain. It has long been recognized that the time domain method are the most suitable methods for nonlinear finite element analysis. Domain type technique such as finite element method of analysis of soil-structure problems involves reflection of waves from the truncated boundaries to the domain of interest, which doesn't represent the actual situation properly. As a remedy to this problem, a number of different approaches have been formulated to confront the

challenges of soil structure interaction problems. Selvadurai et al. (1989) have used infinite elements with sufficient accuracy to model the unbounded saturated soil media. But, coupling the finite element and boundary element or the finite element and infinite element is a very complicated task. Also, for nonlinear analyses such coupled techniques require prohibitive computational cost. The literatures pertaining to nonlinear analyses of concrete gravity dams are diversely oriented. Ibhrahimbegovic et al (1990) devised a method for dynamic analysis of linear structure-foundation systems with local nonlinearities. Wilson (2002) devised a method for doing nonlinear soil structure interaction analysis using fast nonlinear analysis (FNA) method which uses exclusively finite element method.

Non-linear soil-structure interaction analysis for a structure embedded in a half space for a vertical earthquake excitation was carried out by Wolf and Darbre (1986). Wolf and Obernhuber (1985) formulated an indirect boundary element method which uses Green's function in time domain for nonlinear soil-structure interaction analysis for a surface foundation. Abouseeda and Dakoulas (1998) used a combined FE-BE formulation to represent nonlinear seismic soil-structure interaction in two dimensions against incident SV waves. The dam body was modeled with a simple nonlinear hysteretic model using finite element discretization, whereas the elastic half-space was discretized with boundary elements. A more rigorous treatment of the inelastic behavior of soil under cyclic loads can be found in the works of Elgamaal, Gaffar and Prevost (1985, 1987) and Griffiths and Prevost (1988). In theses works, a hardening law expresses the change of the plastic modulus by using multi-yield or boundary surface theory. Recently, emerging generalized plasticity models seem to provide a more convenient platform because they do not require explicit definition of the yield and plastic potential surfaces. Such models have been successfully employed in large deformation analyses of embankment dams and centrifuge tests and provide reasonably accurate results against static and dynamic loading conditions (Zienkiewicz, Pastor, Chan and Xie, 1991). Jianguo et al. (1993) showed that the most soil-structure interaction (SSI) analyses are still conducted assuming linear material behavior or simulating nonlinear effects through an equivalent linearization and the structure (foundation) being closely welded with the surrounding soil. Two kinds of nonlinearities are very important which

needs to be considered: those associated with inelastic soil behavior and those resulting from loss of contact between the foundation and the surrounding soil. A modified lumped parametric model for the analysis of nonlinear SSI effects has been proposed by the author. In the model both nonlinearities are taken into account. The results of tests of the soil-structure system model have been presented, which agree well with those obtained from analysis by using the proposed model.

Generally, FE methods are more suited for complex geometries, material inhomogeniety and nonlinearity in finite domains. A variety of formulations and element types have been developed to tackle such problems (Liao and Wong, 1984; Kausel and Tassoulas, 1981). On the other hand, boundary type methods are superior in handling infinite domains, but they are more suited for linear problems (Beskos, 1987; Ahmad and Banerjee, 1988). Von Estorff and Kausel (1989) used the coupled FE-BE technique to various soil-structure interaction problems such as flexible foundations and tunnels. The inelastic formulation based on coupled FE-BE method was first carried out by Pavlatos and Beskos (1994). Bernal and Youssef (1998) developed another class of method called hybrid-time-frequency-domain (HTFD) procedures which combine both the frequency and time domain techniques in order to solve the nonlinear soil-structure interaction problems. The dual reciprocity boundary element method (DRBEM) was introduced by Nardini and Brebbia (1982) for elastodynamic problems and was extended to time domain problems by Wrobel and Bebbia (1986). Kucukarslan (2004) used DRBEM for dynamic analysis of dam-reservoir-foundation interaction problems in time domain. An efficient coupling procedure was formulated which involving the implementation of Sharan's (1987) boundary condition at the far end of the infinite fluid domain.

## 2.8 SUMMARY OF THE LITERATURE

The review on the existing literature on dynamic analyses of structures considering soil-structure interaction effect can be summarized as follows.

- The finite element method has the distinct advantage of being straightforward in implementation in the analysis of dam-foundation interaction problems and representing any arbitrary geometry, heterogeneity in the dam body and the foundation bed profile.

- Ageing process of the concrete is a very important phenomenon which leads to loss of stiffness of the concrete structure. The ageing of concrete may be caused due various causes such as hygro-chemo-mechanical effects. The leaching of water with various detrimental chemical ingredients into the porous structure of the concrete leads to the reduction of the stiffness of the structure.
- Most of the times, the soil-structure interaction analysis is performed considering the foundation material to be linear, elastic. In reality, the soil/rock foundation has a nonlinear, inelastic stress-strain behavior. Therefore, in order to truly asses the behaviour of the soil-structure system during interaction analyses, the nonlinear material properties of the foundation should be considered.
- Various types of constitutive models are available to characterize the nonlinear behaviour of geologic materials such as nonlinear elastic models, elasto-plastic models and elastoviscoplastic models. The hyperbolic nonlinear, elastic model proposed by Duncan and Chang (1970) is very popular among the researchers throughout. The Von-Mises, Tresca, Mohr-Coulomb and Drucker-Prager models form the major part of the elasto-plastic models available for geomaterials. The elastic-plastic constitutive model suggested by Hoek and Brown (1998) has been used for modeling rock masses very effectively.
- In the time domain method, several kinds of modeling techniques had been developed to represent the radiation condition at finite domain boundary say viscous boundary and damped artificial boundary such that the effect of infinite soil media can be incorporated (Wolf, 1988).
- Coupled analysis of aging dam-reservoir system which takes care of degradation effects of the concrete material with age is necessary to predict the possible generation of stresses in the existing dams for retrofitting.
- FEM has been extensively used for dynamic analysis of many structural systems. In particular, BEM has been widely adopted because of its ability to model infinite compliant media and irregular soil profiles, without the use of fictitious absorbing boundaries at the far field. Modeling of soil media using finite element or boundary element technique itself is a complex problem.

- The coupled method which is a combination of two or more methods, such as coupled Finite Element-Boundary-Element (FE-BE) method or Finite Element-Infinite Element (FE-IE) method used extensively by many investigators (Zienkiewicz, Kelly and Bettess, 1977; Touhei and Ohmachi, 1993).
- Interaction analysis may be carried out either in time domain or in frequency domain (Wolf, 1988).

## 2.9 SCOPE OF THE PRESENT INVESTIGATION

A detailed review of the existing literature on the concrete gravity dam and foundation interaction system reveals that the subject has attracted the widespread attention from researchers all over the world. Though, there are several different areas among which people have directed their investigations from time to time. To fulfil the objectives of the present investigation and considering the areas still unexplored, the scope of the present investigation is limited to the following.

1. Finite element analysis of a concrete gravity dam idealizing the same as two-dimensional plane strain problem considering the geometrical non-linearity.
2. Development of a suitable numerical scheme to predict the dynamic behavior of aged concrete dams considering the material degradation due to long-term ageing.
3. Development of an efficient boundary condition at the sides of the truncated boundaries of the infinite soil domain which would allow the traveling waves to radiate.
4. Development of an iterative scheme for the solution of the dam-foundation coupled system, to obtain response of structural and foundation domains simultaneously.
5. Incorporation of material nonlinearity for the finite element analysis of foundation domain.
6. Parametric study of the dam-foundation coupled system with and without the presence of reservoir water.

# CHAPTER 3

# THEORETICAL FORMULATION

## 3.1 INTRODUCTION

The analysis of a huge structure like concrete gravity dams is generally carried out considering the base of the dam to be fixed. In a word, the dam is assumed to be resting on a rock foundation. The flexibility of the foundation may be considered insignificant in that case. If the rigidity of the foundation is very high compared to the rigidity of the dam material, the assumption of a rigid foundation will lead to safe analysis. But, if the rigidity of the foundation material is comparatively less, then the flexible nature of the foundation should be taken into account during the analysis of gravity dam-foundation system. In that case, the flexibility of the foundation becomes an important issue in analyzing the response of the dam and foundation.

The concrete gets deteriorated with the passage of time due to various hygro-chemo-mechanical actions. Since the dam face is in constant contact with water, concrete degradation due to hygro-mechanical loading is inevitable and should be considered in the analysis procedure. The assessment of the strength of aged concrete is an important issue to be considered during the analysis of the dam against severe earthquake loading. Due to ageing, the dams are subjected to severe environmental effects, which may lead to loss of strength due to material degradation. The consideration of an appropriate material model capable of describing the ageing phenomenon of the concrete will be the key to model its behavior against any kind of loading at a later stage after its construction. The accuracy of the results will be dependent on the assumptions made in building the mathematical model to represent ageing behavior. The design of earthquake resistant concrete dam also necessitates accurate determination of hydrodynamic pressure developed in the adjacent reservoir. The hydrodynamic pressure developed on the dam is dependent on the physical characteristics of the boundaries surrounding the reservoir including reservoir bottom. Westergard (1933) devised a way called added mass approach to model the hydrodynamic pressure resulting from the upstream reservoir water. In this approach, the reservoir water is assumed to be incompressible. Also, it is

assumed that some portion of the reservoir water moves with dam when the earthquake comes. In this method, the interaction effect between the reservoir water and the dam body is ignored. Though, it is not the truly representative of the behavior during the dam and reservoir water during earthquake, this method still remains one of the most favorite among researchers because of its simplicity. In the present work, the added mass approach has been adopted to model the hydrodynamic pressure which develops during any earthquake.

The dynamic soil-structure interaction analysis is a very complex procedure by itself. Most of the literatures show that the interaction analysis has been carried out by considering the foundation domain to be linear, elastic. The assumption of a linear foundation material renders the analysis computationally less demanding. But the actual stress-strain behavior of the soil/rock material is essentially nonlinear in nature. In order to truly represent the actual material behavior of the soil/rock foundation, it is necessary to consider a nonlinear constitutive model. There are a number of methods available to represent nonlinear stress-strain behavior of the soil/ rock material. Amongst them, nonlinear elastic, nonlinear elasto-plastic, nonlinear elasto-viscoplastic methods are some of the very popular methods used to model soil/rock material. Though elasto-plastic and elasto-viscoplastic methods are more suitable to represent soil/rock material, their implementation is very demanding both from point of view of memory space requirement and time of computation. Therefore, a nonlinear elastic model called Duncan-Chang (1970) model has been adopted in the present analysis keeping in mind the disadvantages of using more complex models. The Duncan-Chang model is found to be efficient from the computational point of view yielding very good results.

While evaluating the coupled dam-foundation interaction effect by finite element method, modeling the semi-infinite foundation domain demands special consideration. A proper boundary condition should be implemented in order to correctly represent the semi-infinite foundation domain. The boundary condition should be such that it should be able to radiate the incoming waves or absorb it so that no energy is reflected back into the domain of interest. The coupled dam-foundation response is affected by radiation of waves towards infinity. The boundary condition, which allows the waves to radiate through the artificial boundary without any reflection, is known as radiating boundary

condition or non-reflecting artificial boundary condition since it is applied as an artificial boundary which is physically non-existent. Another type of boundary condition, which makes use of viscous dashpots to absorb the energy of the incoming waves, is known as absorbing or viscous boundary condition. Similar to the absorbing boundary condition, a combination of springs and dashpots could be used to absorb the energy of the incoming waves. This combination of springs and dashpot boundary condition is also local in time and space and is known as Kelvin boundary condition. Both of these two boundary conditions carry simple physical interpretations and are easy to implement in a finite element model. In the present work, viscous dashpots have been used with very good results.

The coupled effects of the dam-foundation system are obtained by introducing an iterative scheme that simulates the interaction behavior. The solution of the coupled system is accomplished by solving the two systems separately with the interaction effects at the foundation-structure interface enforced by the developed iterative scheme. The theoretical formulations for the dam-reservoir coupled systems are presented in three parts. Part A, B and C contain the formulations of the aged dam, foundation and the coupled dam-foundation system respectfully.

## 3.2 SUITABILITY OF FINITE ELEMENT TECHNIQUE

For the dam-foundation having simple boundary, classical solution treating the dam and foundation as continuum may be used effectively. However, if the dam geometry and foundation boundary is not regular, numerical methods such as finite element technique may be used effectively. Due to varied geometric forms of the dam and irregular geometry of the foundation, the finite element method (FEM) is recognized to be one of the most powerful numerical tools for solving such problems. However, computational difficulties arise while trying to model the semi-infinite foundation domain by finite element discretization. In such practical situation, the semi-infinite foundation is truncated by imposing an artificial boundary at a certain distance away from the structure. A suitable boundary condition must be imposed at the truncated boundary to evaluate the effect of radiation damping, so that no spurious wave reflection occurs from the boundary.

### 3.2.1 Selection of Finite Element

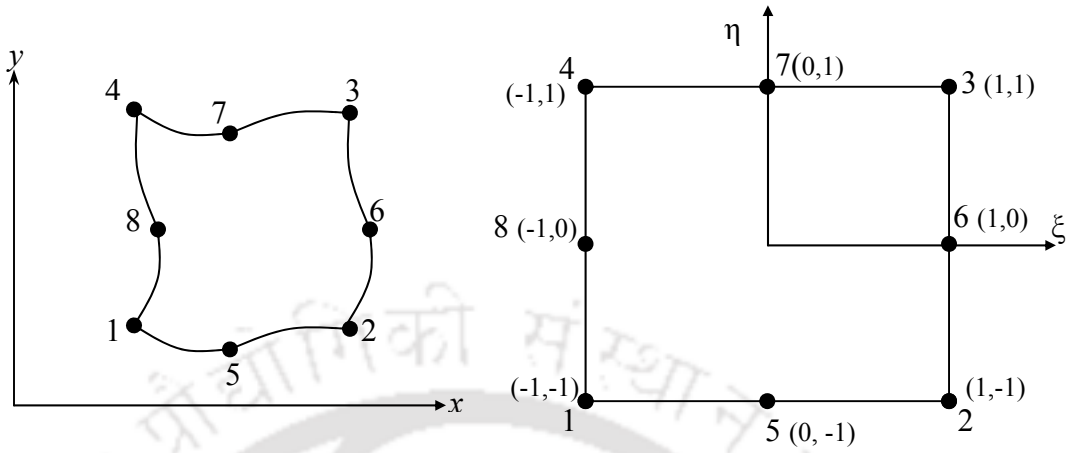


**(a) Cartesian coordinate** **(b) Natural coordinate**

Fig. 3.1 Transformation from Cartesian coordinates to Natural coordinates for eight noded quadrilateral isoparametric elements

In finite element method, a body or a structure is idealized as a continuum. It is discretized into several smaller subdivisions, which are known as finite elements. These elements are connected at finite number of nodes or nodal points. The properties of individual elements are evaluated and then assembled by the numerical integration method to obtain the response of the entire body or the structure. Due to complex geometry of the dam-foundation system, a straightforward analytical solution may not be achievable. In that case, the analyzer has to adopt a proper numerical technique such as finite element method or finite difference method. The use of finite element method has become very popular in handling problems dealing with complex geometries over other existing numerical techniques. In the present case, both dam and the foundation domain are discretized using eight noded quadrilateral isoparametric elements. The eight noded quadratic isoparametric finite elements are one of the most versatile and efficient elements used to model irregular domain geometries. The isoparametric element is oriented in the natural coordinate system ($\xi,\eta$) and is transformed to the global Cartesian coordinate system using Jacobian matrix. The eight nodded element in both the above-mentioned coordinate systems are shown in Fig. 3.1.

### 3.2.2 Shape Functions

The isoparametric elements are chosen because it is able to generate non-rectangular elements having curved sides and arbitrary shapes. Because of this, isoparametric elements are very useful in modeling the domains having arbitrary geometries. Of course, one should be careful about the aspect ratios of the elements while discretizing the domain. Isoparametric elements are formulated using an intrinsic coordinate system (ξ-η), which is defined by the element geometry and not by the element orientation in the global coordinate system. The natural coordinates are always attached to the element and are scaled so that the sides of the parent element are defined by ξ = ±1 and η = ±1.

#### *3.2.2.1 Shape Functions for the Dam and Foundation Domains*

An eight noded quadrilateral element as shown in Fig.3.1 is considered for the discretization of the dam and the foundation domain. The shape functions are derived from an interpolation polynomial in terms of natural coordinates so that the displacements are represented as a function of nodal displacement. The displacement function is represented in natural coordinate system in the following manner

$$u(\xi,\eta)=A_0' + A_1'\xi + A_2'\eta + A_3'\xi^2 + A_4'\xi\eta + A_5'\eta^2 + A_6'\xi^2\eta + A_7'\xi\eta^2 \quad (3.1)$$

The shape functions derived from the interpolation polynomial are as

$$\left.\begin{aligned} N_{di} &= \frac{1}{4}(1+\xi\xi_i)(1+\eta\eta_i)(\xi\xi_i+\eta\eta_i-1) && i=1,2,3,4 \\ N_{di} &= \frac{1}{2}(1+\xi\xi_i)(1-\eta^2) && i=5,7 \\ N_{di} &= \frac{1}{2}(1+\eta\eta_i)(1-\xi^2) && i=6,8 \end{aligned}\right\} \quad (3.2)$$

Here, *i* denotes the node number of the element. The correctness of the shape functions is checked from the relations:

$$\sum N_{di} = 1, \quad \sum \frac{\partial N_{di}}{\partial \xi} = 0 \text{ and } \sum \frac{\partial N_{di}}{\partial \eta} = 0 \quad (3.3)$$

### 3.2.3 Relationship Between Cartesian and Natural Coordinates

The displacements $u$ and $v$ are expressed using the interpolation functions as

$$u = \sum N_{di} u_i \quad \text{and} \quad v = \sum N_{di} v_i \tag{3.4}$$

Here, the shape functions for the dam, $N_{di}$ are functions of the natural coordinates ξ, η. The suffix $i$ represent the node number. For isoparametric formulation, the same interpolation functions are used to represent the geometry in terms of the Cartesian coordinate's $x_i$ and $y_i$ as

$$x = \sum N_{di} x_i \quad \text{and} \quad y = \sum N_{di} y_i \tag{3.5}$$

The relationship between the two coordinate systems may be computed by using the chain rule of partial differentiation as:

$$\begin{pmatrix} \frac{\partial f}{\partial \xi} \\ \frac{\partial f}{\partial \eta} \end{pmatrix} = \begin{pmatrix} \frac{\partial x}{\partial \xi} & \frac{\partial y}{\partial \xi} \\ \frac{\partial x}{\partial \eta} & \frac{\partial y}{\partial \eta} \end{pmatrix} \begin{pmatrix} \frac{\partial f}{\partial x} \\ \frac{\partial f}{\partial y} \end{pmatrix} = [J] \begin{pmatrix} \frac{\partial f}{\partial x} \\ \frac{\partial f}{\partial y} \end{pmatrix} \tag{3.6}$$

where $[J]$ is the Jacobian matrix and $f$ is any function. The derivative operators with respect to Cartesian coordinate system may be represented as

$$\begin{pmatrix} \frac{\partial f}{\partial x} \\ \frac{\partial f}{\partial y} \end{pmatrix} = [J]^{-1} \begin{pmatrix} \frac{\partial f}{\partial \xi} \\ \frac{\partial f}{\partial \eta} \end{pmatrix} \tag{3.7}$$

## 3.3 TIME DOMAIN SOLUTION OF DYNAMIC EQUATION OF MOTION

In a dynamic problem the equation of motion can be expressed as

$$[M]\{\ddot{u}\} + [C]\{\dot{u}\} + [K]\{u\} = \{F\} \tag{3.8}$$

The above equation is known as dynamic equation of motion which is solved by a suitable time stepping scheme. In Eq.(3.8), $[M]$, $[C]$ and $[K]$ are the mass, damping and stiffness matrices of the system respectively. In a linear dynamic system, these values remain constant throughout the time history analysis. The force vector is given by $\{F\}$. If the nonlinearity of the material is considered either by nonlinear elastic or elasto-plastic

method, the stiffness matrix is updated at every time step depending on the state of stress and strains at that time instant. The right hand side load vector $\{F\}$ also updated considering it to be a function of state of stress and strains occurring at that time instant if the visco-plastic algorithm is followed. To obtain the transient response at time $t_N$, the time axis can be discretized into $N$ equal time intervals ($t_N = \sum_{j=1}^{N} j\Delta t$), where displacement $\{u\}$, velocity $\{\dot{u}\}$ and acceleration $\{\ddot{u}\}$ are functions of time. The choice of method for time-history analysis is strongly problem dependent. Various direct time integration methods exist for time history analysis that are proficient for structural dynamics and wave propagation problem. Amongst the explicit methods, the central difference technique is the most popular and widely used because of its simplicity. Besides the very popular implicit Newmark (1959) algorithm there exists another class of method called implicit-explicit methods. Implicit-explicit schemes were first introduced by Belytschko and Mullen (1977) and were given an alternative form by Hughes and Liu (1978) and Park et al (1977). Though simple, the explicit techniques suffer from the need of using excessively small time steps which renders these methods expensive from the computational point of view. Amongst the implicit types of methods, the *Newmark* family of methods is most popular and is given by

$$\{u\}_{j+1} = \{u\}_j + \Delta t\{\dot{u}\}_j + \frac{\Delta t^2}{2}\left[(1-2\beta)\{\ddot{u}\}_j + 2\beta\{\ddot{u}\}_{j+1}\right] \tag{3.9}$$

$$\{\dot{u}\}_{j+1} = \{\dot{u}\}_j + \Delta t\left[(1-\gamma)\{\ddot{u}\}_j + \gamma\{\ddot{u}\}_{j+1}\right] \tag{3.10}$$

Here, $\beta$ and $\gamma$ are chosen to control stability and accuracy. The average and linear acceleration methods are given by $\gamma = \frac{1}{2}, \beta = \frac{1}{4}$ and $\gamma = \frac{1}{2}, \beta = \frac{1}{6}$. By solving Eq. (3.9) for $\{\ddot{u}\}_{n+1}$, then substituting this expression into Eq. (3.10), we obtain

$$\{\ddot{u}\}_{n+1} = \frac{1}{\beta\Delta t^2}\left(\{u\}_{n+1} - \{d\}_n - \Delta t\{\dot{u}\}_n\right) - \left(\frac{1}{2\beta} - 1\right)\{\ddot{u}\}_n \tag{3.11}$$

$$\{\dot{u}\}_{n+1} = \frac{\gamma}{\beta\Delta t}\left(\{u\}_{n+1} - \{u\}_n\right) - \left(\frac{\gamma}{\beta} - 1\right)\{\dot{u}\}_n - \Delta t\left(\frac{\gamma}{2\beta} - 1\right)\{\ddot{u}\}_n \tag{3.12}$$

These equations are substituted into the equation of motion, Eq. (3.8), written at time step $n+1$, and then solved for $\{u\}_{n+1}$. The result is

$$\left[K_{eff}\right]\{u\}_{n+1} = \{F\}_{n+1} + \left[M\right]\left\{\frac{1}{\beta\Delta t^2}\{u\}_n + \frac{1}{\beta\Delta t}\{\dot{u}\}_n + \left(\frac{1}{2\beta}-1\right)\{\ddot{u}\}_n\right\} + \left[C\left\{\frac{\gamma}{\beta\Delta t}\{u\}_n + \left(\frac{\gamma}{\beta}-1\right)\{\dot{u}\}_n + \Delta t\left(\frac{\gamma}{2\beta}-1\right)\{\ddot{u}\}_n\right\}\right] \tag{3.13}$$

Where, $$\left[K_{eff}\right] = \frac{1}{\beta\Delta t^2}\left[M\right] + \frac{\gamma}{\beta\Delta t}\left[C\right] + \left[K\right] \tag{3.14}$$

In this algorithm, $\left[M\right]$ may be chosen to be a diagonal mass matrix. But, an implicit method is more accurate when $\left[M\right]$ is the consistent mass matrix. Also, $\left[K_{eff}\right]$ cannot be a diagonal matrix, because it contains $\left[K\right]$ which is always a fully populated matrix. If $\left[M\right]$ is positive definite, then $\left[K_{eff}\right]$ is nonsingular even if the structure is unsupported or contains a mechanism. Here, the computed displacements are second order accurate. This family of methods can be used with higher time steps and thus requires lesser computational time.

### 3.3.1 Stability Analysis of Newmark Method

Some implicit methods are conditionally stable, but those in common use are unconditionally stable. For the unconditionally stable methods, even very large values of $\Delta t$ do not make calculations blow up (but may destroy accuracy). Stability of an integration scheme implies that the initial conditions for the equations with a large value of $\Delta t / T$ must not be amplified artificially and thus make the integration of lower modes worthless. In a stable scheme, there is no abrupt increase of any errors in displacements, velocities and accelerations at time $t$, due to rounding off during computation. Stability is acquired if the time step chosen is small enough to integrate accurately the response in the highest frequency component. It is important to optimize the size of the time step, so as to obtain accuracy but at the same time avoid an increase in computational cost.

In a practical analysis, the choice of the integration operator depends on the cost of solution that can be determined by the number of time step required in the integration. For a conditionally stable algorithm such as central difference, the time steps for a given

time range considered is determined by the critical time step $\Delta t_{cr}$ and not many choices are available. It can be shown from the literature that the integration scheme is unconditionally stable if $2\beta \geq \gamma \geq 0.5$ and conditionally stable when

$$\gamma \geq \frac{1}{2},\ \beta < \frac{\gamma}{2} \text{ and } \Delta t \leq \frac{\Omega_{crit}}{\omega_{\max}} = \frac{\Omega_{crit} T_{\min}}{2\pi} \tag{3.15}$$

Here, $\omega_{\max}$ and its period $T_{\min}$ correspond to the highest natural frequency obtained by solving the equation

$$\left([K] - \omega^2 [M]\right)\{u\} = \{0\} \tag{3.16}$$

Instability caused by too large a time step is recognized by an unbounded solution that may grow by orders of magnitude per time step, is obviously wrong and causes computer program to stop due to overflow. The $\Omega_{crit}$ is defined as

$$\Omega_{crit} = \frac{\xi\left(\gamma - \frac{1}{2}\right) + \sqrt{\gamma/2 - \beta + \xi^2\left(\gamma - \frac{1}{2}\right)}}{\gamma/2 - \beta} \tag{3.17}$$

in which, $\xi$ is damping ratio. The damping has no effect on stability when $\gamma = \frac{1}{2}$, and that when $\gamma > \frac{1}{2}$ the allowable time step is increased by damping. (In contrast, damping increases the allowable $\Delta t$ of an explicit method. In Eq. (3.17), small damping has small effect, so when damping is uncertain, $\Omega_{crit}$ is obtained by using $\xi = 0$, for which $\Omega_{crit} = \frac{1}{\sqrt{\gamma/2 - \beta}}$. When $\xi > 0$, accuracy is likely to decline, at most from $O\left(\Delta t^2\right)$ to $O\left(\Delta t\right)$, or from $O\left(\Delta t^4\right)$ to $O\left(\Delta t^2\right)$. When $\gamma > \frac{1}{2}$, Newmark method display algorithmic damping, at the cost of reducing guaranteed accuracy from second order to first order. To obtain the highest possible high frequency dissipation, while retaining unconditional stability, the following choice of $\beta$ is appropriate.

$$\text{For } \gamma > \frac{1}{2}, \qquad \text{use} \qquad \beta = \frac{1}{4}\left(\gamma + \frac{1}{2}\right)^2 \tag{3.18}$$

### 3.3.2 Accuracy Analysis of Newmark's method

The errors in the integration may be measured in terms of period elongation and amplitude decay. When the time step to period ratio is larger, the various integration methods exhibit quite different characteristics. For a given $\Delta t / T$, the Wilson-θ method with θ = 1.4 introduces less amplitude decay and period elongation than the Houbolt method, and the Newmark average acceleration method introduces only period elongation and no amplitude decay. If the Newmark constant average acceleration is employed, the high frequency response is retained in the solution. It is observed that the method corresponding to $\gamma$ = 0.5 and $\beta$ = 0.25 has the most desired stability. Therefore, in the present work, the dynamic equilibrium equations are solved using the values of $\gamma$ and $\beta$ as 0.5 and 0.25 respectively.

***PART A***

## 3.4 THEORETICAL FORMULATION FOR DAM

The dam is a huge structure having a long, extended body in the longitudinal direction. The loading on the body of the dam is essentially in its plane arising from the adjacent reservoir water and the inertia force originating due to earthquake. It has been found that a two dimensional analysis produces fairly accurate representation of the response of the dam apart from the sections or regions away from the abutments or supports. For a very important structure, a full three dimensional analysis will be preferred. A two dimensional analysis will be a wiser choice keeping in mind the computational economy and time. For a structure like dam, it can be expected that a plane strain formulation will produce the state of stresses and displacements accurately. In case, a part of the dam body with limited thickness in the z direction is analyzed, plane stress formulation may also be carried out. In the present case, a plane stress formulation has been done to solve the dam-foundation interaction problem. The FEM formulation of the present problem will require:

i. Selection of appropriate shape functions.
ii. Formulation of the mapping between Cartesian and natural coordinates.

iii. Strain-displacement relations.

iv. Building the constitutive matrix to represent the material behavior.

v. Evaluation of the degradation effect with age.

vi. Modification of the constitutive matrix to incorporate the degradation behavior for the structure domain.

vii. Building the stiffness, mass and the damping matrices.

viii. Selection of a suitable numerical scheme for time history analysis

ix. Computation of displacements and stresses.

The selection of shape functions for discretization of the dam, the relationship between the Cartesian and natural coordinates and selection of a suitable numerical scheme for time history analysis are as explained in sections 3.1.3.2, 3.1.4 and 3.1.5 respectively.

### 3.4.1 Strain Displacement Relationships

The relation between strain and displacement is of utmost importance in the finite element formulation for stress analysis problems. Considering small deformations, the generalized strain-displacement relations for the two-dimensional plane strain problems may be written as

$$\left.\begin{aligned} \varepsilon_x &= \frac{\partial u}{\partial x} \\ \varepsilon_y &= \frac{\partial v}{\partial y} \\ \gamma_{xy} &= \frac{\partial v}{\partial x} + \frac{\partial u}{\partial y} \end{aligned}\right\} \tag{3.19}$$

Using Eq. (3.6) the elemental strain may be written as

$$\begin{Bmatrix} \varepsilon_x \\ \varepsilon_y \\ \gamma_{xy} \end{Bmatrix} = \begin{bmatrix} \frac{\partial}{\partial x} & 0 \\ 0 & \frac{\partial}{\partial y} \\ \frac{\partial}{\partial y} & \frac{\partial}{\partial x} \end{bmatrix} \begin{Bmatrix} u \\ v \end{Bmatrix} \tag{3.20}$$

Equation 3.20 can be represented in terms of the shape functions as follows:

$$\begin{Bmatrix} \varepsilon_x \\ \varepsilon_y \\ \varepsilon_{xy} \end{Bmatrix} = \begin{bmatrix} B_1 & 0 \\ 0 & B_2 \\ B_2 & B_1 \end{bmatrix} \begin{Bmatrix} u \\ v \end{Bmatrix} \tag{3.21}$$

Where, $[B_1]$ and $[B_2]$ are the derivative of the shape function $[N_d]$ with respect to $x$ and $y$ respectively. The vectors $\{\bar{u}\}$ and $\{\bar{v}\}$ represent the nodal displacements vectors in $x$ and $y$ directions respectively. The vector of strains at any point inside an element, $\{\varepsilon\}$ may be expressed in terms of nodal displacement as

$$\{\varepsilon\} = [B_0]\{u\} \tag{3.22}$$

where $[B_0]$ is the strain displacement matrix. $\{u\}$ is the nodal displacement vector and may be expressed as

$$\{u\} = \begin{Bmatrix} \bar{u} \\ \bar{v} \end{Bmatrix} \tag{3.23}$$

### 3.4.2 Constitutive Matrix

For the plane strain formulations, a constant longitudinal displacement corresponding to a rigid body translation and rigid body rotations having displacements linear in a direction perpendicular to the cross-section of the dam, do not result in strain. This implies that

$$\varepsilon_z = \gamma_{zx} = \gamma_{xz} = 0 \tag{3.24}$$

Therefore, the constitutive relation for elastic isotropic material can be written as

$$\{\sigma\} = [D]\{\varepsilon\} \tag{3.25}$$

In the above equation, $\{\sigma\}^T = \{\sigma_x, \sigma_y, \tau_{xy}\}$ and $\{\varepsilon\}^T = \{\varepsilon_x, \varepsilon_y, \gamma_{xy}\}$ are the vectors of stress and strain respectively , and $[D]$ is the constitutive matrix defined as

$$[D] = \frac{E_d}{(1+\mu)(1-2\mu)} \begin{bmatrix} (1-\mu) & \mu & 0 \\ \mu & (1-\mu) & 0 \\ 0 & 0 & \dfrac{(1-2\mu)}{2} \end{bmatrix} \tag{3.26}$$

for a material with elastic modulus $E_d$ and Poisson's ratio $\mu$.

### 3.4.3 Degradation Model for Concrete

The concept of degradation of concrete strength is based on the reduction of the net area capable of supporting stresses. The loss of rigidity of the material follows as a consequence of material degradation due to various environmental and loading conditions. Equilibrium of the system is defined by the thermodynamic potential, which is considered here to be strain energy $W(\varepsilon, d)$ and is a function of strain vector $\{\varepsilon\}$ and the damage variable *d*. The expression of $W(\varepsilon, d)$ is as follows:

$$\sigma_i = \frac{\partial W}{\partial \varepsilon_i} \qquad \text{and} \qquad Y = -\frac{\partial W}{\partial d} \tag{3.27}$$

where, $\sigma_i$ =a component of stress vector in engineering sense and $Y$ = Thermodynamic force associated with *d*. The time derivative of specific energy yields

$$\dot{W} = \{\sigma\}^T \{\dot{\varepsilon}\} - Y\dot{d} \tag{3.28}$$

The Clausius Duhem inequality gives a condition on the energy dissipated $W_d$ by the damage process, which is given as

$$\dot{W}_d = Y\dot{d} = \{\sigma\}^T \{\dot{\varepsilon}\} - \dot{W} \geq 0 \tag{3.29}$$

To establish the damage constitutive equation, it is necessary to relate the damage variable $d$ to the other internal variables by some physical hypothesis. The hypothesis of Lemaitre and Chaboche (1978) is empirical in nature. It states any constitutive equation for a damaged material can be derived from the same potential as that for a virgin material by replacing stresses by effective stresses. The effective stresses are defined as

$$\{\dot{\sigma}\} = [M(d)]\{d\} \tag{3.30}$$

where $[M(d)]$ is in general, a symmetric matrix of rank four. For isotropic cases and in the context of strain equivalence, Eq. (3.30) reduces to

$$\{\dot{\sigma}\} = \frac{1}{1-d}\{\sigma\} \tag{3.31}$$

The strain energy of the damaged material is

$$W = \frac{1}{2}\{\sigma\}^T [C(d)]\{\varepsilon\} \tag{3.32}$$

where $[C(d)]$= a second order matrix of material properties. In this case, the effect of

damage is to reduce the stiffness of the material, and we get the following expression:

$$[C(d)] = (1-d)[C_i] \tag{3.33}$$

where, $[C_i]$ = initial stiffness matrix of the undamaged material. The stress vector and the rate of energy dissipation are given by

$$\{\sigma\} = (1-d)[C_i]\{\varepsilon\} \tag{3.34}$$

and $$Y = \frac{1}{2}\{\varepsilon\}^T [C_i]\{\varepsilon\} \tag{3.35}$$

Since $Y$ is a quadratic function of strain $\{\varepsilon\}$, it is always positive. Thus, $d$ is always decreasing as suggested by Eq. (3.29). The isotropic damage model used to model the degradation of concrete due to various chemo-mechanical effects have been derived following the works of Ghrib and Tinawi (1995a). Adopting an analogy given by Ghrib & Tinawi (1995b) to measure the extent of damage in concrete, the orthotropic degradation index can be determined as

$$d_{gi} = \frac{\Omega_i - \Omega_i^d}{\Omega_i} = 1 - \frac{\Omega_i^d}{\Omega_i} \tag{3.36}$$

where $\Omega_i$ = tributary area of the surface in direction $i$; and $\Omega_i^d$ = area affected by degradation. In a scale of 0 to 1, the orthotropic degradation index, $d_{gi}$ = 0 indicates no degradation and $d_{gi}$ = 1 indicates completely degraded material. The index $i$ = 1,2 corresponds with the Cartesian axes $x$ and $y$ in two-dimensional case. The effective plane strain material matrix can be expressed as

$$[D_d] = \frac{E_d}{(1+\mu)(1-2\mu)} \begin{bmatrix} (1-\mu)\Lambda_1^2 & \mu\Lambda_1\Lambda_2 & 0 \\ \mu\Lambda_1\Lambda_2 & (1-\mu)\Lambda_2^2 & 0 \\ 0 & 0 & (1-2\mu)\Lambda_1^2\Lambda_2^2/\left(\Lambda_1^2+\Lambda_2^2\right) \end{bmatrix} \tag{3.37}$$

where $\Lambda_1 = (1 - d_{g1})$ and $\Lambda_2 = (1 - d_{g2})$. In the above equation, $E_d$ is the elastic modulus of the material without degradation. If $d_{g1} = d_{g2} = d_g$, the isotropic degradation model is expressed as

$$[D_d] = (1-d_g)^2 [D] \tag{3.38}$$

where $[D_d]$ and $[D]$ are the constitutive matrices of the degraded and un-degraded model respectively.

### 3.4.4 Evaluation of Degradation Index

The effect of ageing plays a two-way role on concrete. On one hand, the concrete gains strength with the passage of time. On the other hand, it also loses its strength due to detrimental effects of various chemical and mechanical actions. There are relationships suggested in various literatures to predict the gain of compressive strength of concrete for a short period of time. But no such relationships are available to predict its behavior over a longer period of time. All the existing relationships have been derived from the experimental results. To the author's knowledge, such experimental result for mass concrete used for the construction of a concrete dam does not exist, mainly because of difficulties that arise in testing mass concrete consisting of 152 mm maximum size aggregate (MSA). However, various investigators like Andrade et al. (1981), Bittencourt et al. (2001) and Deb and Borsaikia (2006) have carried out mix design of mass concrete using smaller size of aggregates having the same fineness modulus as that of the mass concrete. It was found that the two concrete mixes consisting of different aggregate sizes but having same geometrical proportions and fineness modulus give same compressive strength. This fact has motivated the present formulation for the prediction of the strength of concrete, which is based on experimental results of fifty years of concrete strength (Washa et al., 1989) reported in the literature. Washa et al. (1989) reported the compressive strength of plain cement concrete over a period of fifty years which might have constituents, cement types and curing conditions different than present day concrete. A regression analysis is carried out on the data provided by Washa et al. (1989). But we should be cautious in using the results of regression analyses

#### *3.4.4.1 Degradation as a Function of Time*

Steffens et al. (2003) introduced the parameter "reaction extent" in connection with deterioration of concrete by alkali-silica reaction (ASR). Steffens et al. (2003) says that "In general, the description of the deterioration of concrete structures by ASR involves two basic aspects: the kinetics of the involved chemical reactions leading to the formation of an expansive reaction product, i.e., the swollen gel, and the mechanical damage caused by this formation. Whereas the kinetics are crucial for determining present reaction extent and future expansion potential of the material the mechanical damage is important to give

a realistic description of the material and structural degradation of ASR-affected structures. Presently only few models tend to include both aspects." In the present work, an effort is made to describe the ageing behavior of concrete with the help of a parameter called degradation index. The hygro-chemo-mechanical approach to describe the aging of concrete involves modeling of amorphous gel and water combination process and chemo-mechanical material swelling. The amorphous gel and the chemo-mechanical swelling lead to the formation of porosity in concrete which in turn reduces its strength. The detailed description of the gel formation and other mechanisms are well described in the work of Steffens et al. (2003).

The total porosity of the concrete is considered to be the key factor in determining the effect of chemical and mechanical degradation. A parameter called degradation index (Gogoi and Maity, 2007) has been considered to estimate the interaction effects of hygro-chemo-mechanical actions. The total porosity $\phi$ is defined as the sum of the initial porosity, $\phi_0$ the porosity due to matrix dissolution, $\phi_c$ and the apparent mechanical porosity, $\phi_m$. Bangert et al. (2003) and Kuhl et al. (2004) has suggested the following relationships to relate these parameters

$$\phi = \phi_0 + \phi_c + \phi_m \tag{3.39}$$

Another parameter called the apparent mechanical porosity $\phi_m$ considers the influence of mechanically induced micro-pores and micro-cracks on the macroscopic material properties of the porous material. The parameter $\phi_m$ is obtained as

$$\phi_m = \left[1 - \phi_0 - \phi_c\right] d_m \tag{3.40}$$

Here, $d_m$ is the scalar degradation index. The strain based exponential degradation function (Gogoi and Maity, 2007) is as follows

$$d_m = a_s - \frac{\kappa^0}{\kappa}\left[1 - \alpha_c + \alpha_c\, e^{\left(\beta_c\left[\kappa^0 - \kappa\right]\right)}\right] \tag{3.41}$$

where,

$\kappa^0$ = a variable representing the initial degradation status

$\kappa$ = a variable representing the current degradation status

$a_s, \alpha_c$ and $\beta_c$ are the material parameters.

Both $\kappa^0$ and $\kappa$ depend on the loading history of the material. $\kappa^0$ is given by $f_t$ /$E_0$, where $f_t$ is the static tensile strength and $E_0$ is the elastic modulus of the non-degraded material before any mechanical loading is applied. The value of $d_m$ at any age can be obtained from Eq. (3.41). It can be observed that $d_m$ is dependent on the factor $\kappa$ which depends on the mechanical loading history. For no degradation due to mechanical loading, the value of $\kappa$ may be considered equal to $\kappa^0$ (i.e. $\kappa^0 = \kappa$). Also, in case of no degradation caused by mechanical loading, $\phi_m$ is considered to be zero (i.e. $\phi_m$ = 0). Bangert et al. (2003) outlined the procedure to calculate the values of the mechanical parameters $\alpha_c$ and $\beta_c$. In Eq. (3.41), the value of $a_s$ is considered to lie between 1.0 and 0.0 indicating complete and no degradation (Simo and Ju, 1987) respectively.

To study the effect of time on the process of degradation, the work by Atkin (1994) has been followed. A new parameter $\varsigma$ is introduced to account for the effect of ageing process as a function of time. The value of $\varsigma$ is zero for a freshly laid concrete and $\varsigma = 1$ for a concrete in fully aged condition. The kinetic law of ageing is stated as

$$\dot{\varsigma} = \frac{1}{\tau_a}(1-\varsigma)_m \tag{3.42}$$

The term $\dot{\varsigma}$ represents time derivative of $\varsigma$ and $\tau_a$ is the characteristic time or hygro-chemo-mechanical (HCM) design life of the ageing process, which can be assumed to be the design life of the structure. Integrating Eq. (3.42) with respect to time, the following expressions will be obtained:

$$1-\varsigma = e^{(-\frac{t}{\tau a})} \tag{3.43}$$

Replacing $\varsigma$ with degradation index $d_g$ in Eq. (3.43), variation of degradation index with time can be given as

$$d_g = 1-e^{(-\frac{t}{\tau a})} \tag{3.44}$$

The reaction extent $\xi_\gamma$, for the corresponding characteristic time, $\tau_r$ at constant ambient temperature is given by the following equation as suggested by Steffens et al. (2003).

$$\xi_\gamma = 1 - e^{\left(-\frac{t}{\tau r}\right)} \tag{3.45}$$

Substituting $t$ from Eq. (3.45) in Eq. (3.44) we get the following relation,

$$1 - d_g = (1 - \xi_\gamma)^{\frac{\tau r}{\tau a}} \tag{3.46}$$

The relation between degraded elastic modulus due to porosity of concrete, $E_m$ and the elastic modulus of concrete considering strength gain at a particular age, $E_0$ is given as

$$E_m = (1\text{-}d_g)E_0 \tag{3.47}$$

In order to get the variation of degradation with respect to time, the dimensionless value of total porosity is obtained by multiplying the scalar degradation variable and substituted as reaction constant.

$$E_m = (1 - \phi)^{\frac{t_a}{\tau a}} E_0 \tag{3.48}$$

where $\tau_a$ = the characteristic age or HCM design life for which the structure is designed

$t_a$ = The time corresponding to which degradation index is required

After obtaining the value of degraded elastic modulus $E_m$ from Eq. (3.48), the isotropic degradation index $d_g$ can be determined from the following equation.

$$d_g = 1 - \frac{E_m}{E_0} \tag{3.49}$$

### *3.4.4.2 Gain in Compressive Strength with Age*

Washa, Saemann and Cramer (1989) carried out a series of tests to find out the rate of gain of compressive strength of concrete made in 1937. A curve fitting analysis is carried out to fit these experimental data to obtain a relationship between the gain of compressive strength of concrete with the passage of time. Various concrete specimens of different proportions were moist cured for 28 days before placing it in the outdoor environment on a level ground inside an uncovered cage. The concrete specimens were left in the open to go through harsh weather conditions. They were subjected to cycles of freezing and thawing in each winter and an annual precipitation of snowfall of 0.813 m in an ambient

temperature variation between -32.0°C and 35.0°C.

In engineering problems, an experiment produces a set of data points $(x_1, y_1)$, …., $(x_n, y_n)$, where the abscissas $\{x_k\}$ are distinct. It is often our objective to relate these data with the help of a mathematical function. While choosing the particular mathematical function for the curve fitting of the experimental data sets, the physical behaviour of the system should be kept in mind i.e. the mathematical function should be comprised of physically meaningful parameters. In the present case, we seek to suggest a mathematical function relating the time in years with the compressive strength of concrete. While expressing these experimental data by a mathematical function of the form $y = f(x)$ , some errors are inevitable which may originate from the test conditions of the experiments as well as human or any other errors which can not be accounted for. Therefore, the actual value $f(x_k)$ (Mathews 2001) satisfies

$$f(x_k) = y_k + e_k \tag{3.50}$$

where $e_k$ is the measured error. Some of the methods that can determine how far the curve $y_{ls} = f(x)$ lies from the data are:

$$\left.\begin{array}{ll} \text{Maximum error:} & E_\infty(f) = \max\limits_{1\le k\le N'}\left\{\left|f(x_k) - y_k\right|\right\} \\ \text{Average error:} & E_1(f) = \dfrac{1}{N'}\sum\limits_{k=1}^{N'}\left|f(x_k) - y_k\right| \\ \text{Root-mean-square error:} & E_2(f) = \left[\dfrac{1}{N'}\sum\limits_{k=1}^{N'}\left|f(x_k) - y_k\right|^2\right]^{1/2} \end{array}\right\} \tag{3.51}$$

The *best fit* line passing through these experimental data points is found by minimizing any of quantities expressed in Eq. (3.51) with respect to a particular function *f(x)*. Among the three different error measures expressed in Eq. (3.51), the root mean square error minimization $E_2(f)$ is more popular because it is easy to minimize computationally. The *least squares line* is the line that minimizes the root-mean-square error $E_2(f)$. The assumed function for this purpose may be of the form

$$y_s = f(x) = Ax + B \tag{3.52}$$

In the above equation, $A$ and $B$ can be determined from $N'$ sets of experimental data as follows:

$$A = \frac{\sum_{k=1}^{N'} x_k y_k}{\sum_{k=1}^{N'} x_k} \quad , \quad B = \frac{\sum_{k=1}^{N'} y_k}{N'} - A\frac{\sum_{k=1}^{N'} x_k}{N'} \tag{3.53}$$

For the present work, the fifty years of compressive strength data set corresponds to a concrete specimen of mixed proportion 1:2.51:5.34 (cement : sand : gravel by weight) with water cement ratio of 0.49. Here, the following forms are considered for curve fitting:

$$\left.\begin{array}{ll} \text{I.} & y = C'e^{A\ln x} \\ \text{II.} & y = C'x^{A} \\ \text{III.} & y = C'xe^{A\ln x} \end{array}\right\} \tag{3.54}$$

In the above expression, $C' = e^B$ and $D' = -A$. Data linearization is carried out by transforming points $(x_k, y_k)$ in the $xy$ plane by the operation $(X_k, Y_k) = (\ln(x_k), \ln(y_k))$ in the XY plane for curve I and curve II. In case of curve III, the transformation operation carried out is $(X_k, Y_k) = (\ln(x_k), \ln(y_k/x_k))$ in the XY plane. Then the least squares line is fitted to the points $\{(X_k, Y_k)\}$ to give the predicted results. The predicted results using the above expressions (Eq. 3.54) are plotted in Fig. 3.2. Having attempted curve fitting for fifty year's data of concrete compressive strength with time, following equations are arrived at:

$$f(t) = 43.47e^{0.08\ln t} \tag{3.55}$$

$$f(t) = 43.47t^{0.08} \tag{3.56}$$

$$f(t) = 43.47te^{-0.92\ln t} \tag{3.57}$$

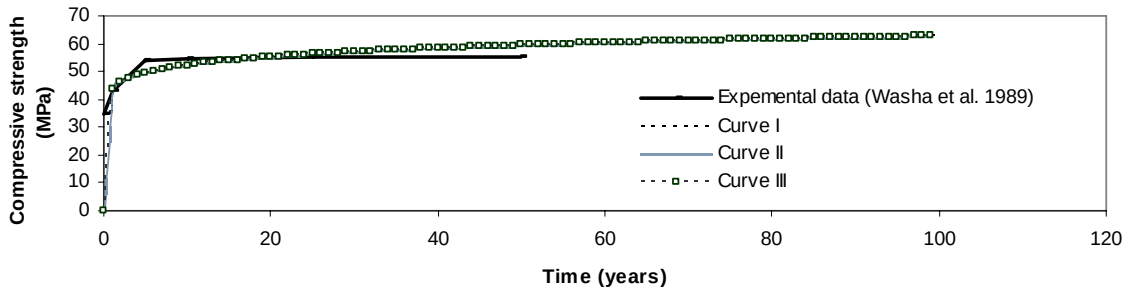


Fig. 3.2 Curve fitting of 50 years of concrete compressive strength

The values of compressive strength obtained are in SI units and $t$ is the age of concrete in years. Equation (3.55) has been obtained by carrying out a least square analysis using a curve of the form $y = C'e^{A \ln x}$ with the necessary transformation of the coordinates as mentioned before. In this case, the values of $C$ and $A$ obtained are 43.47 and 0.08 respectively. Equation (3.56) has been obtained by carrying out a least square analysis using a curve of the form $y = C'x^{A}$ with the necessary transformation of the coordinates as mentioned before. In this case also, the values of $C$ and $A$ obtained are 43.47 and 0.08 respectively. Equation (3.57) has been obtained by carrying out a least square analysis using a curve of the form $y = C'xe^{A \ln x}$ with the necessary transformation of the coordinates as mentioned before. In this case also, the values of $C$ and $A$ obtained are 43.47 and –0.92 respectively. From Fig. 3.2, it can be noticed that the results obtained from Eq. (3.55), Eq. (3.56) and Eq. (3.57) are all similar and these results agree quite well with the experimental data. Since the results obtained from Eq. (3.55), Eq. (3.56) and Eq. (3.57) are almost identical, Eq. (3.56) (as shown by curve II in Fig. 3.2) is chosen for all the further analyses carried out in this work. This choice is done keeping in mind the ease of use and the apparent simplicity of an equation. In the present analysis, Eq. (3.56) has been used to predict the gain of concrete strength with age. The value of static elastic modulus of concrete in SI units (Neville and Brooks, 1987) is obtained from

$$E_0 = 4733\sqrt{f(t_a)} \tag{3.58}$$

## 3.5 STIFFNESS, MASS AND DAMPING MATRICES

The dynamic response of a structure may be derived by minimizing the work of internal, inertial and viscous forces for any small kinematically admissible motion. Using Hamilton's principle for dynamic problems, we can write

$$\int_{t_1}^{t_2} (T - V)dt = 0 \tag{3.59}$$

where $T$ is the total kinetic energy of the system and $V$ is the potential energy of the applied forces. The variable $t$ represents time dimension. Using $q_1$, $q_2$,……, $q_n$ as the generalized coordinates and assuming they are independent, the Euler-Lagrange equations then yield well-known *Lagrange* equation of motion, given as follows in terms

of the Lagrangian $L = T - V$ :

$$\frac{d}{dt}\left(\frac{\partial L}{\partial q_i}\right) - \frac{\partial L}{\partial q_i} = 0 \qquad i = 1,2,.....,n \tag{3.60}$$

To develop Hamilton's principle for continuum from the method of virtual work, D'Alembert principle is employed, which sets forth Newton's law in the following form:

$$\mathbf{F} - \mathbf{ma} = \mathbf{0} \tag{3.61}$$

The vector $-\mathbf{ma}$ is considered a force, with the result that the above equation has a form that corresponding to the equation of statics. For a continuous deformable body the inertia force for the D'Alembert principle is given as $-\boldsymbol{\rho}\dfrac{\mathbf{d^2u}}{\mathbf{dt^2}}$ and is force acting over the entire body. A virtual displacement field $\delta u_i$ at a particular time instant $t$ for a dynamic system can be represented as follows

$$-\iiint_V \rho \frac{d^2 u_i}{dt^2}\delta u_i dv + \iiint_V B_i \delta u_i dv + \iint_S T_i^{(v)} \delta u_i dS = \iiint_V \tau_{ij}\delta\varepsilon_{ij} dv \tag{3.62}$$

The force potential $V$ may be represented as follows

$$V = -\iiint_V B_i u_i dv - \iint_S T_i^{(v)} u_i dS \tag{3.63}$$

where $B_i$ and $T_i^{(v)}$ are the external body loads such that there is overall equilibrium for the body from the viewpoint of rigid body mechanics. The forces $B_i$ and $T_i^{(v)}$ are assumed to be statically compatible. Having included the effect of point loads $\{p\}_i$ , Eq. (3.62) may be expressed in matrix form as follows

$$-\iiint_v \rho\{\delta u\}^T\{\ddot{u}\}dv + \iiint_v \{\delta u\}^T\{b\}dv + \oiint_s \{\delta u\}^T\{T\}dA + \sum_{i=1}^{n}\{\delta u_i\}^T\{p\}_i = \iiint_v \{\delta\varepsilon\}^T[\sigma]dv \tag{3.64}$$

The formulation to include energy dissipation introduces the term $\delta W_{diss}$ which is as follows

$$\delta W_{diss} = \delta\left(\iiint_V \{u\}^T\{f\}dv\right) \tag{3.65}$$

where $\{f\}$ is the dissipation force vector per unit volume. For the case of viscous damping $\{f\}$ is proportional to the velocity. Therefore, it can be said

$$\{f\} = c\{\dot{u}\} \tag{3.66}$$

After dividing the body into small finite elements and considering the

displacement field $\{u\}$ as a function of nodal displacements $\{q\}$and interpolation functions $N_i$, we have

$$u = N_i q_i \tag{3.67}$$

Also, the spatial coordinate of any point inside the body is expressed in terms of each nodal coordinates as follows

$$x = N_i x_i \tag{3.68}$$

The strain field $\{\varepsilon\}$and the stress field $\{\sigma\}$are expressed as follows

$$\{\varepsilon\} = [B]\{q\} \tag{3.69}$$

$$\{\sigma\} = [D]\{\varepsilon\} \tag{3.70}$$

By including the viscous damping, Eq. (3.65) can be expressed as follows

$$\begin{aligned} &-\iiint_v \{\delta q\}^T [N]^T [N]\{\ddot{q}\}dv + \iiint_v \{\delta q\}^T [N]^T \{b\}dv + \oiint_S \{\delta q\}^T [N]^T \{T\}dA \\ &+ \sum_{i=1}^{n} \{\delta q\}^T \{p\}_i - \iiint_v \{\delta q\}^T [N]^T c[N]\{\dot{q}\}dv = \iiint_v \{\delta q\}^T [B]^T [D][B]dv \end{aligned} \tag{3.71}$$

Equation (3.71) may be written in the following manner

$$\{\delta q\}^T ([K]\{q\} + [M]\{\ddot{q}\} + [C]\{\dot{q}\}) = \{\delta q\}^T \{f\} \tag{3.72}$$

Where

$$[K] = \iiint_V [B]^T [D][B]dv \tag{3.73}$$

$$[M] = \iiint_V [N]^T [N]dv \tag{3.74}$$

$$[C] = \iiint_V [N]^T c[N]dv \tag{3.75}$$

$$\{f\} = \iiint_v [N]^T \{b\}dv + \oiint_S [N]^T \{T\}dA + + \sum_{i=1}^{n} \{\delta q_i\}^T \{p\}_i \tag{3.76}$$

The matrices $[K]$, $[M]$, $[C]$ and $\{f\}$ represents stiffness matrix, mass matrix, damping matrix and force vector respectively. Finally, the dynamic equation of equilibrium may be expressed as follows

$$[M]\{\ddot{q}\} + [C]\{\dot{q}\} + [K]\{q\} = \{f\} \tag{3.77}$$

Having used a suffix *d* to identify the domain of concrete gravity dam, Eq. (3.77) can be represented as follows

$$[M]\{\ddot{q}_d\} + [C]\{\dot{q}_d\} + [K]\{q_d\} = \{f_d\} \tag{3.78}$$

where $\{q_d\}, \{\dot{q}_d\}$ and $\{\ddot{q}_d\}$ denotes the displacement, velocity and acceleration of any point inside the dam body. The vector $\{f_d\}$ represents the applied external forces on the structure of the dam. The area integral is computed using Gauss quadrature technique. The elemental area in Cartesian coordinates may be expressed in terms of natural coordinate as

$$dA = dx\,dy = |J|\,d\xi\,d\eta \tag{3.79}$$

Damping is a mechanism which dissipates energy, causing the amplitude of free vibration to decay with time. The various types of damping which influences structural dynamical behavior are viscous damping, hysteresis damping, radiation damping etc. Viscous damping exerts force proportional to velocity, as exhibited by the term $c\dot{u}$ (in case of a 1D problem). A formulation for this kind of problem was developed by Rayleigh (1894). In this case, the energy dissipated is proportional to frequency and to the square of amplitude. Viscous damping is provided by surrounding gas or liquid or by the viscous damper attached to the structure. Radiation damping refers to energy dissipation to a practically unbounded medium, such as soil that supports structure. Among the various types of physical damping, viscous damping is easy to represent computationally in dynamic equations. Fortunately, damping in structural problems is usually small enough regardless of its actual source; its effect on structural response is modeled well by regarding it as viscous. "Small enough" usually means that damping forces $[C]\{\dot{q}\}$ are less than 10% of the other forces in Eq. (3.77). The *Rayleigh damping* , defines the global damping matrix $[C]$ as a linear combination of the global mass and stiffness matrices.

$$[C] = \alpha'[M] + \beta'[K] \tag{3.80}$$

where $\alpha'$ and $\beta'$ are the stiffness and mass proportional damping constants respectively. The relationship between the fraction of critical damping ratio, $\xi$, $\alpha$ and $\beta$ at frequency $\omega$ is given by

$$\xi = \frac{1}{2}\left(\alpha\omega + \frac{\beta}{\omega}\right) \tag{3.81}$$

Damping constants $\alpha'$ and $\beta'$ are determined by choosing the fractions of critical damping ( $\xi_1'$ and $\xi_2'$ ) at two different frequencies ( $\omega_1$ and $\omega_2$ ) and solving simultaneously as follows

$$\left.\begin{aligned}\alpha' &= \frac{2\omega_1\omega_2\left(\xi_2'\omega_2 - \xi_1'\omega_1\right)}{\left(\omega_2^2 - \omega_1^2\right)} \\ \beta' &= \frac{2\left(\xi_1'\omega_2 - \xi_2'\omega_1\right)}{\left(\omega_2^2 - \omega_1^2\right)}\end{aligned}\right\} \qquad (3.82)$$

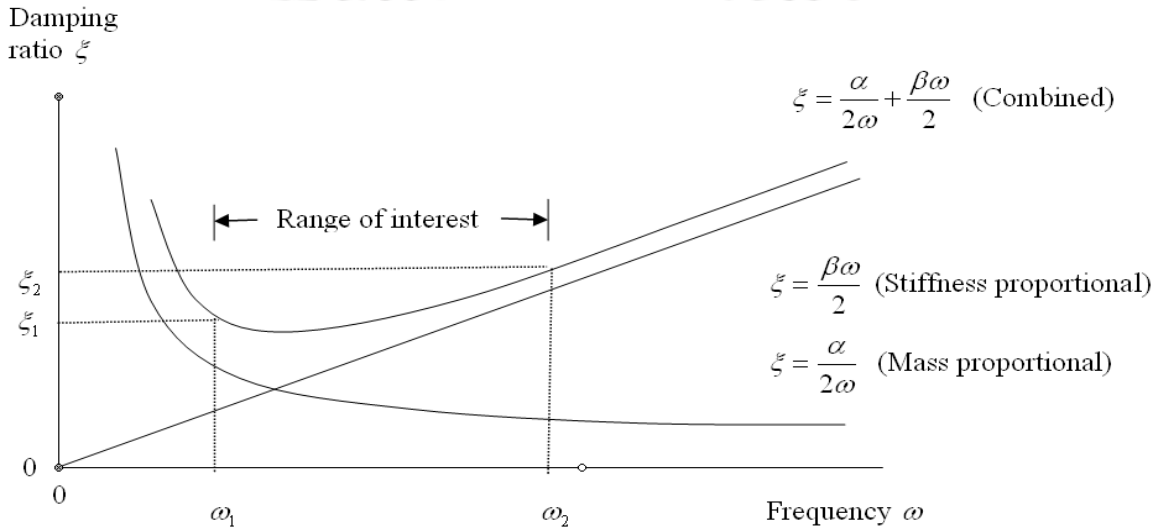


Fig. 3.3 Fraction of critical damping for the proportional-damping scheme

This equation makes damping frequency dependent, as shown in Fig. 3.3. An important property of proportional damping is that vibration modes are orthogonal with respect to the global damping matrix $[C]$. Therefore, the set of coupled equations, as expressed by Eq. (3.77) can be transformed to a set of uncoupled equations. In computational analyses damping can be determined either by phenomenological or spectral damping methods. In the phenomenological approach, the actual physical dissipative mechanism is modelled in details. In the spectral method, viscous damping is introduced as a specified fraction of critical damping. This specific fraction may be determined from (i) experimental observations of vibratory response of the structure; (ii) as a function of frequency; or (iii) a single damping fraction for entire frequency range of a structure.

### 3.5.1 Computation of Stresses

In finite element analysis, once the nodal displacements of an element are obtained, the stresses {σ} can be calculated as

$$\{\sigma_e\} = [D][B_0]\{q_e\} \tag{3.83}$$

where [$D$] is the constitutive matrix, [$B_0$] is the strain displacement matrix, {$\sigma_e$} is the elemental stress vector and {$q_e$} is the elemental displacement vector. The stresses {$\sigma_e$}at any point inside an element are estimated by interpolating the stresses obtained at sampling points. Unfortunately, while determining the stresses at the nodal points, it has been found that they are discontinuous in nature. Efforts to calculate stresses directly at the nodal points have proved them to be very bad sampling points (Zienkiewicz and Taylor 1991), though the nodes are most useful points for output and interpretation of stresses. However, it has been observed that shape function derivatives (and hence stresses) evaluated at the interior of the element is more accurate than those calculated on the element boundary. For two dimensional isoparametric elements, the 2 × 2 Gauss points have been found out to be the optimal sampling points (Barlow, 1976). Hinton and Campbell (1974) have shown how to extrapolate stresses obtained at the Gauss points to the nodal points by using "smoothing" technique.

In finite element analysis, the stresses are computed at four Gauss points (I, II, III and IV) of an element as shown in Fig. 3.4. For example, at point III, $r = s = 1$ and $\xi = \eta = 1/\sqrt{3}$. Therefore, the factor of proportionality is $\sqrt{3}$ ; *i.e.*,

$$r = \xi\sqrt{3} \text{ and } s = \eta\sqrt{3} \tag{3.84}$$

Stresses at any point $P$ in the element are found by the usual shape function equation as

$$\sigma_P = \sum N'_{di}\sigma_i \text{ for } i = 1,2,3,4 \tag{3.85}$$

Where

$$N'_{di} = \frac{1}{4}(1 \pm rr_i)(1 \pm ss_i) \tag{3.86}$$

In the above equation, $\sigma_P$ is $\sigma_x, \sigma_y$ and $\tau_{xy}$ at point $P$. $\sigma_i$ represents $\sigma_{xx}, \sigma_{yy}$ and $\tau_{xy}$ calculated at the nodal points. $N'_{di}$ are evaluated at $r$ and $s$ coordinates of point $P$. Let the point $P$ coincides with the corner 1. To calculate stress $\sigma_{x1}$ at corner 1 from

$\sigma_x$ values at the four Gauss points, substitution of $r$ and $s$ into the shape functions will give

$$\sigma_{xI} = 1.8666\sigma_{xI} - 0.500\sigma_{xII} + 0.134\sigma_{xIII} - 0.500\sigma_{xIV} \tag{3.87}$$

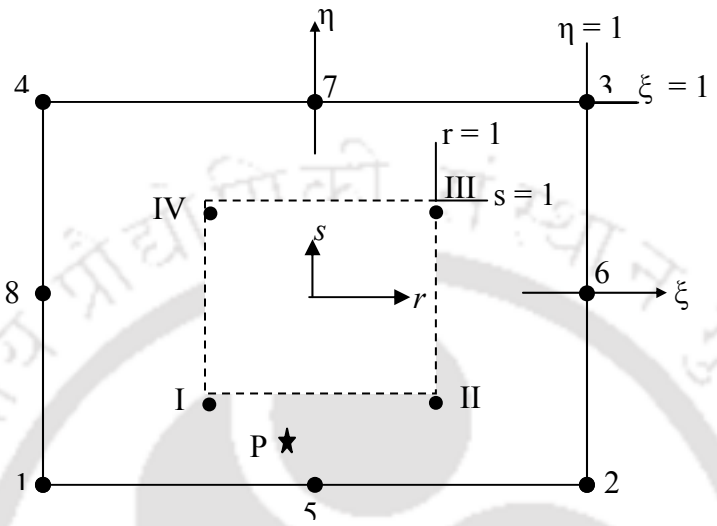


Fig. 3.4 Natural coordinate systems used in extrapolation of stresses from Gauss points

By using the "local stress technique" proposed by Hinton and Campbell (1974), one can find out the nodal point stresses by averaging the stresses obtained at the Gauss points. The resultant extrapolation or transformation matrix may be obtained following least square fit to get the smoothed corner node stresses.

$$\begin{bmatrix} \sigma_1 \\ \sigma_2 \\ \sigma_3 \\ \sigma_4 \\ \sigma_5 \\ \sigma_6 \\ \sigma_7 \\ \sigma_8 \end{bmatrix} = \begin{bmatrix} (1+\sqrt{3}/2) & -0.5 & (1-\sqrt{3}/2) & -0.5 \\ -0.5 & (1+\sqrt{3}/2) & -0.5 & (1-\sqrt{3}/2) \\ (1-\sqrt{3}/2) & -0.5 & (1+\sqrt{3}/2) & -0.5 \\ -0.5 & (1-\sqrt{3}/2) & -0.5 & (1+\sqrt{3}/2) \\ (1+\sqrt{3})/4 & (1+\sqrt{3})/4 & (1-\sqrt{3})/4 & (1-\sqrt{3})/4 \\ (1-\sqrt{3})/4 & (1+\sqrt{3})/4 & (1+\sqrt{3})/4 & (1-\sqrt{3})/4 \\ (1-\sqrt{3})/4 & (1-\sqrt{3})/4 & (1+\sqrt{3})/4 & (1+\sqrt{3})/4 \\ (1+\sqrt{3})/4 & (1-\sqrt{3})/4 & (1-\sqrt{3})/4 & (1+\sqrt{3})/4 \end{bmatrix} \begin{Bmatrix} \sigma_I \\ \sigma_{II} \\ \sigma_{III} \\ \sigma_{IV} \end{Bmatrix} \tag{3.88}$$

Here $\sigma_1$, $\sigma_2$ ……., $\sigma_8$ are the smoothened nodal values and $\sigma_I \ldots \sigma_{IV}$ are the stresses at the Gauss points. The smoothened stress resultants are then modified by finding the average of resultants of all elements meeting at a common node.

## 3.6 HYDRODYNAMIC PRESSURE OF THE RESERVOIR

Figure 3.5 describes the geometry of dam and adjacent reservoir. Assuming the reservoir water to be inviscid and incompressible and its motion to be of small amplitude, the governing equation for hydrodynamic pressure is as follows (Westergaard, 1933):

$$\nabla^2 p = 0 \tag{3.89}$$

Here, $\nabla^2 = \frac{\partial^2}{\partial x^2} + \frac{\partial^2}{\partial y^2}$ and is called the Laplacian operator and $p$ is the hydrodynamic pressure. The solution of Laplace equation (Eq. 3.89) can be expressed in equation (3.90) with the following assumptions:

i. The bottom of the fluid domain is horizontal and rigid.
ii. The fluid-structure interface is vertical.
iii. The fluid domain extends to infinity and its motion is two dimensional.

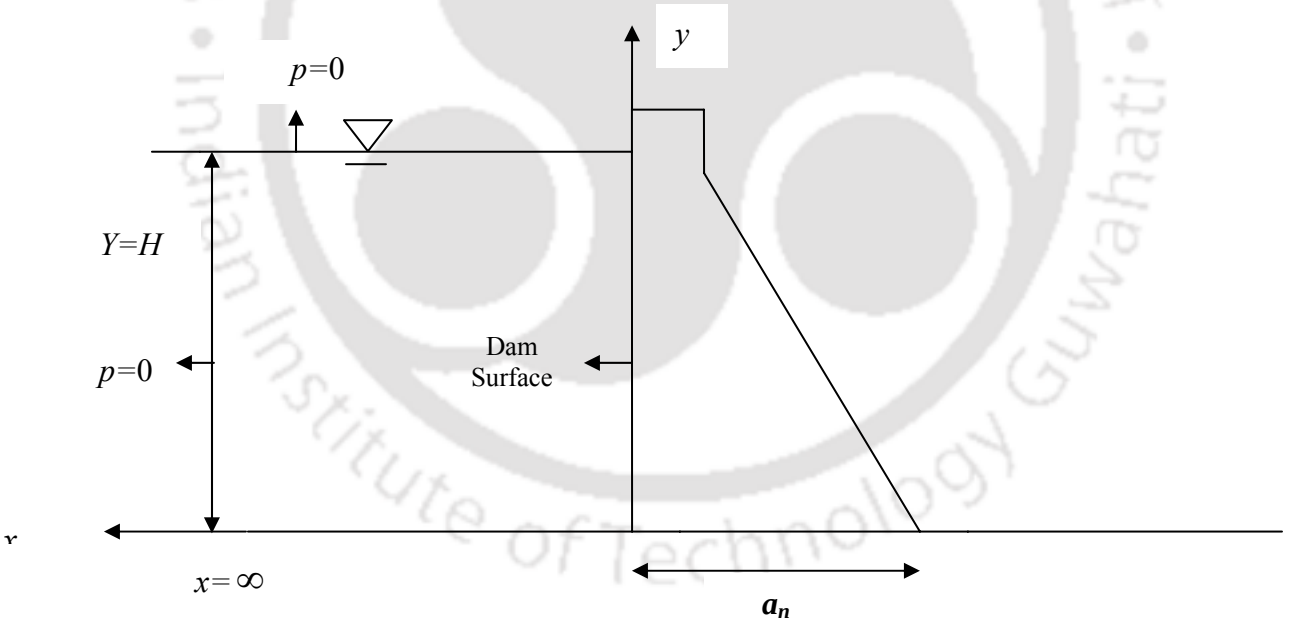


**Fig. 3.5 Geometry of the Reservoir Domain**

The solution is given by

$$p = 2a_n \rho H \sum_{n=1}^{\infty} \frac{(-1)^{n+1}}{\lambda_n^2} e^{\left(-\lambda_n \frac{x}{H}\right)} \cos\left(\lambda_n \frac{y}{H}\right) \tag{3.90}$$

where, $$\lambda_n = \frac{(2n-1)\pi}{2} \tag{3.91}$$

$p$ = Hydrodynamic pressure at the upstream face of the dam.

$a_n$ = The magnitude of acceleration normal to the upstream face of the dam.

$\rho$ = The mass density of water.

$H$ = The height of water at the upstream side of the dam.

$y$ = The variation of distance in the vertical direction.

The hydrodynamic pressure on the dam has been calculated using Eq. (3.91).

## 3.7 FLOWCHART FOR THE DAM ANALYZER

Fig. 3.6 shows a flowchart of the computer program built for the purpose of analyzing the concrete gravity dam with or without considering the effect of ageing under dynamic loading condition. If the original strength of concrete is considered for analyzing the dam body under dynamic loading, the original constitutive matrix is used. If the effect of concrete ageing is to be modeled, the reduced constitutive matrix is determined which is a function of isotropic degradation index. Having determined the reduced/degraded constitutive matrix, the load vector is calculated considering the effect of earthquake loading, hydrodynamic and hydrostatic load and gravity loading etc. After that, Newmark integration is carried out to solve the dynamic equation of motion.

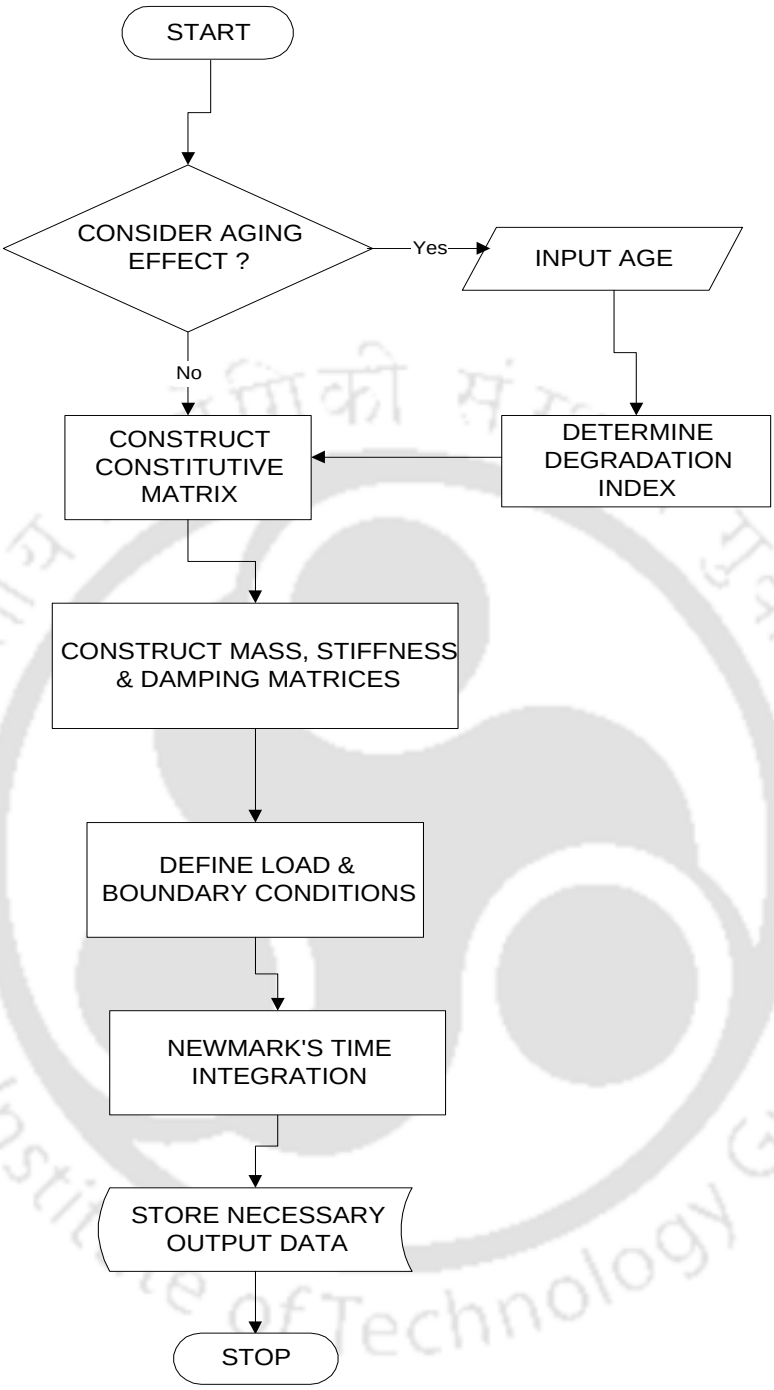


**Fig. 3.6 Flowchart for the dam analyzer with or without considering the effect of concrete degradation**

## ***PART B***

# 3.8 THEORETICAL FORMULATION FOR FOUNDATION

The foundation of the concrete gravity dam has been assumed to be made of rock material. In the present formulation, the nonlinear stress-strain behavior of the rock material has been taken into consideration. The material is also assumed to undergo small displacements when subjected to any kind of loading.

## 3.8.1 Governing Differential Equation for Foundation Domain

In the present work, the foundation domain is analyzed by using finite element method. The foundation domain is discretized by using solid 8 noded isoparametric elements. The formulation for the foundation domain will be essentially similar to that of the structural domain. Therefore the formulation shown in the section 3.2.6 will apply to the foundation domain as well. Having started from Eq. (3.65), the formulation yields Eq. (3.80) which will be used for calculation of displacements, stresses and strains in this domain under the small strain/deformation assumption. We can express the governing differential equation for the foundation as follows

$$[M]\{\ddot{q}_f\}+[C]\{\dot{q}_f\}+[K]\{q_f\}=\{f_f\} \tag{3.92}$$

where $\{q_f\}, \{\dot{q}_f\}$ and $\{\ddot{q}_f\}$ denotes the displacement, velocity and acceleration of any point inside the foundation domain. The vector $\{f_f\}$ represents the applied external forces on the foundation.

## 3.8.2 Constitutive Property for Soil/Rock Material

Constitutive models can be used to describe the stress-strain behavior of soils during numerical calculation of displacements, stresses and strains. They can provide a framework for understanding how soil will behave under different loading conditions, and they can be implemented in the finite element and finite difference codes for use in numerical analyses. In complex loading conditions, such as the foundation-structure-foundation interaction, the use of a proper constitutive model is necessary to make

numerical predictions of soil will deform and transfer stresses. There are many published constitutive models in the literature of varying levels of complexity. Published literature is reviewed to identify important aspects of choosing a constitutive model that would be applicable to soil-structure interaction system.

The stress-strain behavior of soil mass is essentially nonlinear. The nonlinearity significantly influences the behavior of any structure-foundation-soil system. In most of the early investigations into soil-structure interaction phenomena, it is assumed that the stress-strain response of the soil mass is linear, particularly because the solution is then achieved in a single step. In this study, an attempt is made to account for actual nonlinear behaviour of the soil obtained from triaxial test data.

Due to the generality of the hyperbolic model and its ability to represent the stress-strain behaviour of soil ranging from clays and silts through sands, gravels and rockfills, it can be used for partly saturated or fully saturated soils, and either for drained or undrained loading conditions in compacted earth materials or naturally occurring soils (Duncan, 1980). Duncan (1994) also states that simple elasticity models, such as hyperbolic model, can be applied for stable structures where deformations are small, orientation of stresses are constant, and for fully drained or undrained conditions. For accurate predictions of stress-strain behavior near failure and for undrained pore pressures due to application of total stress external loads, Duncan (1994) states that more complex elasto-plastic models, such as Cam-Clay model should be used. Hence, it is possible to make use of such a model in the nonlinear interactive analysis of structure-foundation rock interaction for predicting the behaviour of the structure. Moreover, its implementation with finite element software is not complex. The hyperbolic model described by Duncan and Chang (1970) is a nonlinear elastic constitutive model. Although, soils are inelastic, the model can simulate several important aspects of realistic soil behavior. By using a Young's modulus that is a function of stress level and confining pressure, and a bulk modulus that is a function of confining pressure, the model can simulate nonlinear stress-strain and stress dependency. A brief summary of the description given by Duncan et al (1980) is presented here.

The model uses a hyperbolic curve to represent the stress-strain behavior of a soil mass. The hyperbola is given by the following equation:

$$(\sigma_1 - \sigma_3) = \frac{\varepsilon}{\frac{1}{E_i} + \frac{\varepsilon}{(\sigma_1 - \sigma_3)_{ult}}} \tag{3.93}$$

where

$\varepsilon$ = Axial strain.

$\sigma_1, \sigma_3$ = Major and minor principal stresses respectively.

$(\sigma_1 - \sigma_3)_{ult}$ = Asymptotic value that the hyperbola approaches.

$E_i$ = Initial slope of the stress-strain curve.

$E_i$ is related to the confining pressure by:

$$E_i = KPa\left(\frac{\sigma_3}{Pa}\right)^n \tag{3.94}$$

Where $K$ is the modulus number, $n$ is the modulus exponent, and $Pa$ is the atmospheric pressure. $(\sigma_1 - \sigma_3)_{ult}$ can be related to the soil by the following equation:

$$R_f(\sigma_1 - \sigma_3)_{ult} = (\sigma_1 - \sigma_3)_f \tag{3.95}$$

where $R_f$ is the failure ratio and $(\sigma_1 - \sigma_3)_f$ is the strength of the soil mass. The strength of the soil mass can be expressed in terms of the Mohr-Coulomb failure criterion by the following equation:

$$(\sigma_1 - \sigma_3)_f = \frac{2cCos\phi + 2\sigma_3 Sin\phi}{1 - Sin\phi} \tag{3.96}$$

Here, $c$ = Cohesion of soil/rock material.

$\phi$ = Angle of internal friction for soil/rock material.

The current stress state can be defined by the stress level, *SL*, given by:

$$SL = \frac{(\sigma_1 - \sigma_3)}{(\sigma_1 - \sigma_3)_f} \tag{3.97}$$

The above equations can be combined to produce the following equation for the Tangent Young's modulus, $E_t$ as suggested by Duncan and Chang (1970).

$$E_T = \left[1 - \frac{R_f(1 - \sin\phi)(\sigma_1 - \sigma_3)}{2(C\cos\phi + \sigma_3 \sin\phi)}\right]^2 E_i \tag{3.98}$$

For unloading and reloading, the model uses a different Young's modulus, $E_{ur}$, that is related to confining pressure by:

$$E_{ur} = K_{ur} Pa \left( \frac{\sigma_3}{Pa} \right)^n \tag{3.99}$$

Where only the new parameter is $K_{ur}$ which is the unloading-reloading modulus number. The volume change characteristics are defined by a bulk modulus, $B$, that is related to confining pressure by:

$$B = K_b Pa \left( \frac{\sigma_3}{Pa} \right)^m \tag{3.100}$$

Where $K_b$ the bulk modulus number and $m$ is the bulk modulus exponent. However, for the present analysis, only the Young's modulus of the rock material is varied according to Eq. (3.98). The Posisson's ratio is kept constant throughout the analysis. The value of failure ratio is taken to be 0.80 (Bose and Das, 1997).

### 3.8.3 Nonlinear Solution Algorithm

The average acceleration method for solution of dynamic equation of motion for nonlinear response is adopted here (Chopra, 2007). Because the stiffness matrix is altered at each time step, it is important to take care of the fact that the load equilibrium is achieved at each time step. For that purpose, the modified Newton-Raphson method is employed. The details of the algorithm may be found in the chapter 15 of book by Chopra (2007).

## 3.9 BOUNDARY CONDITIONS FOR FOUNDATION DOMAIN

One of the biggest problems in dynamic soil-structure interaction problems in infinite media is related to the modeling of domain boundaries. Because of limited computational resources the computational domain needs to be kept small enough so that it can be analyzed in a reasonable amount of time. By limiting the domain however an artificial boundary is introduced. As an accurate representation of the soil-structure system this boundary has to absorb all out-going waves and reflect no waves back into the

computational domain. The most commonly used types of domain boundaries are presented in the following section.

### 3.9.1 Fixed or Free Boundary

By fixing all degrees of freedom on the domain boundaries any radiation of energy away from the structure is made impossible. Waves are fully reflected and resonance frequencies can appear that don't exist in reality. The same happens if the degrees of freedom on a boundary are left 'free', as at the surface of the soil. A combination of free and fully fixed boundaries should be chosen only if the entire model is large enough and if material damping of the soil prevents reflected waves to propagate back to the structure.

### 3.9.2 Absorbing Boundary

A way to eliminate waves propagating outward from the structure is to use Lysmer boundaries (1969) boundary condition. This method is relatively easy to implement in a finite element code as it consists of simply connecting dash pots to all degrees of freedom of the boundary nodes and fixing them on the other end. Lysmer boundaries are derived for an elastic wave propagation problem in a one-dimensional semi-infinite bar. It can be shown that in this case a dash pot specified appropriately has the same dynamic properties as the bar extending to infinity (Wolf, 1988).

One dimensional wave propagation – which by definition is local in time and space – can be used to develop the basis of frequency independent transmitting boundaries which are local in space and time. The semi – infinite prismatic rod is the simplest case and is used to derive the absorbing boundary condition for the propagating seismic waves. The radial effects are ignored. This boundary condition, first proposed by Lysmer and Kuhlemeyer (1969) has been used in the present work. The prismatic rod with area $A$, modulus of elasticity $E$, and mass density $\rho$ extending to infinity is shown in Fig. 3.7a. $F$ represents the axial force $u$ the axial displacement. Formulating equilibrium of the infinitesimal element carved out from the axial rod (Fig. 3.7b).

$$F_{,x}\,dx - \rho A dx\ddot{u} = 0 \tag{3.101}$$

Substituting the force-displacement relationship in the above equation

$$F = EAu_{,x} \tag{3.102}$$

Thus, we get the equation of motion

$$u_{,xx} - \frac{\ddot{u}}{c_l^2} = 0 \tag{3.103}$$

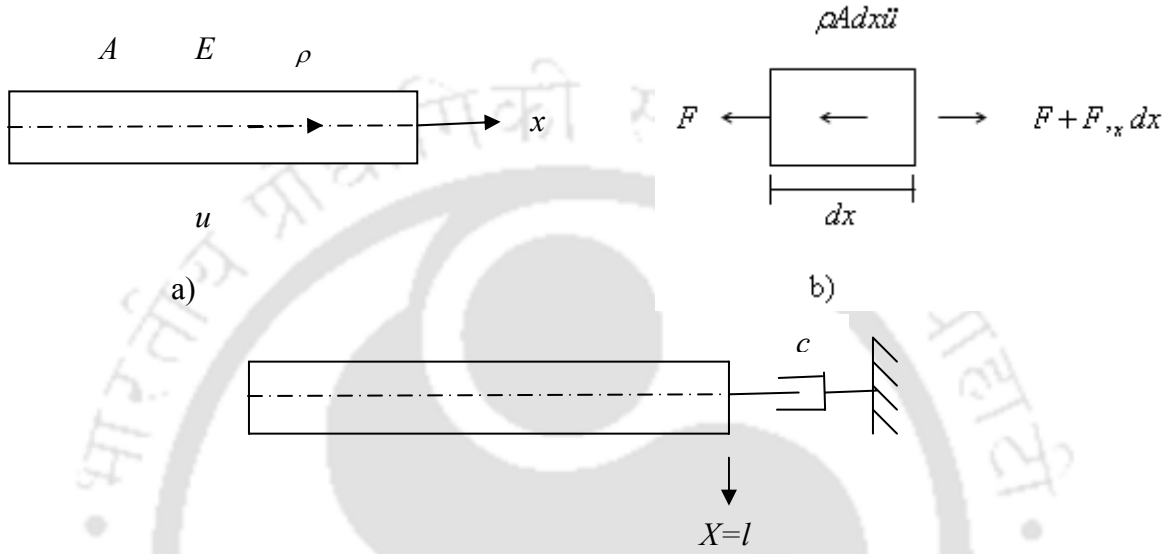


Fig. 3.7 a) Semi-infinite prismatic rod b) Equilibrium of infinitesimal element c) Viscous damper modeling truncating rod

where $c_l$ denotes the rod velocity as given by the following relationship

$$c_l = \sqrt{\frac{E}{\rho}} \tag{3.104}$$

The one dimensional wave equation (Eq. 3.103) can be integrated directly in the time domain after changing the variables $x, t$ to $\xi, \eta$.

$$\xi = t - \frac{x}{c_l} \tag{3.105}$$

$$\eta = t + \frac{x}{c_l} \tag{3.106}$$

Equation (3.103) may be transferred to

$$u_{,\xi\eta} = 0 \tag{3.107}$$

This can be integrated to give

$$u = f(\xi) + g(\eta) \tag{3.108}$$

or, $$u = f\left(t - \frac{x}{c_l}\right) + g\left(t + \frac{x}{c_l}\right) \tag{3.109}$$

where $f$ and $g$ are two arbitrary functions of their arguments. Equation (3.109) is the general solution to the one-dimensional homogenous wave equation. The function $f\left(t - \frac{x}{c_l}\right)$ represents a wave propagating in the positive $x$ direction with a velocity $c_l$, which keeps its original shape; The function $g\left(t + \frac{x}{c_l}\right)$ represents a wave traveling in the negative $x$ direction with the same features. The property of a transmitting boundary located on the artificial boundary $x = l$, described by a differential equation, is addressed next (Fig. 3.7c). When the incident wave $f$ encounters the artificial boundary, this wave must pass through it without any modification so it can continue propagating towards $x = +\infty$. No reflected wave g, which would propagate in the negative $x$ direction, may arise. This wave $f$ satisfies the boundary condition at $x = l$, but $g$ does not. Because the functions $f\left(t - x/c_l\right)$ and $g\left(t + x/c_l\right)$ differ by the signs of the $x/c_l$ terms in the arguments, a differentiation with respect to $x$ is appropriate. This involves a differentiation of $f$ and $g$ with respect to the argument – for instance, $f' = \frac{df\left(t - x/c_l\right)}{d\left(t - x/c_l\right)}$ which is equal to $f_{,x}$. The following differential equations can be obtained:

$$f_{,x} + \frac{\dot{f}}{c_l} = 0 \tag{3.110a}$$

$$g_{,x} + \frac{\dot{g}}{c_l} = 0 \tag{3.110b}$$

Selecting Eq. (3.110a), which is identically satisfied for $f$, as the boundary condition for $u$ at $x = l$ shown below

$$u_{,x}(x=l,t)+\frac{\dot{u}}{c_l}(x=l,t)=0 \tag{3.111}$$

results in $g=0$. This is easily verified by substituting Eq. (3.109) in Eq. (3.110) which leads to $g'=dg\left(t+x/c_l\right)\Big/d\left(t+x/c_l\right)=0$ at $x=l$. Equation (3.111) is also called radiation condition. The physical interpretation of the boundary condition at $x=l$ becomes apparent when Eq. (3.113) is multiplied by *EA*.

$$EAu_{,x}+\frac{EA}{c_l}\dot{u}=0 \tag{3.112a}$$

Or, after substituting Eq. (3.102) and Eq. (3.104),

$$F+c\dot{u}=0 \tag{3.112b}$$

where *c* represents the coefficients of viscous dashpot and is given by

$$c=A\rho c_l \tag{3.113}$$

Equation 3.112b represents equilibrium at the artificial boundary, involving the normal force of a viscous damper with a coefficient *c*, which replaces the part of the rod up to infinity (Fig. 3.7c) and absorbs the incident waves preventing any reflection. *c* is also called the impedance. Because *c* is independent of frequency, this transmitting boundary can be used directly for an analysis in the time domain.

The boundary condition is exact for one dimensional propagation of longitudinal waves. It can also be applied to the propagation of shear waves with the transverse displacement *w* in the rod, by replacing *E* by the shear modulus *G*, and $c_l$ by the shear wave velocity $c_s=\sqrt{\frac{G}{\rho}}$. The one dimensional wave equation then equals

$$w_{,xx}-\frac{\dot{w}}{c_s^2}=0 \tag{3.114}$$

Equation (3.111), (3.112) and (3.113) are transformed to

$$w_{,x}+\frac{\dot{w}}{c_s}=0 \tag{3.115}$$

$$Q+c\dot{u}=0 \tag{3.116}$$

$$c=A\rho c_s \tag{3.117}$$

where $Q$ denotes the transverse shear force. No distinction is made between the shear area and the rod's area. These concepts form the basis of the transmitting boundary consisting of such viscous dampers to approximately model the two and three dimensional cases.

### 3.9.2.1 Viscous Damper for Two Dimensions

For the one dimensional wave propagation in a prismatic rod, the exact transmitting boundary consists of a damper with a coefficient equal to the product of the area *A,* the mass density $\rho$, and either the rod velocity $c_l$ or shear wave velocity $c_s$ for shear waves (Eq. 3.113 and 3.117). Assuming that the waves – for example, in the two dimensional case (Fig. 3.8) – impinge at a right angle on the artificial boundary, the exact transmitting boundary condition is formulated as

$$\sigma(s) + \rho c_p \dot{u}(s) = 0 \tag{3.118}$$

$$\tau(s) + \rho c_s \dot{v}(s) = 0 \tag{3.119}$$

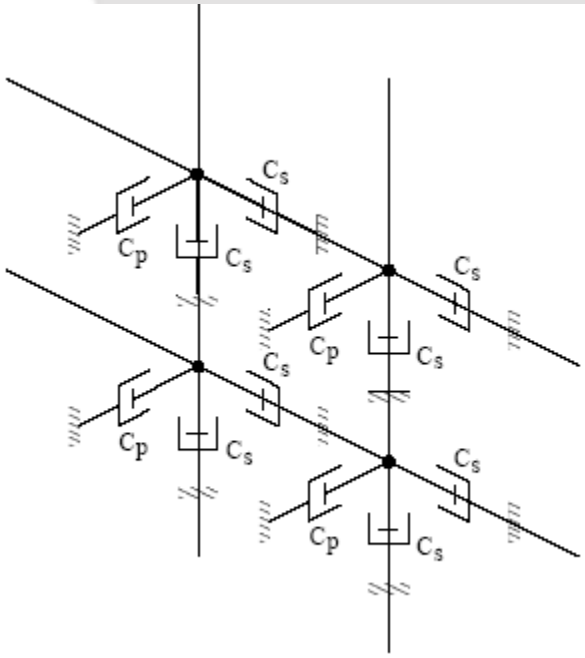


Fig. 3.8 Viscous dashpots connected to each degrees of freedom of a boundary node

Here, in these equations, $\sigma(s)$ and $\tau(s)$ are the normal and shear stresses on the boundary, and $u(s)$and $v(s)$are the normal and shear displacements. The

velocity $c_p$ represents the compressional wave velocity, with $s$ denoting the coordinate on the artificial boundary.

In the three dimensional case, a second equation like Eq. (3.119) is formulated, applicable to the other tangential direction. In discretized form, it is customary to lump the distributed dampers described by Eq. (3.118) and Eq. (3.119), which results in dampers coefficients $c_n$ and $c_t$ in the normal and tangential directions.

$$c_n = A_1 \rho c_p \tag{3.120}$$

$$c_t = A_2 \rho c_s \tag{3.121}$$

The dashpot coefficients $c_s$ and $c_p$, in two mutually orthogonal directions are given by the following expressions:

$$c_s = \sqrt{\frac{G}{\rho}} \tag{3.122}$$

$$c_p = \sqrt{\frac{E(1-\mu)}{(1+\mu)(1-2\mu)\rho}} \tag{3.123}$$

For the three dimensional case, $A_1$ and $A_2$ represent the applicable area which is replaced in the two dimensional case by the applicable length. Usually, the factors $A_1$ and $A_2$ are considered to be equal to 1. $G$ is called the shear modulus and is expressed as

$$G = \frac{E}{2(1+\mu)} \tag{3.124}$$

Where $\mu$ = Poisson's ratio.

This procedure leads to the frequency independent boundary conditions that are local in time and space. If the shape functions of the neighboring finite elements are used instead of crude lumping procedure, a narrow banded damping matrix arises, which is also easy to implement.

However, in general, the directions of the incident waves are not known in advance. In these cases, it may be advantageous to use a 'diffused' version of expression (3.120) and (3.121) as suggested by White et al. (1977). Assuming that wave energy arrives at the boundary with equal probability from all directions, effective factors $A_1$ and $A_2$ are evaluated by minimizing the ratio between the reflected energy and the incident energy over a range of incident angles. For an isotropic medium this results in

$$A_1 = \frac{8}{15\pi}\left(5 + 2S - 2S^2\right) \tag{3.124}$$

$$A_2 = \frac{8}{15\pi}\left(3 + 2S\right) \tag{3.125}$$

Which gives slightly better over-all efficiency than the original approach (Lysmer and Kulhemeyer, 1969). The value of $S$ in Eq. (3.124) and Eq. (3.125) is given by

$$S = \sqrt{\frac{(1-2\mu)}{2(1-\mu)}} \tag{3.126}$$

These local viscous dampers represent the exact solution for *P*- and *S*- waves which impinge at a right angle on the artificial boundary. They are approximate for inclined body waves, whereby the reflected energy is only a small part of the total energy (Lysmer and Kuhlemeyer, 1969). In many cases, the farther one chooses the artificial boundary to be from a source which radiates waves, the more the angle of incidence with respect to the artificial boundary will approach $90^o$. In this way, the viscous dampers will perform better. The same applies as the frequency of excitation becomes higher.

### 3.9.3 The Effect of earth Pressure

In addition to using dashpots, the effect of earth pressure is considered while analyzing the semi-infinite foundation domain. If the effect of earth pressure is not considered, then the configuration of the boundary of the foundation domain may be represented as shown in Fig. 3.9 (a). The application of earth pressure may be considered in two different ways and they are shown in Fig. 3.9 (b) and 3.9 (c) respectively. In Fig. 3.9 (b), all the side nodes at the boundary are fixed with dashpots in both horizontal and tangential directions. The nodes at the base of the foundation are again fixed with dashpots in both horizontal and tangential directions. In Fig. 3.9 (c), the nodes at the base of the boundary are fitted with rollers allowing only horizontal movement. The nodes at the sides of the boundary are fixed with viscous dashpots to absorb the energy of any traveling wave. The perpendicular dashpots to the boundary absorb the p-waves, whereas the dashpots tangential to the boundary absorb the s-waves. In these models, no displacement constraints are used. Therefore, the horizontal at rest earth pressure is applied at the boundary nodes situated at the both sides of the foundation domain. This is done by

recording the reaction forces in the model with fixed boundaries and applying them with opposite sign to the model with absorbing boundaries (Preisig, 2002).

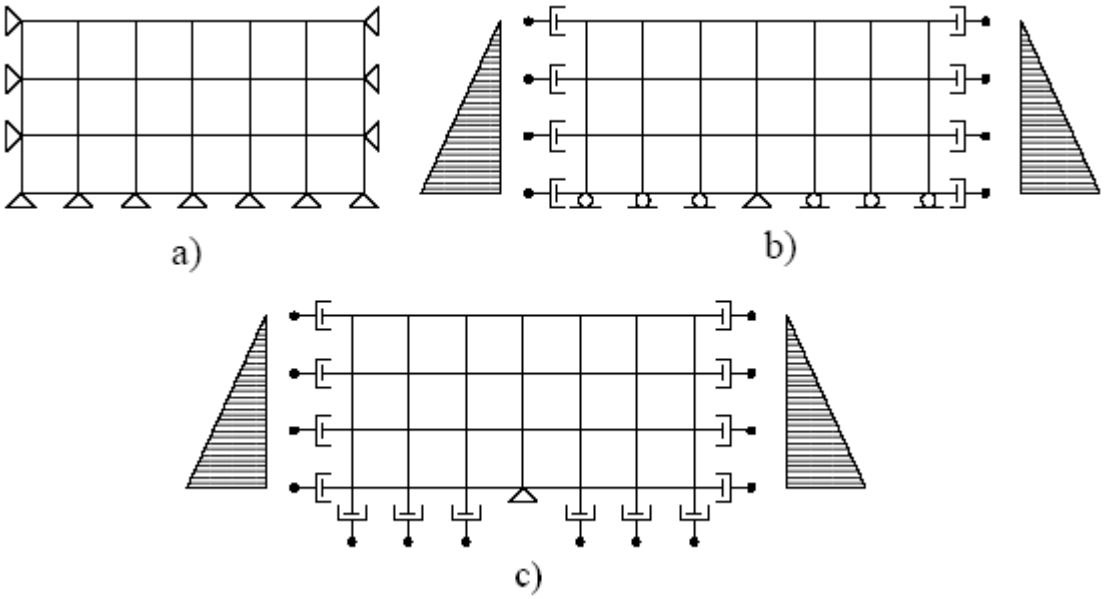


Fig. 3.9 Boundary conditions for 2-D model

This configuration of boundary conditions has no fixed point in *x*-direction. Because the dash pots only provide resistance to high velocity motions the model is very sensitive to low frequency components of the motion. The slightest imbalance in acceleration causes the entire model to move as a rigid body in *x*-direction (Preisig, 2002). To avoid this, the node at the center of the base is fully fixed in the following analyses. Keeping the center node at the base of the foundation as fixed, two varieties of boundary conditions are tested. First, all the bottom nodes are provided with rollers allowing only horizontal movements as shown in Fig. 3.9 (b) and second, the boundary nodes at the bottom of the base are fitted with dashpots as shown in Fig. 3.9 (c). However, in both these cases, the side nodes of the foundation domains are attached to dashpots in both normal and tangential directions. A detailed description of the use of dashpots can be found in the works by Preisig (2002).

### 3.9.4 Finite Element Implementation

The finite element implantation of viscous dashpots is easy. It simply requires adding to the diagonal position of the damping matrix of the amount of dashpot coefficient as

expressed by Eq. (3.120) and (3.121) respectively. The nodal points attached with viscous dashpots achieve more stiffness in that particular d.o.fs. As a result, they act like energy absorber coming from the traveling earthquake waves.

### 3.9.5 Flowchart for the foundation analyzer

Fig. 3.10 shows the flowchart of the computer implementation of the material nonlinearity modeled as per Duncan-Chang theory. If the foundation material is considered to be linear, elastic, then the time integration is carried out with elastic stiffness matrix. If the effect of material nonlinearity is to be determined, then the Young's modulus of the foundation is altered at each time step as per the following Eq. (3.98). With this changed Young's modulus, the new constitutive matrix is built which is used for the calculation of displacements, stresses and strains. The boundary condition at the sides of the foundation boundaries are altered to take into account of the effect of attached viscous. The load vector is calculated considering the effect of gravity loading, seismic and any other imposed loads. Finally, the Newmark integration is carried to solve the dynamic equation of motion.

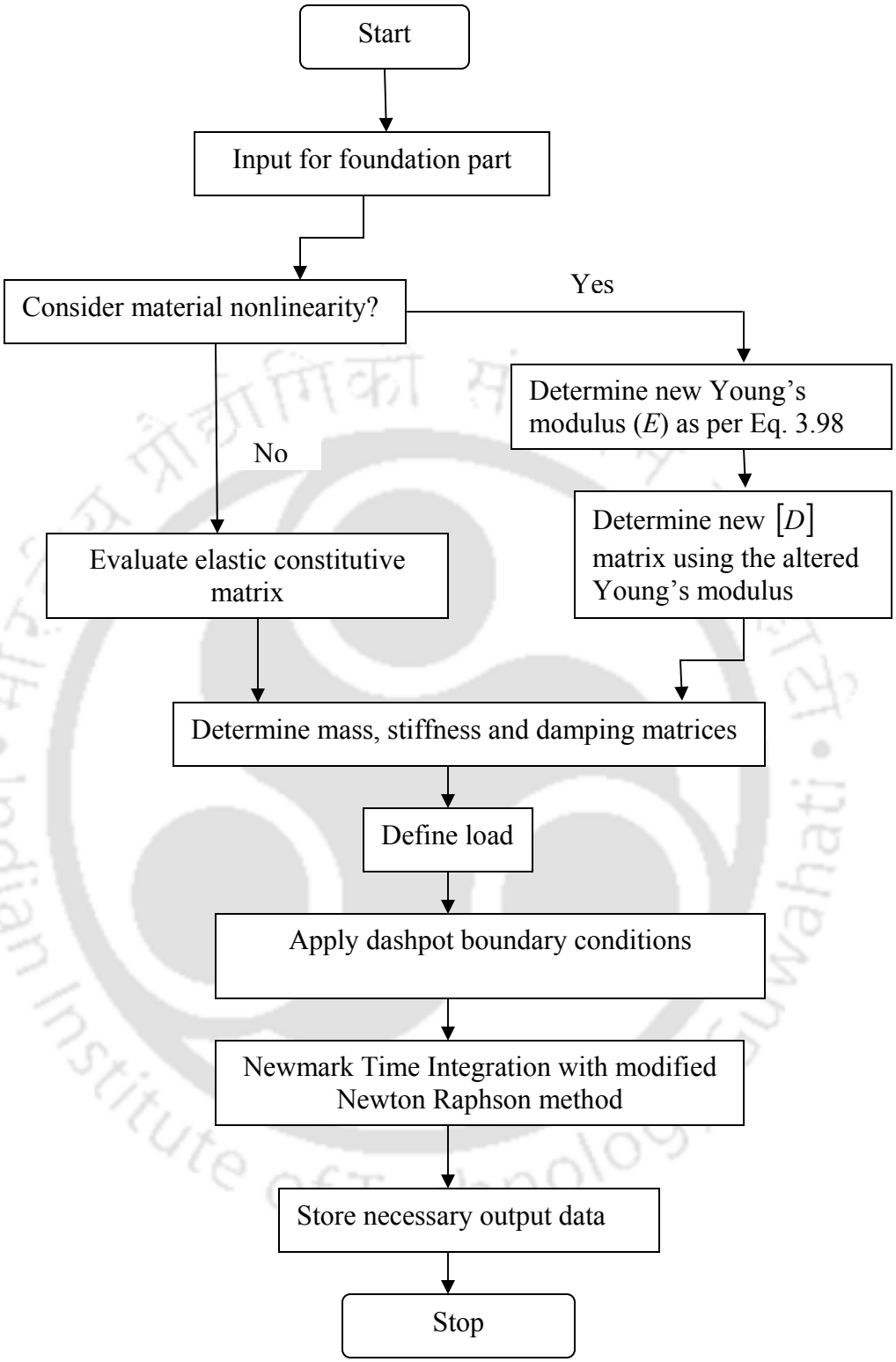


**Fig. 3.10 Flowchart for foundation analyzer with or without considering the effect of material nonlinearity**

## ***PART C***

# 3.10 DAM-FOUNDATION COUPLED SYSTEM

In the dam-foundation interaction problems, the dam and the foundation do not vibrate as separate systems under external earthquake excitations, rather they act together in a coupled way. Therefore, these problems have to be dealt in a coupled way. An iterative scheme is developed in the present study to achieve the coupled effect of dam-reservoir system.

## 3.10.1 Iterative Scheme

The equations of motion for dam and foundation system are written separately as follows:

$$M_d\ddot{x}_d + C_d\dot{x}_d + K_d x_d = f_d \tag{3.127}$$

$$M_f\ddot{x}_f + C_f\dot{x}_f + K_f x_f = f_f + f_{if} \tag{3.128}$$

Here, $M_d$, $C_d$, $K_d$ and $f_d$ are the mass, damping, stiffness and the applied load matrices respectively for the dam part. The load vector $f_d$ includes the hydrodynamic forces developed from reservoir water, the earthquake forces, self weight of the dam body and any other external forces if present. $M_f$, $C_f$, $K_f$ and $f_f$ are the mass, damping, stiffness and the applied load matrices respectively for the soil domain. The vector $f_{if}$ is the vector of interactive force for the soil region exerted by the dam body. The vector $f_{if}$ is generated during successive iteration at the interface nodes of dam and foundation. The vectors of acceleration, velocity and displacement for the dam part at any time step $t$ are represented by $\ddot{x}_d, \dot{x}_d$ and $x_d$. The vectors $\ddot{x}_f, \dot{x}_f$ and $x_f$ also carry similar meaning for the foundation part.

The damping matrix $C$ has been assumed to be the Rayleigh damping matrix and is constructed as a linear combination of $M$ and $K$ matrices which are multiplied by two suitably chosen scalars $\alpha$ and $\beta$. It is expressed as follows:

$$C = \alpha M + \beta K \tag{3.129}$$

The matrices $M_d, M_s$ and $K_d, K_s$ are built from the following formulae:

$$M_d = \int_{\Omega_d} [N_d]^T \rho_d [N_d] d\Omega_d \tag{3.130}$$

$$M_f = \int_{\Omega_f} [N_f]^T \rho_f [N_f] d\Omega_f \tag{3.131}$$

$$K_d = \int_{\Omega_d} [B_d]^T [D_d][B_d] d\Omega_d \tag{3.132}$$

$$K_f = \int_{\Omega_f} [B_f]^T [D_f][B_f] d\Omega_f \tag{3.133}$$

Where $[B_d], [B_f]$ are the strain displacement matrices and $[N_d], [N_f]$ are the matrices for the shape functions for dam and the soil foundation portions respectively. Also $[D_d], [D_f]$ are the constitutive matrices and $\rho_d, \rho_f$ represent the material densities for dam and foundation part respectively.

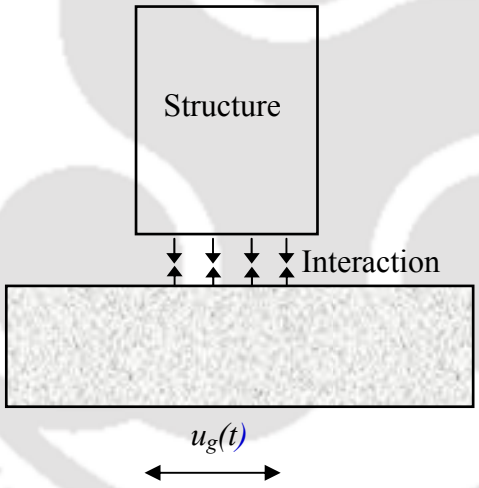


Fig. 3.11 Soil structure interaction employed through reaction forces at the interface

The iterative scheme has been developed to determine the responses of the dam-foundation coupled system (Fig. 3.11). At any instant of time $t$, the equation of motion for the dam part Eq. (3.127) is solved first with the applied load $f_d$ considering dam to be fixed at the bottom i.e. at the dam-foundation interface nodes. The exerted forces give rise to reaction forces at the common nodes of dam-foundation interface. The reaction forces generated at the common interface nodes of structure and foundation are then applied in the opposite direction at the common nodes of the foundation system to solve

Eq. (3.128) at the same time instant $t$. These reaction forces applied in the opposite direction for the foundation part is termed as $f_{if}$.

After solving the foundation part against the applied load of ($f_f + f_{if}$), the common interface nodes for the foundation part will undergo some displacement. These displacements are then fed into Eq. (3.127) i.e. the structural analyzer in the next instant of time ($t + \Delta t$) as the known displacements at the common interface nodes of dam and foundation. Subsequently, the response of the dam needs to be solved again with the changed boundary conditions which will be different from the earlier step. As a result, the developed reaction forces at the common interface nodes will be different from earlier step and therefore, the foundation domain is solved again with the modified reaction forces developed at the dam-foundation interface at the same time step. In this way iterations are continued for a particular time step $t$ until the displacements and stresses for both the dam and foundation part are found to be converged with a certain level of tolerance. The displacements ($x$) of both the domain at a particular time step are assumed to be converged if the following relationships are satisfied:

$$\frac{\left|\{x_d\}_{i+1}^t - \{x_d\}_i^t\right|}{\left|\{x_d\}_i^t\right|} \le \varepsilon \quad \text{and} \quad \frac{\left|\{x_f\}_{i+1}^t - \{x_f\}_i^t\right|}{\left|\{x_f\}_i^t\right|} \le \varepsilon \tag{3.134}$$

Here, $i$ is the number of iteration, $\varepsilon$ is a small pre-assigned tolerance value and $t$ is a particular time instant. Thus this iteration process goes on until the displacements and stresses between two successive iterations converge in both the dam and foundation domain.

### 3.10.2 Flowchart of the Iterative Scheme

A flow chart of the iterative scheme for the solution method of coupled dam-foundation system is presented in Fig. 3.12. In the flowchart, $t_0$ stands for the initial time instant and $t_n$ stands for the final time instant. The term $\Delta t$ represents the time step of the implicit-explicit Newmark's method used for the numerical integration of the dynamic equation of motion. The most costly operation involved in the above algorithm is to successively solve two separate systems of equations at each iteration. But in the present case,

matrices involved in the solution of the system equations are decomposed into triangular forms at the beginning of the of the iteration, and thereby only two forward-eliminations and backward substitutions are required at each iteration step. Thus, the time required to obtain the coupled response for a particular time instant is minimized in the developed iterative scheme.

This method of interaction is able to model the influence of the structure on the foundation. Also, the foundation is allowed to influence the structure domain by inducing the common interface displacements to be used as known displacements for the structure domain to be solved in the successive iterations. Thus the changed boundary condition for the structure domain simulates the flexibility of the foundation.

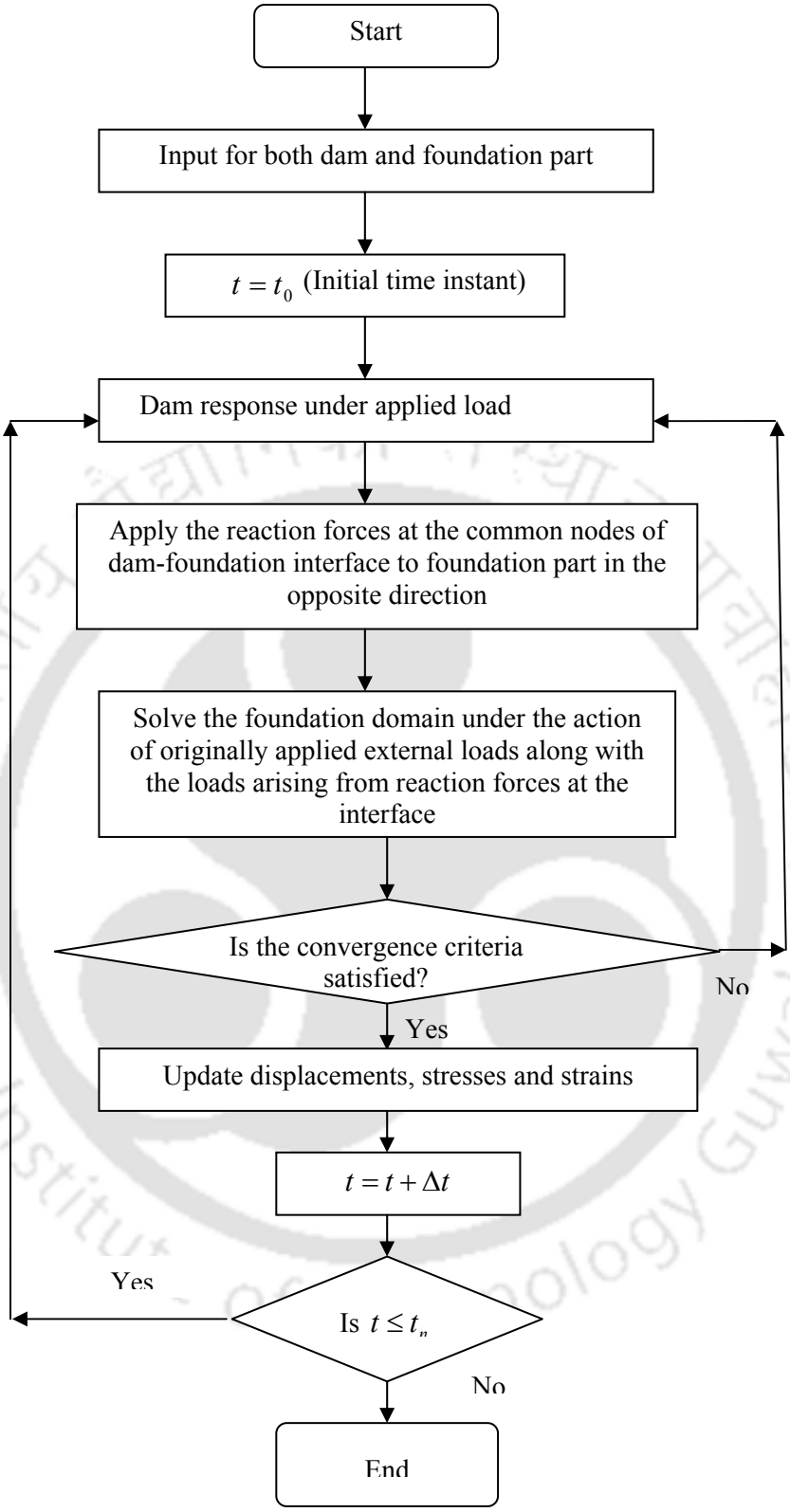


**Fig. 3.12 Flowchart of the proposed algorithm for dam-foundation interaction analysis**

# CHAPTER 4

# NUMERICAL RESULTS AND DISCUSSIONS

## 4.1 INTRODUCTION

In the present work, a technique to estimate the seismic response of an aged concrete dam is developed. A term called isotropic degradation index is introduced to estimate the response of concrete gravity dam against earthquake loading at a later stage after its construction. The illustrated method simulates the time dependent degradation of concrete due to various environmental factors and mechanical loading. A set of computer programs are developed to predict the dynamic behavior of a concrete gravity dam adjacent to an unbounded reservoir lying over infinite soil media. The reduced strength of the concrete material due to isotropic degradation is used to find out its response at a later stage of its life. A benchmark problem employing such a numerical algorithm for seismic analysis of an aged concrete dam situated on a flexible foundation and considering soil-structure interaction does not exist in the available literature. Therefore, for the validation and critical evaluation of the computer codes developed in the present investigation (as described in the formulation), different benchmark problems are solved separately for each part.

The iterative soil-structure interaction (SSI) algorithm proposed in this work is evaluated by determining the effect of soil-structure interaction on Koyna gravity dam against Koyna earthquake (1967) accelerations. The results are divided into three parts. In the first part, the behavior of the dam structure alone is analyzed considering the effect of ageing of concrete. Further, the analysis is also carried out for the dam considering empty and full reservoir condition. In the second part, response of the foundation domains is obtained considering both linear and nonlinear constitutive properties of the materials. Proper boundary conditions consisting of viscous dashpots are imposed on the foundation domains in order to represent the semi-infinite nature of the domain. The third part of this chapter deals with the effect of interaction between dam and foundation domain through the developed iterative algorithm. The results of the analyses are presented to highlight the importance of nonlinear behaviour of the foundation materials as well as the reduced strength of concrete due to ageing phenomenon considering a coupled soil-structure systems. The effect of hydrodynamic pressure on the dam has also been included while carrying out coupled dam-foundation interaction analysis.

# PART – I

## 4.2 Analysis of Dam

In this section, a concrete gravity dam is analyzed subjected to earthquake accelerations. The effect of concrete degradation due to various environmental factors and mechanical loading is investigated. This procedure is helpful to predict the behavior of aged concrete under any type of loading at a later stage of its construction. A parameter called degradation index which varies from 0 to 1 indicating the state of non-degraded and fully degraded material is introduced. The scope of the present investigation is to determine the effect of ageing on the seismic response of the dam. The constitutive matrix being a function of this degradation index changes at various stages of its life and is therefore instrumental in predicting the behavior of the concrete gravity dam at different stages of its life. The problem related to the dynamic response of the dam with and without degradation is discussed here. However, the effects of hydrodynamic pressure are ignored while studying the influence of ageing on the response of the concrete dam in order to emphasize the effect of ageing behaviour.

### 4.2.1 Validation of the Algorithm

In order to check the accuracy of the algorithm developed in this study, the Pine Flat Dam (Fenves and Chopra, 1985) is considered and eigen value analysis is carried out. The maximum crest displacements due to the South East (S69E) component of the ground motion at Taft Lincoln School Tunnel on 21$^{st}$ July, 1952 are presented in Table 4.1 for comparison. A little variation in the results is observed which may be due to different finite element mesh size for representing the dam.

**Table 4.1 Fundamental period and maximum crest displacement of Pine Flat Dam**

| **Fundamental period (sec)** | | **Max Crest Displacement (mm)** | |
|---|---|---|---|
| **Fenves & Chopra (1985)** | **Present** | **Fenves & Chopra (1985)** | **Present** |
| 0.317 | 0.320 | 26.93 | 26.58 |

### 4.2.2 Discretization of Dam

In order to investigate the response of the structure ravaged by various environmental, chemical and mechanical actions, a simplified section of Koyna gravity dam (Fig. 4.1) is chosen for the analysis purpose.

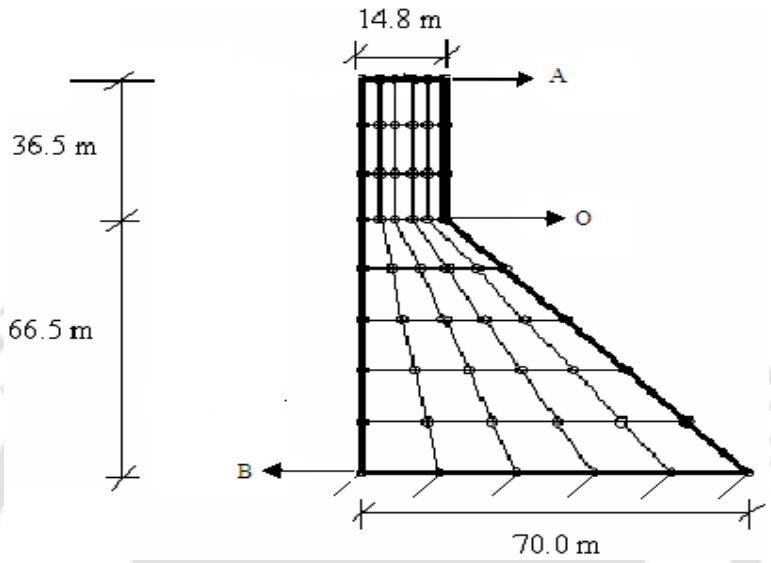


Fig. 4.1 Geometry and finite element discretization of Koyna dam

For simplicity, the upstream face of the Koyna gravity dam is considered to be straight which is slightly different from the real configuration (Chopra & Chakrabarti 1972). Similarly, on the downstream face of the dam, the section above the neck to the top is also considered to be straight ignoring the slight inclination of the portion in reality. The dimension and the material properties of the dam in the present case are: height of the dam = 103.0 m; width at the top of the dam is 14.80 m and at the base is 70.0 m, modulus of elasticity = 31500 MPa; Poisson's ratio = 0.235 and mass density = 2415.816 kg/m$^3$. Structural damping is considered as 3%. The dam is discretized with 8-noded quadratic elements as shown in Fig. 4.1 and is analyzed using plane strain formulation. In order to arrive at an economic mesh grading for the dam portion, a concentrated horizontal load of 1000 kN (acting in the +ve $x$ direction) is applied at the rightmost crest point of the structure and the static analysis is carried out considering the bottom nodes of the dam to be fixed. Also, the eigen value analysis is carried out to observe the convergence of natural frequencies and time periods. The structure is discretized with different mesh grading and the convergences of results for the time periods and the crest displacements at the rightmost upstream crest node (point 'A') obtained for different discretizations are

presented in Table 4.2. It is observed from the tabular results that results converge sufficiently for a discretization of 5 (horizontal) × 7 (vertical). However, a mesh grading of 5 (horizontal) × 8 (vertical) is chosen for the sake of better accuracy during the interaction analysis between dam and foundation.

**Table 4.2 Convergence of time periods and horizontal displacement of the dam**

| Mesh Size | Time Period (sec) | | Horizontal Crest Displacement (m) | |
|---|---|---|---|---|
| $N_h \times N_v$ | Mode 1 | Mode 2 | $u$ | $v$ |
| 3×5 | 0.3431 | 0.1270 | 0.00546 | -0.000746 |
| 4×5 | 0.3437 | 0.1273 | 0.00550 | -0.000756 |
| 5×5 | 0.3440 | 0.1275 | 0.00551 | -0.000762 |
| 4×6 | 0.3438 | 0.1275 | 0.00550 | -0.000756 |
| 5×6 | 0.3441 | 0.1276 | 0.00551 | -0.000762 |
| 4×7 | 0.3440 | 0.1276 | 0.00552 | -0.000772 |
| 5×7 | 0.3442 | 0.1277 | 0.00554 | -0.000778 |
| 4×8 | 0.3440 | 0.1276 | 0.00552 | -0.000772 |
| 5×8 | 0.3442 | 0.1277 | 0.00554 | -0.000778 |
| 4×9 | 0.3441 | 0.1277 | 0.00553 | -0.000772 |
| 5×9 | 0.3442 | 0.1277 | 0.00554 | -0.000778 |
| 4×10 | 0.3440 | 0.1276 | 0.00552 | -0.000772 |
| 5×10 | 0.3442 | 0.1277 | 0.00554 | -0.000778 |

### 4.2.3 Selection of Time Step ($\Delta t$)

The selection of a suitable time step is required to ensure minimum computational effort needed to obtain results with desired accuracy. For this purpose, the gravity dam shown in Fig. 4.1 is subjected to unit ramp acceleration. The material properties are same as described in section 4.2.2. Newmark's (1957) average acceleration method is chosen to determine the displacement of its crest under the ramp load in horizontal direction. A study is carried out by varying the time step sizes $\Delta t$ (i.e. 0.1 sec, 0.01 sec, 0.005 sec, 0.001 sec etc.) as shown in Fig. 4.2. From the figure, it can be observed that, the horizontal crest displacement converges with sufficient accuracy at a time step of 0.01 sec. Therefore, from the computational efficiency as well as from the point of view of accuracy, a time step size of 0.01 sec is used for subsequent analysis.

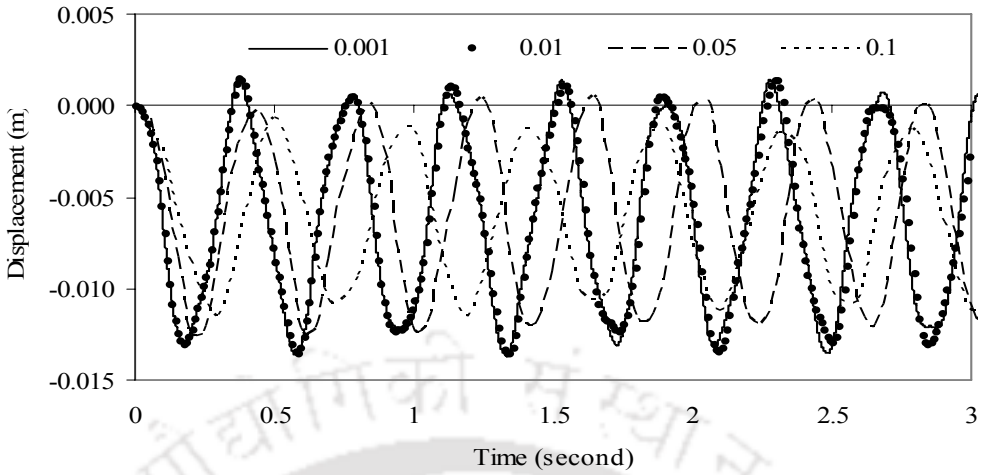


Fig.4.2 Horizontal displacement at the top of the dam subjected to ramp acceleration

### 4.2.4 Evaluation of Degradation Index

It is a known fact that concrete gains compressive strength with age. This phenomenon is predicted by a curve fitting on 50 years of compressive strength data published by Washa et al. (1989). In the referred literature, the specimens were cured for 28 days and then placed outdoors to subject it to change in severe weather conditions of 25 cycles of freezing and thawing each winter, annual precipitation including snowfall of about 0.813 m and air temperature variation between -32.0°C and 35.0°C. For the present work, the same data is chosen. The fifty years of compressive strength data set corresponds to a concrete specimen of mixed proportion 1.0:2.51:5.34 (cement: sand: gravel by weight) with water cement ratio of 0.49.

The elastic modulus of concrete ($E_0$) considering the strength gain with age is obtained from Eq. (3.58). Having obtained the value of $E_0$, the degraded elastic modulus $E_m$ is calculated from Eq. (3.48). The degraded elastic modulus is found out as a function of the elastic modulus considering the gain of strength with age is obtained using Eq. (3.56).

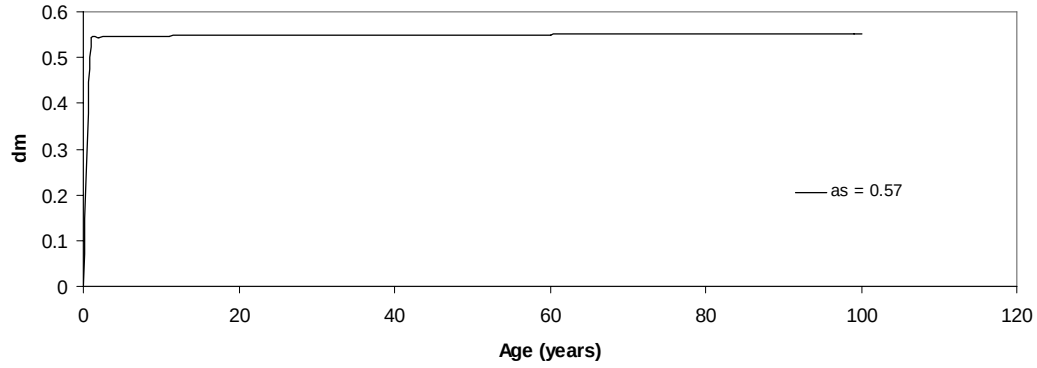


Fig. 4.3 The variation of the parameter $d_m$ with age in years

In case of hygro-chemo-mechanically induced degradation, the total porosity $\phi$ of concrete is expressed as the summation of initial porosity $\phi_0$, chemically induced porosity $\phi_c$ and mechanically induced porosity $\phi_m$ according to Eq. (3.39). The values of $\phi_0$ and $\phi_c$ are considered to be 0.2 (Kuhl et al., 2004; Gogoi and Maity, 2007). Following Eq. (3.40), the value of mechanically induced porosity $\phi_m$ is expressed as a function of scalar degradation parameter $d_m$, which can be calculated from Eq. (3.41). The variation of the degradation parameter $d_m$ with age is shown in Fig. 4.3. In Eq. (3.41), the values of material parameters $\alpha_m, \beta_m, \phi_0$ and $\kappa^0$ are considered to be 0.9, 1000, 0.2 and $1.1\times10^{-4}$, respectively (Kuhl et al., 2004). The value of $\phi_c$ may be considered to be equal to 0.0 and 0.2 in the absence of silt deposited on the upstream face due to chemical degradation and in the presence of the same respectively. The maximum allowable range of values for $d_m$ should lie between 1.0 and 0.0 indicating complete and no degradation of concrete, respectively. The value of the material parameter $a_s$ is varied from 0.4 to 1.0 for a HCM (hygro-chemo-mechanical) design life of 100 years. The variation of elastic modulus with different values $a_s$ is plotted in Fig. 4.4. The elastic modulus is calculated by using Eq. (3.58). It is observed that considering $a_s$=1.0 reduces the value of elastic modulus of concrete to a very low value which is practically incorrect. Thus, to study the effect of maximum allowable degradation due to mechanically induced porosity during its design life on the strength of concrete, the elastic modulus is obtained for different values of $a_s$. It is observed that with a decreasing value of $a_s$ the decrease in elastic modulus of concrete is reduced i.e., the extent of degradation is reduced. Having observed the effects of the different values of the material parameter $a_s$, the value is fixed at 0.57 for further

analyses (Gogoi and Maity, 2007). The proposed technique can be used effectively to estimate the degradation of concrete in the concrete gravity dam due to aggressive environmental effect.

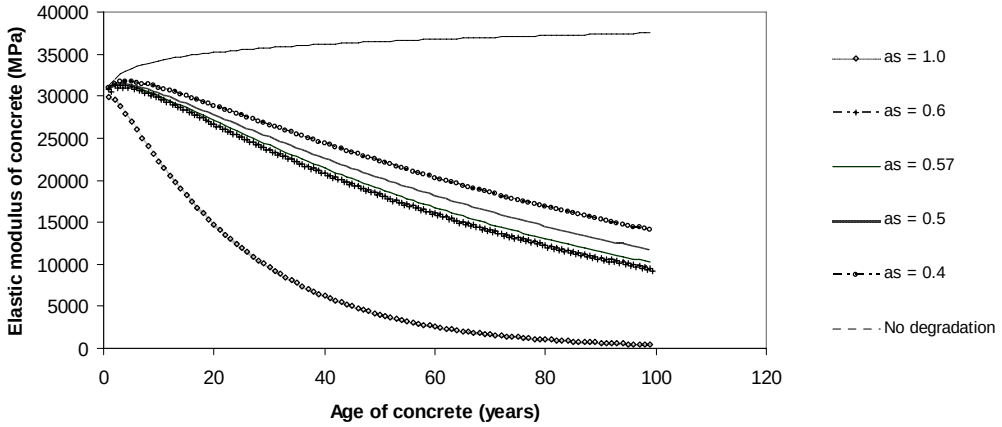


Fig. 4.4 Variation of elastic modulus of concrete with age (Design life = 100 years)

### 4.2.5 Response of Aged Dam

The Koyna dam is located on the western side of India, about 200 kilometers south of Mumbai, in the state of Maharashtra and was constructed in 1962. In the present work, the effect of ageing is investigated by carrying out static and eigen value analyses on this dam under empty reservoir condition. A 1000 kN horizontal static load is applied on the crest of the upstream side of the dam from left to right. The effect of isotropic degradation of concrete is investigated on the Koyna dam subjected to Koyna earthquake (1967) acceleration. The Koyna earthquake accelerogram is shown in Fig. 4.5. In the present work, the analysis is carried out without any initial degradation, after completion of construction, considering concrete has not degraded at all. Under the hygro-chemo-mechanical actions, the isotropic degradation index $d_g$ calculated following Eq. (3.49) is 19.1% after 25 years of construction for a HCM design life $\tau_a$ equal to 100 years. If the HCM design life $\tau_a$ is changed to 50 years, the value of isotropic degradation index obtained after 25 years of construction is 34.5%. Therefore, the consideration of higher HCM design life yields lesser value of degradation index and vice versa at a particular year after construction. Correspondingly, for a higher HCM design life the degradation of concrete will be lower and vice versa because the degradation of concrete increases with the increase of the value of degradation index.

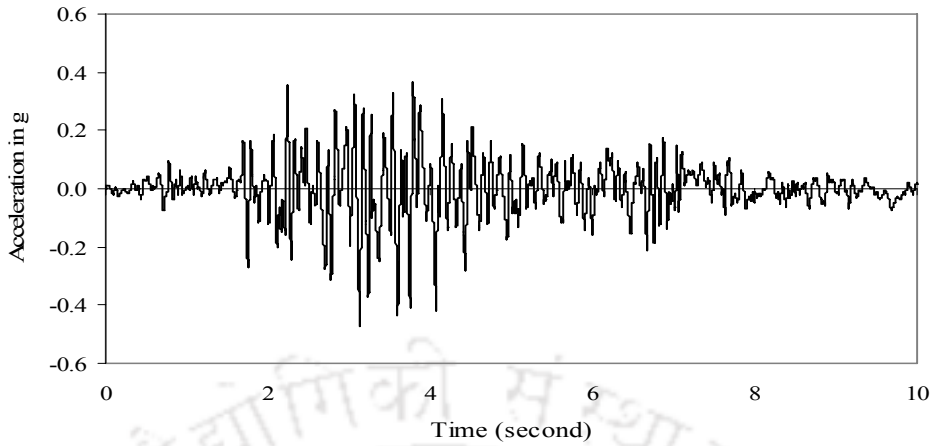


Fig.4.5 Horizontal accelerogram of Koyna earthquake, December 11, 1967

In Fig. 4.6, the variation of degradation index for different HCM design life (i.e. 50 years and 100 years respectively) with age is plotted. The static elastic modulus $E_0$ is determined from Eq. (3.58) which is a function of the compressive strength of concrete. The compressive strength of concrete at any age may be approximated by Eq. (3.56) proposed in the present work. It is observed that the degradation index of the concrete is less if the HCM design life ( $\tau_a$ ) is higher and vice versa.

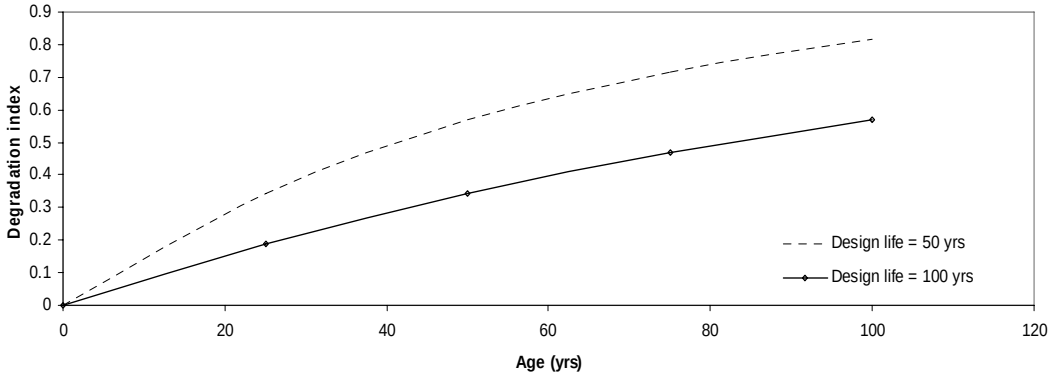


Fig. 4.6 Variation of degradation index with age of concrete for different HCM design life

Degradation of dam material under the hygro-chemo-mechanical actions will lead to reduction of concrete strength and stiffness along the horizontal, vertical or in both directions. Following the works of Gogoi (2007), a study is carried out to evaluate the response on the change of natural frequency of the dam due to degradation along the width and height of the dam. It is observed from Fig. 4.7 that with an increase in damage caused by degradation, the natural frequency of the structure reduces. This behavior is

mainly attributed to the reduced stiffness of the structure with increased degradation which makes the structure more flexible. If the degradation only occurs in the horizontal direction, then the rate of reduction of natural frequency is comparatively lower than the case when the degradation is caused along the vertical direction. This phenomenon clearly indicates that the degradation experienced along horizontal direction is comparatively lesser than the degradation experienced along the vertical direction. It may be because the extent along the vertical direction of the dam is more than the extent in horizontal direction. Moreover, the rate of reduction in frequency of the dam is higher in case of isotropic degradation compared to the other two orthotropic cases. This phenomenon is observed because, in case of isotropic degradation, the reduction of stiffness occurs along both horizontal and vertical directions whereas, in case of orthotropic degradation, the loss of stiffness occurs along one direction only.

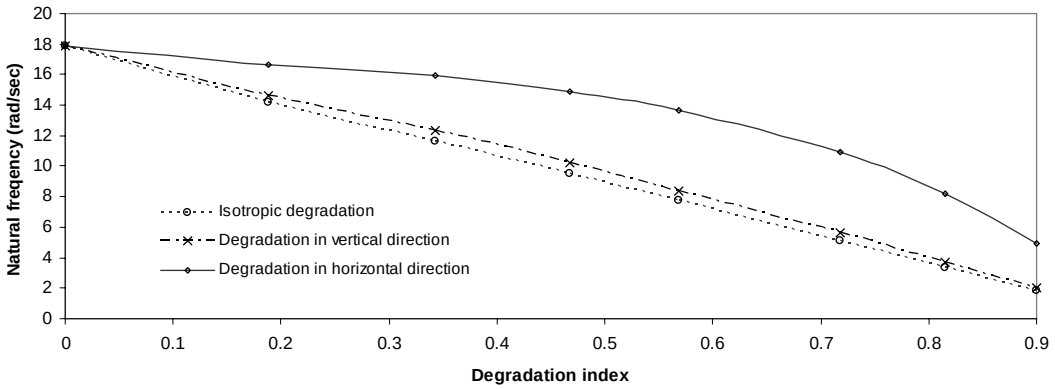


Fig. 4.7 Variation in frequency of dam with initial degradation

Table 4.3 shows the values of first natural frequency and the time period corresponding to first natural frequency in seconds. It is observed that natural frequency of the dam reduces with passage of time if the HCM design life of concrete is considered to be fixed at a particular value. Correspondingly, the time period increases at a later stage. This phenomenon is attributed to the fact that the concrete suffers more degradation with time. Therefore, the structure becomes more flexible with passage of time due to reduction of its stiffness which leads to progressive reduction of the natural frequency. Also, for a particular age, the natural frequency increases with the increase of HCM design life of concrete and vice versa. Correspondingly, the time periods decreases with the increase of HCM design life of concrete in years at a particular age of the dam. Consideration of lesser value of HCM design life inflicts more degradation to the

concrete which makes the structure more flexible in nature. That is the reason for decrease in natural frequency when the value of HCM design life is less at a particular age and vice versa.

**Table 4.3 Natural frequencies and time periods of aged dam**

| | 1st natural frequency (rad/sec) | Time periods (sec) corresponding to 1st natural frequency |
|---|---|---|
| Non-degraded dam | 16.50 | 0.381 |
| After 25 yrs; HCM-50 | 11.48 | 0.547 |
| After 50 yrs; HCM-50 | 7.64 | 0.822 |
| After 25 yrs; HCM-100 | 14.15 | 0.444 |
| After 50 yrs; HCM-100 | 11.63 | 0.540 |

The comparisons of the horizontal crest displacement of the structure after 25 years of construction and 50 years of construction are presented in Fig. 4.8, corresponding to HCM design life of concrete equal to 100 yrs and empty reservoir condition. Just after the construction, the analysis is carried out assuming the concrete has not degraded at all. The maximum and minimum values of the horizontal crest displacements are 6.34 cm and -5.49 cm, respectively, after 25 years of construction. After 50 years of construction, the similar values are obtained as 5.66 cm and -6.02 cm respectively. Without considering degradation, the maximum and minimum values of horizontal crest displacements obtained are 3.40 cm and -3.93 cm respectively. Therefore, it is observed that the displacement increases with aging after 50 years of construction because degradation of concrete is more at a later age.

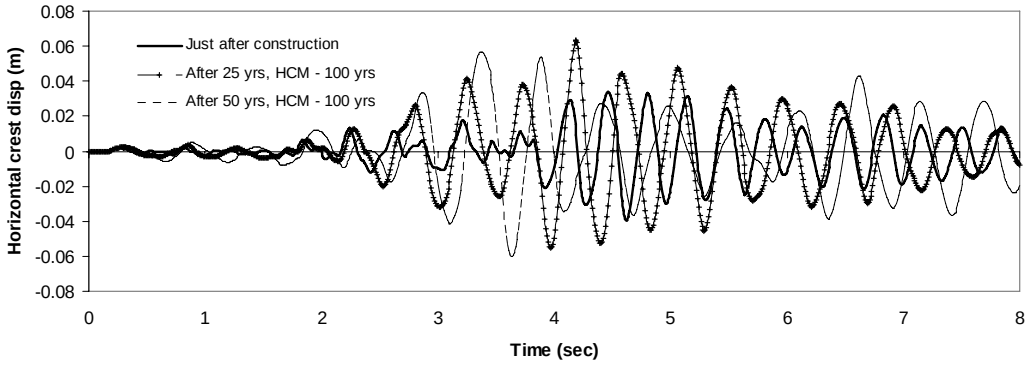


Fig. 4.8 Comparison of horizontal crest displacement vs. age under empty reservoir condition just after construction, after 25 and 50 years of construction (HCM design life = 100 yrs)

Similar analyses are carried out in order to compare the values of major principal stresses occurring at point O (as shown in Fig. 4.1) just after construction, at the end of $25^{th}$ and $50^{th}$ year of construction under the empty reservoir condition. The variation of major principal stresses with time is plotted in Fig. 4.9. The HCM design life of concrete is considered to be equal to 100 years. Just after construction, considering no degradation of concrete has taken place, the maximum amount of major principal stress observed is 7.61 MPa. It is observed that the maximum value of the major principal stress obtained after 25 years of construction is 6.85 MPa whereas that obtained after 50 years of construction is 5.25 MPa. The major principal stress values have decreased at the age of 50 years because the stiffness of the material reduces by a large amount due to high degradation experienced at a later stage of its life. Fig. 4.10 shows the variation of minor principal stress vs. time at the point 'O' (as shown in Fig. 4.1). The value of the minimum minor principal stress observed at the immediate end of construction is -6.78 MPa. The value of minimum minor principal stress obtained after 25 years of construction is -8.99 MPa. At the end of 50 years of construction, the minimum value of minor principal stress is obtained as -5.54 MPa. In this case also, the value of the minor principal stress is observed to decrease at a later stage of its life because the material loses its stiffness due to high amount of degradation. However, at the end of $25^{th}$ year of construction, the value of minor principal stress is found to be even lesser than that observed just after construction of the dam. This can be attributed to the observation that the generated stresses are directly proportional to the amount of displacement as well as the constitutive properties of the material. Due to degradation of the concrete, the structure will experience more displacement and its constitutive matrix will reduce. The reduction of constitutive matrix makes the structure more flexible and gives rise to lesser stresses. After a certain number of years, whether the structure will exhibit more or less stresses compared to the non-degraded state shall depend on the relative increase in displacement and the reduction of the constitutive properties. It is inferred that if the percentage reduction of the constitutive matrix of the structure is more than the percentage increase in the displacement of the structure, then the amount of stresses developed shall be lesser compared to the case of non-degraded analysis and vice versa.

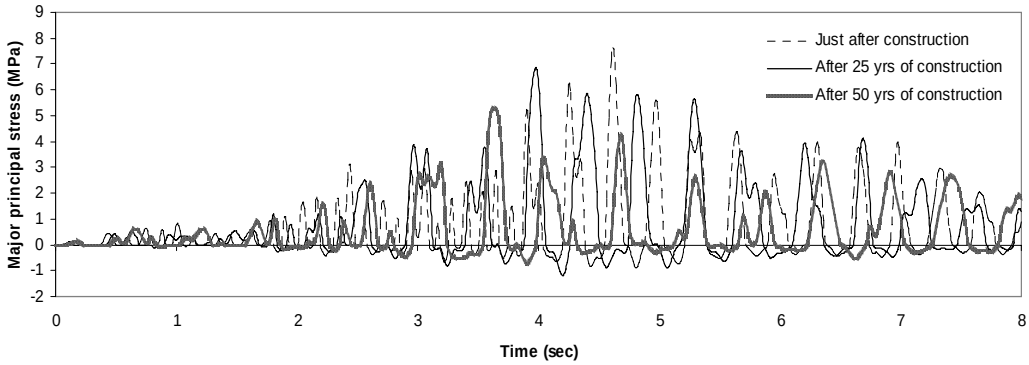


Fig. 4.9 Comparison of major principal stress vs time at point O under empty reservoir condition just after construction, 25th and 50th year of construction (HCM design life = 100 years)

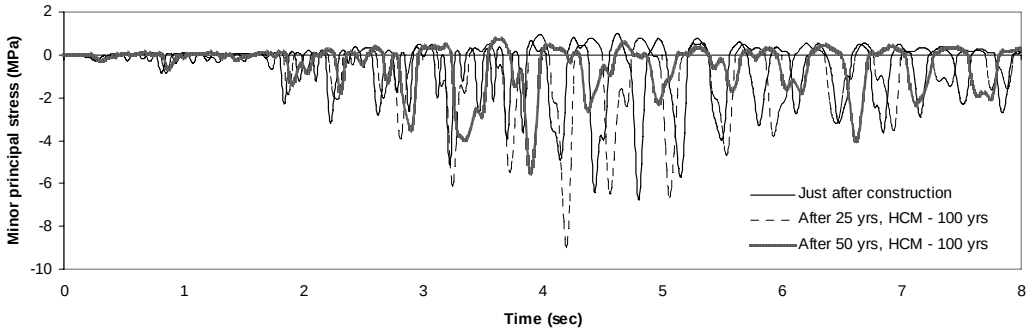


Fig. 4.10 Comparison of minor principal stress vs time at point O under empty reservoir condition just after construction, 25th and 50th year of construction (HCM design life = 100 years)

From Fig. 4.9, it may be observed that the maximum major principal stress occurs at 4.62 sec just after construction of the dam. Fig. 4.11 (i) and Fig. 4.11 (ii) show the contour plot of the major and minor principal stresses (both $\sigma_{p1}$ and $\sigma_{p3}$) throughout the body of the dam at 4.62 sec. From Fig. 4.10, it is observed that the minimum value of minor principal stress occurs at 4.81 sec. Fig. 4.12 (i) and Fig. 4.12 (ii) plot the distribution of major and minor principal stress (both $\sigma_{p1}$ and $\sigma_{p2}$) throughout the body of the dam at 4.81 sec. From Fig. 4.9, it may be seen that the maximum value of major principal stress occurs at 3.98 sec after 25th year of construction of the dam. The contour plot of the variation of major and minor principal stresses (both $\sigma_{p1}$ and $\sigma_{p3}$) at 3.98 sec is shown in Fig. 4.13 (i) and Fig. 4.13 (ii). At the end of 25 years after the construction of the dam, the minimum value of minor principal stress is observed to develop at 4.20 sec. The variation of major and minor principal stresses (both $\sigma_{p1}$ and $\sigma_{p2}$) at the end of 4.20

sec is plotted in Fig. 4.14 (i) and Fig. 4.14 (ii). Fig. 4.9 shows that the maximum major principal stress takes place at 3.64 sec after 50 years of construction of the dam. Fig. 4.15 (i) and Fig. 4.15 (ii) display the contour variation of major and minor principal stress throughout the body of the dam at the end of 3.64 sec. Fig. 4.10 shows that the minimum value of minor principal stress takes place at 3.91 sec after 50 years of construction of the dam. Fig. 4.16 (i) and Fig. 4.16 (ii) show the contour plot of major and minor principal stresses at 3.91 second.

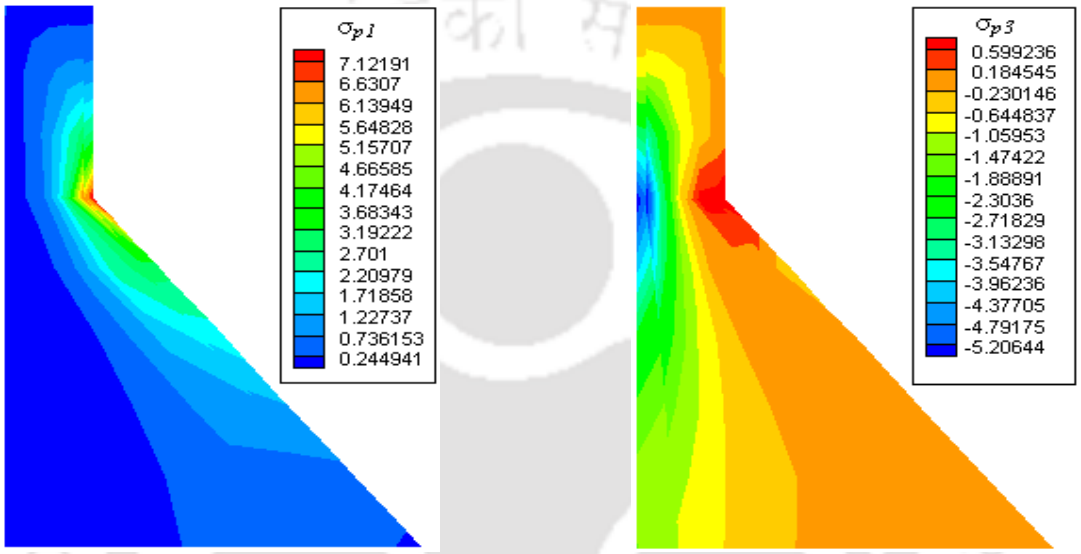


(i) (ii)

Fig. 4.11 Contour for principal stress (i) $\sigma_{p1}$ and (ii) $\sigma_{p3}$ at 4.62 seconds just after construction

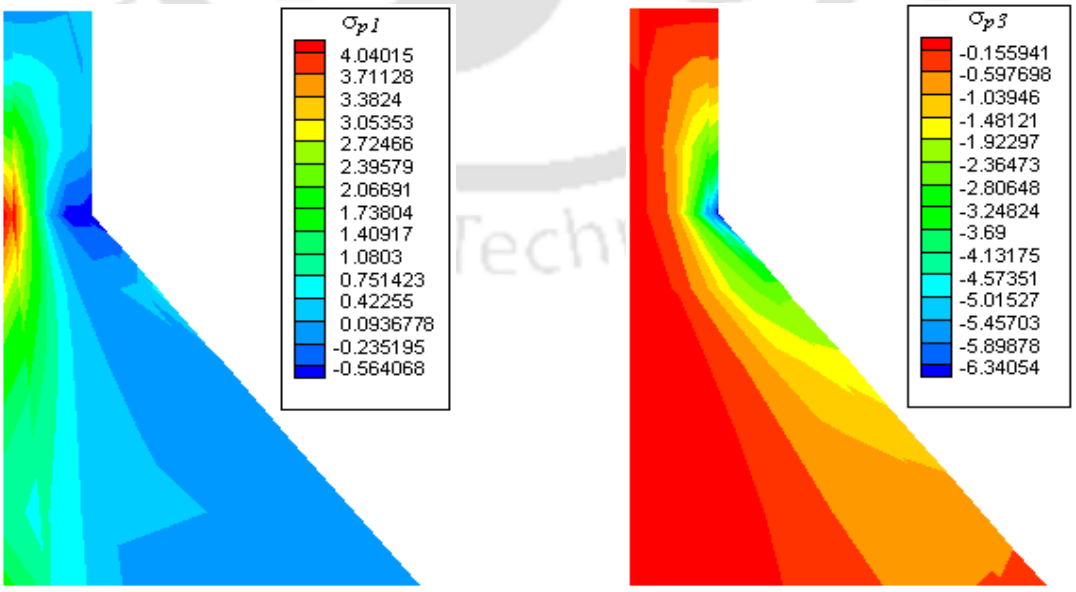


(i) (ii)

Fig. 4.12 Contour for principal stress (i) $\sigma_{p1}$ and (ii) $\sigma_{p3}$ at 4.81 seconds just after construction

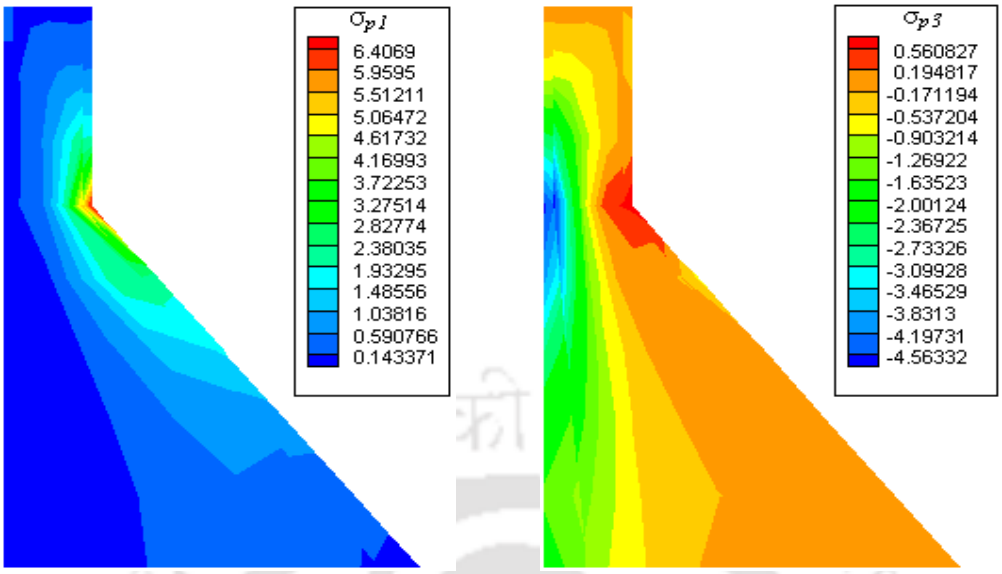


(i) (ii)

Fig. 4.13 Contour for principal stress (i) $\sigma_{p1}$ and (ii) $\sigma_{p3}$ at 3.98 seconds at the end of 25th year

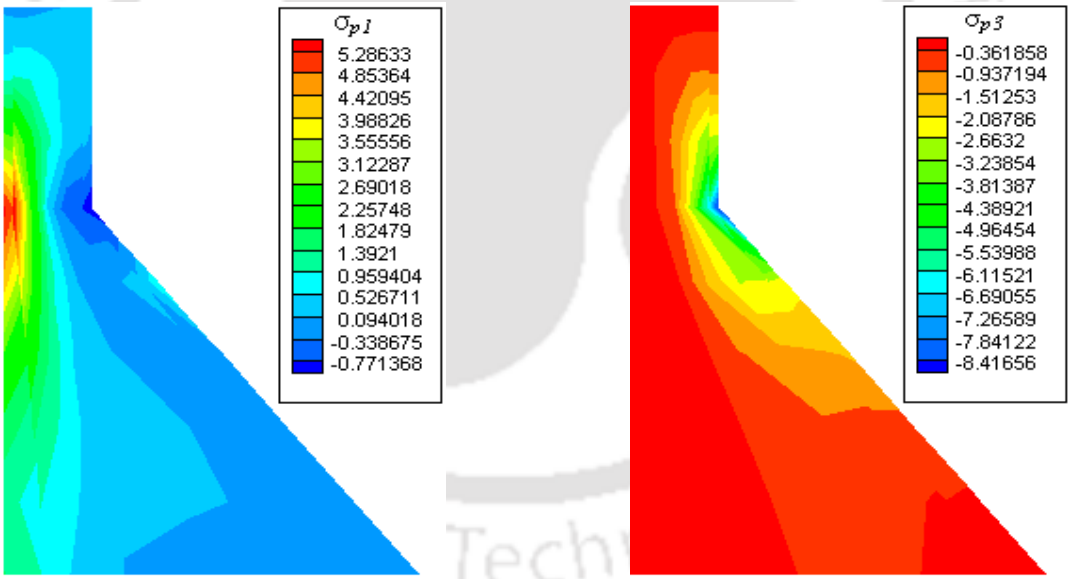


(i) (ii)

Fig. 4.14 Contour for principal stress (i) $\sigma_{p1}$ and (ii) $\sigma_{p3}$ at 4.20 seconds at the end of 25th year

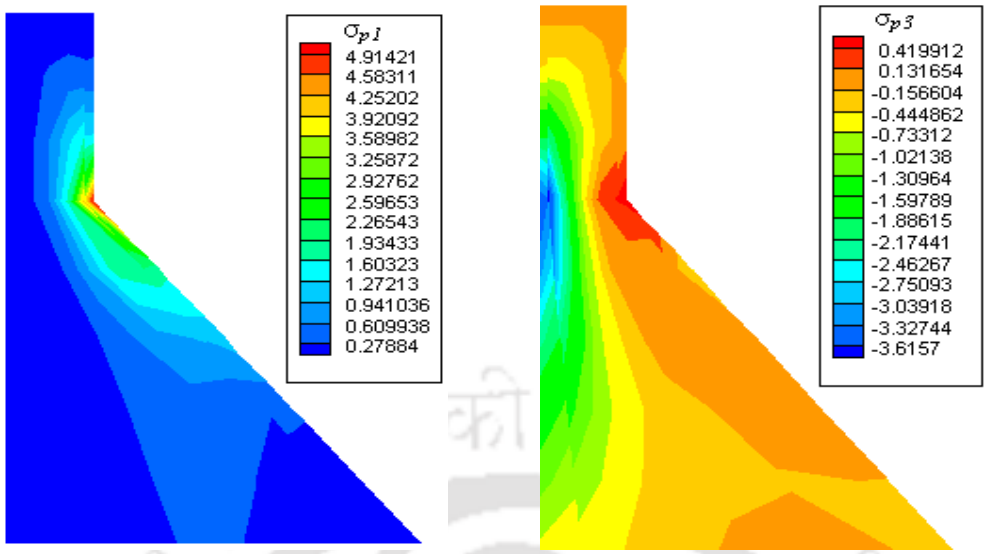


(i) (ii)

Fig. 4.15 Contour for principal stress (i) $\sigma_{p1}$ and (ii) $\sigma_{p32}$ at 3.64 seconds at the end of 50$^{th}$ year

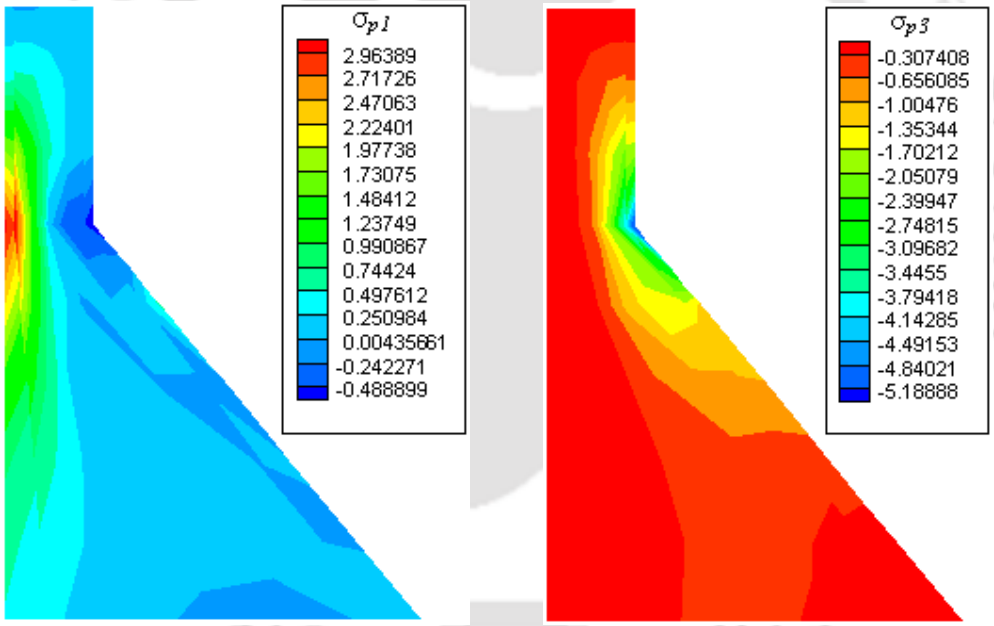


(i) (ii)

Fig. 4.16 Contour for principal stress (i) $\sigma_{p1}$ and (ii) $\sigma_{p3}$ at 3.91 seconds at the end of 50$^{th}$ year

Fig. 4.11 to Fig. 4.16 presents the contour plots of major and minor principal stresses at those time instants when major and minor principal stresses have attained their peak values. It is observed from Fig. 4.11 (i), Fig. 4.13 (i) and Fig. 4.15 (i) that whenever the major principal stresses are highest, the neck region (point 'O' in Fig. 4.1) of the dam experiences the highest tensile stress. Fig. 4.11 (ii), Fig. 4.13 (ii) and Fig. 4.15 (ii) show that the compressive stress occurs along the vertical upstream face of the dam opposite to the neck region of the dam. Similarly, Fig. 4.12(i), Fig. 4.14 (i) and Fig. 4.16(i) reveal

that whenever minor principal stresses are lowest, the tensile stresses are generated along vertical upstream side of dam (opposite to point 'O' of Fig. 4.1) of the dam. Also, Fig. 4.12(ii), Fig. 4.14 (ii) and Fig. 4.16(ii) display that the compressive stresses accumulates near the neck region.

### 4.2.6 Effect of Hydrodynamic Pressure on Dam

The hydrodynamic pressure on upstream side of the dam is calculated using Eq. (3.90). The self weight of the dam is ignored during the analyses. Fig. 4.17 shows the variation of pressure at heel of the dam body (point 'B' as shown in Fig. 4.1) calculated using Eq. 3.90 with respect to time. It may be seen that the maximum and minimum pressure obtained at point 'B' are 273068.18 N/m$^2$ and -355588.78 N/m$^2$ respectively.

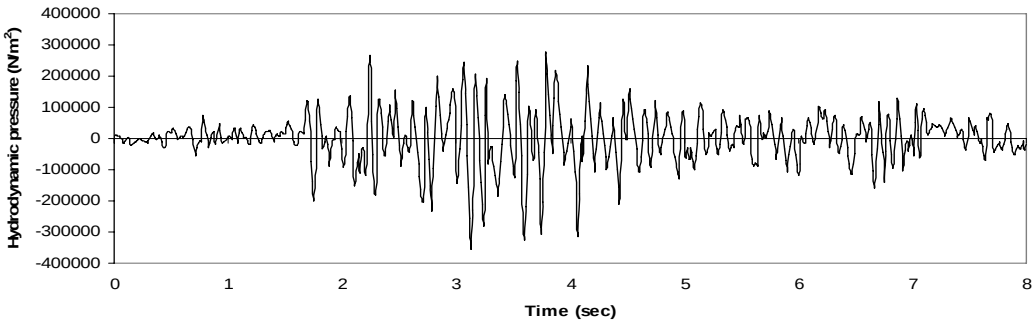


Fig. 4.17 Variation of hydrodynamic pressure calculated at heel node (point 'B') with respect to time

While calculating the hydrodynamic pressure using Eq. (3.90), a convergence study is carried out to determine how many terms designated by the index *'m'* under the summation sign are required. Fig. 4.18 shows the variation of normalized hydrodynamic pressure $\left(\frac{p}{a_n \rho H}\right)$ at 4 second along the upstream face of the dam using different values of *'m'* in Eq. (3.90). It is observed that the normalized pressure calculated over the height of the dam converges fairly well for a value of $m = 10$. However, for further calculations, a value of $m = 10$ is used.

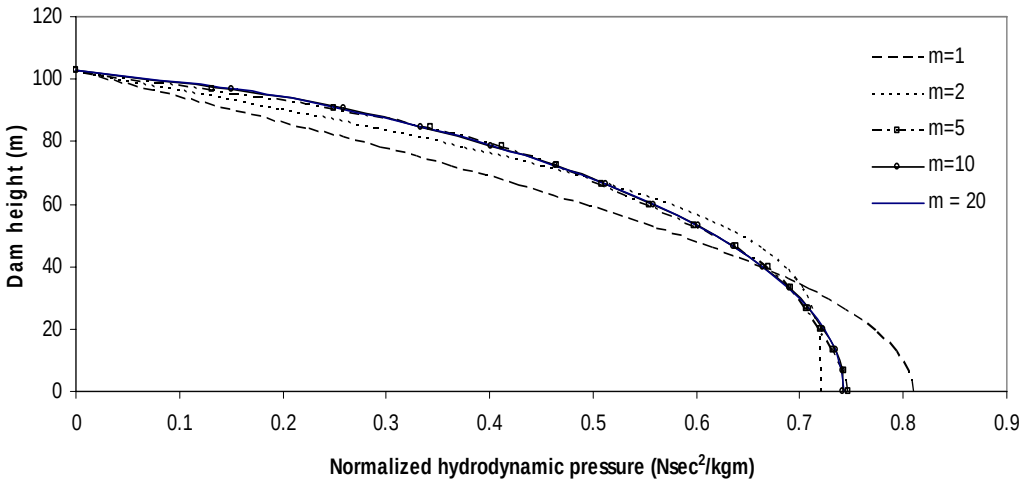


Fig. 4.18 Convergence of normalized hydrodynamic pressure along dam height

At each year after the construction of the dam, comparisons are made to assess the relative increment of the responses when the hydrodynamic pressure is considered in the analyses. Fig. 4.19 depicts the comparison between horizontal crest displacements of dam under reservoir empty and reservoir full condition. If the hydrodynamic pressure is ignored, then the peak displacements are 3.40 cm and -3.93 cm just after the construction of the dam is over. If the hydrodynamic pressure is considered in the analysis, the peak magnitudes of displacements increase to 6.18 cm and -7.23 cm respectively. Therefore an increase of 81.8% and 84.0% is observed when the effect of hydrodynamic pressure is taken into account. Fig. 4.20 shows the comparison of major principal stress values observed at neck node (point 'O' as shown in Fig. 4.1) under full reservoir and empty reservoir conditions respectively. Under empty reservoir condition, the maximum value of major principal stress observed at point 'O' is 14.30 MPa whereas the magnitude of maximum major principal stress at that node is 7.61 MPa under the empty reservoir condition. Therefore, a rise of 87.90% is observed if the effect of hydrodynamic pressure is considered in the analysis. Fig. 4.21 shows the variation of minor principal stress observed at point 'O'. The minimum value of minor principal stress observed at the neck node is -12.60 MPa when the effect of hydrodynamic pressure is considered. The minimum major principal stress at the neck is -6.78 MPa if the contribution of hydrodynamic pressure is ignored. Therefore, a rise of 85.80% is observed in the peak value of minor principal stress observed at point 'O' when the analysis is carried out under full reservoir condition.

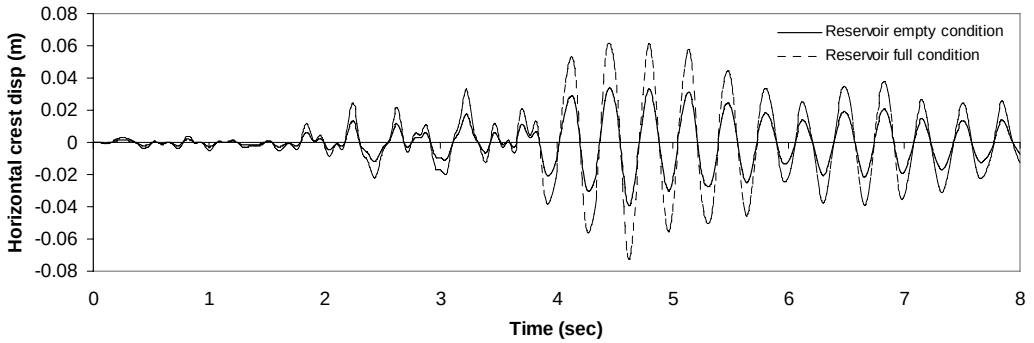


Fig. 4.19 Comparisons of horizontal crest displacement just after construction under reservoir empty and reservoir full conditions (HCM design life – 100 years)

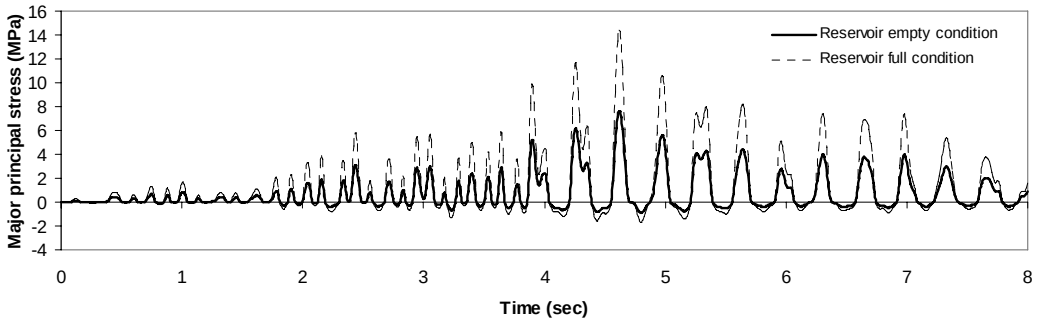


Fig. 4.20 Comparisons of major principal stress at neck just after construction under reservoir empty and reservoir full conditions (HCM design life – 100 years)

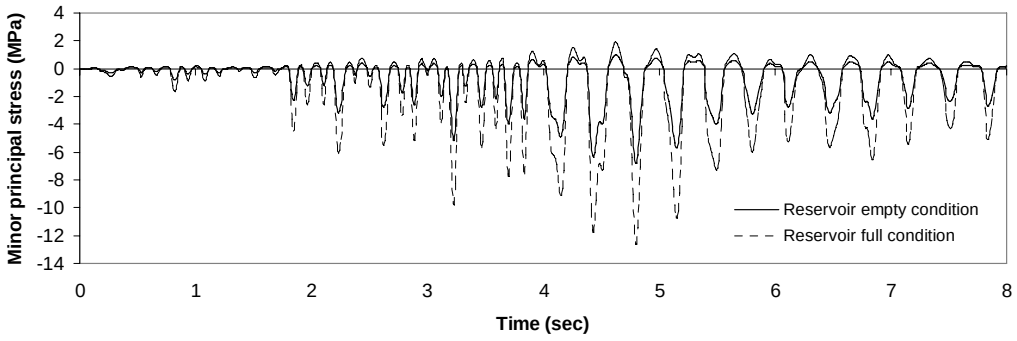


Fig. 4.21 Comparisons of minor principal stress at neck just after construction under reservoir empty and reservoir full conditions (HCM design life – 100 years)

Fig. 4.22 shows the comparison of horizontal crest displacement observed for the analyses carried under full reservoir and empty reservoir conditions after 25 years of construction. The peak values of horizontal crest displacements observed under empty reservoir conditions are 6.34 cm and -5.49 cm respectively. The same values observed under full reservoir analysis are 11.70 cm and -10.10 cm respectively. Therefore, a rise of

84.50% and 84.0% in the peak responses is observed when the hydrodynamic pressure is considered in the analysis. Fig. 4.23 and Fig. 4.24 display the variation of major and minor principal stress values observed at neck node (point 'O') under full and empty reservoir conditions respectively. The maximum value of major principal stress under full reservoir condition is 13.0 MPa whereas the same attains a value of 6.85 MPa under empty reservoir condition. A rise of 89.8-% is observed in this case. From Fig. 4.24, it may be observed that the minimum value of minor principal stresses under full and empty reservoir conditions are -16.80 MPa and -8.99 MPa respectively. Therefore, a rise of 86.90% is observed if the effect of hydrodynamic pressure is included in the analysis.

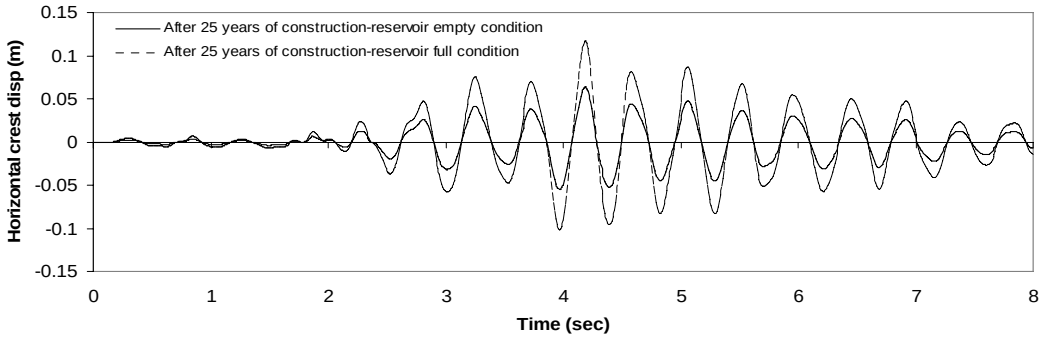


Fig. 4.22 Comparisons of horizontal crest displacement after 25 years of construction under reservoir empty and reservoir full conditions (HCM design life – 100 years)

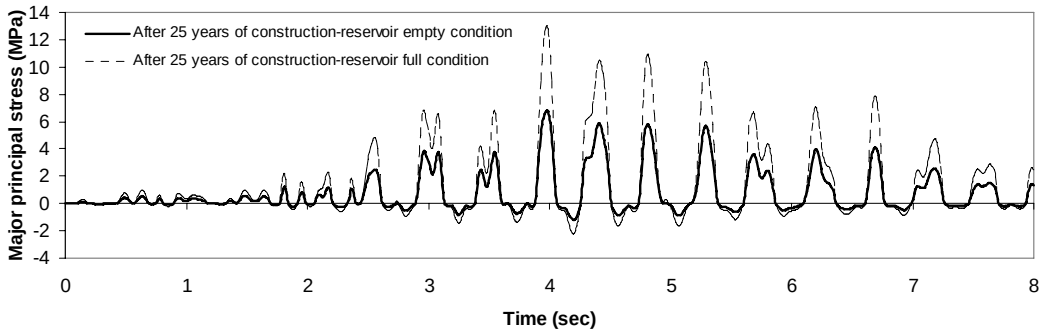


Fig. 4.23 Comparisons of major principal stress at neck after 25 years of construction under reservoir empty and reservoir full conditions (HCM design life – 100 years)

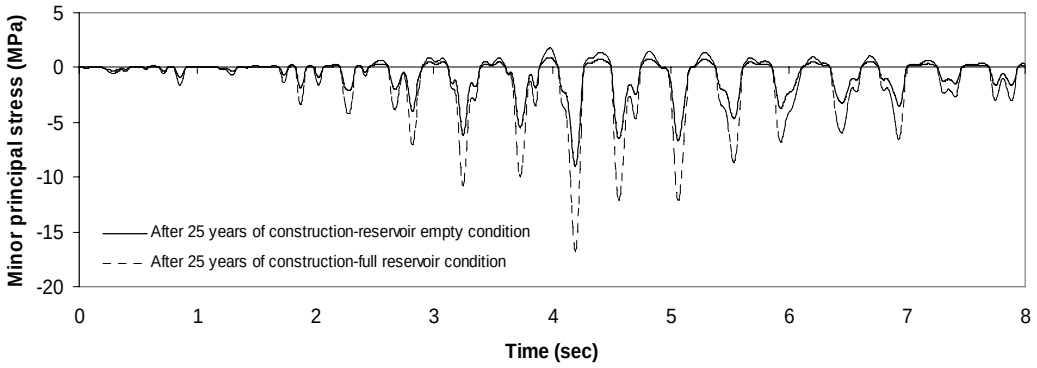


Fig. 4.24 Comparisons of minor principal stress at neck after 25 years of construction under reservoir empty and reservoir full conditions (HCM design life – 100 years)

Fig. 4.25 shows the comparison of horizontal crest displacements observed at the end of 50 years of construction of the dam under full and empty reservoir conditions. When the hydrodynamic pressures are not incorporated in the analysis, the maximum and minimum displacements observed are 5.66 cm and -6.02 cm respectively. If the analysis is carried out under full reservoir condition, the maximum and minimum displacements are obtained as 10.20 cm and -11.20 cm respectively. Therefore, a rise of 80.20% and 86.0% are observed for the respective quantities.

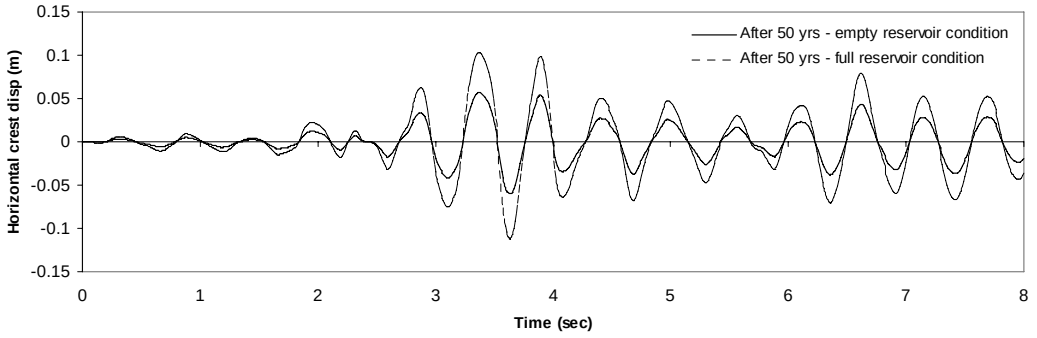


Fig. 4.25 Comparisons of horizontal crest displacement after 50 years of construction under reservoir empty and reservoir full conditions (HCM design life – 100 years)

Fig. 4.26 shows the comparison of major principal stresses for reservoir empty and reservoir full conditions after 50 years of construction. Under empty reservoir conditions, the maximum value of major principal stress observed at point 'O' is 5.25 MPa whereas the same is found out to be equal to 10.30 MPa. Therefore, a rise of 96.20% is observed in the value of major principal stress if the hydrodynamic pressure is taken into account. Fig 4.27 displays the comparison of minor principal stresses observed

at point ‘O’ at the end 50 years of construction under empty and full reservoir conditions. If the hydrodynamic pressure is ignored, the minimum value of minor principal stress observed is -5.54 MPa. The same quantity is found out to be equal to -10.50 MPa when the hydrodynamic pressure is included in the analysis. Therefore, a rise of 89.50% is observed in this case.

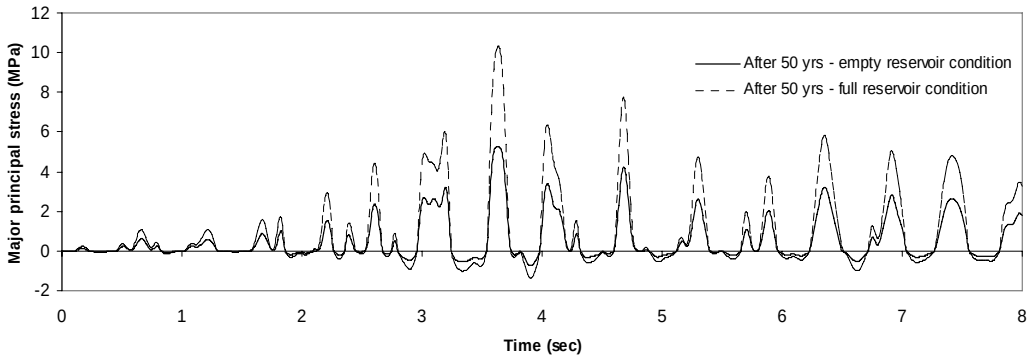


Fig. 4.26 Comparisons of major principal stress at neck after 50 years of construction under reservoir empty and reservoir full conditions (HCM design life – 100 years)

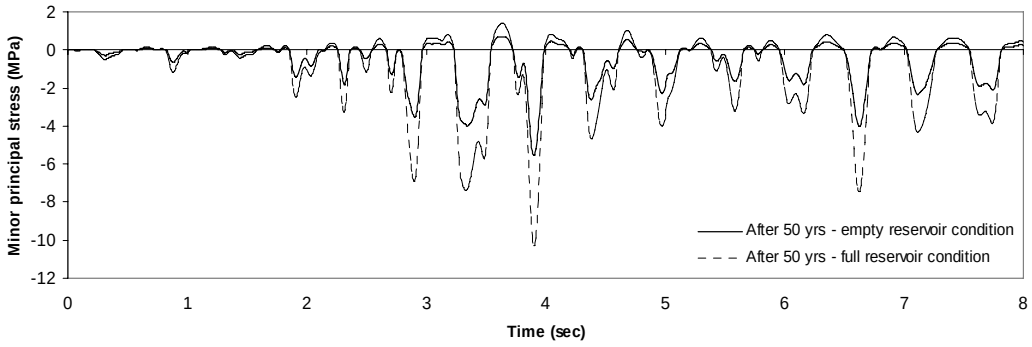


Fig. 4.27 Comparisons of minor principal stress at neck after 50 years of construction under reservoir empty and reservoir full conditions (HCM design life – 100 years)

Table 4.4 displays the numerical values of horizontal crest displacement observed at node ‘A’ (as shown in Fig. 4.1), major and minor principal stresses obtained at node ‘O’ (as shown in Fig. 4.1) for different ages under empty and full reservoir conditions. The HCM design life of concrete is taken as 100 years. It is noticed that the consideration of hydrodynamic pressure produces higher responses compared to that of empty reservoir condition.

**Table 4.4 Comparison of maximum values of horizontal crest displacements, major and minor principal stresses computed under empty and full reservoir conditions (HCM design life = 100 years)**

| | Horizontal crest displacement (cm) | Major principal stress (MPa) | Minor principal stress (MPa) |
|---|---|---|---|
| Just after construction (reservoir empty condition) | 3.40<br>-3.93 | 7.61 | -6.78 |
| Just after construction (reservoir full condition) | 6.18<br>-7.23 | 14.30 | -12.60 |
| After 25 years (reservoir empty condition) | 6.34<br>-5.49 | 6.85 | -8.99 |
| After 25 years (reservoir full condition) | 11.70<br>-10.10 | 13.0 | -16.80 |
| After 50 years (reservoir empty condition) | 5.66<br>-6.02 | 5.25 | -5.54 |
| After 50 years (reservoir full condition) | 10.20<br>-11.20 | 10.30 | -10.50 |

### 4.2.7 Summary of Findings

The following conclusions are drawn based on the results obtained in Chapter 4 (Part I):

i) A time domain model (as proposed by Gogoi and Maity, 2007) to describe the ageing process of concrete due to various hygro-chemo-mechanical actions has been used to investigate the behavior aged concrete gravity dam. The model is capable to describe the behavior of aged concrete.

ii) A parameter called isotropic degradation index $d_m$ is used as suggested by Gogoi and Maity (2007) to describe the time dependent degradation phenomenon of concrete. The maximum allowable range of values for $d_m$ should lie between 1.0 and 0.0 indicating complete and no degradation of concrete, respectively.

iii) The isotropic degradation index is also a function of a parameter hygro-chemo-mechanical (HCM) design life. The consideration of higher HCM design life yields lesser value of degradation index and vice versa at a particular year after construction. Correspondingly, for a higher HCM design life the degradation of concrete will be lower and vice versa because the degradation of concrete increases with the increase of the value of degradation index.

iv) As the degradation index of concrete increases, the elastic modulus and the stiffness reduces as the concrete suffers more and more degradation due to ageing effect over a larger stretch of time. As a result, higher displacements and lesser stresses are observed to develop in the body of the dam.

v) The natural frequency of the structure decreases and the fundamental time period of the structure increases with the increase in degradation of the concrete dam.

vi) The contour plots of major and minor principal stresses reveal that whenever the major principal stresses are highest, the neck region of the dam experiences highest tensile stresses. Also, the maximum compressive stresses are found to occur along the vertical upstream face of the dam. Whenever minor principal stresses are lowest, the compressive stresses are observed near the neck region of the dam. The tensile stresses are found to accumulate near the vertical upstream face of the dam just opposite to the neck region of the dam body.

vii) The "added mass" approach proposed by Westargaard (1933) is a simple and effective way to simulate the effect of hydrodynamic pressure on the dam.

viii) Consideration of the effect of hydrodynamic pressure on the body of the dam (full reservoir condition) produces higher displacements and stresses compared to the case when the effect of hydrodynamic pressure is ignored (empty reservoir condition).

# PART –II

## 4.3 ANALYSIS OF FOUNDATION

In the present analysis, the concrete gravity dam is considered to be situated on rock foundation. When the behavior of Koyna gravity dam under the effect of SSI is ascertained, the underlying rocky foundation is modeled considering linear, elastic as well as nonlinear, elastic material properties. Since the stress-strain behavior of rock is essentially nonlinear, a proper nonlinear stress-strain model known as Duncan-Chang model is chosen to represent its nonlinear characteristics. In the following section, some results related to the foundation characteristics are presented. The foundation domain underlying Koyna gravity dam is analyzed considering the linear as well as the nonlinear behavior of the foundation material. The side nodes at the truncated boundary of the foundation are attached to viscous dashpots in order to absorb the traveling earthquake waves and thereby, preventing them from being reflected from the truncated boundary. The bottom nodes at the base of the foundation are attached to rollers allowing only horizontal translations. The boundary conditions for the foundation domain are implemented as described in section 3.3.3.4. The results of analysis of the foundation used for solving Koyna dam-foundation interaction problem are presented next.

### 4.3.1 Material Properties of Foundation

At the sides of the foundation domain, viscous dashpots are attached to absorb the energy of the incident earthquake waves. The boundary condition used in the present analyses is depicted in Fig. 3.9 (b). The Young's modulus of foundation rock is considered to be 1.75e+10 $N/m^2$. The Poisson's ratio is assumed as 0.2. The mass density of the foundation material is assumed to be 1800.0 $kg/m^3$. For simulation of nonlinear behavior of the foundation rock, the cohesion ($C$) and angle of internal friction ($\phi$) are assumed to be equal to 1500 $kN/m^2$ and $40^0$ respectively (Deb, 2006).

### 4.3.2 Discretization of Foundation Domain

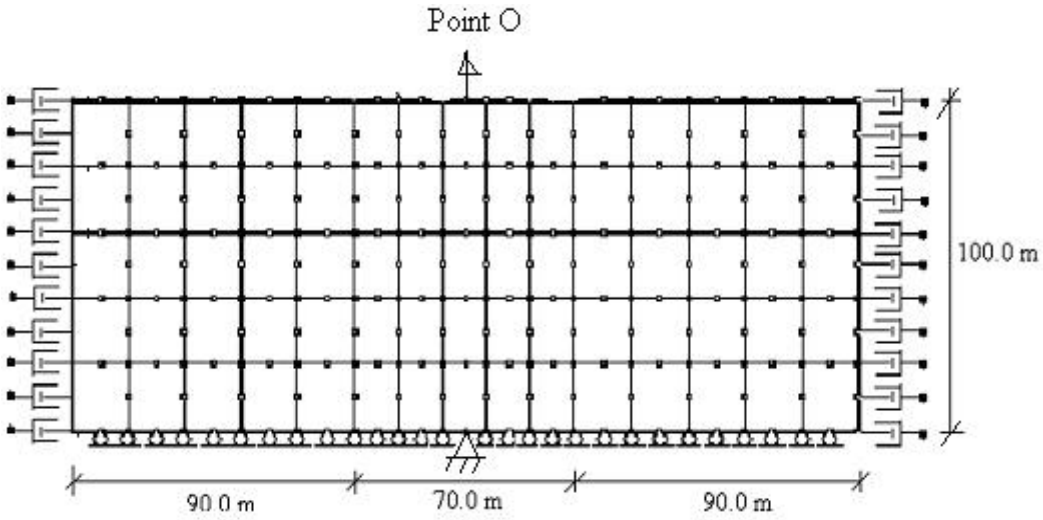


Fig. 4.28 Geometry and finite element discretization of foundation domain

In order to arrive at an optimum mesh grading for this particular problem, the response of the dam and the foundation domain under the action of a given load was found out. The foundation domain is analyzed against Koyna earthquake (1967) loading and the maximum and minimum value of horizontal displacement observed at node point 'O' (as shown in Fig. 4.28) is noticed. During analysis, the side nodes at the boundary are considered to be fitted with viscous dashpots in both normal and tangential directions which act as absorbing dampers to prevent reflection of waves from the boundary. The middle point at the base of the boundary is kept fixed to prevent rigid body motion in $x$ – direction. All the other nodes are fitted with rollers as shown in Fig. 4.28. The effect of earth pressure is simulated as suggested by Preisig (2002) in section 3.9.3. The time periods for the first two nodes were also noted. The convergence of these values was investigated for different mesh grading. The values of time periods in seconds as well as the horizontal component of displacement (in meters) observed at point are tabulated in Table 4.5. It was noted that the values converged for a discretization of 15H×5V fairly accurately. Thus, the discretization of 15H×5V is chosen for the present problem.

**Table 4.5 Convergence of time periods and displacement at the middle point of the surface of the foundation for different mesh sizes**

| Foundation With Mesh Size | Time Period (sec) | | Maximum +ve value of the horizontal displacement (m) | Maximum -ve value of the horizontal displacement (m) |
|---|---|---|---|---|
| $N_v \times N_h$ | Mode1 | Mode 2 | | |
| 10×2 | 0.4666 | 0.1635 | 0.00177 | -0.00216 |
| 10×4 | 0.4645 | 0.1636 | 0.00197 | -0.00238 |
| 10×5 | 0.4669 | 0.1636 | 0.00198 | -0.00239 |
| 11×2 | 0.4132 | 0.1635 | 0.00207 | -0.00248 |
| 11×4 | 0.4251 | 0.1636 | 0.00208 | -0.00251 |
| 11×5 | 0.4303 | 0.1636 | 0.00226 | -0.00249 |
| 12×4 | 0.4646 | 0.1636 | 0.00222 | -0.00243 |
| 12×5 | 0.4669 | 0.1636 | 0.00221 | -0.00242 |
| 13×4 | 0.4251 | 0.1636 | 0.00227 | -0.00246 |
| 13×5 | 0.4303 | 0.1636 | 0.00226 | -0.00244 |
| 14×4 | 0.4646 | 0.1636 | 0.00220 | -0.00242 |
| 14×5 | 0.4669 | 0.1636 | 0.00221 | -0.00243 |
| 15×4 | 0.4251 | 0.1636 | 0.00225 | -0.00245 |
| 15×5 | 0.4303 | 0.1636 | 0.00225 | -0.00243 |
| 16×4 | 0.4646 | 0.1636 | 0.00224 | -0.00240 |
| 16×5 | 0.4669 | 0.1636 | 0.00223 | -0.00239 |
| 17×4 | 0.4251 | 0.1636 | 0.00225 | -0.00245 |
| 17×5 | 0.4304 | 0.1636 | 0.00225 | -0.00244 |

### 4.3.3 Selection of Time Step ($\Delta t$)

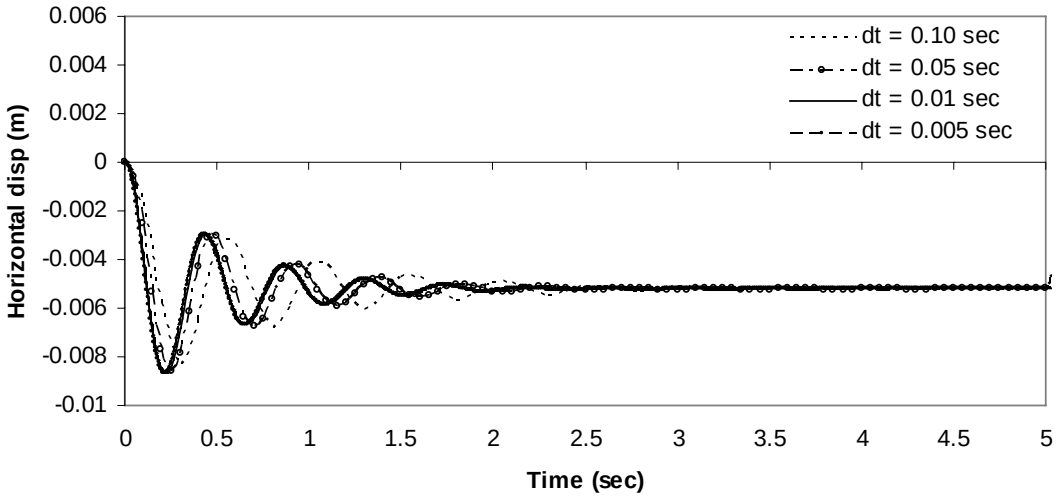


Fig 4.29 Horizontal displacement at of point 'O' of foundation subjected to unit horizontal ramp acceleration

Similar to the analyses of dam domain, the foundation domain for Koyna gravity dam is also subjected to unit horizontal ramp acceleration with different time step values. The Newmark's average acceleration method which is unconditionally stable is adopted for the present solution. A study is carried out with different time steps to obtain a convergent value of a particular response in the present analysis. The initial time step $\Delta t$ is chosen as the $1/100^{th}$ of the fundamental period. Time histories of horizontal displacements at the top of the structure subjected to unit sinusoidal acceleration for different time steps are shown in Fig. 4.29. From the results it is observed that a time step of 0.01 second may be considered, at which sufficient level of convergence is obtained.

### 4.3.4 Selection of Foundation Size without Dashpot

For accurate analysis of the semi-infinite foundation domain with finite element method, it is important to fix a suitable dimension in both horizontal and vertical direction of the foundation domain. The foundation domain is discretized with the mesh division of 15H × 5V (as obtained in section 4.3.2) considering different width and height of the foundation domain. The middle point at the surface of the foundation domain is denoted by point 'O'. A horizontal sinusoidal load of 1000 kN is applied on the middle point

(point ‘O’) of the surface of the foundation. At first, it is attempted to fix the width and height of the foundation domain without considering viscous dashpots at the sides of the foundation domain. The side nodes of the foundation domain (as shown in Fig. 4.35) are considered to be free to move along two orthogonal directions. Fig. 4.30 shows the plot of horizontal displacement observed at point ‘O’ under applied sinusoidal load of 1000 kN. It may be seen that the displacements attains a constant value with the increase in the size of the foundation domain. It is also observed that there are some undulations in the beginning of the response which are later fizzled out. From the figure, it is seen that if the foundation width is more than 4.0b, then the responses become almost constant.

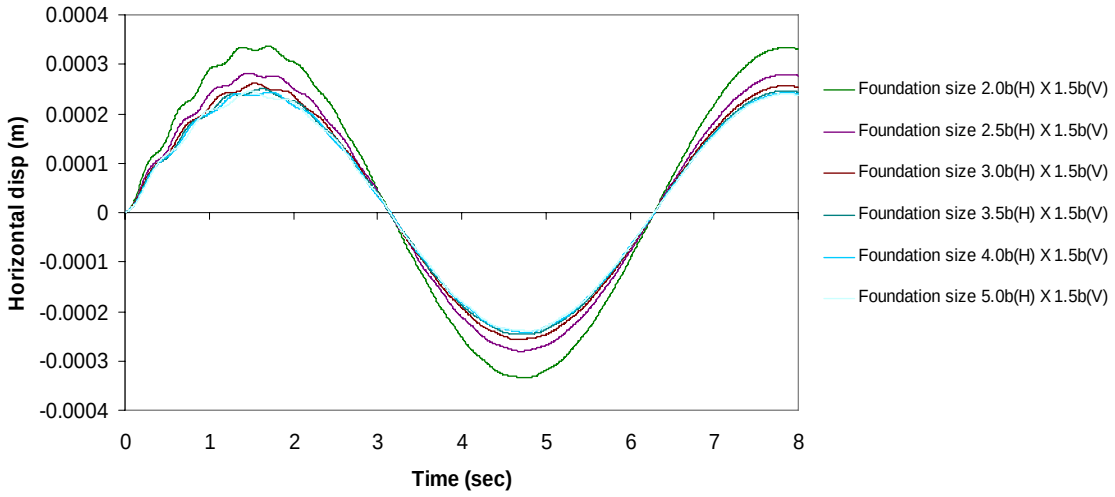


Fig. 4.30 Horizontal displacement at point ‘O’ of the foundation domain when side nodes are kept free

### 4.3.5 Selection of Foundation Size with Dashpot

Next, the dashpots are attached to the nodes at the side boundary of the foundation domain. The foundation domain is discretized with the mesh division of 15H × 5V (as obtained in section 4.3.2) considering different width and height of the foundation domain. The nodes at the side of the boundary are attached to viscous dashpots to absorb the incoming waves. A horizontal sinusoidal load of 1000 kN is applied on the middle point (point ‘O’) of the surface of the foundation. The horizontal component of displacement is noted after carrying out the dynamic analysis. Fig. 4.31 shows the response of horizontal displacement observed at point ‘O’. It is seen that the undulation

which occurred when the analyses are carried out in the absence of the viscous dashpots are no longer present in this case. It may be seen that the responses attain similar values when the foundation width reaches 4.0b and onwards.

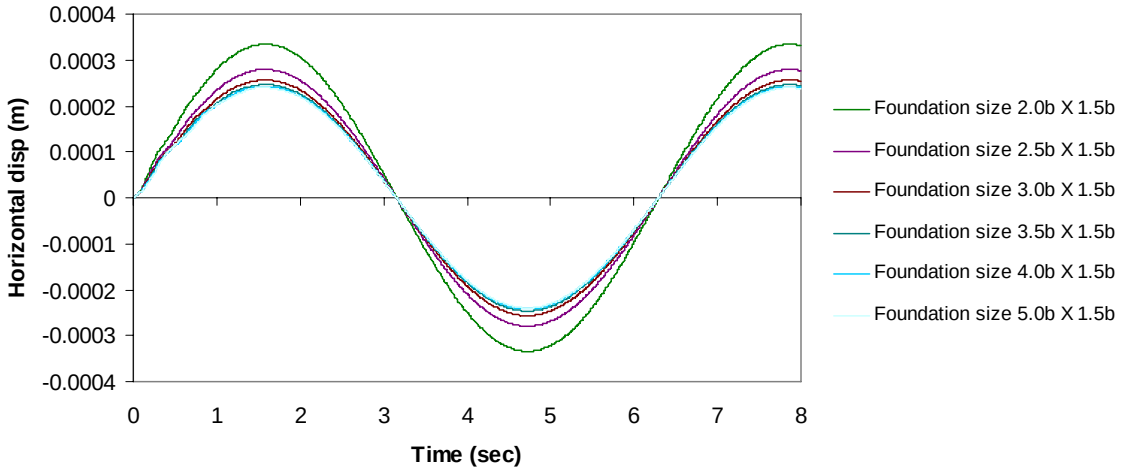


Fig. 4.31 Horizontal displacement at point 'O' of the foundation domain when side nodes are attached to viscous dashpots

Next, the effect of earth pressure is incorporated along with the dashpots at the sides of the boundary. The horizontal at rest earth pressure is applied at the boundary nodes situated at the both sides of the foundation domain. This is done by recording the reaction forces in the model with fixed boundaries and applying them with opposite sign to the model with absorbing boundaries (as shown in Fig. 3.9(b)). The horizontal displacement at point 'O' is plotted in Fig. 4.32 under the application of a horizontally applied sinusoidal load of 1000 kN. It is seen that responses have reduced in this case and the differences of responses are also reduced if such a boundary condition is adopted compared to two earlier cases. Also, the responses attain constant values with lesser width of the foundation domain. It is seen that the responses become similar if the foundation width is 3.0b or more. From this analysis, the width and the depth of the foundation domain are considered to be 250.0 m ($\approx 3.5b$) and 100.0 m ($\approx 1.5b$) respectively. The foundation domain with the applied boundary conditions is presented in Fig. 4.35. At the base of the foundation domain, the middle node is kept fixed. All the other nodes at the base are attached with rollers allowing translations only in the horizontal direction. The fixation of the middle node at the base of the foundation domain

is required in order to guard against the rigid body movement in *x*-direction. The reason for using such boundary condition for the foundation domain is that similar boundary condition has been adopted during dam-foundation interaction analyses by Presisig, 2002. The slightest imbalance in forces causes the entire model to move as a rigid body in *x*-direction (Preisig, 2002). To avoid such rigid body motion, the node at the center of the base is fully fixed in the following analyses.

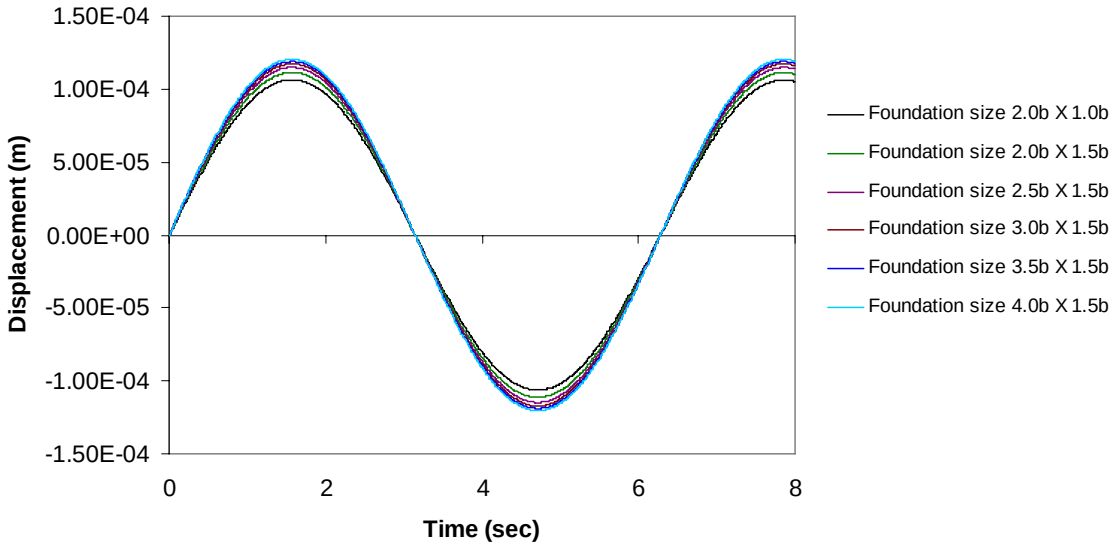


Fig. 4.32 Horizontal displacement at point 'O' of the foundation domain when side nodes are attached to viscous dashpots (the effect of earth pressure considered)

### 4.3.6 Effect of Foundation Nonlinearity

Fig. 4.33 shows the effect of foundation nonlinearity on the response of horizontal displacements of point O with that of the linear material. With the considered values of cohesion (1500 kN/m$^2$) and angle of internal friction (40$^0$), the maximum and minimum displacements for nonlinear material are 2.86 mm and -2.90 mm respectively. The same values for displacements with linear, elastic material properties are 2.25 mm and -2.43 mm respectively. Therefore, a rise of 27.11% and 19.34% has been observed respectively when nonlinear properties of foundation are considered.

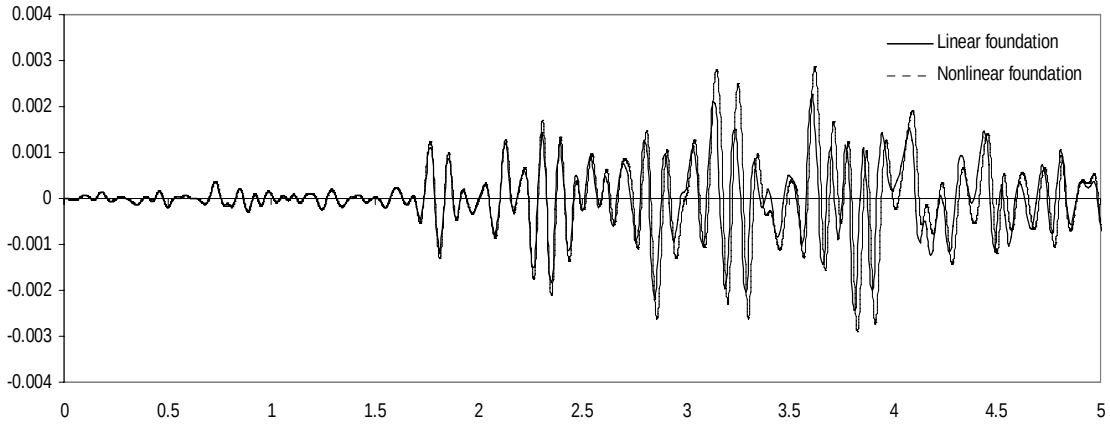


Fig. 4.33 Comparison between linear and nonlinear response of point O
($C$ = 1500 kN/m$^2$, $\phi$=40$^0$)

Fig. 4.34 shows the comparison of major principal stress for linear and nonlinear foundation material found out at point 'O'. For linear foundation properties, the maximum of major principal stress is observed to be 0.0570 MPa. For nonlinear Duncan Chang foundation material, the maximum principal stress is found out to be 0.0646 MPa. Therefore, a rise of 13.33% has been observed for analysis considering nonlinear material properties. Fig. 4.35 shows the comparison of minor principal stress for linear and nonlinear foundation material found out at point O. For linear foundation properties, the maximum value of the minor principal stress is observed to be -0.0570 Mpa. For nonlinear Duncan Chang foundation material, the maximum principal stress is found out to be -0.0646 MPa. Therefore, a rise of 13.33% has been observed for analysis considering nonlinear material properties.

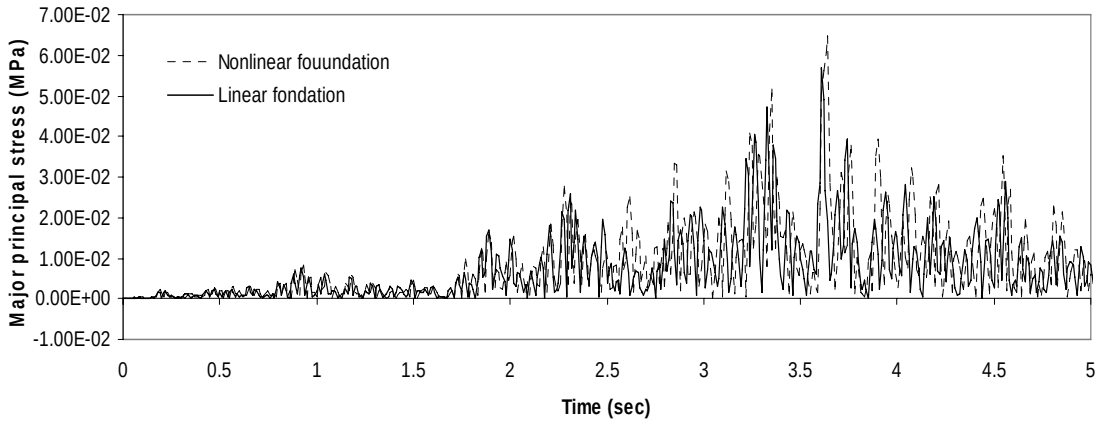


Fig. 4.34 Comparison between linear and nonlinear response of major principal stress at point O ($C$ = 1500 kN/m$^2$, $\phi$=40$^0$)

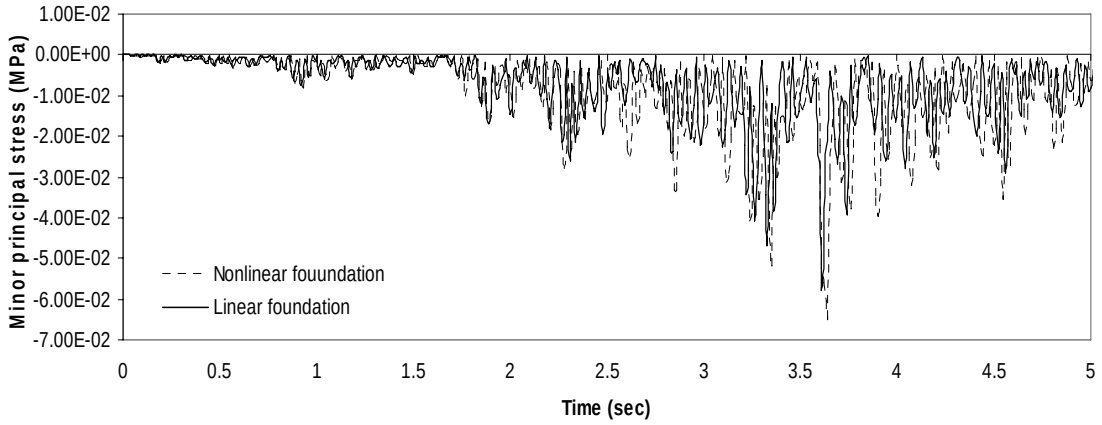


Fig. 4.35 Comparison between linear and nonlinear response of major principal stress at point O ($C$ = 1500 kN/m$^2$, $\phi$=40$^0$)

Table 4.6 displays the maximum values of horizontal displacements, major and minor principal stresses observed at point 'O' (as shown in Fig. 4.28). It is seen that the consideration of nonlinear material properties of the foundation produces higher responses.

**Table 4.6 Responses observed at point 'O' (as shown in Fig. 4.28)**

| | Horizontal disp (m) | Major principal stress (MPa) | Minor principal stress (MPa) |
|---|---|---|---|
| Linear foundation | 0.00225 | 0.0570 | -0.0570 |
| | -0.00243 | | |
| Nonlinear foundation | 0.00286 | 0.0646 | -0.0646 |
| | -0.00290 | | |

Fig. 4.36 shows the variation of tangent Young's modulus calculated following Eq. (3.98) with respect to time. The variation is calculated by carrying out the nonlinear analysis of the foundation domain against Koyna earthquake (1967) (Krishna, Chandrasekharan and Saini, 1969) motion. Also, the value of linear, elastic Young's modulus is plotted against time and their comparison is shown. It may be recalled that the value of Young's modulus (1.75e+10 $N/m^2$) remains unchanged during linear analysis process whereas the effective value of tangent Young's modulus varies according to Eq. (3.98). From Fig. 4.36, it may be seen that the lowest value of tangent Young's modulus obtained is 1.14 e+10 $N/m^2$ during nonlinear analysis. Therefore, a maximum reduction of 34.8% of the original Young's modulus is obtained during nonlinear analysis.

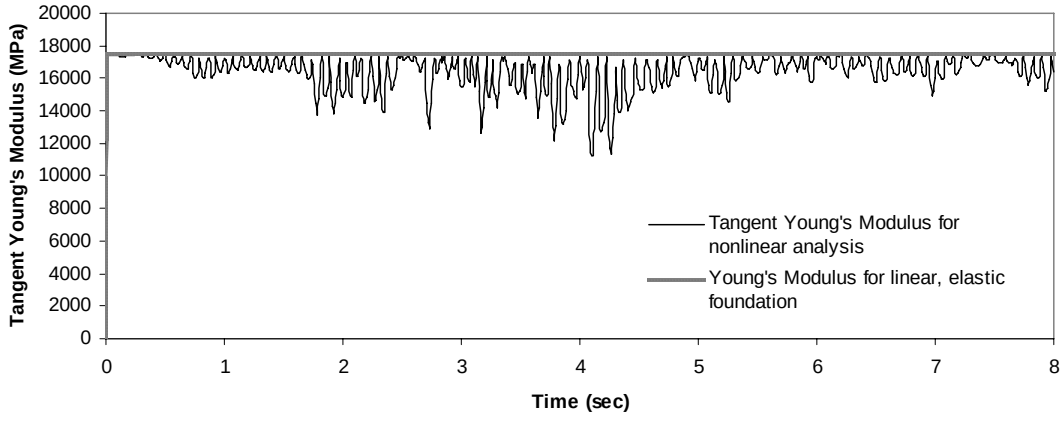


Fig. 4.36 Variation of tangent Young's modulus for nonlinear foundation with time

From Fig. 4.34, it may be observed that the maximum values of horizontal displacements occur at 3.61 seconds for linear analysis. Fig. 4.37 shows the contour plot

of major principal stresses throughout the foundation domain at 3.61 seconds. It may be noticed that there is a concentration of tensile stresses along the left side of the foundation domain. Also, the middle of foundation along the base experiences tensile stresses. Fig. 4.38 displays the contour plot of minor principal stresses over the body of the foundation domain at 3.61 second. It may be seen that the compressive stresses are predominant along the right side of the foundation. Also, the left-middle portion at the base experiences the concentration of compressive stresses at that particular time instant.

Fig. 4.35 displays that the minimum value of horizontal displacements occurs at 3.81 seconds for linear analyses. Fig. 4.39 shows the contour plot of major principal stresses throughout the body of the dam at 3.81 seconds when the linear material properties of the foundation are considered in the analysis. From Fig. 4.39, it may be seen that the tensile stresses occur along the right side of the foundation. The top right corner along the right boundary as well as the left-middle portion along the base of the foundation domain is heavily stressed with tensile stresses. Fig. 4.40 shows the contour variation of minor principal stresses over the foundation domain. It reveals that maximum compressive stresses are found to occur along the left side of the boundary of the foundation domain. Also, right-middle portion along base of the foundation experiences the occurrences of compressive stresses.

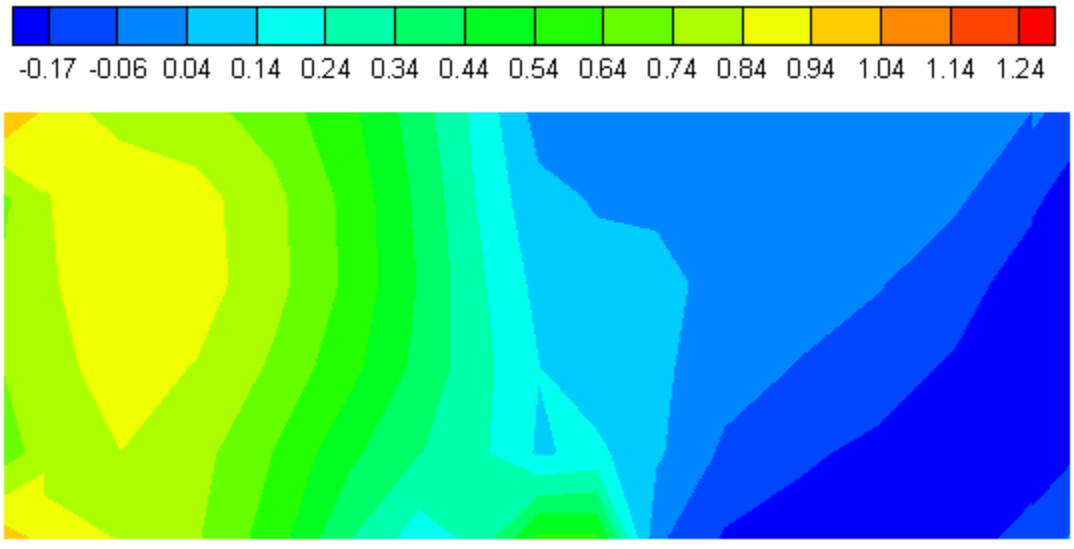


Fig. 4.37 Contour plot of major principal stress (MPa) of linear, elastic foundation for Koyna gravity dam at 3.61 seconds

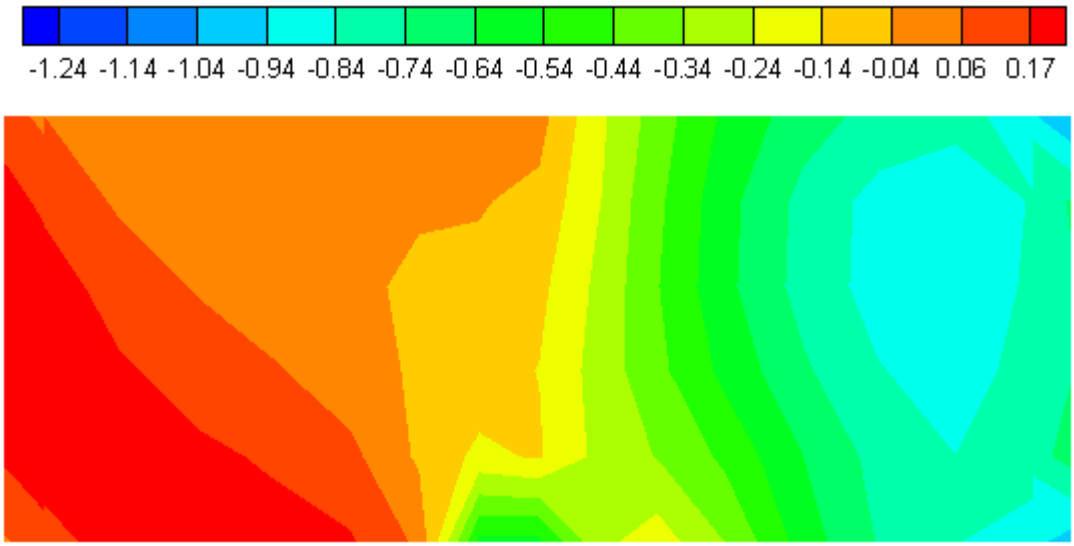


Fig. 4.38 Contour plot of minor principal stress (MPa) of linear, elastic foundation for Koyna gravity dam at 3.61 seconds

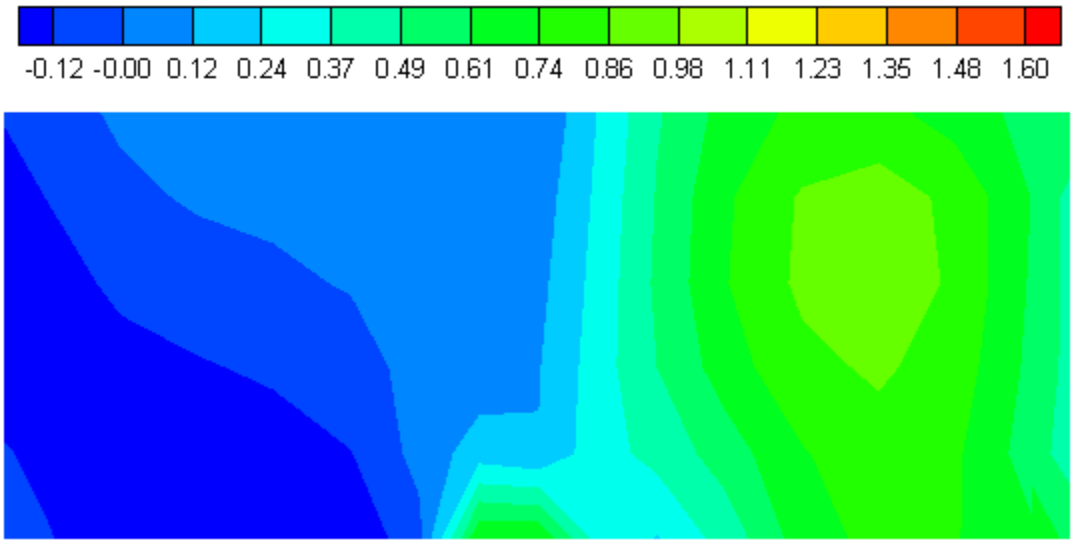


Fig. 4.39 Contour plot of major principal stress (MPa) of linear, elastic foundation for Koyna gravity dam at 3.81 seconds

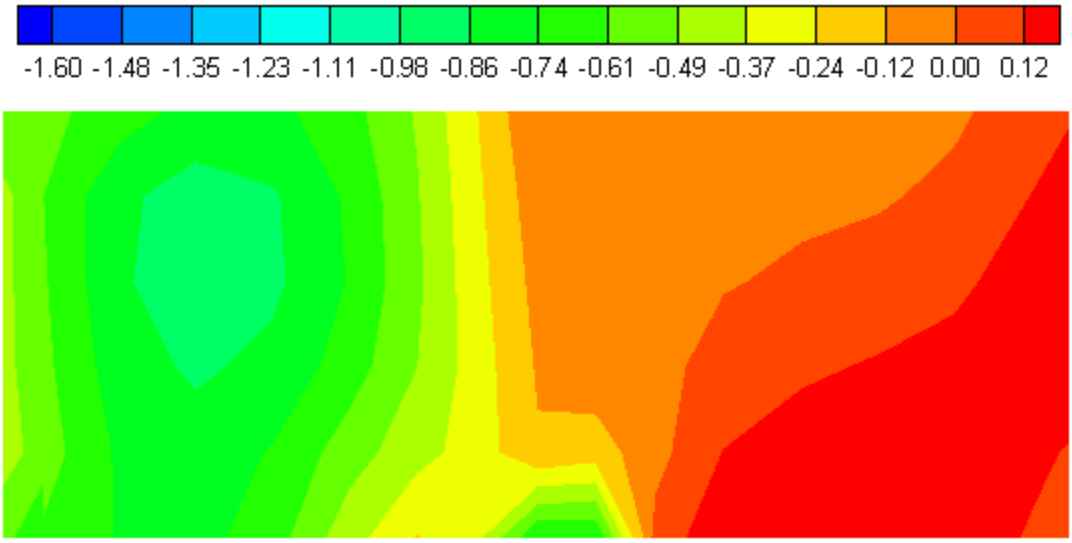


Fig. 4.40 Contour plot of minor principal stress (MPa) of linear, elastic foundation for Koyna gravity dam at 3.81 seconds

From Fig. 4.34, it may be noticed that the maximum and minimum values of displacements occur at 3.63 seconds and 3.84 seconds respectively for nonlinear analysis of the foundation. Fig. 4.41 displays the contour variation of major principal stresses throughout the foundation domain at 3.63 seconds. The figure shows that the maximum tensile stresses occur along the left side of the boundary of the foundation. Also, there is concentration of the tensile stresses at the right-middle portion of the base of the foundation domain. Fig. 4.42 shows the contour plot of minor principal stresses obtained during nonlinear analysis at 3.63 seconds. It may be observed from the figure that the minimum value of minor principal stresses occur along the right side of the boundary. Also, the left-middle portion of the base of the boundary experiences the concentration of compressive stresses.

Similarly, Fig. 4.43 displays the contour variation of major principal stresses throughout the foundation domain for nonlinear analysis at 3.84 seconds. It may be observed that the tensile stresses are predominant along the right side of the boundary of the foundation domain. Also, the left-middle portion at the base of the foundation experiences concentration of tensile stresses. Fig. 4.44 exhibits the contour plot of the minor principal stresses over the body of the foundation domain. It is observed that there is concentration of compressive stresses along the left side of the boundary of the

foundation. Also, the right-middle portion at the base of the foundation experiences some amount of compressive stresses.

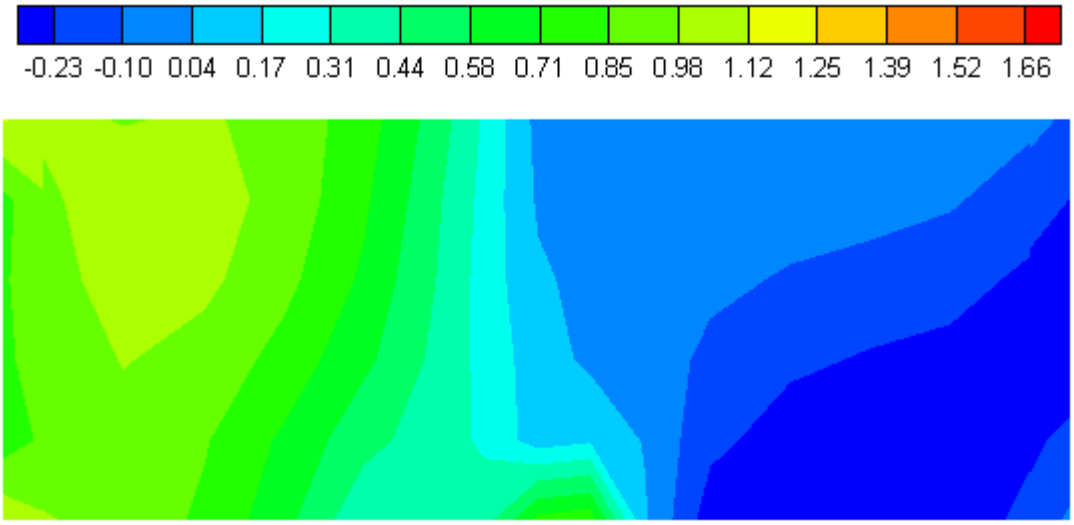


Fig. 4.41 Contour plot of major principal stress (MPa) of nonlinear foundation for Koyna gravity dam at 3.63 seconds

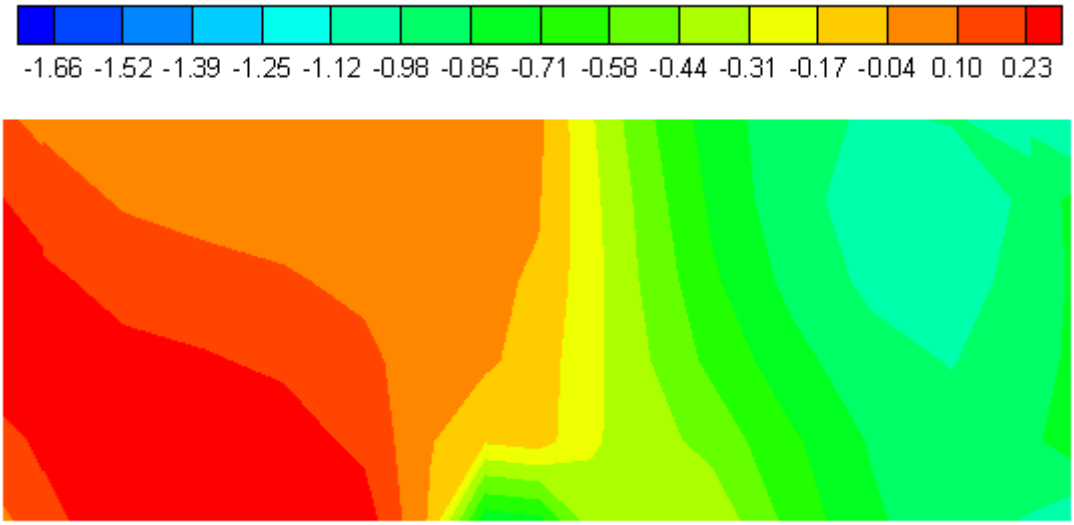


Fig. 4.42 Contour plot of minor principal stress (MPa) of nonlinear foundation for Koyna gravity dam at 3.63 seconds

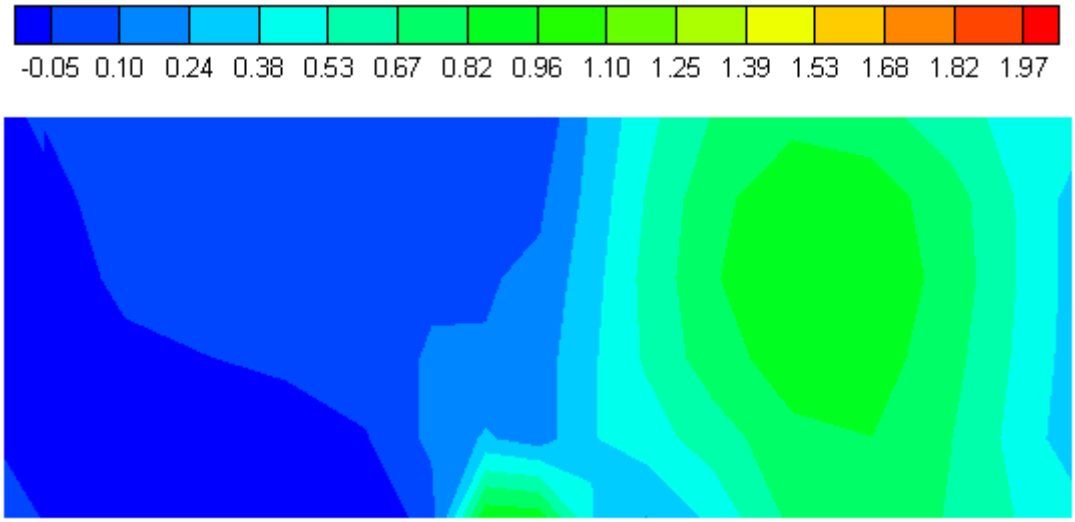


Fig. 4.43 Contour plot of major principal stress (MPa) of nonlinear foundation for Koyna gravity dam at 3.84 seconds

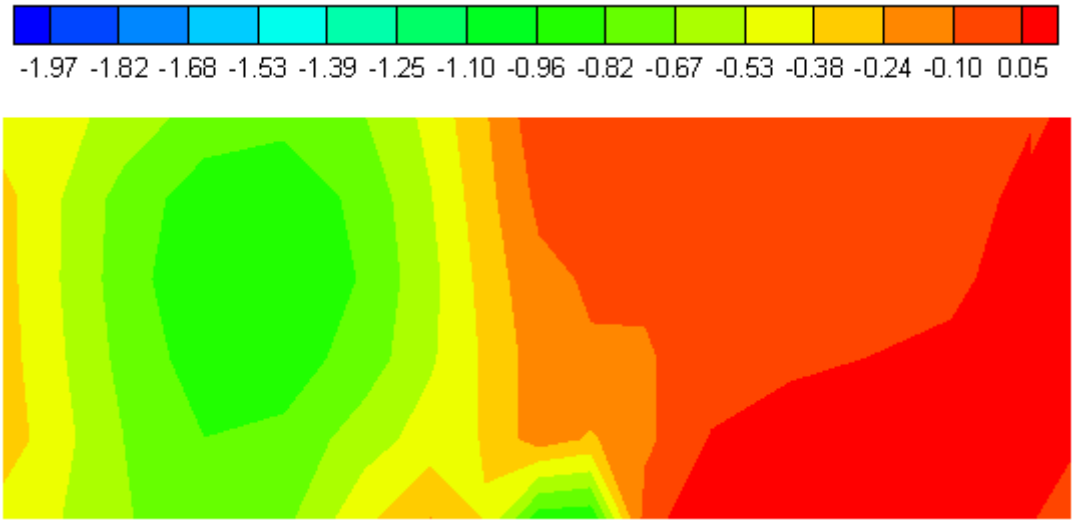


Fig. 4.44 Contour plot of minor principal stress (MPa) of nonlinear foundation for Koyna gravity dam at 3.84 seconds

Therefore, it is observed for both linear and nonlinear analyses of the foundation domain that whenever the displacement at point ‘O’ (as shown in Fig. 4.28) reaches the maximum value, tensile stresses are found to occur along vertical boundary in the left. Also, the middle of foundation along the base experiences tensile stresses. It is further noticed that whenever displacement at point ‘O’ (as shown in Fig. 4.28) attains the lowest

value, maximum compressive stresses are found to occur along the left side of the boundary of the foundation domain. Also, right-middle portion along base of the foundation experiences the accumulation of compressive stresses. Because, the middle node at the base of the foundation domain is considered to be fixed as suggested by Preisig (2002) in section 3.9.3, the concentration of stresses are experienced near the middle portion along the base of the foundation domain.

### 4.3.7 Summary of Findings

Following conclusions may be drawn based on the results obtained in Chapter 4 (Part II):

i) The nonlinear, elastic Duncan-Chang (1970) model is able to simulate the nonlinear properties of the foundation domain. The use of nonlinear, elastic model produces higher displacements and stresses for the foundation domain.

ii) The use of viscous dashpot boundary conditions (Lysmer and Kuhlemeyer, 1969) at the boundary nodes effectively absorbs the energies of the travelling waves and thus prevents spurious reflections. In this way the viscous dashpots help to truncate the foundation domain to a smaller size domain.

iii) It is observed for both linear and nonlinear analyses of the foundation domain that whenever the displacement at mid point on the surface of the foundation reaches the maximum value, tensile stresses are found to occur along vertical boundary in the left. It is further noticed that whenever displacement attains the lowest value, maximum compressive stresses are found to occur along the left side of the boundary of the foundation domain.

# PART III

# 4.4 ANALYSIS OF DAM-FOUNDATION COUPLED SYSTEM

## 4.4.1 Validation of the Proposed Iterative Scheme

In the present work, an iterative technique for analyzing the dam-foundation interaction problem is suggested. In order to validate the proposed algorithm, it is tested against an already published problem. For this purpose, a concrete gravity dam-foundation prototype resting on rock foundation is chosen. The same dam-foundation interaction problem has been previously analyzed by Yazdchi et al (1999). Yazdchi et al. (1999) analyzed a dam-foundation interaction problem using coupled finite element and boundary element technique. Both the dam and foundation domains are treated as linear, elastic in nature. While solving the same dam-foundation interaction problem using the proposed iterative technique in the present work, the side nodes of the discretized finite elements in the foundation portions are considered to be attached to viscous dashpots. These dashpots are helpful in absorbing the energies of the incoming waves and thus preventing them from being reflected inside the foundation domain. The dam and the foundation domain are discretized using two-dimensional, plane strain, isoparametric finite elements. A $2\times2$ Gauss integration rule is adopted for the calculation of both the stiffness and mass matrices. The dimensions of the dam prototype (originally solved by Yazdchi et al., 1999) are depicted in Fig. 4.45. The width of the base of the dam is 10.0 m. The height of the dam is 15.0 m out of which the crest portion is of 6.0 m in length. The width of the crest is considered as 2.0 m. The width and the depth of the foundation part are considered to be 100.0 m and 50.0 m respectively. The material properties of the dam and the foundation part are taken same and are as follows:

The Young's modulus: 30.0 GPa

The Poisson's ratio : 0.20

The mass density : 2600.0 kg/m$^3$

The dam-foundation interaction problem solved by Yazdchi et al. (1999) is solved by the proposed iterative method for soil-structure interaction analysis. The procedure for

choosing the discretization of the dam domain is described in section 4.2.2. A mesh grading of 4 (horizontal) × 10 (vertical) for the dam domain is chosen for the analysis purpose. The dimensions and the mesh discretization adopted for the dam prototype is shown in Fig. 4.45. Similarly, for foundation domain, a mesh grading of 12 (horizontal) × 4 (vertical) is chosen for the analysis. In order to simulate the semi-infinite nature of the foundation domain, viscous dashpots are attached to the sides of the boundary of the foundation domain. The horizontal extent of the foundation portion is truncated at a certain distance from both the upstream and the downstream face of the dam. The procedure for determining the range of foundation domain is described in section 4.3.4.

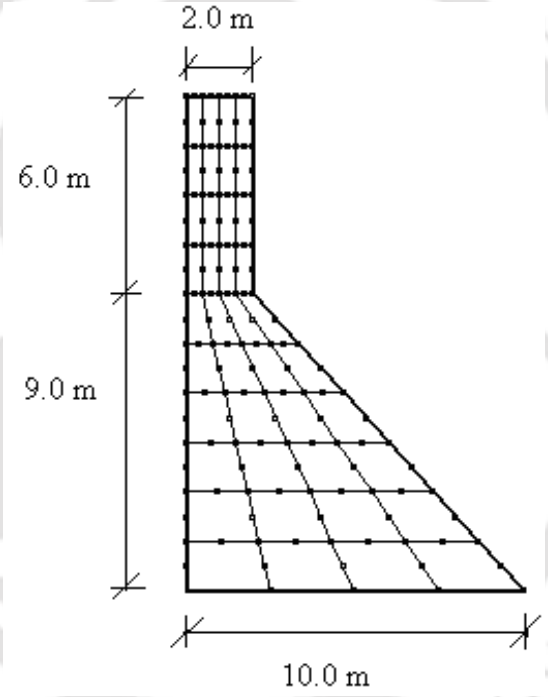


Fig. 4.45 The geometry and mesh division of dam (Yazdchi et al, 1999)

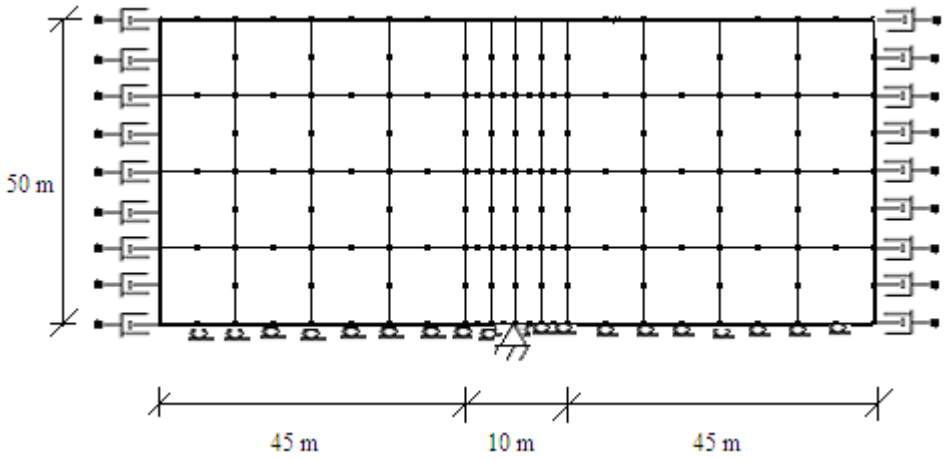


Fig. 4.46 Geometry and finite element discretization of foundation domain (Yazdchi et al., 1999)

The dam-foundation interaction analysis is carried out by considering both dam and foundation domain to be linear, elastic and isotropic in nature. The theoretical details of the interaction analysis are presented in chapter – 3, part C, section 3.10.

For the purpose of validation of the proposed soil-structure interaction method, the results obtained are compared with those reported by Yazdchi et al. (1999). The Koyna earthquake acceleration is applied to the dam prototype with a scaling factor of 2.5 as is done by Yazdchi et al. (1999). The earthquake acceleration data is presented in Fig. 4.5. When the same dam-foundation model is solved by the proposed iterative scheme in the present work, the effect of viscous damping and the hydrodynamic pressure is also considered in similar way as is done by Yazdchi et al. (1999). Also, the interaction analysis is carried out considering the effects of its self weight and the hydrostatic pressure of the dam which produced initial acceleration in the dam body.

Different boundary conditions are tested on the dam-foundation coupled model. First, the side boundary nodes are fully kept fixed as shown in Fig. 3.9 (a). Then, these nodes are released and fitted with dashpots in both normal and tangential direction. The perpendicular dashpots to the boundary absorb the p-waves, whereas the dashpots tangential to the boundary absorb the s-waves. Keeping the center node at the base of the foundation as fixed, two varieties of boundary conditions are tested. First, all the bottom nodes are provided with rollers allowing only horizontal movements as shown in Fig. 3.9 (b) and second, the boundary nodes at the bottom of the base are fitted with dashpots as

shown in Fig. 3.9 (c). However, in both these cases, the side nodes of the foundation domains are attached to dashpots in both normal and tangential directions. A detailed description of use of dashpots can be found in the works by Preisig (2002). In the present work, the hydrodynamic pressures at the upstream face of the dam are calculated from Eq. (3.90). These hydrodynamic forces are applied on the upstream face of the dam.

Table 4.7 shows the comparison between the horizontal crest displacements obtained by Yazdchi et al (1999) and that of the proposed method for different $E_f/E_d$ (impedance ratio) ratios. In spite of the differences in boundary conditions, the proposed model yields horizontal displacement at the crest node close to that of Yazdchi et al. (1999). The slight discrepancy between the two results might be due to i) use of different methods and numerical tools for the solution of the coupled system and ii) different mesh sizes considered for the problem. Moreover it is observed that the results from the model where bottom nodes are provided with rollers are closer to that of Yazdchi et al (1999) compared to the results obtained from the model where the bottom nodes are also attached to dashpots. Therefore, in subsequent calculations, the bottom nodes of the foundation domain are provided with rollers except for the center node which will remain fully fixed to prevent any type of rigid body translation.

The use of dashpots as a viscous boundary to absorb the traveling earthquake waves serve as a simple and effective approach in dealing with semi-infinite foundation domain. But, one should be cautious while using them because they are local in nature. They should be placed far away from the source of originating waves. On the other hand, the boundary element method used by Yazdchi et al. (1999) satisfies the radiation boundary condition automatically. However, if the nonlinearity of the foundation material is to be considered in the analysis, then the use of boundary element method would become difficult since it is more suited to linear analysis. Also, the mathematical complexities involved with boundary element method makes it unattractive from the user's point of view. The implementation of dashpots at the foundation boundary allows us to use finite element method exclusively for the entire dam and foundation domain which is a much simpler method than the boundary element method. Also, finite element methods are more efficient in modeling nonlinear behavior of the material than the boundary element method.

**Table 4.7 Comparison of maximum horizontal crest displacements**

| Horizontal crest displacements (mm) | | Yazdchi (et al, 1999) | Staggered method with boundary conditions as per Fig. 3.9 (b) | % of deviation | Staggered method with boundary conditions as per Fig. 3.9 (c) | % of deviation |
|---|---|---|---|---|---|---|
| Impedance ratio ($E_f/E_d$) | 0.5 | 6.89 | 6.99 | 1.45 | 7.14 | 3.63 |
| | | -7.53 | -7.20 | 4.38 | -7.38 | 1.99 |
| | 1.0 | 4.38 | 4.72 | 7.76 | 4.94 | 12.79 |
| | | -4.41 | -4.28 | 2.95 | -4.69 | 6.35 |
| | 2.0 | 4.27 | 4.11 | 3.74 | 4.36 | 2.11 |
| | | -3.85 | -3.97 | 3.12 | -3.99 | 3.64 |
| | 4.0 | 4.11 | 3.90 | 5.11 | 3.95 | 3.89 |
| | | -3.70 | -3.57 | 3.51 | -3.47 | 6.22 |

Table 4.8 tabulates the range of numbers of iteration required for different time steps. It is seen that, if the impedance ratio is more, the number of iterations required are less and vice versa. In other words, if the foundation is rigid, less number of iterations per time step is required to achieve convergence as per Eq. (3.134). Also, if the foundation is relatively more flexible, the number of iterations required are comparatively higher. Though these iterations add to the overhead required for solving the interaction problem, it is seen that if the proper storage technique such as skyline methods is applied, it speeds up the solution process as the soil-structure interaction algorithm divides the total domain into two sub-domains and enables us to work with smaller matrix sizes.

**Table 4.8 Iteration counts for different impedance ratios**

| Impedance ratios | $E_f/E_d = 0.5$ | $E_f/E_d = 1.0$ | $E_f/E_d = 2.0$ | $E_f/E_d = 4.0$ |
|---|---|---|---|---|
| Iteration count | 2-95 | 2-60 | 2-35 | 2-20 |

### 4.4.2 Response of Dam-Foundation Coupled System

After validating the proposed iterative method for soil-structure interaction analysis, it is applied to Koyna gravity dam and underlying rock foundation system. The dam and foundation domains are subjected to Koyna earthquake (1967) acceleration. The foundation material is assumed to be of hard rock. The width and the depth of the foundation are assumed to be 250.0 m and 100.0 m respectively. The geometry of the dam-foundation system chosen for the analysis purpose is shown in Fig. 4.47. The material properties of the dam are as follows:

Following the works of Gogoi and Maity (2007), the Young's modulus of dam body is assumed to be 3.15 GPa. The Poisson's ratio is taken to be 0.20 and the mass density is assumed as 2415.816 kg/m$^3$.

The Young's modulus of the foundation varied in each time step according to the relationship expressed in Eq. (3.98) as proposed by Duncan-Chang model (1970). In this way, the nonlinear nature of the stress-strain behavior of the foundation material is simulated. The material properties of the foundation are as follows:

The Young's modulus of foundation rock is considered to be 1.75 GPa. The Poisson's ratio is assumed as 0.2. The mass density of the foundation material is assumed to be 1800.0 kg/m$^3$ (Owen and Hinton, 1980). The cohesion of the rock foundation is considered to be 1500 kN/m$^2$ and angle of internal friction is taken as $40^0$ (Deb, 2006).

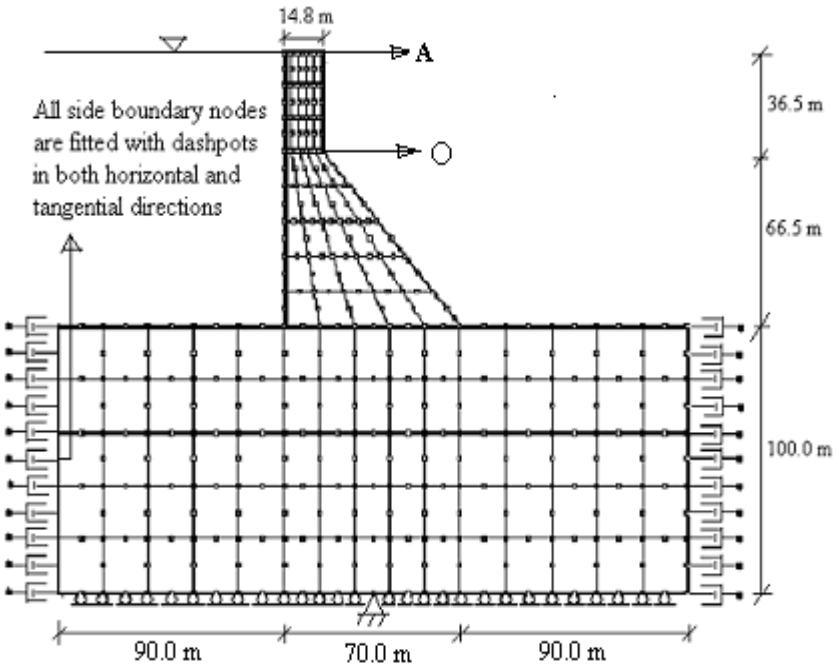


Fig. 4.47 The geometry and boundary condition of the Koyna dam-foundation system

Analyses are carried out to arrive at an optimum mesh grading for this particular problem, the details of which are provided in section 4.2.2, part I of chapter 4. A mesh grading of 5 (horizontal) × 8 (vertical) is selected for the dam domain. Similar analyses are carried out to find an optimum mesh grading for the foundation domain as well. The details of these analyses are provided in section 4.3.2, part II of chapter 4. A mesh grading of 15 (horizontal) × 5 (vertical) is found suitable for the analysis purpose.

Fig. 4.48 shows the comparison of interaction analyses with non-degraded dam and linear/nonlinear foundation material with the above mentioned material properties. If the foundation material is considered to be linear, elastic, then the maximum and minimum horizontal crest displacements are found out to be 7.04 cm and -7.21 cm respectively. The interaction analysis with nonlinear material properties produced maximum and minimum crest displacements as 8.18 cm and -8.02 cm. Therefore, a variation of 16.19% and 11.23% are observed with the results of linear foundation material properties.

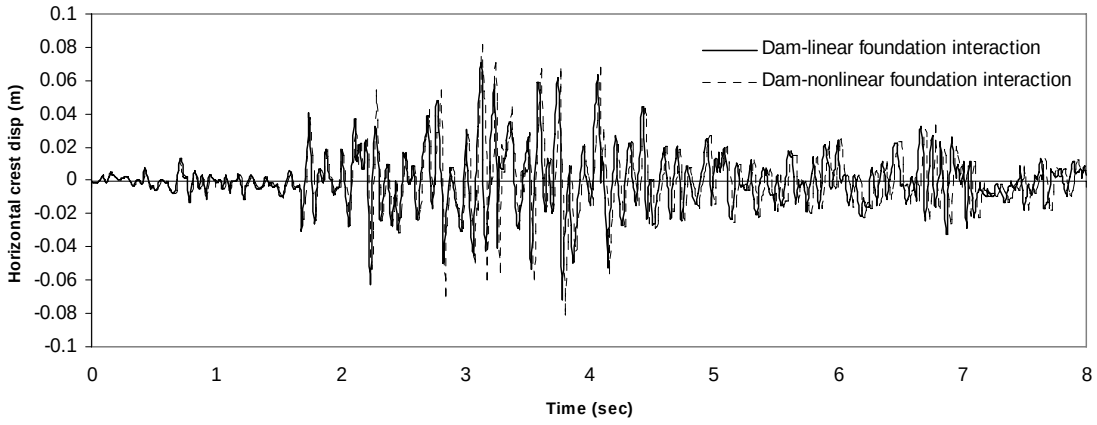


Fig. 4.48 Comparison of horizontal crest displacements between non-degraded dam and linear/nonlinear foundation ($C$ = 150.0e+4 N/m$^2$ and $\phi$ = 40.0$^0$)

Fig. 4.49 shows the variation of major principal stress vs. time for non-degraded dam and linear/nonlinear foundation interaction analyses. The maximum values are observed to be 15.30 MPa and 16.45 MPa respectively for interaction analyses of dam with linear and nonlinear foundation material. For nonlinear analysis, the major principal stress is observed to rise by 7.52% compared to the case where foundation material is assumed to be linear, elastic. Fig. 4.50 shows the variation of minor principal stress vs.

time for non-degraded dam and linear/nonlinear foundation material. The maximum values of principal stress are observed to be -14.50 MPa and -15.90 MPa respectively for interaction analyses of dam and foundation with both linear and nonlinear material properties. Therefore, for nonlinear case, an increase of 9.65% in the magnitude of minor principal stress is noticed.

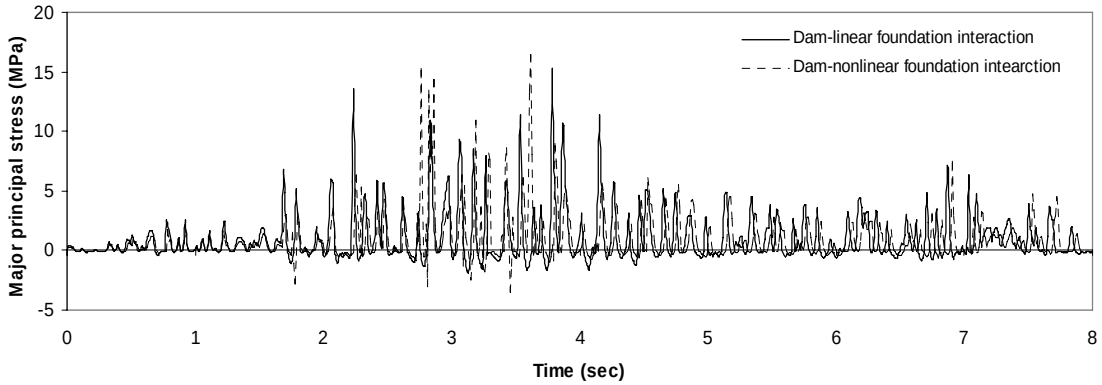


Fig. 4.49 Comparison of major principal stress vs time for non-degraded dam and linear/nonlinear foundation at the neck ($C$ = 150.0e+4 N/m$^2$ and $\phi = 40.0^0$)

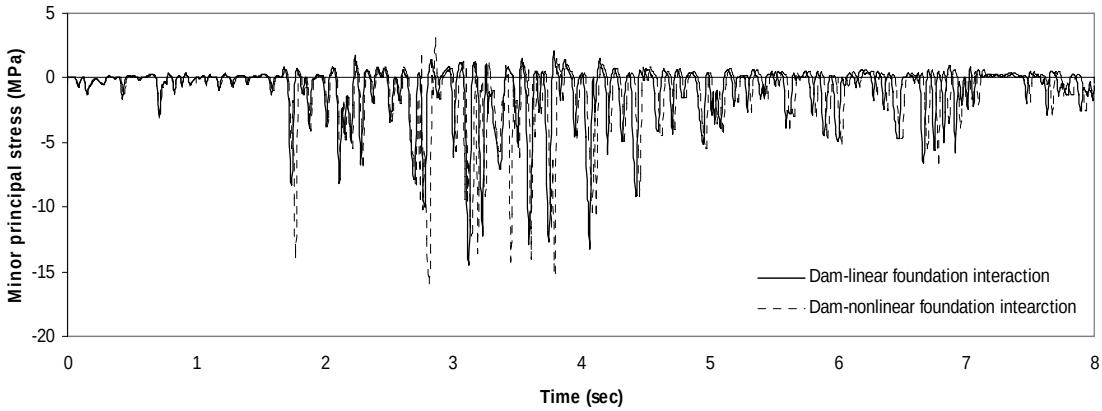


Fig. 4.50 Comparison of minor principal stress vs time for non-degraded dam and linear/nonlinear foundation at the neck ($C$ = 150.0e+4 N/m$^2$ and $\phi = 40.0^0$)

Fig. 4.49 shows that the maximum value of major principal stress occurs at 3.79 sec. if the foundation material is considered to be linear, elastic in nature. At 3.79 sec, the contour plots of major and minor principal stresses throughout the dam-foundation system are presented in Fig. 4.51. Fig. 4.51 (i) reveals that the maximum tensile stress occurs near the neck and toe region and Fig. 4.51 (ii) shows that the maximum compressive stress occurs near the heel portion of the dam body. Also, there is

concentration of compressive stresses opposite to the neck region along the vertical upstream side of the dam. From Fig. 4.50 it may be noticed that the minimum value of minor principal stress occurs at 3.13 sec. Fig. 4.52 plots the variation of major and minor principal stresses throughout the dam and foundation domain at 3.13 sec. Fig. 4.52 (i) depicts that the maximum tensile stress is experienced near the heel region of the dam body as well as opposite to the neck region along the vertical upstream face of the dam. Fig. 4.52 (ii) displays that the maximum compressive stress is found to occur near the neck region as well as the toe portion of the dam.

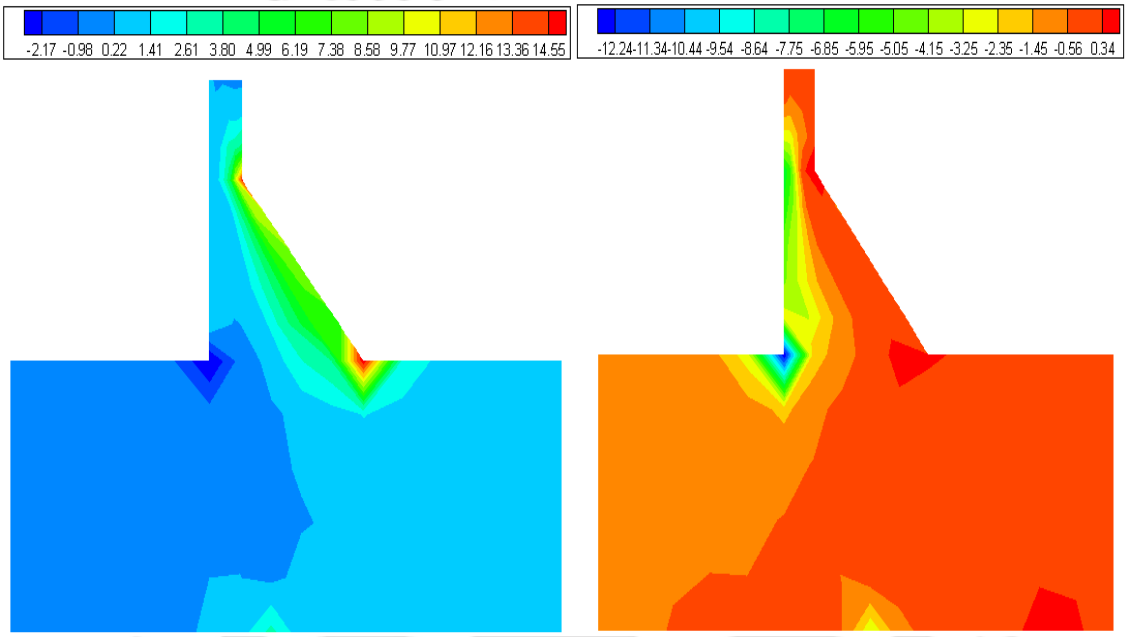


(i) (ii)

Fig. 4.51 Contour for principal stress (i) $\sigma_{p1}$ and (ii) $\sigma_{p3}$ at 3.79 seconds just after construction under full reservoir condition for non-degraded dam and linear foundation interaction

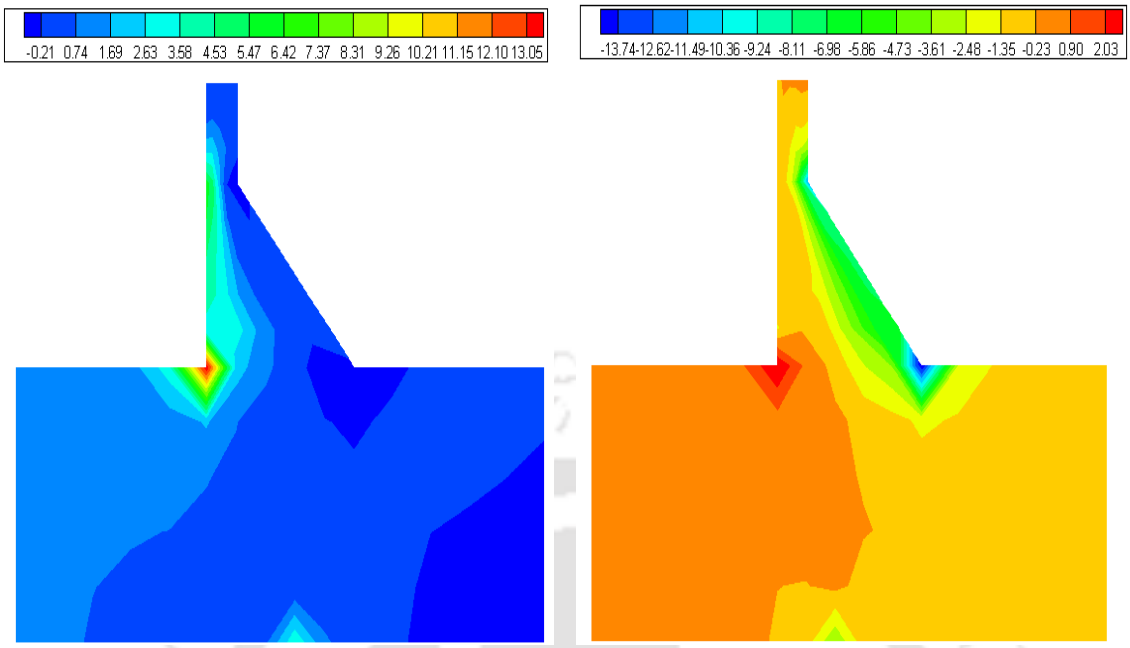


(i) (ii)

Fig. 4.52 Contour for principal stress (i) $\sigma_{p1}$ and (ii) $\sigma_{p3}$ at 3.13 seconds just after construction under full reservoir condition for non-degraded dam and linear foundation interaction

Fig. 4.49 shows that the maximum major principal stress occurs at 3.62 sec if the foundation material is considered to be nonlinear in nature. Fig. 4.53 shows the contour plots of major and minor principal stresses throughout the body of the dam and foundation. Fig. 4.53 (i) indicates that tensile stresses are accumulated near the neck region and the toe of the dam. The foundation domain experiences mostly compressive stresses of small amount. Fig. 4.53 (ii) displays that the compressive stresses are generated near the heel of the dam. Also, the vertical upstream face opposite to the neck region experiences concentration of compressive stresses. Fig. 4.50 also shows that the minimum value of minor principal stress occurs at 2.81 sec. Fig. 4.54 plots the distribution of major and minor principal stresses throughout the dam body at that particular time instant. Fig. 4.54 (i) shows that the maximum tensile stress occurs near the heel as well as opposite to the neck region along vertical upstream face of the dam. Fig. 4.54 (ii) displays that the neck as well as the toe portion of the dam body experiences maximum compressive stress. The maximum compressive stresses occur near the heel portion of the dam.

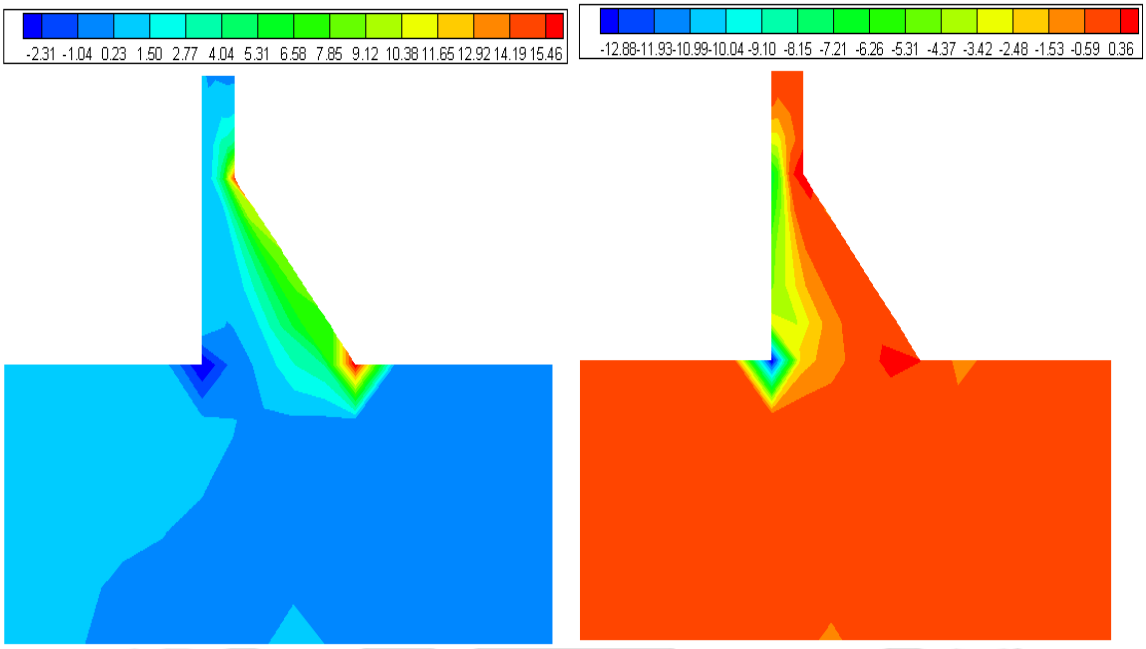


(i) (ii)

Fig. 4.53 Contour for principal stress (i) $\sigma_{p1}$ and (ii) $\sigma_{p3}$ at 3.62 seconds just after construction under full reservoir condition for non-degraded dam and nonlinear foundation interaction

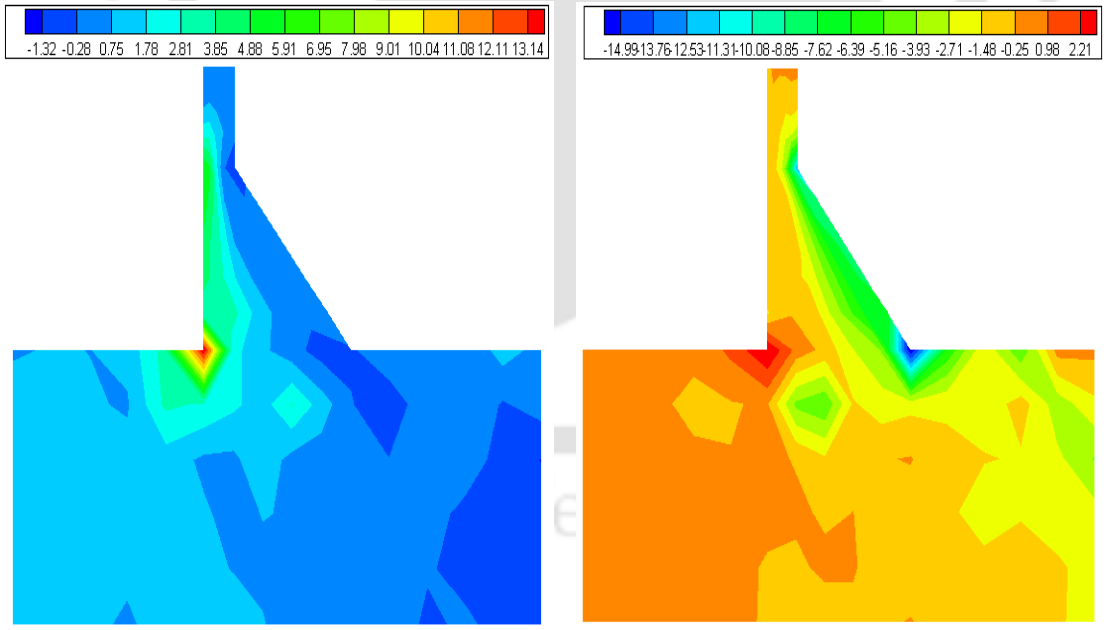


(i) (ii)

Fig. 4.54 Contour for principal stress (i) $\sigma_{p1}$ and (ii) $\sigma_{p3}$ at 2.81 seconds just after construction under full reservoir condition for non-degraded dam and nonlinear foundation interaction

***Comparison between linear/nonlinear responses after 25 years (HCM-50)***

The dam-foundation interaction analyses are carried out to find the response of the degraded dam at different ages after its construction. The horizontal crest displacement, major and minor principal stresses are calculated at the end of 25 years of construction. The hygro-chemo-mechanical (HCM) design life (as mentioned in section 3.4.4.1) of concrete is assumed to be 50 years. Fig. 4.55 shows the response of the horizontal crest displacement vs. time for interaction analyses considering both linear and nonlinear (Duncan-Chang material) properties of foundation. The maximum and minimum horizontal crest displacements are found to be 13.80 and -13.30 cm for degraded dam and linear foundation analysis. However, for degraded dam and nonlinear foundation interaction analyses, the maximum and minimum displacements are found to be 15.30 cm and -14.70 cm respectively. Therefore, a rise of 10.87% and 10.53% are observed if the foundation material is considered to be Duncan-Chang material instead of linear, elastic material.

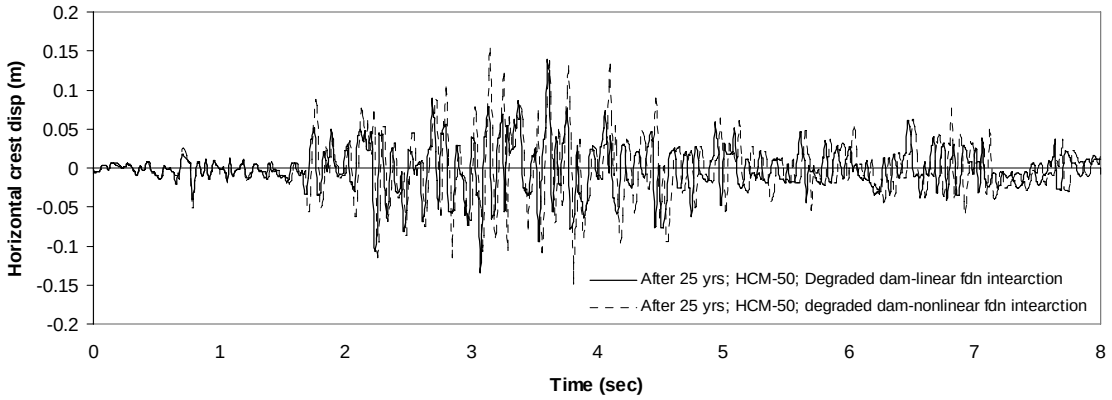


Fig. 4.55 Comparison of horizontal crest displacements between degraded dam (HCM design life-50 years) and linear/nonlinear foundation after 25 years of construction

Fig. 4.56 shows the results of major principal stresses vs. time. The major principal stress is found out to be 11.50 MPa and 12.60 MPa respectively for degraded dam and linear/nonlinear foundation interaction analyses. Therefore, the consideration of foundation nonlinearity produced a response which is 9.57% higher than results of dam and linear foundation interaction analysis. Fig. 4.57 displays the comparison of minor principal stress vs. time for dam and linear/nonlinear foundation interaction. The maximum value of minor principal stress is found out to be -11.11 MPa and -12.20 MPa

for interaction analyses considering the linearity and nonlinearity of the foundation material, respectively. In this case, consideration of nonlinearity of the foundation material increased the response by 9.81%. Therefore, it is observed that the consideration of nonlinear material behavior produces higher responses in the structure.

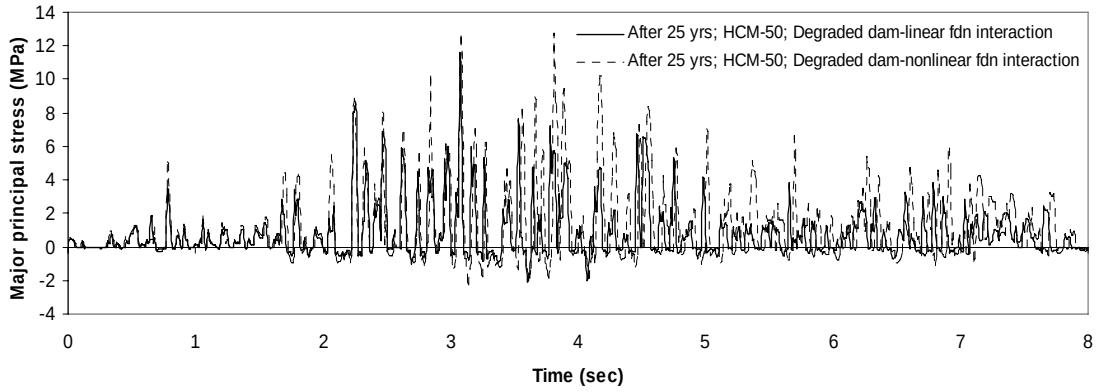


Fig. 4.56 Major principal stress vs time for degraded dam (HCM design life-50 years) and linear/nonlinear foundation interaction at neck after 25 years of construction

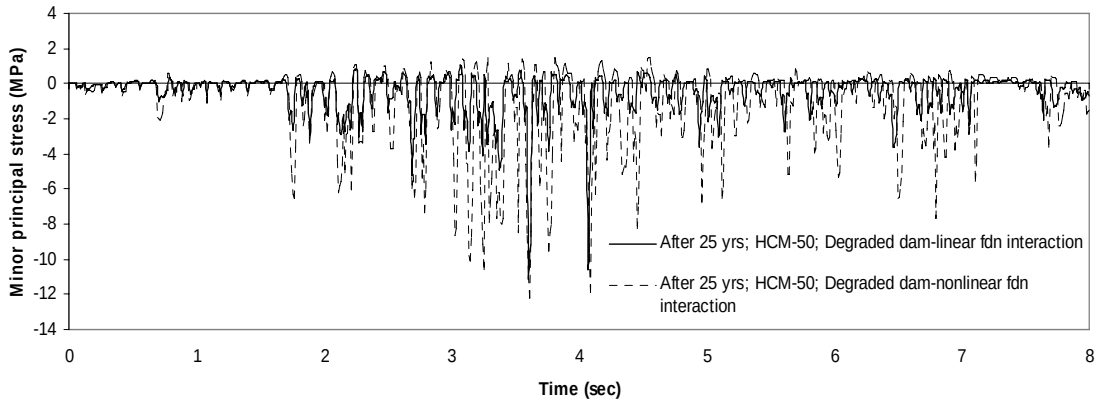


Fig. 4.57 Minor principal stress vs time for degraded dam (HCM design life-50 years) and linear/nonlinear foundation interaction at neck after 25 years of construction

From Fig 4.56, it may be found that the maximum major principal stress occurs at 3.07 sec when foundation material is simulated as linear, elastic material. Fig. 4.58 presents the distribution of major and minor principal stresses throughout the domain of the dam and foundation at 3.07 sec. Fig. 4.58 (i) reveals that the maximum tensile stresses accumulates near the neck as well as toe of the dam. Fig. 4.58 (ii) displays that the maximum compressive stresses occurs near heel of the dam as well as along the vertical upstream side opposite to the neck region. From Fig. 4.57, it may be seen that the

minimum value of minor principal stress is obtained at 3.60 sec. Fig. 4.59 plots the variation of major and minor principal stresses throughout the body of the dam at 3.60 sec. Fig. 4.59 (i) displays that the maximum tensile stresses occur at the heel as well as along the vertical upstream side of the dam opposite to the neck region. Fig. 4.59 (ii) reveals that compressive stresses are generated near the neck region of the dam body.

Fig. 4.56 indicates that the maximum major principal stress occurs at 3.08 sec if the foundation material is modeled as nonlinear Duncan-Chang material. Fig. 4.60 shows the variation of major and minor principal stresses throughout the dam-foundation domain at 3.08 sec. Fig. 4.60 (i) reveals that the maximum tensile stresses accumulate near the neck as well as toe of the dam. Fig. 4.60 (ii) demonstrates that the maximum compressive stresses occur near the heel of the dam. Also, the vertical upstream side opposite to the neck of the dam experiences compressive stresses. Fig. 4.57 also reveals that the minimum minor principal stress occurs at 3.62 sec. Fig. 4.61 plots the distribution of major and minor principal stresses throughout the dam at 3.62 sec. Fig. 4.61 (i) shows that the maximum tensile stresses occur near the heel and also along the vertical upstream side opposite to the neck area. Fig. 4.61 (ii) shows that compressive stresses are generated near the neck region of the dam body.

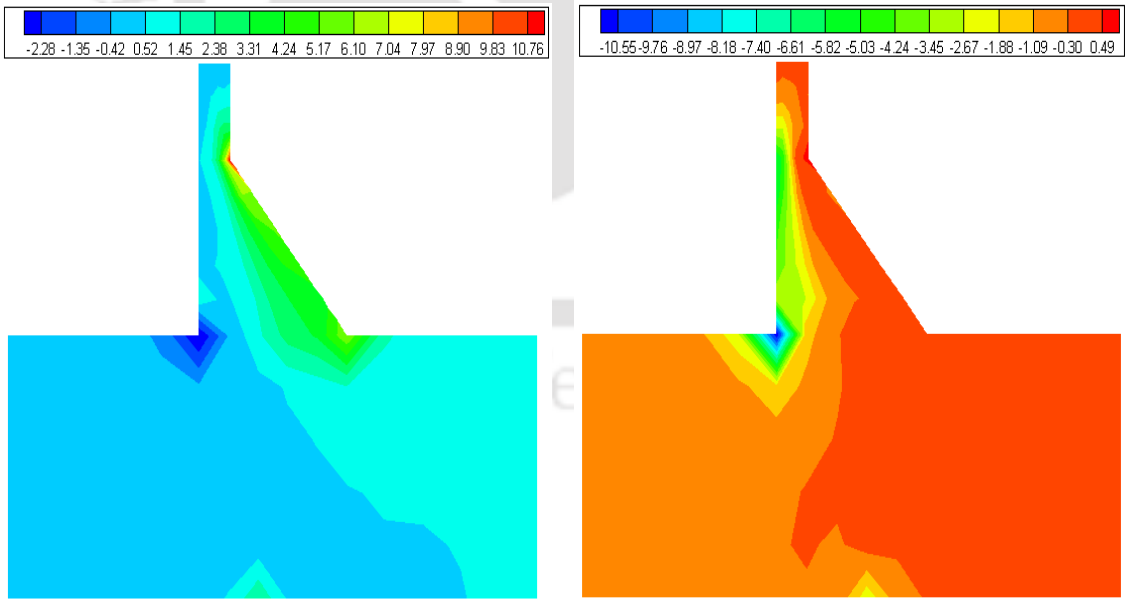


(i) (ii)

Fig. 4.58 Contour for principal stress (i) $\sigma_{p1}$ and (ii) $\sigma_{p3}$ at 3.07 seconds after 25 years for degraded dam (HCM-50) and linear foundation interaction (full reservoir condition)

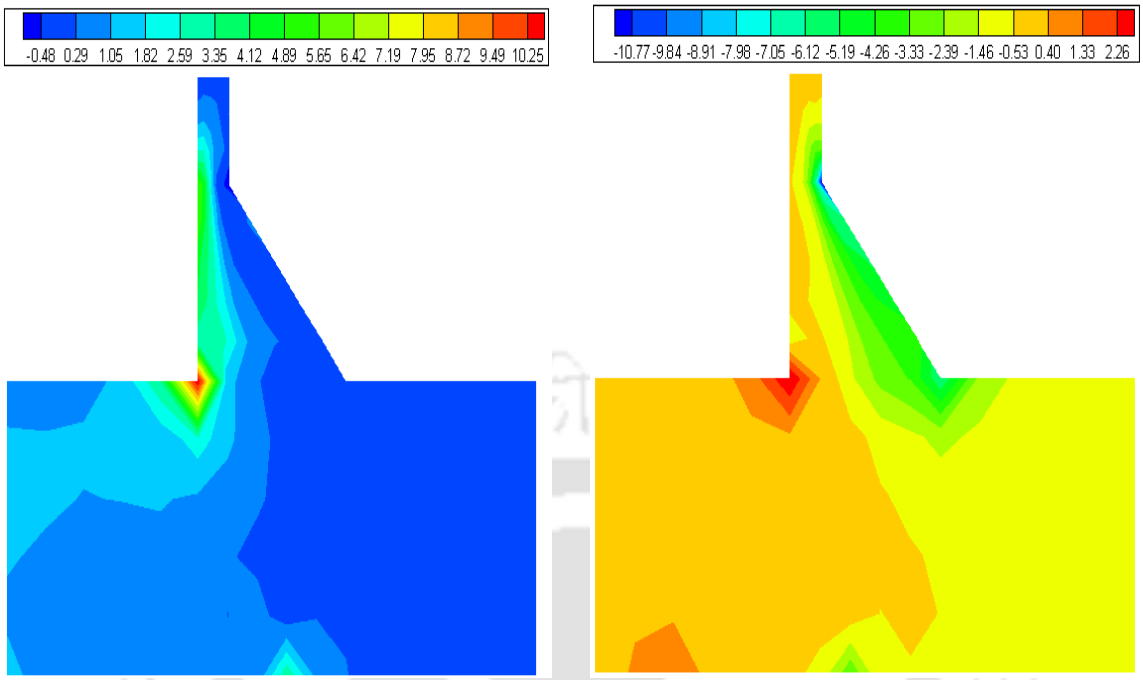


(i) (ii)

Fig. 4.59 Contour for principal stress (i) $\sigma_{p1}$ and (ii) $\sigma_{p3}$ at 3.60 seconds after 25 years for degraded dam (HCM-50) and linear foundation interaction (full reservoir condition)

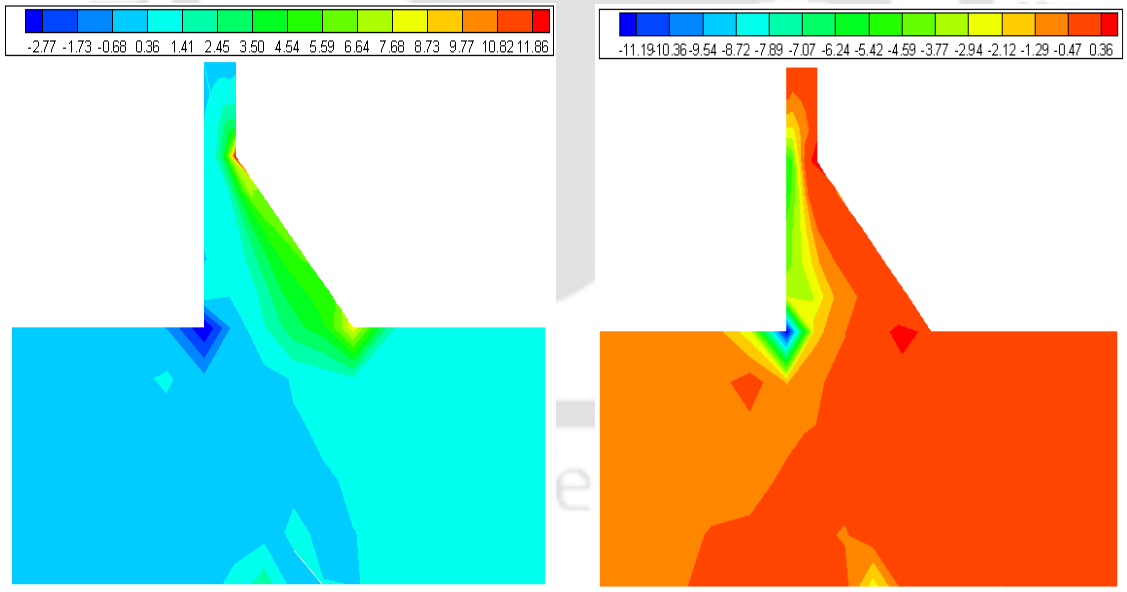


(i) (ii)

Fig. 4.60 Contour for principal stress (i) $\sigma_{p1}$ and (ii) $\sigma_{p3}$ at 3.08 seconds after 25 years for degraded dam (HCM-50) and nonlinear foundation interaction (full reservoir condition)

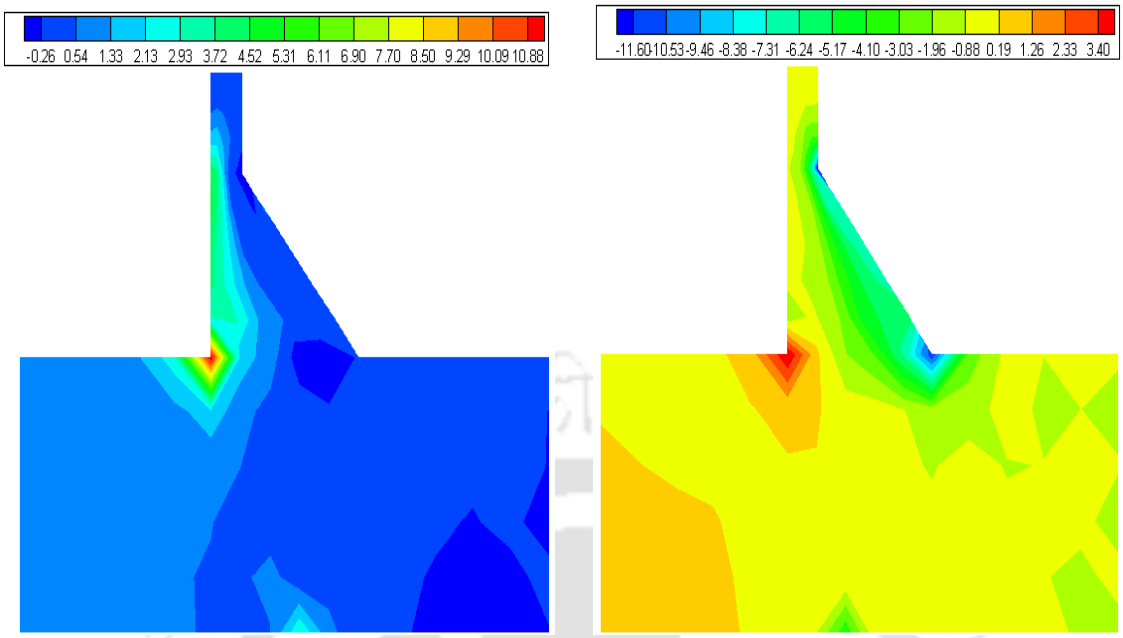


(i) (ii)

Fig. 4.61 Contour for principal stress (i) $\sigma_{p1}$ and (ii) $\sigma_{p3}$ at 3.62 seconds after 25 years for degraded dam (HCM-50) and nonlinear foundation interaction (full reservoir condition)

***Comparison between linear/nonlinear responses after 25 years (HCM-100)***

The HCM design life is increased to 100 years from previous value of 50 years. The dam-foundation interaction response is computed at the end of 25 years after construction. Fig. 4.62 shows horizontal crest displacement vs. time plot for degraded dam and linear/nonlinear foundation interaction analyses. If the linearity of the foundation material is considered, the maximum and minimum horizontal crest displacements are found out to be 12.10 cm and -10.90 cm. If the nonlinearity of the foundation is considered, then the resulting displacements are 13.30 cm and -11.97.cm respectively. Therefore, an increase of 9.92% and 9.82% are noticed if the material nonlinearity of the foundation region is taken into account. Fig. 4.63 shows the variation of major principal stress vs. time for degraded dam and linear/nonlinear foundation interaction analyses. In case of linear, elastic foundation, the maximum major principal stress is obtained as 14.40 MPa. If the foundation material is simulated as Duncan-Chang material, then the resulting maximum major principal stress is found out to be 15.30 MPa. Therefore, an increase of 6.25% is observed in this case. Fig. 4.64 plots the variation of minor principal stress vs. time for degraded dam and linear/nonlinear foundation. The maximum minor principal stress is

found out to be -17.19 MPa if the foundation material is considered to be elastic. The maximum minor principal stress is found out to be -18.20 MPa for dam and nonlinear foundation interaction. Therefore, an increase of 5.88% is observed for nonlinear foundation case compared to the linear foundation case. The consideration of nonlinear foundation material behavior gives rise to higher displacement values and stresses in the body of the dam.

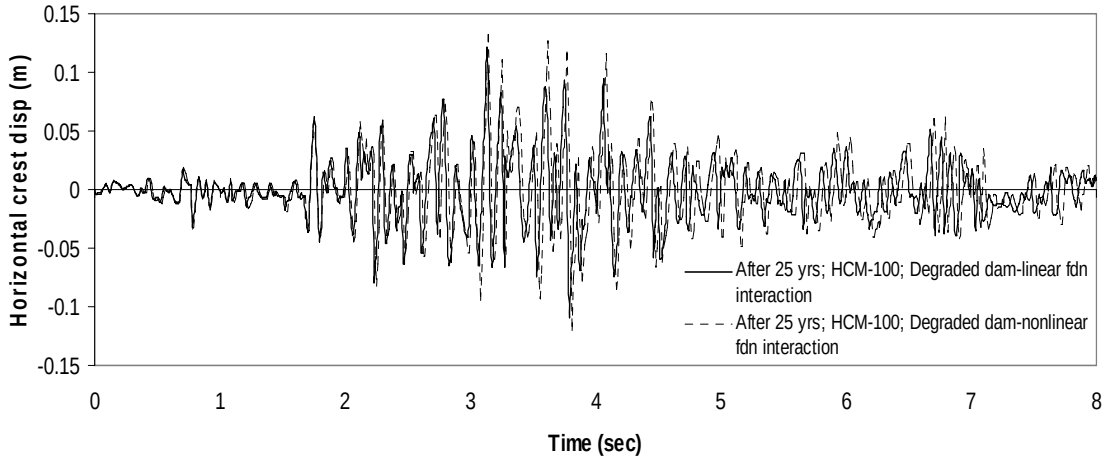


Fig. 4.62 Comparison of horizontal crest displacements between degraded dam (HCM design life-100 years) and linear/nonlinear foundation after 25 years of construction

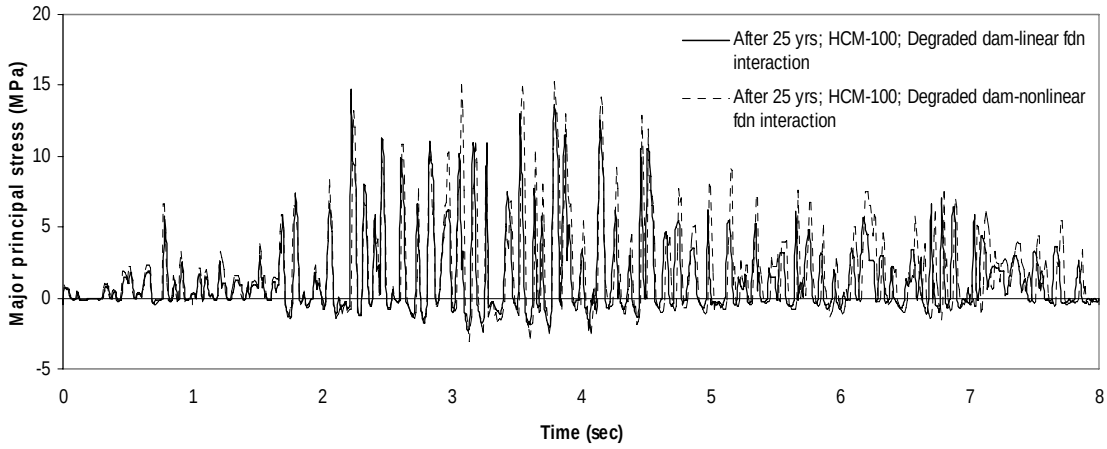


Fig. 4.63 Major principal stress vs time for degraded dam (HCM design life-100 years) and linear/nonlinear foundation interaction at neck after 25 years of construction

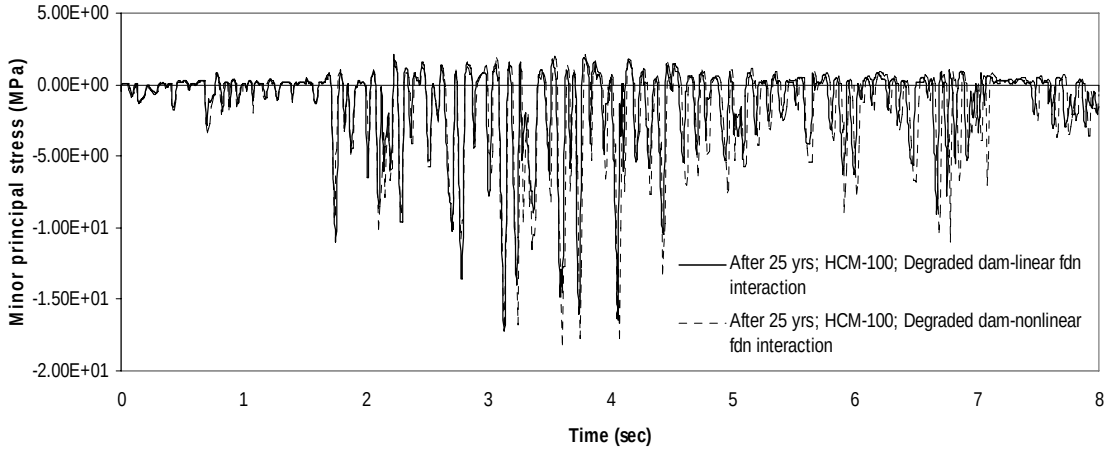


Fig. 4.64 Minor principal stress vs time for degraded dam (HCM design life-100 years) and linear/nonlinear foundation interaction at neck after 25 years of construction

If the foundation properties are considered to be linear, elastic in nature, it may be found out from Fig. 4.63 that the maximum major principal stress occurs at 2.23 sec. Fig. 4.65 displays the major and minor principal stress variation throughout the body of the dam and foundation. Fig. 4.65 (i) displays that the tensile stresses are concentrated near the neck and the toe region of the dam. Minimum compressive stress is observed to occur at the heel of the dam. Fig. 4.65 (ii) reveals that maximum compressive stress occurs near the heel of the dam body. Also, the vertical upstream side opposite to the neck of the dam experiences compressive stress. Fig. 4.64 shows that the minimum value of minor principal stress occurs at 3.13 sec. Fig. 4.66 plots the distribution of major and minor principal stresses at 3.13 sec. Fig. 4.66 (i) show that tensile stresses are developed near the heel as well as along the vertical upstream side of the dam opposite to the neck portion. Fig. 4.66 (ii) displays that the compressive stresses are concentrated near the neck region of the dam body. Also, the toe of the dam experiences accumulation of compressive stresses.

If the foundation properties are simulated as nonlinear Duncan-Chang material, it may be found out from Fig. 4.63 that the maximum major principal stress occurs at 3.80 sec. Fig. 4.67 depicts the major and minor principal stress variation throughout the dam-foundation domain at 3.80 sec. Fig. 4.67 (i) displays that the tensile stresses are concentrated near the neck and the toe region of the dam body. Fig. 4.67 (ii) reveals that

maximum compressive stresses are concentrated near the heel of the dam body. Also, the vertical upstream side opposite to the neck region experiences accumulation of compressive stresses. Fig. 4.64 shows that the minimum value of minor principal stress occurs at 3.61 sec. Fig. 4.68 displays the contour plots of major and minor principal stresses at 3.61 sec. Fig. 4.68 (i) show that tensile stresses are generated near the heel as well as along the vertical upstream side of the dam opposite to the neck portion. Fig. 4.68 (ii) displays that the compressive stresses are concentrated near the neck region of the dam body. Also, the toe of the dam suffers concentration of compressive stresses.

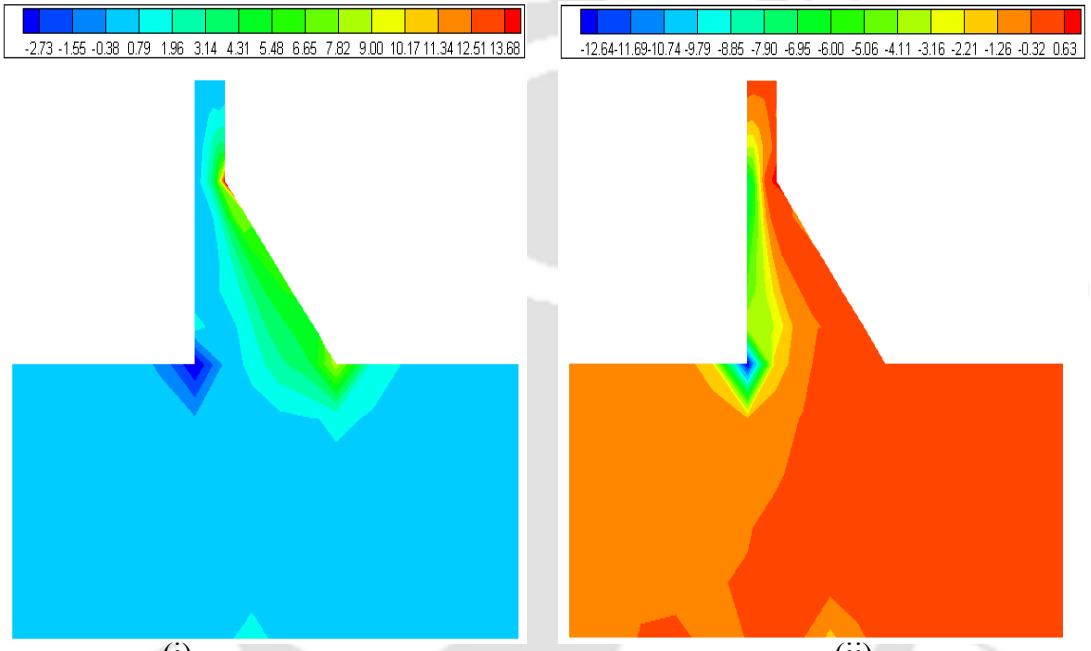


(i) (ii)

Fig. 4.65 Contour for principal stress (i) $\sigma_{p1}$ and (ii) $\sigma_{p3}$ at 2.23 seconds after 25 years for degraded dam (HCM-100) and linear foundation interaction (full reservoir condition)

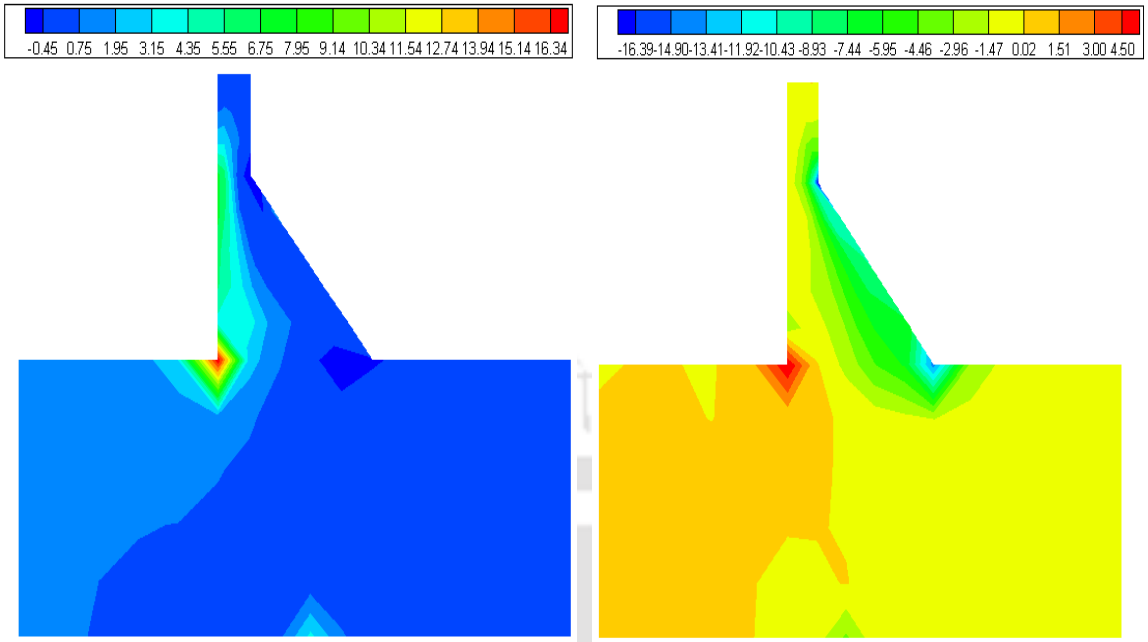


(i) (ii)

Fig. 4.66 Contour for principal stress (i) $\sigma_{p1}$ and (ii) $\sigma_{p3}$ at 3.13 seconds after 25 years for degraded dam (HCM-100) and linear foundation interaction (full reservoir condition)

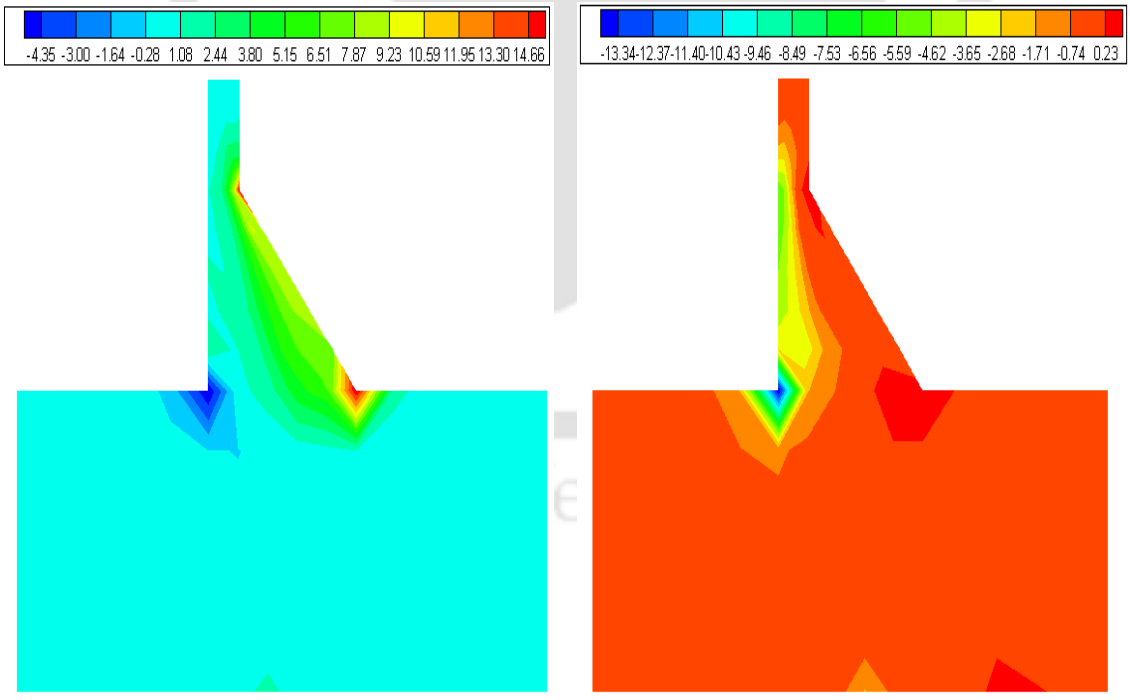


(i) (ii)

Fig. 4.67 Contour for principal stress (i) $\sigma_{p1}$ and (ii) $\sigma_{p3}$ at 3.80 seconds after 25 years for degraded dam (HCM-100) and nonlinear foundation interaction (full reservoir condition)

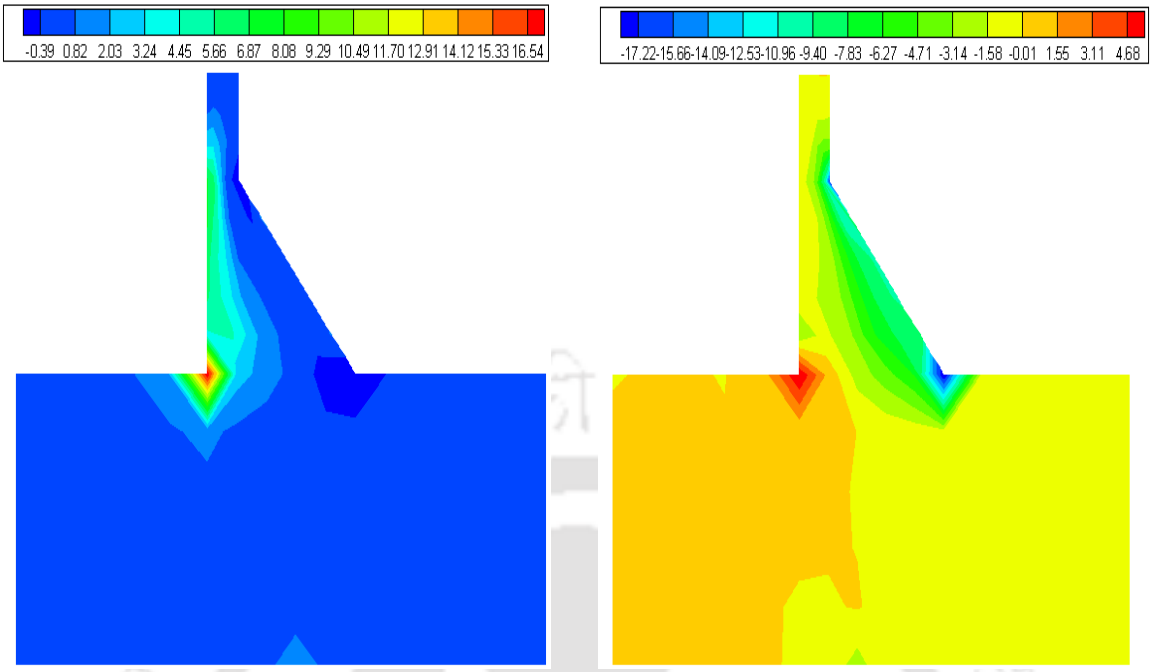


(i) (ii)

Fig. 4.68 Contour for principal stress (i) $\sigma_{p1}$ and (ii) $\sigma_{p3}$ at 3.61 seconds after 25 years for degraded dam (HCM-100) and nonlinear foundation interaction (full reservoir condition)

***Comparison between linear/nonlinear responses after 50 years (HCM-50)***

The responses of dam-foundation interaction are investigated after 50 years of construction of the dam. The HCM design life used in the analyses is considered to be 50 years. Fig. 4.69 shows the response of the horizontal crest displacement vs. time for interaction analyses considering both linear and nonlinear (Duncan-Chang material) foundation. The maximum and minimum horizontal crest displacements are found out to be 18.70 cm and -18.40 cm for degraded dam and linear foundation analysis. However, for degraded dam and nonlinear foundation interaction analyses, the maximum and minimum displacements are found out to be 20.90 cm and -20.40 cm respectively. Therefore, an increase of 11.86% and 10.87% are observed if the foundation material is considered to be Duncan-Chang material instead of linear, elastic material. Fig. 4.70 and Fig. 4.71 show the results of major and minor principal stresses vs. time for the similar analyses. The major principal stress is found to be 8.18 MPa and 9.10 MPa respectively for degraded dam and linear/nonlinear foundation interaction analyses. Therefore, the consideration of foundation nonlinearity gave a response which is 11.25% higher than

results of dam and linear foundation interaction analysis. The maximum value of minor principal stress is found to be -8.50 MPa and -9.50 MPa respectively for interaction analyses considering the linearity and nonlinearity of the foundation material. In this case, consideration of nonlinearity of the foundation material increased the response by 11.76%. In this case also, degraded dam and nonlinear foundation interaction analysis produced higher responses (i.e., displacements and stresses) compared to degraded dam-linear foundation interaction.

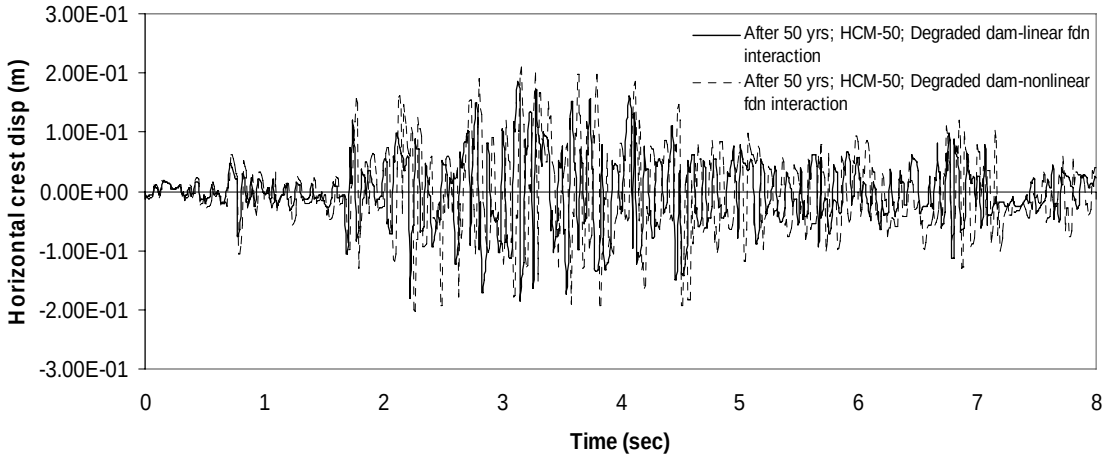


Fig. 4.69 Comparison of horizontal crest displacements between degraded dam (HCM design life-50 years) and linear/nonlinear foundation after 50 years of construction

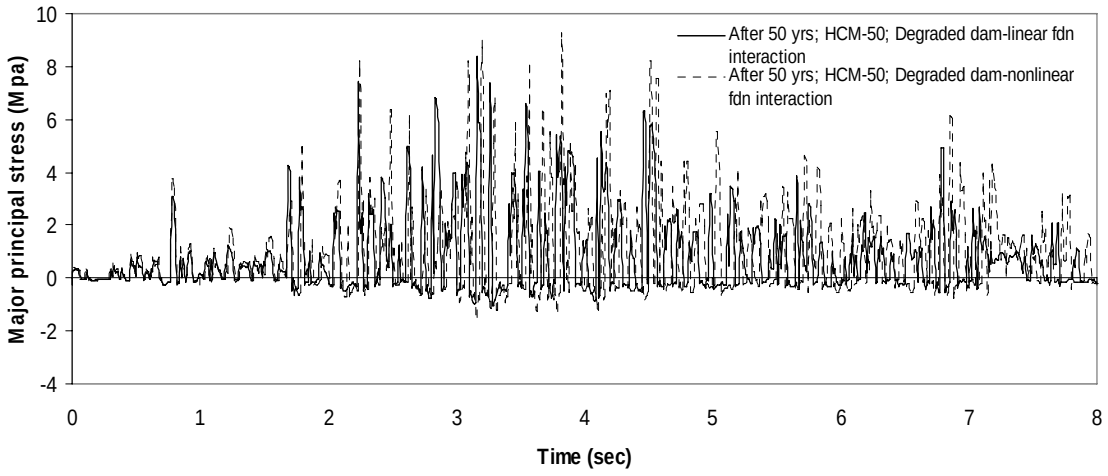


Fig. 4.70 Major principal stress vs time for degraded dam (HCM design life-50 years) and linear/nonlinear foundation interaction at neck after 50 years of construction

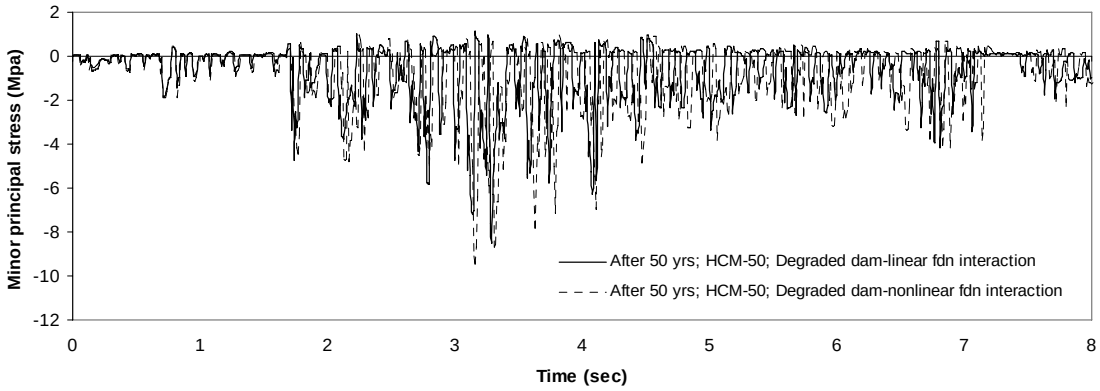


Fig. 4.71 Minor principal stress vs time for degraded dam (HCM design life-50 years) and linear/nonlinear foundation interaction at neck after 50 years of construction

The contour plots of major and minor principal stresses are presented when dam-foundation interaction analyses are carried out after 50 years of the construction of the dam. The HCM design life of concrete is considered to be 50 years. If the foundation material is considered to be linear, elastic then Fig. 4.70 shows that the major principal stress occurs at 3.17 sec. Fig. 4.72 plots the distribution of major and minor principal stresses throughout the body of the dam and foundation. Fig. 4.72 (i) displays that the tensile stresses are concentrated near the neck and the toe portion of the dam. Fig. 4.72 (ii) shows that the compressive stresses are generated near the heel portion of the dam as well as along the vertical upstream face. Fig. 4.80 reveals that minimum value of the minor principal stress occurs at 3.29 sec. Fig. 4.73 plots the distribution of minor principal stresses throughout the body of the dam at 3.29 sec. Fig. 4.73 (i) shows that the maximum tensile stresses occur near the heel as well as along the vertical upstream face of the dam opposite to the neck region. Fig. 4.73 (ii) reveals that the compressive stresses are mostly found to occur near neck region of the dam body.

The contour plots of major and minor principal stresses are studied if the nonlinear properties of the foundation domain are taken into account. Fig. 4.70 shows that the maximum value of major principal stress occurs at 3.81 sec. Fig. 4.74 demonstrates the contour variation of major and minor principal stresses throughout the dam-foundation domain at 3.81 sec. Fig. 4.74 (i) show that the tensile stresses gather near the neck and toe region. From Fig. 4.74 (ii) it is seen that the compressive stresses gather near the heel portion of the dam as well as along the vertical upstream side. Also, Fig.

4.71 shows that the minimum value of minor principal stresses occur at 3.15 sec. Fig. 4.75 depicts the variation of major and minor principal stresses at 3.15 sec. Fig. 4.75 (i) shows that the maximum principal stresses occur near the heel as well as along the vertical upstream face of the dam. Fig. 4.75 (ii) reveals that the compressive stresses are generated near the neck and the toe portion of the dam.

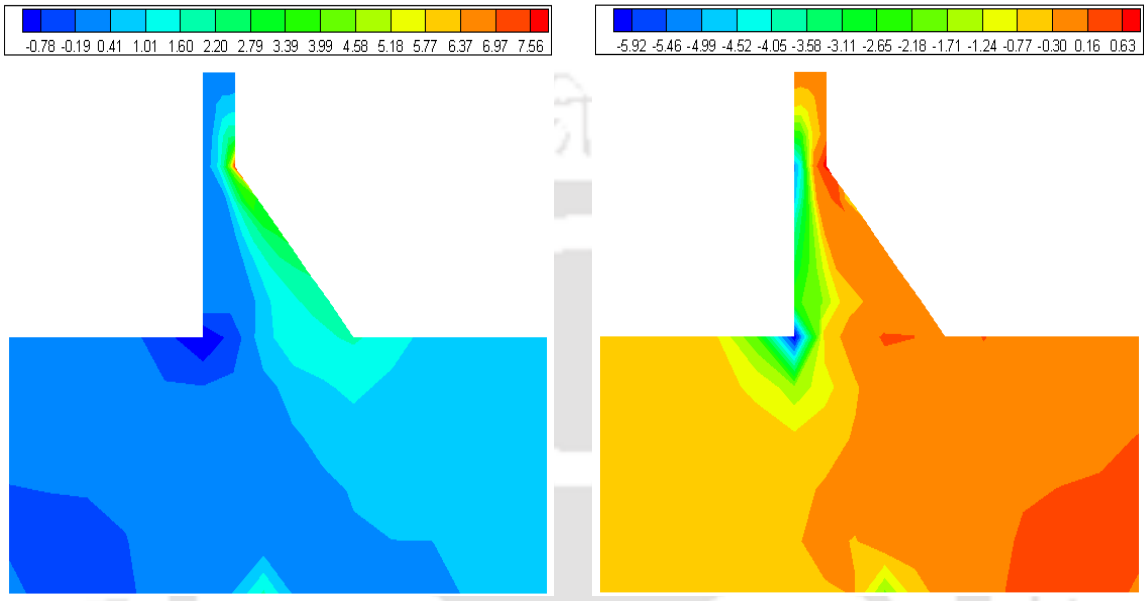


(i) (ii)

Fig. 4.72 Contour for principal stress (i) $\sigma_{p1}$ and (ii) $\sigma_{p3}$ at 3.17 seconds after 50 years for degraded dam (HCM-50) and linear foundation interaction (full reservoir condition)

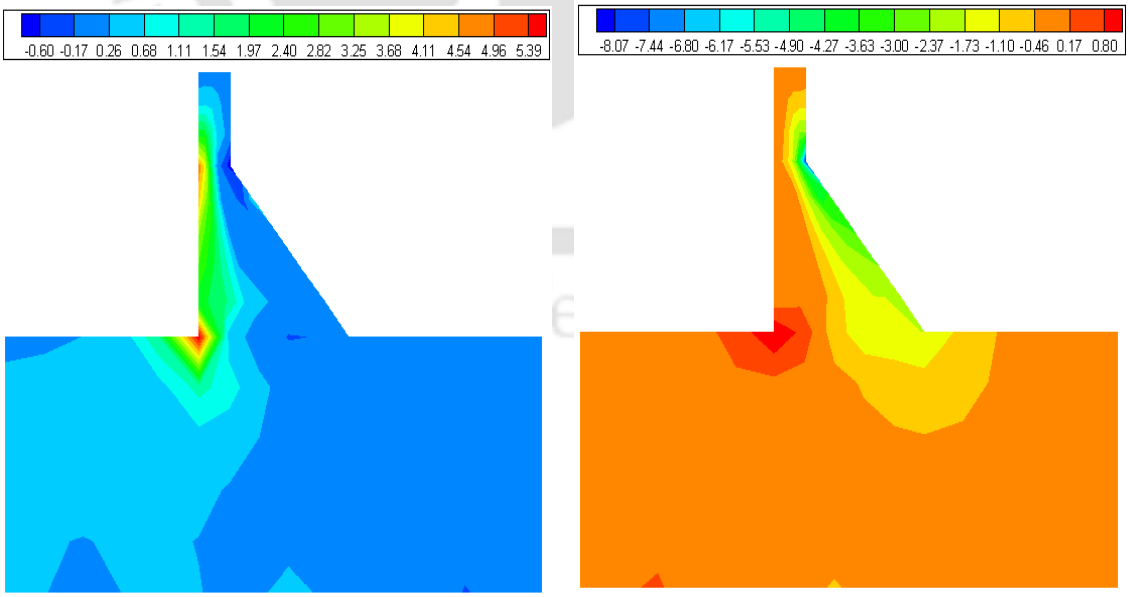


(i) (ii)

Fig. 4.73 Contour for principal stress (i) $\sigma_{p1}$ and (ii) $\sigma_{p3}$ at 3.29 seconds after 50 years for degraded dam (HCM-50) and linear foundation interaction (full reservoir condition)

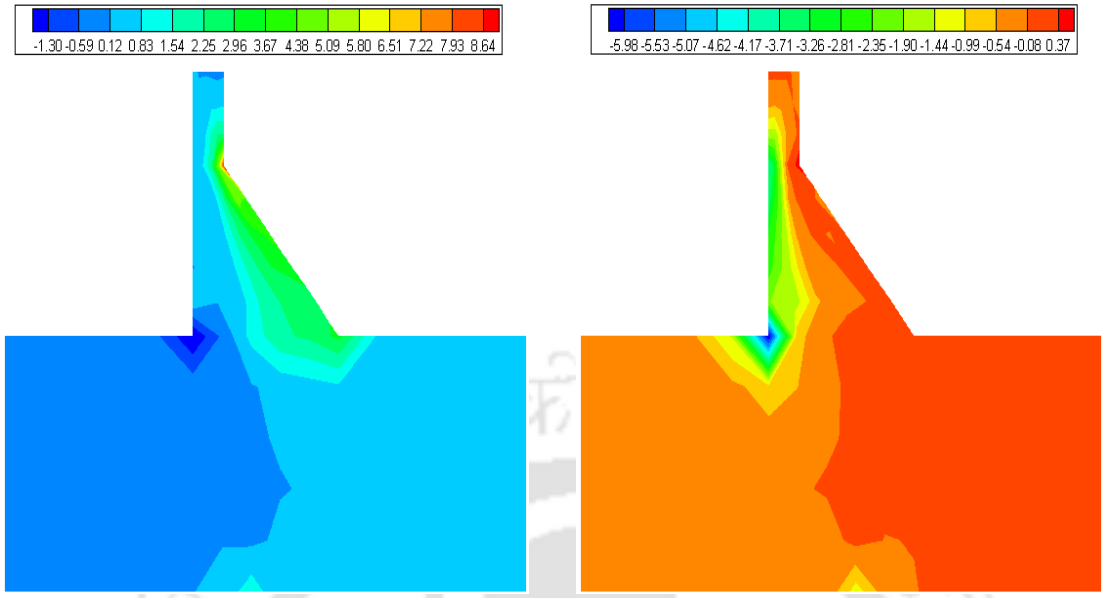


(i) (ii)

Fig. 4.74 Contour for principal stress (i) $\sigma_{p1}$ and (ii) $\sigma_{p3}$ at 3.81 seconds after 50 years for degraded dam (HCM-50) and nonlinear foundation interaction (full reservoir condition)

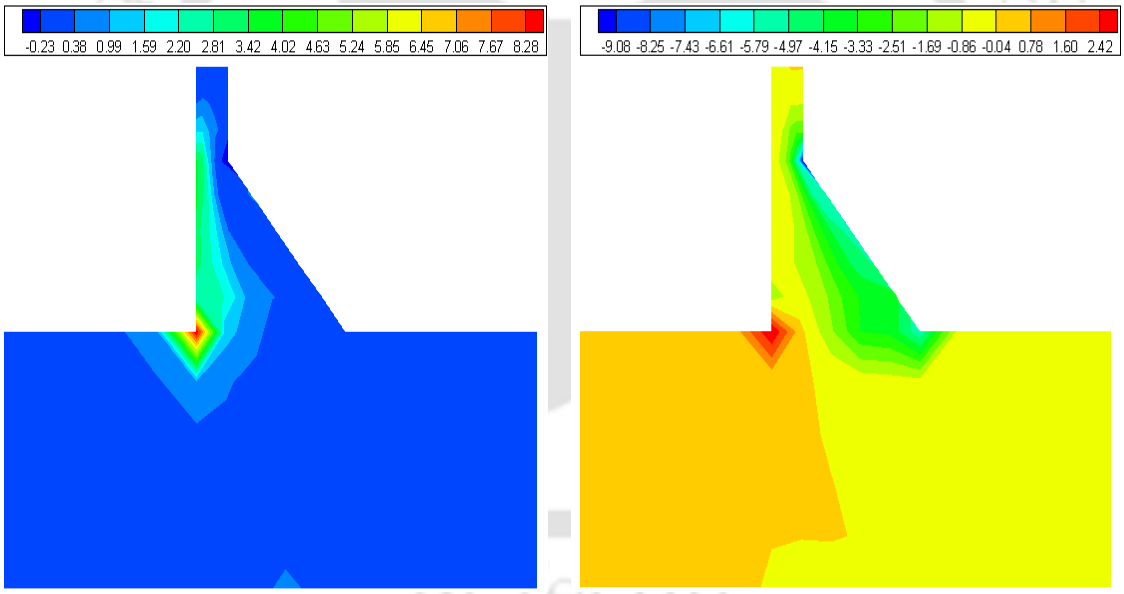


(i) (ii)

Fig. 4.75 Contour for principal stress (i) $\sigma_{p1}$ and (ii) $\sigma_{p3}$ at 3.15 seconds after 50 years for degraded dam (HCM-50) and nonlinear foundation interaction (full reservoir condition)

***Comparison between linear/nonlinear responses after 50 years (HCM-100)***

Fig. 4.76 presents the horizontal crest displacement with respect to time for degraded dam and linear/nonlinear foundation interaction analyses. The HCM design life is

considered to be 100 years. The dam-foundation interaction response is computed at the end of 50 years after construction. If the foundation material is considered to be linear-elastic, the maximum and minimum horizontal crest displacements are found out to be 15.40 cm and -15.20 cm. If the nonlinearity of the foundation is considered, then the resulting displacements are 17.10 cm and -16.80 cm respectively. Therefore, an increase of 11.04% and 10.53% are noticed if the material nonlinearity of the foundation region is taken into account. Fig. 4.77 shows the variation of major principal stress vs. time for degraded dam and linear/nonlinear foundation interaction analyses. In case of linear, elastic foundation, the maximum major principal stress is obtained as 10.80 MPa. If the foundation material is idealized as Duncan-Chang material, then the resulting maximum major principal stress is found out to be 11.90 MPa. An increase of 10.20% is observed in this case. The variation of minor principal stress vs time for degraded dam and linear/nonlinear foundation analyses are plotted in Fig. 4.78. The maximum minor principal stress is found out to be -11.40 MPa if the foundation material is considered to be elastic. For Duncan-Chang foundation material, the maximum minor principal stress is found out to be -12.60 MPa. Therefore, an increase of 10.53% is observed for nonlinear foundation case compared to the linear foundation case. Here also, it is found that if the nonlinear properties of the foundation are included in the analysis, it produces higher displacements and stresses in the dam body compared to the case when foundation material is considered to be linear, elastic.

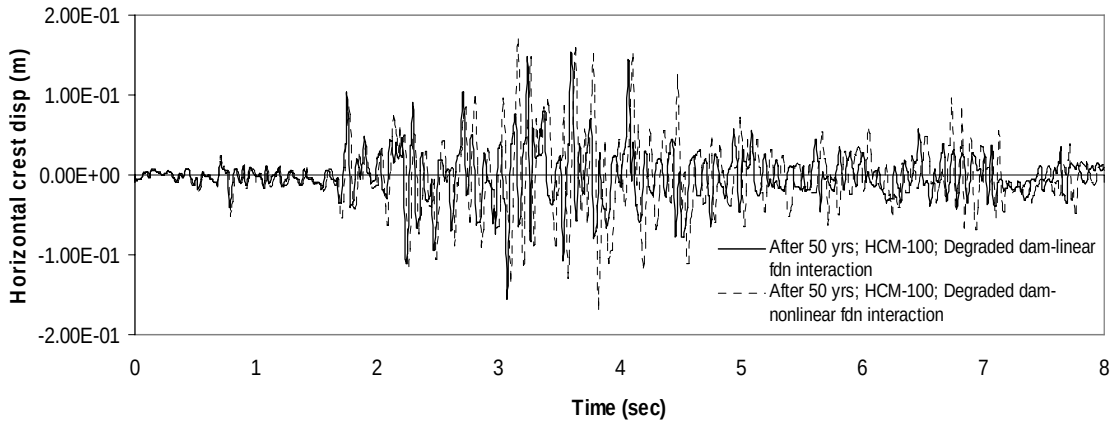


Fig. 4.76 Comparison of horizontal crest displacements between degraded dam (HCM design life-100 years) and linear/nonlinear foundation after 50 years of construction

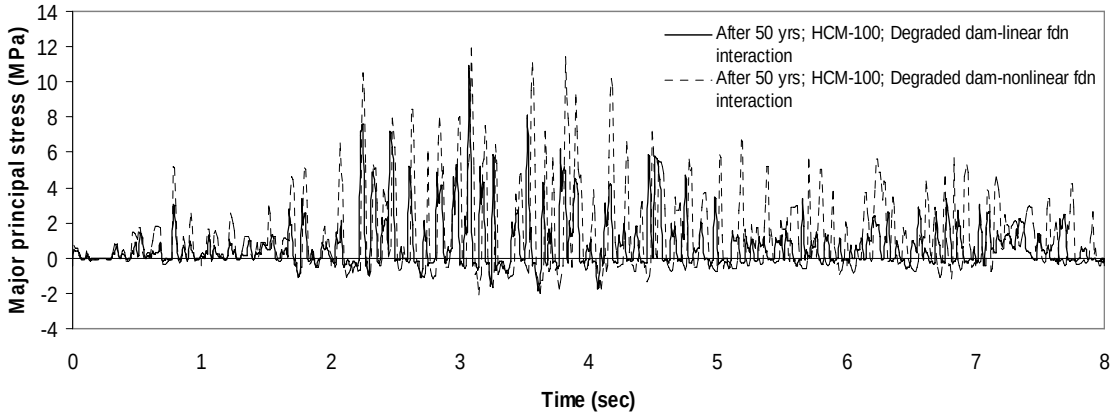


Fig. 4.77 Major principal stress vs time for degraded dam (HCM design life-100 years) and linear/nonlinear foundation interaction at neck after 50 years of construction

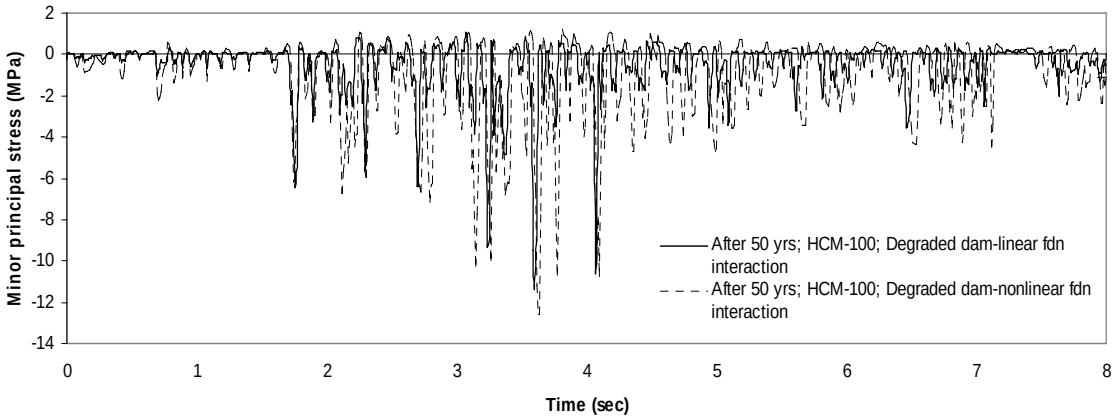


Fig. 4.78 Minor principal stress vs time for degraded dam (HCM design life-100 years) and linear/nonlinear foundation interaction at neck after 50 years of construction

Next the contour plots of major and minor principal stresses are drawn when HCM design life of concrete is considered to be equal to 100 years and the dam-foundation interaction analyses are carried out after 50 years of the construction of the dam. If the foundation material is considered to be linear, elastic then Fig. 4.77 shows that the major principal stress occurs at 3.06 sec. Fig. 4.79 plots the distribution of major principal stresses throughout the dam-foundation domain at 3.06 sec. Fig. 4.79 (i) demonstrates that the tensile stresses are concentrated near the neck and the toe portion of the dam. Fig. 4.79 (ii) shows that the heel portion of the dam as well as along the vertical upstream face opposite to the neck region experiences compressive stresses. Fig. 4.78 reveals that minimum value of the minor principal stress occurs at 3.59 sec. Fig. 4.80

plots the distribution of minor principal stresses throughout the body of the dam at 3.59 sec. Fig. 4.80 (i) shows that the maximum tensile stresses occur near the heel as well as along the vertical upstream side of the dam opposite to the neck region. Fig. 4.80 (ii) reveals that the compressive stresses are found to occur near neck and toe region of the dam body.

The contour plots of major and minor principal stresses are studied if the nonlinear properties of the foundation domain are taken into account. Fig. 4.77 shows that the maximum value of major principal stress occur at 3.09 sec. Fig. 4.81 displays the contour variation of major and minor principal stresses in dam-foundation at 3.09 sec. From Fig. 4.81 (i), it is found that the tensile stresses occurs near the neck and toe region. From Fig. 4.81 (ii) it may be seen that the compressive stresses gather near the heel portion of the dam as well as along the vertical upstream side opposite to the neck region. Also, Fig. 4.78 shows that the minimum value of minor principal stresses occur at 3.63 sec. Fig. 4.82 depicts the variation of major and minor principal stresses over the dam's body at 3.63 sec. Fig. 4.82 (i) shows that the maximum principal stresses occur near the heel as well as along the vertical upstream face of the dam. Fig. 4.82 (ii) reveals that the compressive stresses are generated near the neck and toe region.

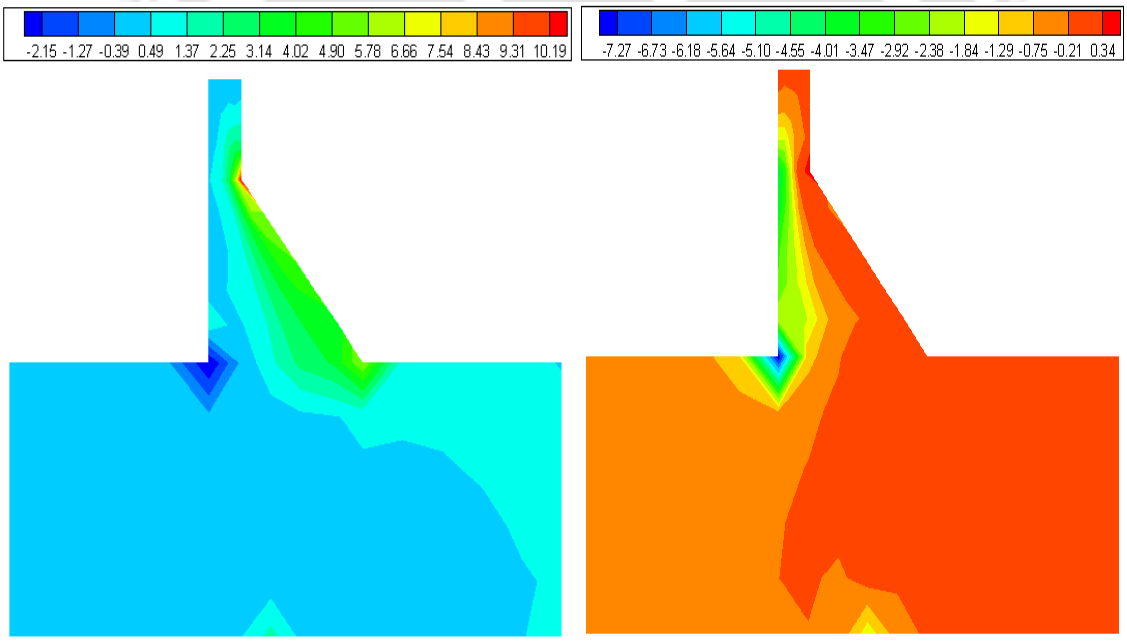


(i) (ii)

Fig. 4.79 Contour for principal stress (i) $\sigma_{p1}$ and (ii) $\sigma_{p3}$ at 3.06 seconds after 50 years for degraded dam (HCM-100) and linear foundation interaction (full reservoir condition)

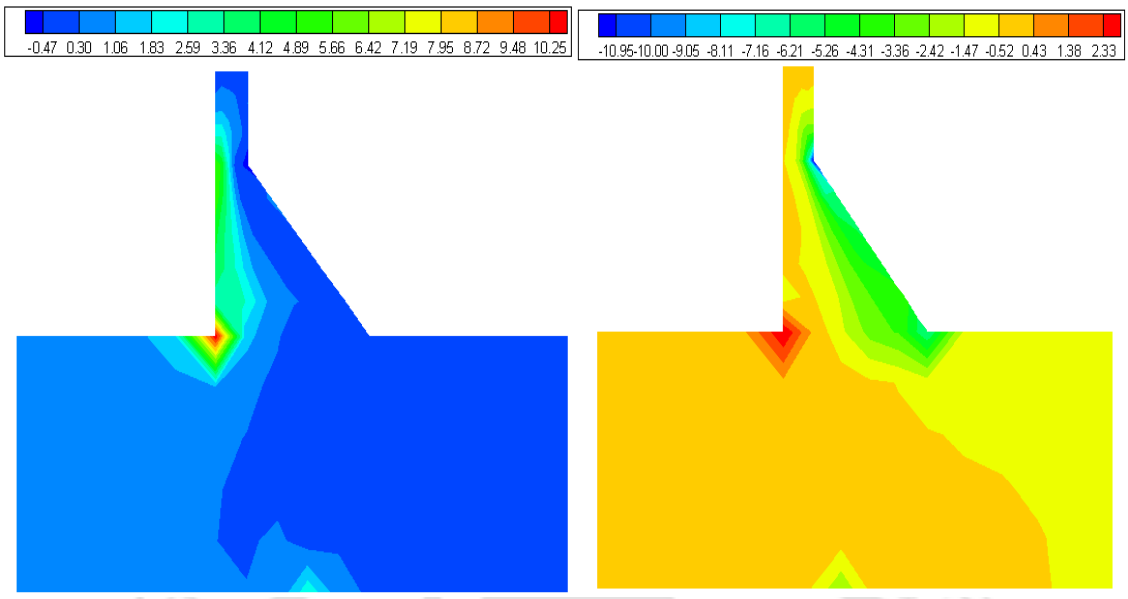


(i) (ii)

Fig. 4.80 Contour for principal stress (i) $\sigma_{p1}$ and (ii) $\sigma_{p3}$ at 3.59 seconds after 50 years for degraded dam (HCM-100) and linear foundation interaction (full reservoir condition)

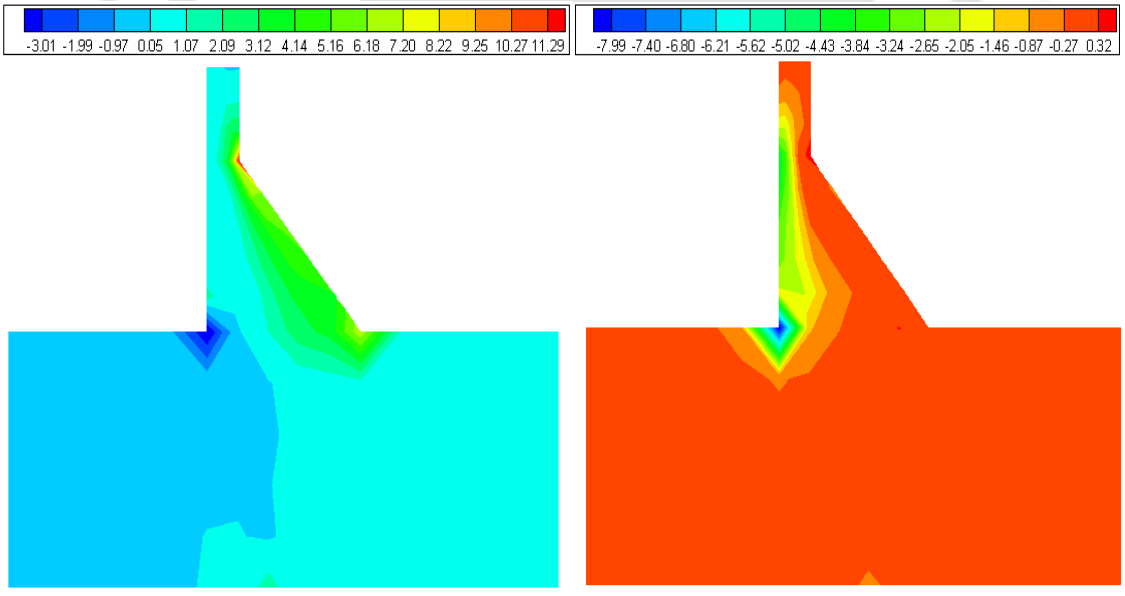


(i) (ii)

Fig. 4.81 Contour for principal stress (i) $\sigma_{p1}$ and (ii) $\sigma_{p3}$ at 3.09 seconds after 50 years for degraded dam (HCM-100) and nonlinear foundation interaction (full reservoir condition)

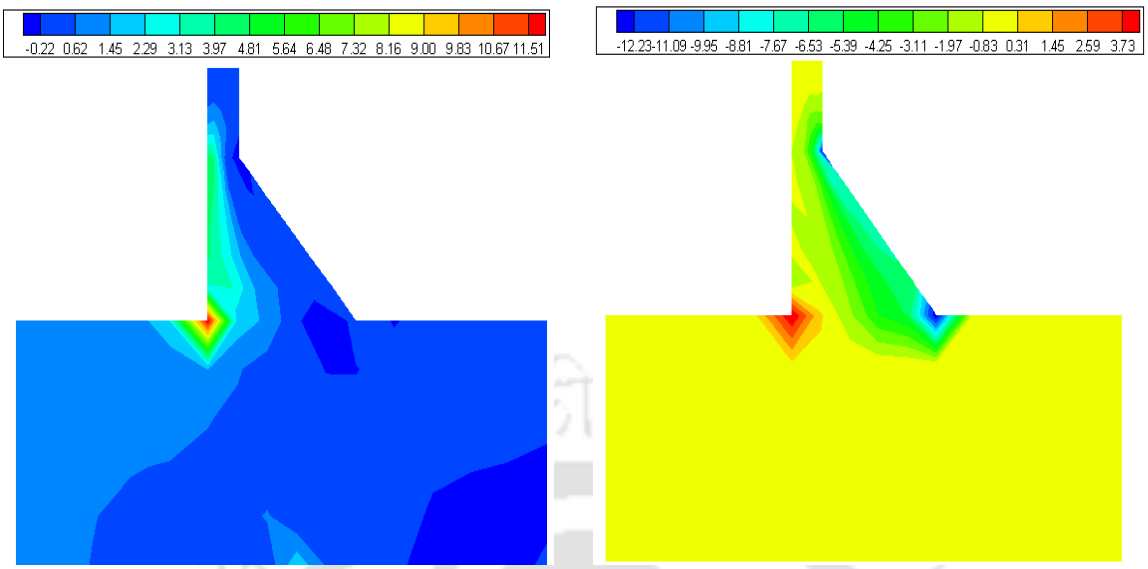


(i) (ii)

Fig. 4.82 Contour for principal stress (i) $\sigma_{p1}$ and (ii) $\sigma_{p3}$ at 3.63 seconds after 50 years for degraded dam (HCM-100) and nonlinear foundation interaction (full reservoir condition)

Therefore, the contour plots reveal that the neck and toe region experiences maximum tensile stresses whenever the major principal stress reaches its maximum value. At that particular moment, compressive stresses gather near the heel region of the dam body as well as along vertical upstream face of the dam. Further it is noticed that there is accumulation of compressive stresses at the neck region whenever the minor principal stress reaches its minimum value. Also, it is observed that the tensile stresses develop near the heel of the dam when minor principal stress reaches its minimum value.

At the end the maximum and minimum values of horizontal crest displacements, major and minor principal stresses are shown in a tabulated form. Table 4.9 displays the corresponding values. It may be observed that the displacements increase if the dam-foundation interaction analyses are carried out at a later age of the dam. With passage of time, the concrete endures more degradation and therefore, its strength and stiffness reduces. Because of this, more displacements are achieved at a later date. However, stresses reduce because the dam structure becomes more flexible with increase in degradation of its material. Furthermore, if the HCM design lives of concrete are reduced, the displacements increase and stresses reduce. If the HCM design life of concrete is more, the initial stiffness is higher. As a result, loss of stiffness of concrete becomes lesser with compared to the case when HCM design life of concrete is lesser. That is why,

at a particular age of the dam, for higher HCM design life, less displacements are obtained from dam-foundation interaction analyses.

Further, it is noticed that the displacement values obtained for the dam after fifty years of construction is considerably high. The investigator opines that such high displacements are unlikely to be sustained by concrete because when such high displacements will occur, concrete might suffer cracks. Consideration of linear, elastic material properties for concrete may not suffice to describe its proper behavior. A model capable of describing crack formation and propagation for concrete material should preferably be used for describing its behavior for more realistic prediction. Also, a proper nonlinear constitutive matrix for concrete is preferable for better prediction of material behavior at later age after construction. Regrettably, such analyses are not within the scope of present work.

**Table 4.9 Horizontal crest displacements, major and minor principal stresses at the neck under full reservoir condition**

| Different cases | Horizontal crest displacements (cm) | | Major principal stress (MPa) | Minor principal stress (MPa) |
|---|---|---|---|---|
| | Maximum (+ve) value | Minimum (-ve) value | | |
| Non-degraded dam-linear foundation interaction | 7.04 | -7.21 | 15.30 | -14.50 |
| Non-degraded dam-nonlinear foundation interaction | 8.18 | -8.02 | 16.45 | -15.90 |
| After 25 yrs; HCM-50; Degraded dam-linear foundation interaction | 13.80 | -13.30 | 11.50 | -11.11 |
| After 25 yrs; HCM-50; Degraded dam-nonlinear foundation interaction | 15.30 | -14.70 | 12.60 | -12.20 |
| After 25 yrs; HCM-100; Degraded dam-linear foundation interaction | 12.10 | -10.90 | 14.40 | -17.19 |

| | | | | |
|---|---|---|---|---|
| After 25 yrs; HCM-100; Degraded dam-nonlinear foundation interaction | 13.30 | -11.97 | 15.30 | -18.20 |
| After 50 yrs; HCM-50; Degraded dam-linear foundation interaction | 18.70 | -18.40 | 8.18 | -8.50 |
| After 50 yrs; HCM-50; Degraded dam-nonlinear foundation interaction | 20.90 | -20.40 | 9.10 | -9.50 |
| After 50 yrs; HCM-100; Degraded dam-linear foundation interaction | 15.40 | -15.20 | 10.80 | -11.40 |
| After 50 yrs; HCM-100; Degraded dam-nonlinear foundation interaction | 17.10 | -16.80 | 11.90 | -12.60 |

### 4.4.3 Parametric Studies for Dam-Foundation Interaction Analyses under Full Reservoir Condition

#### *4.4.3.1 Effect of HCM Design Life on Dam-Foundation Coupled Response*

The effect of HCM design life on the response of dam-foundation interaction analyses has been studied for linear and nonlinear foundation. The HCM design life of the concrete of the dam region is altered and the interaction analyses are carried out at the end of 25 years after construction of the structure. Fig. 4.83 shows the comparison of horizontal crest displacement under earthquake loading for HCM design lives of 50 years and 100 years respectively. It is observed that the horizontal crest displacement reduces if the design life of the dam structure is considered more. For a design life of 50 years, the maximum and minimum values of the horizontal crest displacements are found out to be 13.80 cm and -13.30 cm respectively. For a design life of 100 years, the same quantities are found out to be 12.10 cm and -10.90 cm respectively. Therefore, the maximum and minimum values of the horizontal crest displacements reduces by 12.30% and 18.0% respectively if the design life of the concrete of the dam region is increased from 50 years to 100 years. The consideration of higher HCM design life imparts greater initial strength

in concrete. Therefore, if the HCM design life is more, the initial strength of concrete is higher than the case when HCM design life is lower. That is why, if HCM design life of concrete increases, the corresponding horizontal crest displacement obtained from dam-foundation interaction analysis reduces.

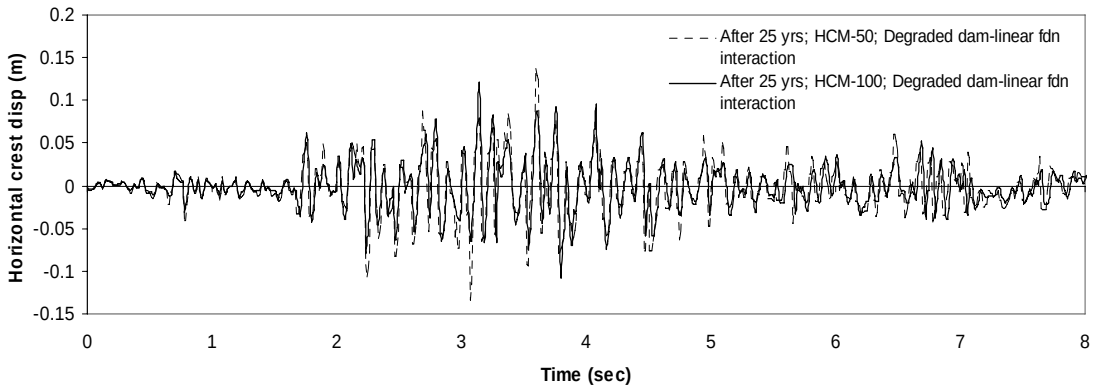


Fig. 4.83 Comparison of horizontal crest displacement between degraded dam-linear foundation interaction after 25 years of construction for different HCM design lives

Fig. 4.84 plots the variation of major principal stress vs. time for dam-linear foundation interaction analyses at the end of 25 years after construction for different values of HCM design life. If the deign life is considered to be 50 years, the maximum major principal stress is found out to be 11.50 MPa whereas, the maximum major principal stress is obtained as 14.40 MPa when the HCM deign life is increased to 100 years. Therefore, it is observed that consideration of higher design life yields more stress compared to the case when design life is reduced. A reduction of 20.14% takes place when the design life is reduced to 50 years from 100 years. With lower design life, the degradation index obtained is more which in turn reduces the constitutive matrix $([D])$ of the material. Also, at a later age of the material, the loss of stiffness is also higher due to higher value of degradation index. For this reason, less stresses may be obtained due to more displacement with lower design life. Since, the generated stress $\{\sigma\}$ is equal to $[D][B]\{u\}$, the comparative severity between the decrement of the $[D]$ matrix and the increment of $\{u\}$ vector will actually determine whether the generated stress will be more or less. In this case, higher stresses are obtained when the design life is 100 years compared to the design life of 50 years. Therefore, the decrement in $[D]$ matrix due to

consideration of lower design life is more predominant than the increase in $\{u\}$ vector. Similarly, Fig. 4.85 plots the distribution of minor principal stresses with respect to time for dam-foundation interaction analyses with HCM design life 50 years and 100 years. With HCM design life 100 years, the minimum value of the minor principal stress is obtained as -17.19 MPa and with design life 50 years; the minimum value of minor principal stress is obtained as -11.11 MPa. Therefore, a reduction of 35.36% in the values of minor principal stress occurs if the design life is reduced to 50 years from 100 years. Here also, while changing the design life from 100 years to 50 years, the reduction in $[D]$ matrix for consideration of lower design life governs the relative increase or decrease in the value of generated stresses.

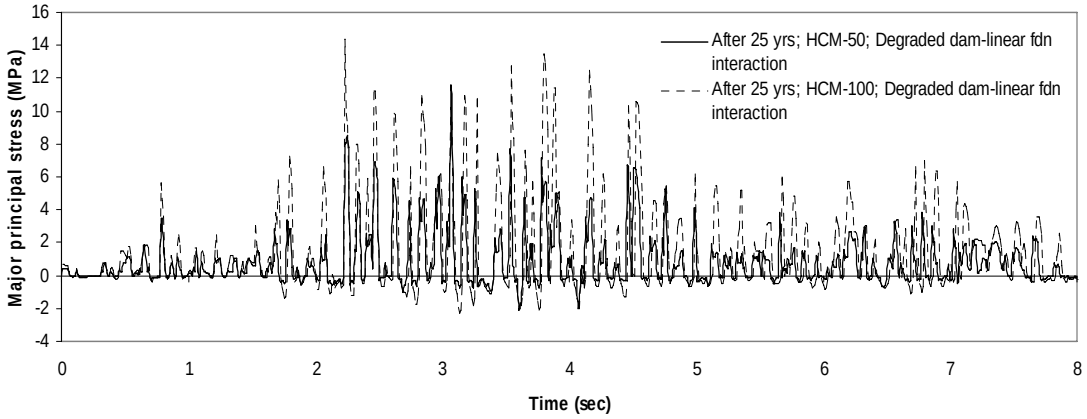


Fig. 4.84 Major principal stress vs. time at neck from degraded dam-linear foundation interaction after 25 years of construction with different HCM design lives

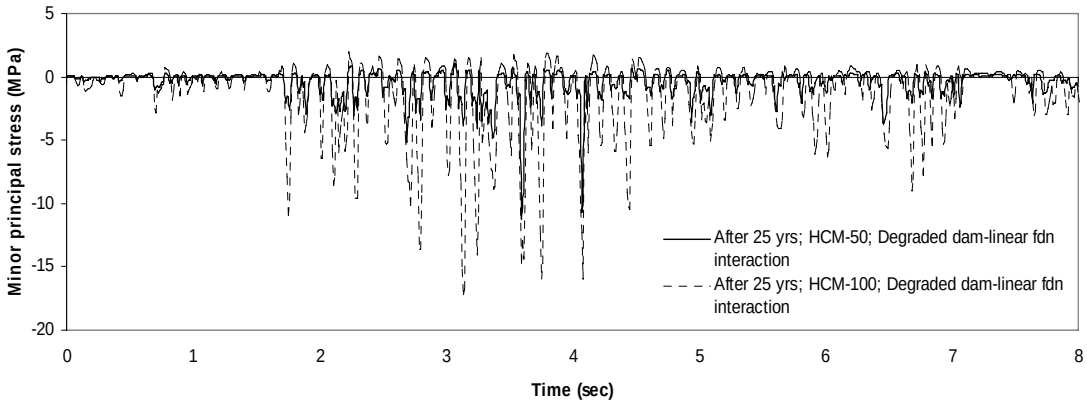


Fig. 4.85 Minor principal stress vs. time at neck from degraded dam-linear foundation interaction after 25 years of construction with different HCM design lives

Similar analyses are carried out varying the HCM design life of the concrete of the dam considering the nonlinear material properties of the foundation. Fig. 4.86 shows the variation of horizontal crest displacements vs time for degraded dam and nonlinear foundation analyses. For interaction analysis with HCM design life of 50 years, the maximum and minimum values of horizontal crest displacements are found to be 15.30 cm and -14.70 cm respectively. When the design life is increased to 100 years, similar values are found out to be 13.30 cm and -11.97 cm respectively. Therefore, a reduction of 13.10% and 18.57% in the magnitudes of maximum and minimum values of resulting horizontal crest displacement from the degraded dam-nonlinear foundation interaction analyses is observed if the design life is reduced 50 years from 100 years. The results show the similar trend as when the foundation material is considered to be linear, elastic. The consideration of higher design life of concrete produces lesser displacements as compared to the case when the HCM design life of concrete is less.

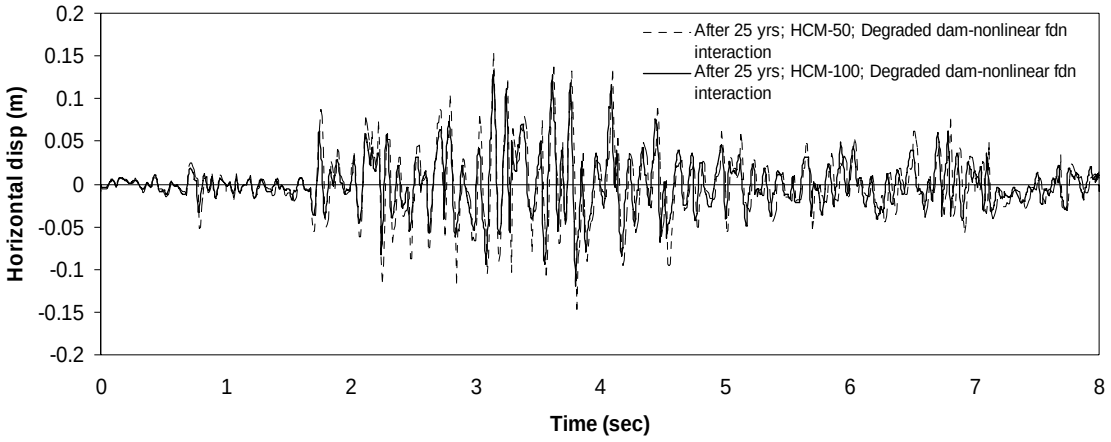


Fig. 4.86 Horizontal crest displacement vs time between degraded dam-nonlinear foundation interactions after 25 years of construction for different HCM design lives

Fig. 4.87 and Fig. 4.88 represent the variations of major and minor principal stress vs. time for degraded dam and nonlinear foundation interaction analysis. It is observed that the major and minor principal stresses are lesser when HCM design life is 50 years as compared to the case when HCM design life is 100 years. A similar trend is observed when the foundation material is considered to be linear, elastic in nature (as seen from Fig. 4.84 and 4.85).

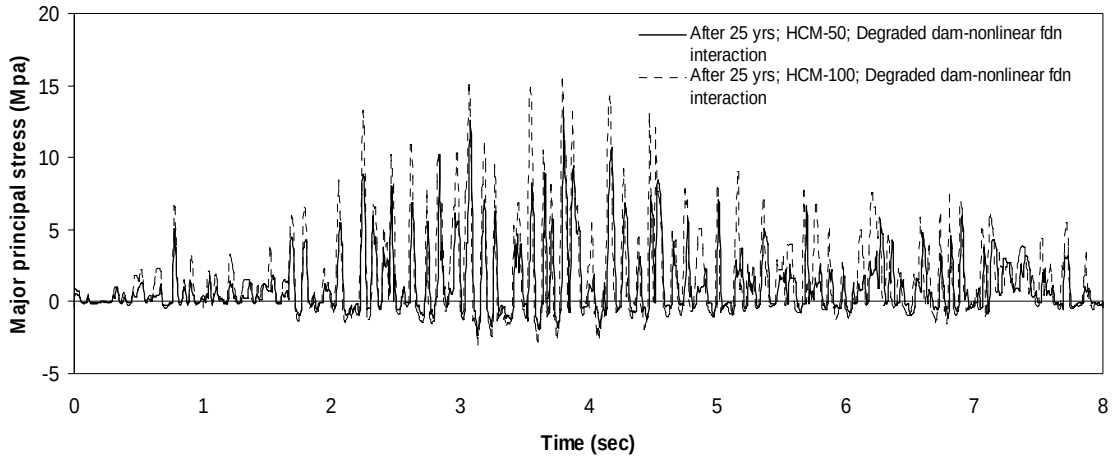


Fig. 4.87 Major principal stress vs. time at the neck from degraded dam-nonlinear foundation interaction after 25 years of construction with different HCM design lives

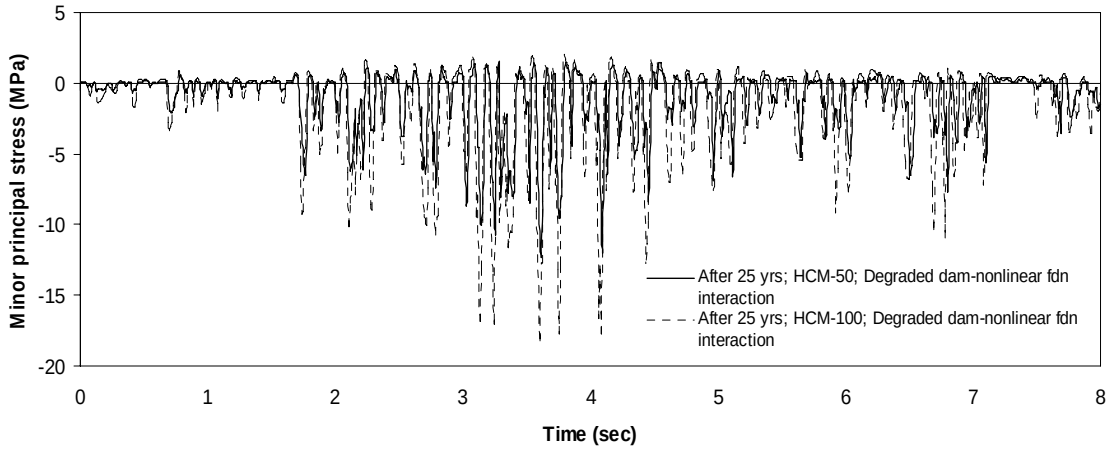


Fig. 4.88 Minor principal stress vs. time at the heel from degraded dam-nonlinear foundation interaction after 25 years of construction with different HCM design lives

The responses of the dam-foundation interaction analyses are plotted at the end of 50 years of construction of the dam. The HCM design lives are varied between 50 years and 100 years. The material properties of the foundation are considered to be linear, elastic. Fig. 4.89 plots the variation of horizontal crest displacements obtained after dam-foundation interaction analyses. If the HCM design life is considered to be equal to 100 years, the maximum values of horizontal crest displacements are obtained to be equal to 15.40 cm and -15.20 cm. If HCM design life dam is considered to be equal to 50 years, the maximum and minimum values of horizontal crest displacements are found out to be

equal to 18.70 cm and -18.40 cm. Therefore a reduction of 17.65% and 17.39% is observed in the values of maximum and minimum horizontal crest displacements if HCM design life is increased to 100 years from that of 50 years.

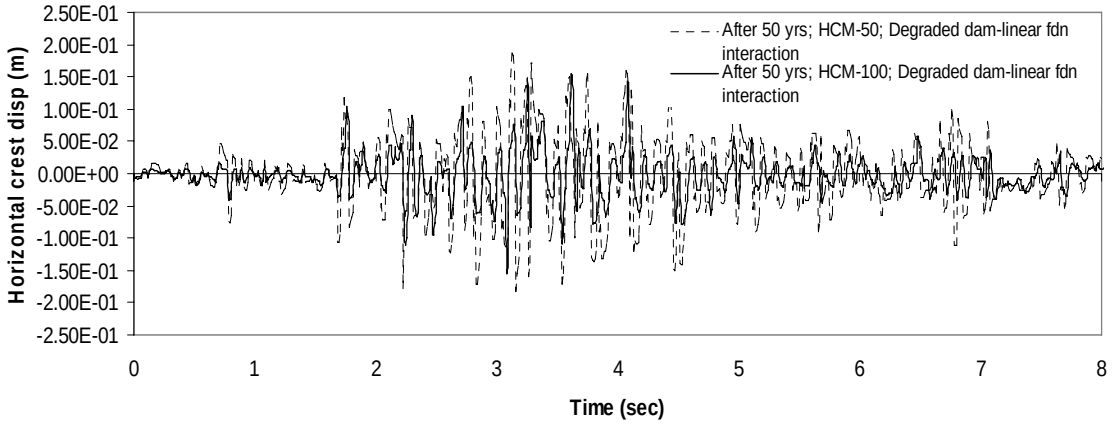


Fig. 4.89 Horizontal crest displacement vs. time between degraded dam-linear foundation interaction after 50 years of construction for different HCM design lives

Fig. 4.90 and Fig. 4.91 depict the variation of major and minor principal stresses at the end of 50 years for different HCM design lives of concrete. Fig. 4.90 shows that the maximum value of major principal stress is obtained as 10.80 MPa if the HCM design life is 100 years. If the HCM design life is considered to be equal to 50 years, the maximum value of major principal stress is found out to be 8.18 MPa. Therefore a reduction of 24.10% is observed in the value of major principal stresses if the HCM design life is changed to 50 years from that of 100 years. Fig. 4.91 displays the variation of minor principal stresses observed at the neck point of the dam body. If the HCM design life is considered to be equal to 50 years, the minimum value of minor principal stress is obtained as -8.50 MPa. If the HCM design life is changed to 100 years, the minimum value of minor principal stress is obtained as -11.40 MPa. Therefore, a reduction of 25.44% is observed in the value of minor principal stress if the HCM design life is changed to 50 years from 100 years.

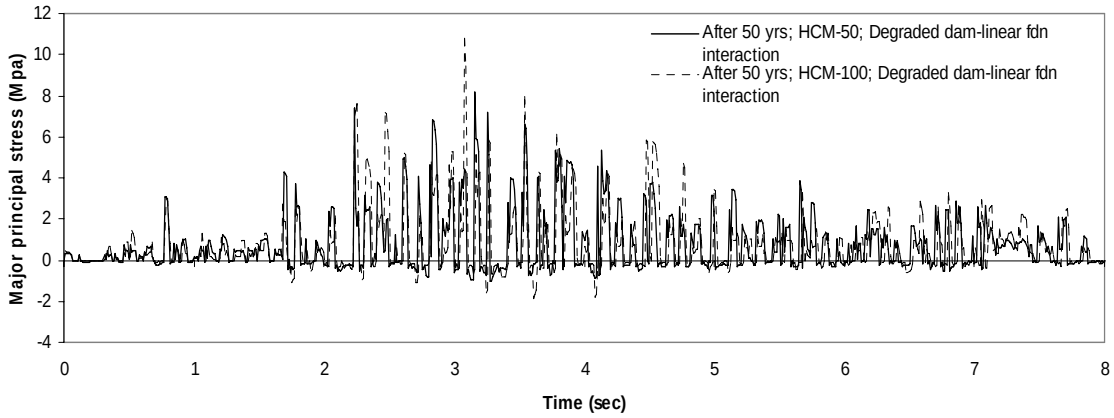


Fig. 4.90 Major principal stress vs. time at the neck from degraded dam-linear foundation interaction after 50 years of construction with different HCM design lives

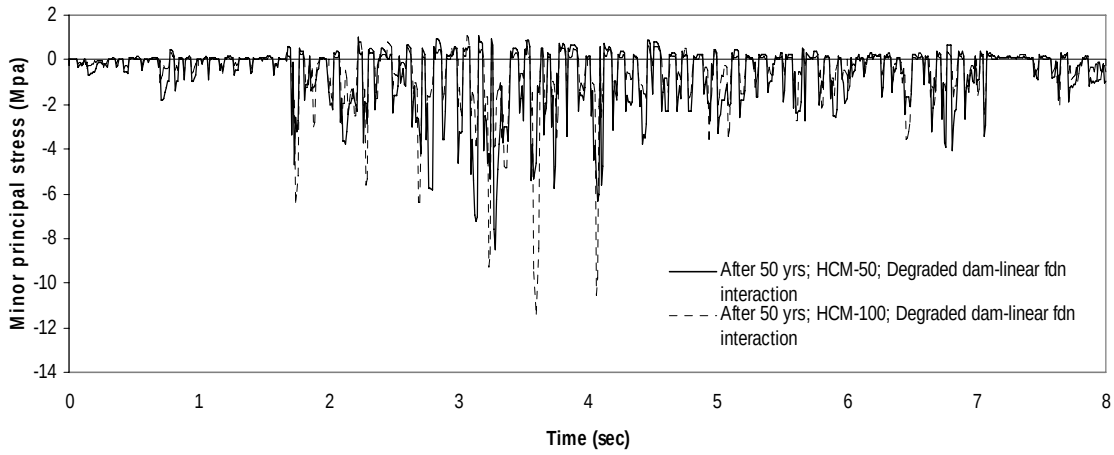


Fig. 4.91 Minor principal stress vs. time at the neck from degraded dam-linear foundation interaction after 50 years of construction with different HCM design lives

Next, the comparison of the results at the end of 50 years of construction of the dam is carried out when the foundation material is considered to be nonlinear Duncan-Chang material. Fig. 4.92 shows the variation of horizontal crest displacements for HCM design lives of 50 years and 100 years respectively. It may be seen that the maximum and minimum values of horizontal crest displacements are 20.90 cm and -20.40 cm respectively when the HCM design life of concrete is considered to be equal to 50 years. If the HCM design life of concrete is increased to 100 years, the corresponding values of horizontal crest displacements are found to be equal to 17.10 cm and -16.80 cm respectively. Therefore, a reduction of 18.18% and 17.65% are observed if the HCM design life of concrete is changed to 100 years from that of 50 years.

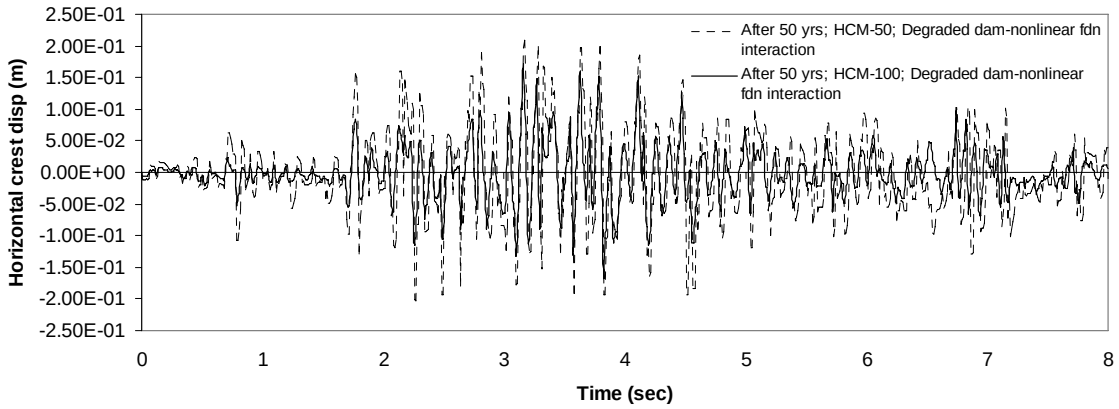


Fig. 4.92 Horizontal crest displacements vs. time from degraded dam-nonlinear foundation interaction after 50 years of construction with different HCM design lives

Fig. 4.93 shows the variation of major principal stresses observed at neck node if the HCM design life of concrete is considered to be equal to 100 years, the maximum value of major principal stress is obtained as 11.90 MPa. If the HCM design life of concrete is taken as 50 years, the corresponding value is 9.10 MPa. Therefore, a reduction of 23.50% is observed in the value of major principal stress if the HCM design life is reduced to 50 years from 100 years.

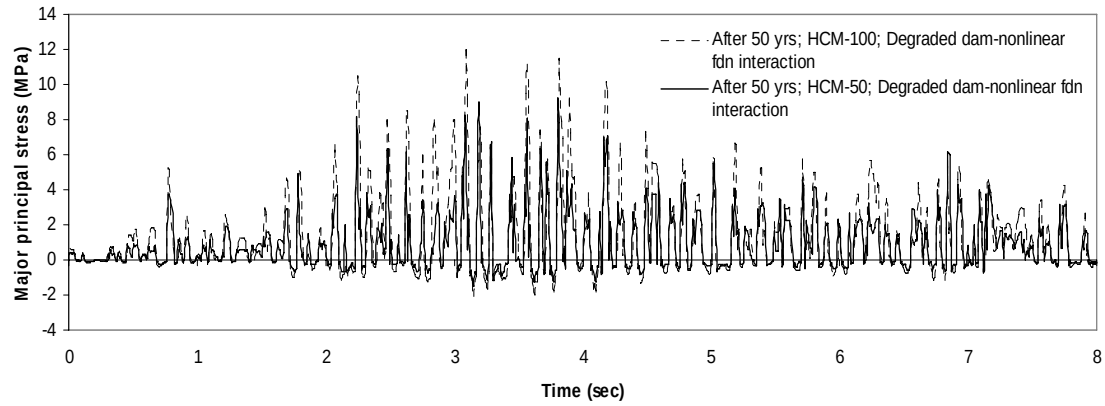


Fig. 4.93 Major principal stress vs. time at the neck from degraded dam-nonlinear foundation interaction after 50 years of construction with different HCM design lives

Fig. 4.94 shows the variation of minor principal stress vs. time plotted at the neck node ‘O’ as shown in Fig. 6.5. When the HCM design life of concrete is 50 years, the dam and nonlinear foundation interaction yields the value of minor principal stress as -9.50 MPa. The same value is obtained as -12.60 MPa when the HCM design life of

concrete is 100 years. Therefore, a reduction of 24.60% may be observed in the value of minor principal stress at point 'O' when HCM design life of concrete is reduced to 50 years from 100 years.

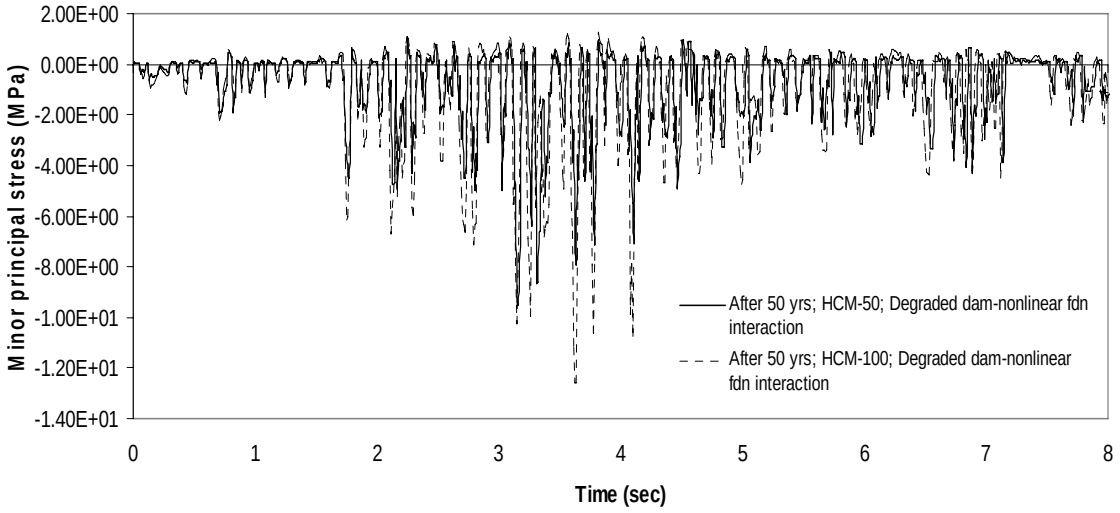


Fig. 4.94 Minor principal stress vs. time at the neck from degraded dam-nonlinear foundation interaction after 50 years of construction with different HCM design lives

### 4.4.4 Dam-Foundation Interaction Analyses under Empty and Full Reservoir Conditions

A comparative study is carried out to determine the relative variations between the results of dam-foundation interaction analyses under empty and full reservoir conditions. In section 4.4.4, the results pertaining to dam-foundation interaction analyses under full reservoir conditions are presented. Just like the case of dam-foundation interaction analyses under full reservoir condition, interaction analyses between dam and foundation are carried out under empty reservoir condition. The hydrodynamic pressure arising from Eq. 3.90 is neglected during such analyses. Following plots show the difference between the case of empty and full reservoir condition analyses.

Fig. 4.95 displays the variations between the horizontal crest displacements observed during dam and linear foundation interaction analysis just after the construction of the dam is over. It is observed that the maximum and minimum values of the horizontal crest displacements under empty reservoir conditions are 4.02 cm and -4.18

cm respectively. If the effect of hydrodynamic pressure is considered in the analysis, the values are obtained as 7.04 cm and -7.21 cm respectively. Therefore a rise of 75.12% and 72.49% are observed in the values of maximum and minimum horizontal crest displacements if the effect of hydrodynamic pressure is considered in the analysis.

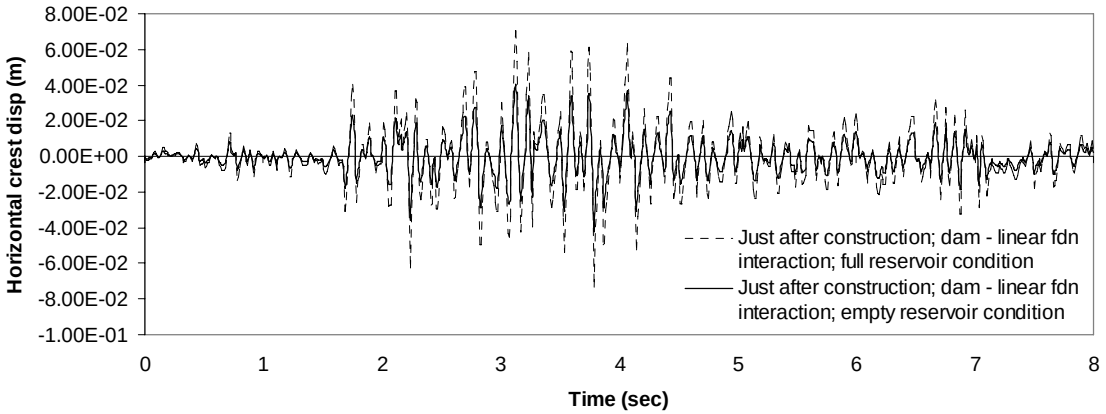


Fig. 4.95 Horizontal crest displacements for dam and linear foundation interaction analysis just after construction under empty and full reservoir condition

Fig. 4.96 displays the comparative values of major principal stresses for dam and linear foundation interaction analyses just after construction of the dam. Under empty reservoir condition, the maximum value of major principal stress is found out to be 8.75 MPa whereas the same value is obtained as 15.30 MPa under full reservoir condition. Therefore, a rise of 74.86% is observed if the analysis is carried out under full reservoir condition. Fig. 4.97 shows the variation of minor principal stresses obtained during analyses under full and empty reservoir conditions. The minimum value of minor principal stress under empty reservoir conditions is -8.23 MPa. If the effect of hydrodynamic pressure is considered in the analysis, the same value is found out to be equal to -14.50 MPa. Therefore, a rise of 76.18% is obtained for minor principal stress when reservoir full condition is considered.

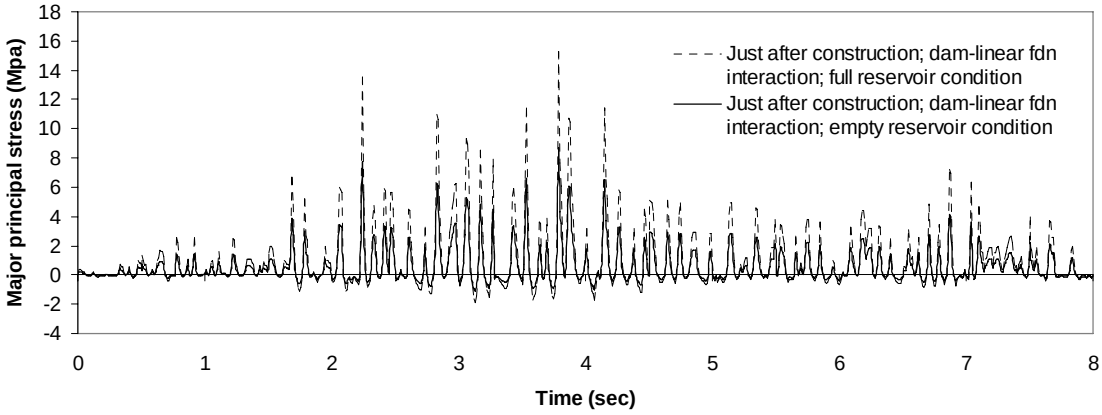


Fig. 4.96 Major principal stress for dam and linear foundation interaction analysis just after construction under empty and full reservoir condition

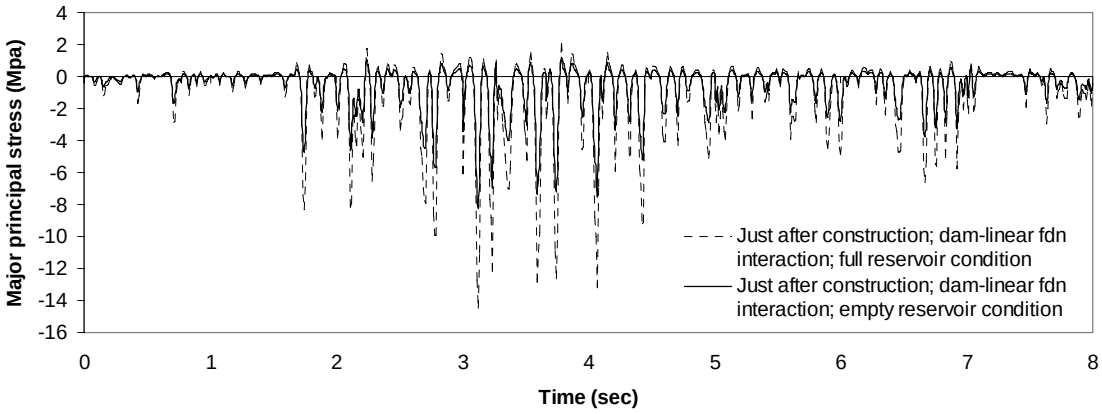


Fig. 4.97 Minor principal stress for dam and linear foundation interaction analysis just after construction under empty and full reservoir condition

For all other cases where the degradation of the concrete is taken into account, similar graphs are plotted by carrying out analyses without considering the effect of hydrodynamic pressure. Similar profiles with same phase differences as in the case of analyses considering the effect of hydrodynamic pressure are obtained in theses cases. Only, the magnitudes of graphs are reduced in such cases. The peak values of horizontal crest displacements, major and minor principal stresses found during dam-foundation interaction analyses under empty reservoir condition and full reservoir condition are tabulated in Table 4.10.

**Table 4.10 Comparison of horizontal crest displacements, major and minor principal stresses at the neck between empty and full reservoir condition**

| Different cases | | Horizontal crest displacements (cm) | | Major principal stress (MPa) | Minor principal stress (MPa) |
|---|---|---|---|---|---|
| | | Maximum (+ve) value | Minimum (-ve) value | | |
| Non-degraded dam-linear foundation interaction | Empty reservoir | 4.02 | -4.18 | 8.75 | -8.27 |
| | Full reservoir | 7.04 | -7.21 | 15.30 | -14.50 |
| Non-degraded dam-nonlinear foundation interaction | Empty reservoir | 4.73 | -4.66 | 9.38 | -9.05 |
| | Full reservoir | 8.18 | -8.02 | 16.45 | -15.90 |
| After 25 yrs; HCM-50; Degraded dam-linear foundation interaction | Empty reservoir | 7.56 | -7.28 | 6.36 | -6.03 |
| | Full reservoir | 13.80 | -13.30 | 11.50 | -11.11 |
| After 25 yrs; HCM-50; Degraded dam-nonlinear foundation interaction | Empty reservoir | 8.37 | -8.05 | 6.93 | -6.61 |
| | Full reservoir | 15.30 | -14.70 | 12.60 | -12.20 |
| After 25 yrs; HCM-100; Degraded dam-linear foundation interaction | Empty reservoir | 6.79 | -6.12 | 8.01 | -9.44 |
| | Full reservoir | 12.10 | -10.90 | 14.40 | -17.19 |
| After 25 yrs; HCM-100; Degraded dam-nonlinear foundation interaction | Empty reservoir | 7.47 | -6.72 | 8.51 | -9.98 |
| | Full reservoir | 13.30 | -11.97 | 15.30 | -18.20 |

| | | | | | |
|---|---|---|---|---|---|
| After 50 yrs; HCM-50; Degraded dam-linear foundation interaction | Empty reservoir | 10.15 | -9.90 | 4.38 | -4.52 |
| | Full reservoir | 18.70 | -18.40 | 8.18 | -8.50 |
| After 50 yrs; HCM-50; Degraded dam-nonlinear foundation interaction | Empty reservoir | 10.95 | -10.70 | 4.86 | -5.04 |
| | Full reservoir | 20.90 | -20.40 | 9.10 | -9.50 |
| After 50 yrs; HCM-100; Degraded dam-linear foundation interaction | Empty reservoir | 8.24 | -8.11 | 5.67 | -5.95 |
| | Full reservoir | 15.40 | -15.20 | 10.80 | -11.40 |
| After 50 yrs; HCM-100; Degraded dam-nonlinear foundation interaction | Empty reservoir | 9.05 | -8.72 | 6.21 | -6.56 |
| | Full reservoir | 17.10 | -16.80 | 11.90 | -12.60 |

Therefore, it is observed that higher responses are produced during full reservoir analyses compared to that of empty reservoir analyses. During empty reservoir analyses, the external hydrodynamic force (as expressed by Eq. 3.90) is not considered in the analyses. But, the effect of hydrodynamic force is imposed as an external force during full reservoir analyses. That is why; higher responses are produced during full reservoir analyses.

### 4.4.5 Summary of Findings

The findings from this chapter's results are summarized below:

i) The validation of the proposed iterative soil-structure interaction algorithm with a published problem by Yazdchi et al. (1999) proves its effectiveness in modeling soil-structure interaction problems.

ii) The interaction analysis between degraded dam and foundation yields more displacements compared to the case of interaction analysis between non-degraded dam and foundation interaction.

iii) If the nonlinear behaviour of foundation material is considered during SSI analyses, the responses (i.e displacements and stresses) increase compared to the case when foundation is considered to be linear, elastic.

iv) The hygro-chemo-mechanical (HCM) design life of concrete has a significant influence on the response of the dam during interaction analyses. Consideration of lesser HCM design life leads to more and more degradation of the concrete which in turn produces higher displacements. If the HCM design life of concrete is higher, the corresponding degradation of concrete is lower. Therefore, the resultant displacements are also lower compared to the case when HCM design life of concrete is relatively lower.

v) The contour plot drawn at the moment when major principal stress reaches its maximum value reveals that there is significant concentration of tensile stresses at the neck and toe region of the dam. Also, the contour plots drawn at the moment when minor principal stress attains the minimum value shows that the neck and toe regions experience accumulation of compressive stresses. It is observed that the neck region of the dam is highly stressed due to dam-foundation interaction effects. This probably explains why the cracks normally generate first at the neck region.

vi) The magnitude of responses of dam-foundation interaction analyses during full reservoir condition is higher than that during empty reservoir condition with same phase differences.

# CHAPTER 5

# CONCLUSIONS AND SCOPE OF FURTHER WORK

## 5.1 CONCLUSIONS

Based on the present work, the following conclusions are drawn:

- The work presents a methodology for the analysis of concrete gravity dam subjected to seismic excitations considering soil-structure interaction effects. A time domain model (as proposed by Gogoi and Maity, 2007) to describe the ageing process of concrete due to various hygro-chemo-mechanical actions has been used in the interaction analyses.
- As the concrete of the dam suffers degradation due to various hygro-chemo-mechanical actions, the stiffness of the structure reduces. As a result, the displacements increase due to earthquake excitation.
- The natural frequencies of the structure decrease with the increase in the value of degradation index.
- The contour plots of major and minor principal stresses reveal that whenever the major principal stresses are highest, the neck region of the dam experiences highest tensile stresses. Also, the maximum compressive stresses are found to occur along the vertical upstream face of the dam. Whenever minor principal stresses are lowest, the compressive stresses are observed near the neck region of the dam. The tensile stresses are found to accumulate near the vertical upstream face of the dam just opposite to the neck region of the dam body.
- The “added mass” approach proposed by Westargaard (1933) is a simple and effective way to simulate the effect of hydrodynamic pressure on the dam.
- The use of viscous dashpot boundary conditions (Lysmer and Kuhlemeyer, 1969) at the boundary nodes effectively absorbs the energies of the travelling waves and thus prevents spurious reflections.
- The nonlinear, elastic Duncan-Chang (1970) model is able to simulate the nonlinear properties of the foundation domain. The use of nonlinear, elastic model produces higher displacements and stresses for the foundation domain.

- It is observed for both linear and nonlinear analyses of the foundation domain that whenever the displacement at mid point on the surface of the foundation reaches the maximum value, tensile stresses are found to occur along vertical boundary in the left. It is further noticed that whenever displacement attains the lowest value, maximum compressive stresses are found to occur along the left side of the boundary of the foundation domain.
- The validation of the proposed soil-structure interaction algorithm proves its effectiveness in modeling soil-structure interaction problems.
- The degraded concrete suffers significant reduction of the stiffness. Therefore, the interaction analysis between degraded dam and foundation yields more displacements compared to the case of interaction analysis between non-degraded dam and foundation interaction.
- Consideration of nonlinear behavior of foundation in the dam-foundation interaction analysis yields more displacements and stresses compared to the case when the foundation behavior is considered to be linear, elastic.
- The hygro-chemo-mechanical (HCM) design life of the dam also bears a significant effect on the response of the dam-foundation interaction analysis. Consideration of lesser HCM design life leads to more and more degradation of the concrete which in turn produces higher displacements. If the HCM design life of concrete is higher, the corresponding degradation of concrete is lower. Therefore, the resultant displacements are also lower comparatively to case when HCM design life of concrete is relatively lower.
- The contour plot drawn at the moment when major principal stress reaches its maximum value reveals that there is significant concentration of tensile stresses at the neck and toe region of the dam. Also, the contour plots drawn at the moment when minor principal stress attains the minimum value shows that the neck and toe regions experience accumulation of compressive stresses. It is observed that the neck region of the dam is highly stressed due to dam-foundation interaction effects. This probably explains why the cracks normally generate first at the neck region.

- The magnitude of responses of dam-foundation interaction analyses during full reservoir condition is higher than that during empty reservoir condition with same phase differences.

## 5.2 SCOPE OF FURTHER WORK

The present work elaborates efficient solution scheme for the soil-structure coupled problems. There are certain aspects, which can be the extensive part of the present work and these can be as follows.

1. In the present study nonlinear properties are considered for foundation material through Duncan-Chang model nonlinear, elastic model. However, more rigorous nonlinear models such as elasto-plastic models (i.e. Mohr-Coulomb, Drucker-Prager models) may be used for the same.
2. The research may be extended to study the fully coupled effect of the dam-foundation-reservoir system.
3. Though an attempt is made to develop a method of solving SSI analysis, this method cannot take into account for any discontinuity or inhomogeneity or layered effect. Further research is required to overcome this constraint
4. The semi-infinite domain has been simulated by using viscous dashpots at the foundation boundaries. Other local and non-local boundary conditions including infinite elements, boundary elements etc. may be explored and compared to arrive at an efficient but simple algorithm to implement actual boundary conditions for the seismic analysis of dam-foundation coupled system.
5. Three-dimensional dynamic SSI analysis of dam with and without layering of soil is also an area where further work can be carried out.

# REFERENCES


Abouseeda H. and Dakoulas P. (1996) "Response of earth dams to P and SV waves using coupled FE-BE formulation", *Earthquake Engineering and Structural Dynamics*, 25, 1177-1194.

Ahmad S. and Banerjee P. K. (1998) "Multi-domain BEM for two dimensional problems of elastodynamics", *International Journal of Numerical Methods for Engineering*, 26, 891-911.

Andrade W. P., Tomaz R. J., Biitencourt R. M. and Guerra E. (1981) "A mix design for mass concrete", *Proceedings of Brazilian Concrete Institute*.

Ang H. S. and Newmark N. M. (1972) "Development of a transmitting boundary for numerical wave motion calculations", Report 2631, Defense Atomic Support Agency, April.

Antes H. (1985) "A boundary element procedure for transient wave propagations 2D isotropic elastic media", *Finite Elements in Analysis and Design*, 1, 313-323.

Antes H. and Von Estorff O. (1989) "Dynamic response analysis of rigid foundations and elastic structures by boundary element method", *Soil Dynamics and Earthquake Engineering*, 8, 68-74.

Atkin P. W. (1994) *Physical Chemistry*, 5th Edition, Oxford University Press, Oxford, U.K.

Bangert F., Grasberger S., Kuhl D., Meschke G. (2003) "Environmentally induced deterioration of concrete: physical motivation and numerical modelling", *Engineering Fracture Mechanics*, 70, 891–910.

Barros H. F., Marques C. M. S. and Martins R. A. F. (1991) "A symmetric formulation in non-associated plasticity", *International Journal for Numerical Methods in Engineering*, 38, 25-29.

Bathe K. J., Snyder M. D., Cimento A. P. and Rolph III, W. D. (1980) "On some current procedures and difficulties in finite element analysis of elastic-plastic response", *Computers & Structures*, 12, 607-624.

Batta V. and Pekau O. A. (1996) “Application of boundary element analysis for multiple cracking in conrete gravity dams”, *Earthquake Engineering and Structural Dynamics*, 25, 15-30.

Bayliss A. and Turkel E. (1980) “Radiation boundary conditions for wave-like equations”, *Communications on Pure and Applied Mathematics*, 33, 707–725.

Bazant Z. P. (1994) “Creep and thermal effects in concrete structures: a conceptus of some new developments”, *Computational modelling of Concrete Structures, International Conf. EURO-C*, H. Mang, N. Bicanic and R. de Borst. eds., Pineridge Press, Swansea, Wales, 461-480.

Bazant Z. P., Hauggaard A. B., Baweja S. and Ulm F. J. (1997) “Microprestress-solidification theory for concrete creep. I: Aging and drying effects”, *Journal of Engineering Mechanics, ASCE*, 123(11), 1188-1194.

Bazant Z. P. and Xiang Y. (1997) “Crack growth and lifetime of concrete under long time loading”, *Journal of Engineering Mechanics, ASCE*, 123(4), 350-358.

Beer G. and Meek J. L. (1981) “Infinite domain elements”, *International Journal for Numerical Methods in Engineering*, 17(1), 43-52.

Belytchko T. and Mullen R. (1977) “Stability of explicit-implicit time integration”, *International Journal for Numerical Methods in Engineering*. 12, 1575-1586.

Bernal D. and Youssef A. (1998) “A hybrid time frequency domain formulation for nonlinear soil structure interaction”, *Earthquake Engineering and Structural Dynamics*, 27, 673-685.

Beskos D. E. (1987) “Boundary element methods in dynamic analyses”, *Applied Mechanics Review*, 40, 1-23.

Bettess P. (1977) “Infinite Elements”, *International Journal for Numerical Methods in Engineering*, 11(1), 53-64.

Bettess P. (1980) “More on infinite elements”, *International Journal for Numerical Methods in Engineering*, 15, 1613-1626.

Bettess P. (1981) “Dynamic analysis of offshore structures”, *Applied Mathematical Modeling*, 5(2), 127.

Bittencourt R. M., Fontoura J. T. F., Andrade W. P. and Monteiro P. J. M (2001) "Mass concrete mixtures based on fineness modulus and geometrical gradation", *Journal of Materials in Civil Engineering, ASCE,* 13(1), 33-40.

Bose S. K. and Das S. C. (1997) "Nonlinear finite element analysis of stresses and deformations beneath rigid footings", *Computers & Structures*, 62(3), 487-492.

Bouaanani N., Paultre P. and Proulx J. (2003) "A closed-form formulation for earthquake-induced hydrodynamic pressure on gravity dams", *Journal of Sound and Vibration*, 261, 573-582.

Bustamante I. J. and Flores A. (1966) "Water pressure on dams subjected to earthquakes", *Journal of Engineering Mechanics Division, Proceedings of ASCE*, Oct, 15-127.

Byfors J. (1980) "Plain concrete at early ages", *Research Report F3:80*, Swedish Cement and Concrete Research Institute, Stockholm, Sweden.

Cervera M., Oliver J. and Faria R. (1995) "Seismic evaluation of concrete dams via continuum damage models", *Earthquake Engineering and Structural Dynamics*, 24(9), 1225-1245.

Cervera M., Oliver J. and Prato T. (1999a) "Thermo-Chemo-Mechanical Model for Concrete. I: Hydration and Aging", *Journal of Engineering Mechanics, ASCE*, 125, 1018 -1027.

Cervera M., Oliver J. and Prato T. (1999b) "Thermo-Chemo-Mechanical Model for Concrete. II: Damage and Creep", *Journal of Engineering Mechanics, ASCE*, 125, 1028- 1039.

Cervera M., Oliver J. and Prato T. (2000a) "Simulation of construction of RCC dams I: Temperature and aging", *Journal of Structural Engineering, ASCE*, 126(9), 1053-1061.

Cervera M., Oliver J. and Prato T. (2000b) "Simulation of construction of RCC dams. II: Stress and Damage" *Journal of Structural Engineering, ASCE,* 126(9), 1062-1069.

Chandrashaker R. and Humar J. L. (1993) "Fluid-foundation interaction in the seismic response of gravity dams", *Earthquake Engineering and Structural Dynamics*, 22, 1067-1084.

Chavez J. W. and Fenves G. L. (1995) “Earthquake analysis of concrete gravity dams including base sliding”, *Earthquake Engineering and Structural Dynamics*, 24, 673-686.

Chen J. (1980) “Analysis of local variations in free field seismic ground motion', *Ph.D. Dissertation*, University of California,Berkeley.

Chopra A. K. (1967) “Hydrodynamic pressures on dams during earthquakes”, *Journal of Engineering Mechanics, ASCE*, 93, 205-223.

Chopra A. K. (1968) “Earthquake behavior of reservoir-dam systems”, *Journal of Engineering Mechanics Division, ASCE*, 93,1475-1500.

Chopra A. K. (1975) “An examination of standard earthquake design forces for concrete gravity dams”, *Proceedings of International Symposium*, Swansea, UK, Sept. 8-11.

Chopra A. K. (2007) Dynamics of Structures: Theory and Applications to Earthquake Engineering ($2^{nd}$ eds) *Prentice Hall of India*, New Delhi.

Chuhan Z., Chengda Y. and Guanglun W. (2001) “Numerical simulation of reservoir sediment and effects on hydrodynamic response of arch dams”, *Earthquake Engineering and Structural Dynamics*, 30, 1817-1837.

Clarke M. J. and Hancock G. J. (1990) “A study of incremental iterative strategies for non-linear analysis”, *International Journal for Numerical Methods in Engineering*, 29, 1365-1391.

Clayton R. and Engquist B. (1977) "Absorbing boundary conditions for acoustic and elastic wave equations". *Bulletin of Seismological Society of America*, 67(6), 1529-1540.

Cohen M. and Jennings P. C. (1984) “Silent boundary methods for transient analysis”. In: Belytschko T. and Hughes T. J. R. (ed.): *Computational Methods for Transient Analysis*; Chap. 7, 301-357, Elsevier Science Publishers, Amsterdam.

Cole D. M., Kosloff D. D. and Minster J. B. (1978) “A numerical boundary integral equation method for elastodynamics. I”, *Bulletin of Seismological society of America*, Vol. 68(5), 1331-1557.

Copen M. D., Lindholm E.A. and Tarbox G. S. (1977) Design of concrete dams. Handbook of Dam Engineering, Nostrand Reinhold; 385-465.

Coulomb C. A. (1773), “Essai sur une application des Regles de Maximis et Minimis a quelques Problemes de Statique, relatifs a l Architecture,” Memoires par divers Savants, 1776 (read in 1773) “Coulomb’s Memoir on Statics”, Cambridge University Press, Cambridge, England, 1972.

Cruse T. A. (1968) “A direct formulation and numerical solution of the transient elastodynamic problems II”, *Journal of Mathemetical Analysis and Computations*, 22(2), 341-355.

Cruse T. A. and Rizzo F. J. (1968) “A direct formulation and numerical solution of the transient elastodynamic problems I”, *Journal of Mathemetical Analysis and Computations*, 22(1), 244-259.

Dai D. N. (1992) “An improved boundary element formulation for wave propagation problems”, *Engineering Analysis with Boundary Elements*, 10(4), 277-281

Deb S. K. and Borsaikia A. C. (2006) “Design of mass concrete mix for gravity dam based on fineness modulus and geometrical gradation”, *Indian Concrete Journal*, 80(1), 52-56.

Deb D. (2006) *Finite Element Method: Concepts and Applications in Geomechanics*, Prentice Hall of India, New Delhi.

Desai C. S. and Galagoda H. M. (1989) “Earthquake analysis with generalized plasticity model for saturated soils”, *Earthquake Engineering and Structural Dynamics*, 18, 903-919.

DiMaggio F.L. and Sandler I.S (1971) Material models for granular soils. J. Eng. Mech. Div. ASCE, 97(EM3): 935-950.

Dravinski M. (1982) “Influence of interface depth upon strong ground motion”, *Bulletin of Seismological Society of America*, 72, 597-614.

Drucker D. C. and Prager W. (1952) “Soil mechanics and plastic analysis or limit design” Quarterly of Applied Mathematics, 10, 157-175.

Drucker D. C., Gibson R. E. and Henkel D. J. (1957) “Soil mechanics and work hardening theories of plasticity”. Trans. ASCE, 122, 338-346.

Duncan J. M. and Chang C. Y. (1970) “Non-linear analysis of stress and strain in soils”, Journal of Soil Mechanics and Foundation Engineering Division, ASCE, 96(SM5), 1629-1634.

Duncan J. M., Byrne P., Wong K. S. and Mabry P., (1980) “Strength, Stress-Strain and Bulk Modulus Parameters for Finite Element Analyses of Stresses and Movements in Soil Masses”, Report Number UCB/GT/80-01, University of California, Berkeley, California, USA, 70 p.

Duncan J. M. (1994) “The role of advanced constitutive relations in practical application.” *Proceedings 12th International Conference on Soil Mechanics and Foundation Engineering*, New Delhi, India, 5, 31-48.

El-Aidi B. and Hall J. F. (1989) “Nonlinear earthquake response of concrete gravity dams”, *Earthquake Engineering and Structural Dynamics*, 187, 837-865.

Elgamal A. W., Ghaffar M. A. and Prevost J. H., (1985) “Nonlinear hysteretic response of soil systems”, *Journal of Engineering Mechanics, ASCE*, 111, 882-897.

Elgamal A. W., Ghaffar M. A. and Prevost J. H., (1987) “Elasto-plastic seismic shear response of 3-D earth dams: Application”, *Journal of Geotechnical Engineering Division*, ASCE, 113, 1309-1325.

El-Gebeily M., Elleithy W. M. and Al-Gahtani H. (2002) “Convergence of the domain decomposition finite element-boundary element methods”, *Computer Methods in Applied Mechanics and Engineering*, 191, 4851-4867.

Elleithy W. M. and Tanaka M. (2003) “Interface relaxation algorithms for BEM-BEM coupling and FEM-BEM coupling”, *Computer Methods in Applied Mechanics and Engineering*, 192, 2977-2992.

Engquist B. and Majda A. (1977) "Absorbing boundary conditions for numerical solutions of waves". *Math. Comp.*, 31(139), 629-651.

Fahjan Y. M., Borekci O. S. and Erdik M. (2003) “Earthquake-induced hydrodynamic pressures on 3D rigid dam-reservoir system using DRBEM and a radiation matrix”, *International Journal for Numerical Methods in Engineering*, 56(10), 1511-1532.

Felippa C. A. and Park K. C. (1980) “Staggered transient analysis procedures for coupled mechanical systems: formulation”, *Computer Methods in Applied Mechanics and Engineering*, 24, 61-111.

Feng K. (1983) “Finite element method and natural boundary conditions”, International Proceedings of the International Congress of Mathematicians; 1439-1453.

Fenves G. and Chopra A. K. (1984) “Earthquake analysis and response of concrete gravity dams”, *Report No.UCB/EERC-84/10, Earthquake Engineering Research Center, University of California, Berkley, California*.

Fenves G. L. and Chopra A. K. (1987) “Simplified analysis of concrete gravity dams”, *Journal of Structural Engineering, ASCE*, 113(8), 1688-1708.

Fok K. L., Hall J. F. and Chopra A. K. (1986) “EACD-3D, A computer program for three-dimensional earthquake analysis of concrete dams”, *Earthquake Engineering Research Center, Report No. UCB/EERC-86/09, University of California, Berkeley*, July.

Frantziskonis G., Desai C. S. and Somasundaram S. (1986) “Constitutive model for nonassociative behavior”, Journal of Engineering Mechanics, ASCE, 112(9), 932-946.

Ghaemian M and Ghobarah A. (1999) “Nonlinear seismic response of concrete gravity dams with dam-reservoir interaction”, *Engineering Structures*, 21, 306-315.

Ghrib F. and Tinawi R. (1995a) “Nonlinear behavior of concrete gravity dams using damage mechanics”, *Journal of Engineering Mechanics, ASCE*, 121(4), 513-527.

Ghrib F. and Tinawi R. (1995b) “An application of damage mechanics for seismic analysis of concrete gravity dams”, *Earthquake Engineering and Structural Dynamics*, 24(2), 157-173.

Givoli D. (1991) “Non-reflecting boundary conditions”, *Journal of Computational Physics*, 94, 1-29.

Givoli D. (1992) “Numerical methods for problems in infinite domains”, *Studies in Applied Mechanics*, 33, Elsevier, Amsterdam.

Givoli D. and Patlashenko I. (1998) “Optimal local non-reflecting boundary conditions” *Applied Numerical Methods*, 27, 367-384.

Gogoi I. (2007) “Dynamic response of ageing concrete gravity dams with unbounded reservoir”, *Doctoral Thesis*, IIT Guwahati.

Gogoi I. and Maity D. (2007) “Influence of sediment layers on dynamic behavior of aged concrete dams” *Journal of Engineering Mechanics, ASCE*, 133(4), 400-413.

Griffiths D. V. (1990) “Failure criteria interpretation based on Mohr-Coulomb friction”, *Journal of Geotechnical Engineering*, ASCE, 116(6), 986-999.

Griffiths D. V. and Prevost J. H. (1988) “The properties of anisotropic conical failure surfaces in relation to Mohr-Coulomb criterion”, *International Journal for Numerical and Analytical Methods in Geomechanics*, 12(5), 497-504.

Grote M. J and Keller J. B. (1996) “Nonreflecting boundary conditions for the time scattering”, *Journal of Computational Physics*, 127, 52–65.

Haggblad B. and Nordgren G. (1987) “Modelling nonlinear soil-structure interaction using interface elements, elastic-plastic soil elements and absorbing infinite elements”, *Computers & Structures*, 26(1), 307-324.

Hird C. C. and Russell D. (1990) “A benchmark for soil-structure interface elements”, *Computers & Geotechnics*, 10(2), 139-147.

Hoek, E. and E.T. Brown (1980),” Underground Excavation in Rock”, Instn. Mine Metallurgy, London.

Hoek, E. and E.T. Brown (1988),” The Hoek and Brown Failure Criterion – A 1988 Update”, 15th Canadian Symposium of Rock mechanics, Toronto, pp. 31-38, Dept., of Civil Engineering, Univ. of Toronto.

Hoek, E. and E.T. Brown (1997),”Practical Estimate of Rock Mass Strength”, *Int. J. Rock Mech. Min. Sci. and Geomesh Abstr.*, Vol. 34, No. 8, pp. 1165-1186.

Huan R. N and Thompson L. L. (2000) “Accurate radiation boundary conditions for the time-dependent wave equation on unbounded domains”, *International Journal for Numerical Methods in Engineering*, 47, 1569–1603.

Hubert F.X., Burlion N. and Shao J.F. (2001) “Consequences of dessication on mechanical damage of concrete”, *Fracture Mechanics of Concrete Structures*, 1, 223-230.

Hughes T. J. R. and Liu W. K. (1978) “Implicit-explicit finite elements in finite element analysis: Stability theory”, *Journal of applied Mechanics*, ASME, 45, 371-374.

Hughes T. J. R. and Liu W. K. (1978) “Implicit-explicit finite elements in finite element analysis: Implementation and numerical examples”, *Journal of applied Mechanics*, ASME, 45, 375-378.

Ibrahimbegovic A. and Wilson E. (1990) “A methodology for dynamic analysis of linear structure-foundation systems with local nonlinearities”, *Earthquake Engineering and Structural Dynamics*, 19, 1197-1208.

Israil A. S. and Banerjee P. K. (1991) “Interior stress calculations in two dimensional time domain transient BEM analysis”, *International Journal of Solids and Structures*, 27, 915-927.

Jahromi H. Z., Izzuddin B. A. and Zdravkovic L. (2007) “Partitioned analysis of nonlinear soil-structure interaction using iterative coupling”, *Interaction and Multiscale Mechanics*, 1(1), 33-51.

Jahromi H. Z., Izzuddin B. A. and Zdravkovic L. (2009) “A domain decomposition approach for coupled modeling nonlinear soil-structure interaction”, *Computer Methods in Applied Mechanics and Engineering*, 198(33), 2738-2749.

Jianguo X., Danmin W. and Tieming F. (1993) “A modified lumped parametric model for nonlinear soil-structure interaction analysis”, *Soil Dynamics and Earthquake Engineering*, 12, 273-282.

Karabalis D. L. and Beskos D. E., (1984): ‘Dynamic response of 3D rigid surface foundation by time domain BEM’, *Earthquake Engineering and Structural Dynamics*, 12, pp. 73-93.

Karabalis D.L. and Beskos D.E. (1985) “Dynamic response of three-dimensional flexible foundations by time domain BEM and FEM”, *Soil Dynamics and Earthquake* Engineering, 24(2), 91-101.

Kausel E. (1988) “Local transmitting boundaries”, *Journal of Engineering Mechanics*, ASCE, 114, 1011-1027.

Kausel E. and Tassoulas J. T. (1981) “Transmitting boundaries: a closed-form comparison”, *Bulletin of Seismological Society of America*, 71, 143-159.

Keller J. B. and Givoli D. (1989) “Exact Non-reflecting boundary conditions”, *Journal of Computational Physics*, 82(1), 172-192.

Kellezi L. (2000) “Local transmitting boundaries for transient elastic analysis”, *Soil Dynamics and Earthquake* Engineering, 19(7), 533-547.

Khalili N., Valliappan S., Tabatabaie Y. J. and Yazdchi M. (1997) “ID infinite element for dynamic problems in saturated porous media”, *Communications in Numerical Methods in Engineering* ,13, 727-738.

Krajcinovic D. (1989) “Damage mechanics”, *Mechanics of Materials*, 8, 117-197.

Krishna J., Chandrasekaran A. R. and Saini S. S. (1969) "Analysis of Koyna accelerogram of December 11, 1967", *Bulletin of Seismological Society of America*, 59 (4), 1719-1731.

Küçükarslan S. (2003) "Dam-reservoir interaction including the reservoir bottom effects in time domain", *16th ASCE Engineering Mechanics Conference, July 16-18, 2003, University of Washington, Seattle.*

Kucukarslan S. (2004) "Dynamic analysis of dam-reservoir-foundation interaction in time domain", *Computational Mechanics*, 33, 274-281.

Kuhl D, Bangert F, Meschke G. (2004) "Coupled chemo-mechanical deterioration of cementitious materials. Part I: Modeling", *International Journal of Solids and Structures*, 41, 15 - 40.

Léger P. and Katsouli M. (1989) "Seismic stability of concrete gravity dams", *Earthquake Engineering and Structural Dynamics*; 18, 889-902.

Lemaître J. and Chaboche J. L. (1989) "Aspect phénoménologique de la rupture par endommagement", *Journal de mécanique appliquée*, Paris, France, 23, 317-367.

Levtcitch, V., Kvasha, V., Boussalis, H., Chaissakos, A. and Kosmatopoulos, E. (2004), "Seismic performance capacities of old concrete", 13th World Conference on Earthquake Engineering, Vancouver, Canada, August 1-6, paper no. 2182.

Liao Z. P. and Wong H. L., (1984) "A transmitting boundary for the numerical simulation of elastic wave propagation", *Soil Dynamics and Earthquake Engineering*, 3, 174-183.

Lindman E. L. (1973) "On getting all of the waves out of the box", Proc. Sixth Conf. on Numerical Simulation of Plasmas, Lawrence Berkeley Laboratory, Berkeley, Calif., 42-45.

Lindman E. L. (1975) "Free-space boundary conditions for the time dependent wave equation", *Journal of Computational Physics*, 18, 66-78.

Lindvall A. (2001) "Environmental actions and response: Reinforced concrete structures exposed in road and marine environments", *Licentiate of Engineering Thesis*, Chalmers University of Technology, Göteborg, Sweden.

Lord Rayleigh. (1885) "Ueber die Methode der Dämpfung bei der Bestimmung des Ohms", *Annalen der Physik*, 260(2), 214-215.

Lysmer J. and Kuhlemeyer R. L. (1969) “Finite dynamic model for infinite media”, *Journal of Engineering Mechanics*, ASCE, 95(EM4), 859-877.

Oliver J., Cervera M., Oller S. and Lubliner J., (1990) “Isotropic damage models and smeared crack”, *Computer Aided Analysis and Design of Concrete Structures*, Pineridge Press, Swansea England, 945-957.

Maity D. and Bhattacharyya S. K. (2003) “A parametric study on fluid structure interaction problems”, *Journal of Sound and Vibration*, 263, 917-935.

Manolis G. D. and Beskos D. E. (1981) “Dynamic stress concentration studies by boundary integrals and Laplace transforms”, *International Journal for Numerical Methods in Engineering*, 17(4), 573–599.

Mathews J. H. (2001) Numerical Methods for Mathematics, Science and Engineering, *Prentice-Hall of India*, New Delhi, 257-314.

Mazars J. and Pijaudier-Cabot G. (1989), “Continuum Damage Theory – Application to Concrete”, *Journal of Engineering Mechanics, ASCE*, 115(2), 345-365.

Mazzotti C., Savoia M. and Tralli A. (2001) “Isotropic damage model for nonlinear creep behaviour of concrete in compression”, *Fracture Mechanics of Concrete Structures*, 1, 255-262.

Medina F. and Penzien J. (1982) “Infinite elements for elastodynamics”, *Earthquake Engineering and Structural Dynamics*, 10, 699-709.

Moser W., Antes H. and Beer G. (2005) **“**Soil-structure interaction and wave propagation problems in 2D by a Duhamel integral based approach and the convolution quadrature method”, Computational Mechanics, 36, 431-443.

Nardini D. and Brebbia C. A. (1982) “A new approach to free vibration analysis using boundary elements”, Boundary Element methods in Engineering, ed. C. A. Brebbia, Springer – Verlag, Berlin.

Neville A. M. and Brooks J. J. (1987) “Elasticity and creep”, *Concrete Technology*, Pearson Education (Singapore) Pte. Ltd., 4th Indian Reprint, 209-234.

Newmark N. M. (1959) “A method of computation for structural dynamics”, Journal of Engineering Mechanics Division. ASCE 85, No. EM3, 67-94.

Ng P. C. F., Pyrah C. and Anderson W. F. (1997) “Assessment of three interface elements and modification of interface elements in CRISP90”, *Computers & Geotechnics*, 21(4), 315-339.

Olson L. G. and Bathe K. J. (1985a) “An infinite element for analysis of transient fluid-structure interactions”, *Engineering Computations*, 2, 319-330.

Olson L. G. and Bathe K. J. (1985b) “Analysis of fluid-structure interactions. A direct symmetric coupled formulation based on the fluid velocity potential”, *Computers and Structures*, 21, 21-32.

Pandey A. K., Kumar G. and Sharma S. P. (1994) “An iterative approach for soil-structure interaction in tall buildings”, *Engineering Fracture Mechanics*, 47(2), 169-176.

Paul D.K., Zienkiewicz O.C. and Hinton E. (1981) “Transient dynamic analysis of reservoir-dam interaction using staggered solution schemes”, *Numerical Methods for Coupled Problems, Proceedings of International Conference held at University College, Swansea, 7th-11th September*, Pineridge Press, Swansea, U.K., pp. 321-331.

Park K. C., Felippa C. A. and Deruntz H. A., (1977) “Stabilization of staggered solution procedures for fluid structure interaction analysis”, In: *Computational Methods for Fluid-Structure Interaction Problems*, Ed. T. Belytschko and T. L. Geers, ASME Applied Mechanics Symposia Series, AMD, 26, 94-124.

Pavlatos G. D. and Beskos D. E., (1994) “Dynamic elastoplastic analysis by BEM/FEM”, *Engineering Analysis with Boundary Elements*, 14, 51-63.

Pekau O. A., Chuhan Z. and Lingmin F. (1991) “Seismic fracture analysis of concrete gravity dams”, *Earthquake Engineering and Structural Dynamics*, 20, 335-354.

Peyer L., Royet P. and Boissier D. (2006) “Dam ageing diagnosis and risk analysis: development of methods to support expert judgment”, *Canadian Geotechnical Journal*, 43, 169-186.

Prandtl L. (1921) “Eindringungs Festigkeit und Festigkeit von Schneiden”, *Zeitschrift für Angewandte Mathematik und Mechanik*, 1, 15.

Prandtl L. (1924) Proc. 1st International Congress of Applied Mechanics, Delft, 1924, 43–54.

Preisig M. (2002) “Nonlinear finite element analysis of dynamic soil-foundation-structure interaction”, Dissertation submitted for Master of Science in Civil Engineering, University of California, Davis. Swiss Federal Institute of Technology, Lausanne.

Proulx J. and Paultre P. (1997) “Experimental and numerical investigation of dam–reservoir–foundation interaction for a large gravity dam”, *Canadian Journal of Civil Engineering*, 24 (1), 90-105.

Reinoso E., Wrobel L. C. and Power H. (1997) “Three dimensional scattering of seismic waves from topographic structures”, *Soil Dynamics and Earthquake Engineering*, 16(1), 41-61.

Rizos, D. C. and Wang, Z. (2002) “Coupled BEM–FEM solutions for direct time domain soil–structure interaction analysis”, *Engineering Analysis with Boundary Elem*ents, 26, 877-888.

Sain T. and Chandra Kishen J. M. (2003) “Residual life assessment of concrete structures”, *Proceedings of Structural Engineering Convention, 2003, An International Meet, IIT Kharagpur, India, Ed. Bhattacharyya S.K.*, 161-169.

Saini S. S., Bettess P., Zienkiewicz O. C. (1978) “Coupled hydrodynamic response of concrete gravity dams using finite and infinite elements”, *Earthquake Engineering and Structural Dynamics*, 6, 363-374.

Scott R. F. (1985) “Plasticity and constitutive relations in soil mechanics”, *Journal of Geotechnical Engineering*, ASCE, 111(5), 563-604.

Selvadurai A. P. S. and Karpurapu R. (1989) “Composite infinite element for modeling unbounded saturated soil media”, *Journal of Geotechnical Engineering*, ASCE, 115(11), 1633-1646.

Sharan S. K. (1987a) “Time domain analysis of infinite fluid vibration”, *International Journal of Numerical Methods in Engineering*, 24, 945-958.

Sharan S. K. (1987b) “A non-reflecting boundary in fluid-structure interaction”, *Computers and Structures*; 26, 841-846.

Shetty M. S. (1998) Concrete Technology. *S. Chand & Company,* New Delhi.

Simo J. and Ju J. (1987) “Strain and stress-based continuum damage models – I. Formulation”, *International Journal of Solids and Structures*, 23(7), 821-840.

Sitharam T. G., Sridevi J. and Shimizu N. (2001) "Practical equivalent continuum characterization of jointed rock masses", *International Journal of Rock Mechanics and Mineral Science*, 38, 437-448.

Sitharam T. G. and Madhavi Latha G. (2002), "Simulation of excavation in jointed rock masses using practical equivalent continuum model", *International Journal of Rock Mechanics and Mineral Science*, 39, 517-525.

Sitharam T. G., Majhi V. B. and Verma A. K. (2005) "Equivalent continuam analysis of jointed rock mass" Alaska Rocks, The 40th U.S. Symposium on Rock Mechanics (USRMS), American Rock Mechanics Association (ARMA), June 25-29.

Sloan S. W. and Booker J. R. (1992) "Integration of Tresca and Mohr-Coulomb constitutive relations in plane strain elastoplasticity", *International Journal for Numerical Methods in Engineering*, 33, 163-196.

Spyrakos C. C., Beskos D. E. (1986) "Dynamic response of flexible strip foundation by boundary and finite elements", *Soil Dynamics and Earthquake Engineering*, 5(2), 84-96.

Stefanou G. D. (1983) "Aspects of soil-structure-water interaction problems", *Computers & Structures*, 16(5), 629-638.

Steffens A., Li K. and Coussy O. (2003) "Ageing approach to water effect on alkali–silica reaction degradation of structures", *Journal of Engineering Mechanics, ASCE*, 129(1), 50-59.

Tan H. and Chopra A. K. (1995) "Earthquake analysis of arch dams including dam-water-foundation rock interaction", *Earthquake Engineering and Structural Dynamics*; 24, 1453-1474.

Tan H. and Chopra A. K. (1996) "Dam-foundation rock interaction effects in frequency response functions of arch dams". *Earthquake Engineering and Structural Dynamics*, 24, 1475-1489.

Tekie P. B. and Ellingwood B. R. (2003) "Seismic fragility assessment of concrete gravity dams", *Earthquake Engineering & Structural Dynamics*, 32(14), 2221-2240.

Thompson, L. L. and Huan, R. N. (2000a) "Implementation of exact non-reflecting boundary conditions in the finite element method for the time dependent wave equation", *Computer Methods in Applied Mechanics and Engineering*, 187, 137-159.

Thompson L. L. and Huan R. N. (2000b) “Computation of the far field solutions based on exact non-reflecting boundary conditions for the time dependent wave equation”, *Computer Methods in Applied Mechanics and Engineering*, 190, 1551-1577.

Thompson L. L., Huan R. N. and He D. T. (2001) “Accurate radiation boundary conditions for the two-dimensional wave equation on unbounded domains”, *Computer Methods in Applied Mechanics and Engineering*, 191, 331–351.

Torkamani M. A. M. and Alsanusi S. (1989) “Elasto-plastic analysis of a plane stress problem using linearized yield surface and mixed hardening rule”, *Computers & Structures*, 31(6), 935-956.

Touhei T. and Ohmachi T., (1993) “A FE-BE method for dynamic analysis of dam-foundation-reservoir system in the time domain”, *Earthquake Engineering and Structural Dynamics*, 22, 195-209.

Tresca H. (1868) “Memoire sur l’ecoulement des corps solides soumis a de fortes pressions”, Memoires Presentees par Divers Savants, 18, 733-799. (presented 1864).

Tresca H. (1872) “Memoire sur le poinconnage des metaux”, Memoires des Savants Etrangers, 20, 617-838. (presented 1869).

Ulm F. J. and Coussy O. (1995) “Modelling of thermochemomechanical couplings of concrete at early ages”, *Journal of Engineering Mechanics, ASCE*, 121(7), 785-794.

U. S. Army Corps of Engineers (1977) The evaluation of dam safety. *Proceedings of Engineering Foundation Conference*, Pacific Grove, California, Nov- Dec.

U. S. Bureau of Reclamation: Arch Dams. In Concrete Dams. Design Standards No.2 Denver: U.S. Department of the Interior 1965.

U. S. Bureau of Reclamation: Gravity Dams. In Concrete Dams. Design Standards No.2 Denver: U.S. Department of the Interior 1966.

U. S. Bureau of Reclamation (1976) Design of gravity dams, *Design manual for concrete gravity dams*, Denver.

Valliappan S. and Zhao C. (1992) “Dynamic response of concrete gravity dams including dam-water-foundation interaction”, *International Journal for Numerical and Analytical Methods in Geomechanics*, 16, 79-99.

Vargas-Loli L. M. and Fenves G. L. (1989) “Effects of concrete cracking on the earthquake response of gravity dams”, *Earthquake Engineering and Structural Dynamics*, 18, 575-592.

Viladkar M. N., Godbole P. N. and Noorzaei J. (1991a) “Some new three dimensional infinite elements”, *Computers & Structures*, 34(3), 455-467.

Viladkar M. N., Noorzaei J. and Godbole P. N. (1991b) “Soil-structure interaction in plane frames using coupled finite-infinite elements”, *Computers & Structures*, 39(5), 535-546.

Viladkar M. N., Noorzaei J. and Godbole P. N. (1994a) “Behavior of infinite elements in an elasto-plastic domain”, *Computers & Structures*, 51(4), 337-342.

Viladkar M. N., Noorzaei J. and Godbole P. N. (1994b) “Interactive analysis of a space frame-raft-soil system considering soil nonlinearity”, *Computers & Structures*, 51 (4), 343-356.

Von Estorff O. and Antes H. (1991) “On FEM-BEM coupling for fluid structure interaction analyses in the time domain”, *International Journal for Numerical Methods in Engineering*, 31, 1151-1168.

Von Estorff O. and Hagen C. (2005) “Iterative coupling of FEM and BEM in 3D elastodynamics”, *Engineering Analysis with Boundary Elements*, 29, 775-787.

Von Estorff O. and Kausel E., (1989): “Coupling of boundary and finite elements for soil-structure interaction problems”, *Earthquake Engineering and Structural Dynamics*, 18, 1065-1075.

Von Estorff O. and Prabucki M. J. (1990) “Dynamic response in time domain by coupled boundary and finite elements”, *Computational Mechanics*, 6, 35-46.

Von Kármán T. (1933) “Discussion of water pressures on dams during earthquakes”, *Transactions of ASCE*, 98, 434-436.

Von Mises R. (1913) “Mechanik der festen Korper im plastisch-deformablen Zu-stand”, Nachrichten der Koniglicher Gesellschaft der Wissenschaft, Gottingen, Mathematik-Physik Klasse, 582-592.

Von Mises R (1928), "Mechanik der plastischen Formänderung von Kristallen", *Z. Angrew. Math. Mech*, 8, 161

Washa G. W., Saemann J. C. and Cramer S. M. (1989) “Fifty year properties of concrete made in 1937”, *ACI Materials Journal*, 86(4), 367-371.

Wei Z., Peric D. and Owen D. R. J. (1996) “Consistent linearization for the exact stress update of Prandtl-Reuss non-hardening elastoplastic models”, *International Journal for Numerical Methods in Engineering*, 39, 1219-1235.

Werner P. and Sundquist K. (1949) “On hydrodynamic earthquake effects”, *Transactions of American Geophysical Union*, 30(5), 636-657.

Westergaard H. M. (1933) “Water pressure on dams during earthquakes” *Transactions of ASCE*, 98, 418-472.

White W., Valliappan S. and Lee I. K. (1977) “Unified boundary for finite dynamic models”, *Journal of Engineering Mechanics Division*, ASCE, 103, 949-964.

Wilson E. (2002) “Three dimensional static and dynamic analysis of structures: A physical approach with emphasis on earthquake engineering”, *Computers & Structures*, Inc., Berkeley, California, 3rd edition, 234-249.

Withey, M. O. (1961) “Fifty year compression test of concrete”, *ACI Journal Proceeding*, 58 (6), 695-712.

Wolf J. P. (1985) Dynamic Soil-Structure Interaction, Prentice-Hall, Englewood Cliffs, NJ.

Wolf J. P. (1988) Soil-structure-interaction in time domain, Prentice Hall, Englewood Cliffs, NJ.

Wolf J. P and Darbre G. R. (1986) “Nonlinear soil-structure interaction analysis based on the boundary element method in time domain with application to embedded foundation”, *Earthquake Engineering and Structural Dynamics*, 13, 83-100.

Wolf J. P and Obernhuber P. (1985) “Nonlinear soil-structure interaction analysis using Green’s function of soil in the time domain”, *Earthquake Engineering and Structural Dynamics*, 13, 213-223.

Wolf J. P. and Song C. (1996) “Finite element modeling of unbounded media”, Wiley, New York.

Wong H. L. (1982) "Effect of surface topography on the diffraction of P, SV, and Rayleigh waves," *Bulletin of Seismological Society of America*, 72(4), 1167-1183.

Wrobel L. C., Brebbia C. A. and Nardini D. (1981) “The dual reciprocity boundary element formulation for transient heat conduction” Springer-Verlag.

Wrobel L. C. and Brebbia C. A. (1986) “The Dual Reciprocity Boundary Element Formulation for Non-Linear Diffusion Problems”, *Computer Methods in Applied Mechanics and Engineering*, 65, 147-164.

Yazdchi M., Khalili N. and Valliappan S. (1999) “Dynamic soil-structure interaction analysis via coupled finite element-boundary element method”, *Soil Dynamics And Earthquake Engineering*, 18, 499-517.

Yun C. B., Kim D. K. and Kim J. M. (2000) “Analytical frequency-dependent infinite elements for soil-structure interaction analysis in two-dimensional medium”, *Engineering Structures Engineering Structures* , 22, 258–271.

Zangar C. N. (1952) “Hydrodynamic pressures on dams due to horizontal earthquakes engineering”, *Monograph No.11, Bureau of Reclamation*.

Zhang X., Wegner J. L. and Haddow J. B. (1999) “Three-dimensional dynamic soil-structure interaction analysis in time-domain”, *Earthquake Engineering and Structural Dynamics*, 28, 1501-1524.

Zhao C. and Liu T. (2003) “Non-reflecting artificial boundaries for transient scalar wave propagation in a two dimensional infinite homogenous layer”, *International Journal for Numerical Methods in Engineering*, 58, 1435-1456.

Zienkiewicz O. C. and Newton R. E. (1969) “Coupled vibration of a structure submerged in a compressible Fluid”, *Proceedings of International Symposium on Finite Element Techniques, Stuttgart*.

Zienkiewicz O. C., Kelly D. W. and Bettes P. (1977) “The coupling of the finite element methods and boundary solution procedures”, *International Journal for Numerical Methods in Engineering*, 11, 355-377.

Zienkiewicz O. C., Pastor M., Chan A. H. C. and Xie Y. M. (1991) “Computational approaches to the dynamics and statics of saturated and unsaturated soils”, *Advanced Geotechnical Analysis*, Chapter 1, 1-45, Ed. P.K. Banerjee and R. Butterfield, Elsevier.

Zienkiewicz O. C. and Taylor R. L. (1991) The Finite Element Method, Vol.2, Solid and Fluid Mechanics, Dynamics and Nonlinearity, McGraw-Hill Book Co. U.K.

# PUBLICATIONS BASED ON PRESENT WORK

Following are the publications based on the present work:

**Journal:**

1. A. Burman, D. Maity and S. Sreedeep and I. Gogoi (2011) "Long term influence of concrete degradation on dam-foundation interaction", *International Journal of Computational Methods*, Vol. 8 (3), 397-423.
2. A. Burman, D. Maity and S. Sreedeep (2010) "Iterative analysis of concrete gravity dam-nonlinear foundation interaction", *International Journal of Engineering, Science and Technology*, Vol. 2 (4), 85-99.
3. A. Burman, D. Maity and S. Sreedeep (2009) "The Behavior of Aged Concrete Gravity Dam under the Effect of Isotropic Degradation Caused by Hygro-Chemo-Mechanical Actions", *International Journal of Engineering Studies*, Vol. 1 (2), 105–122.

**Conference:**

1. Burman, A., Chakravarty, D., Maity, D (2008) "Influence of Material Nonlinearity of Foundation in the Dam Foundation Interaction Analysis" Paper accepted in 14WCEE held in October 12-17, Beijing, China.